Chem Soc Rev

REVIEW ARTICLE

View Article Online
View Journal | View Issue

Cite this: *Chem. Soc. Rev.*, 2021, **50**, 3755

Biochemical and artificial pathways for the reduction of carbon dioxide, nitrite and the competing proton reduction: effect of 2nd sphere interactions in catalysis

Sk Amanullah, Paramita Saha, Abhijit Nayek, Md Estak Ahmed and Abhishek Dey *

Reduction of oxides and oxoanions of carbon and nitrogen are of great contemporary importance as they are crucial for a sustainable environment. Substantial research has been dedicated to these areas in the last few decades. These reductions require both electrons and protons and their thermodynamic potentials often make them compete with hydrogen evolution reaction *i.e.,* the reaction of protons and electrons to generate H_2. These reactions are abundant in the environment in microorganisms and are facilitated by naturally occurring enzymes. This review brings together the state-of-the-art knowledge in the area of enzymatic reduction of CO_2, NO_2^- and H^+ with those of artificial molecular electrocatalysis. A simple ligand field theory-based design principle for electrocatalysts is first described. The electronic structure considerations developed automatically yield the basic geometry required and the 2nd sphere interactions which can potentially aid the activation and the further reduction of these small molecules. A systematic review of the enzymatic reaction followed by those reported in artificial molecular electrocatalysts is presented for the reduction of CO_2, NO_2^- and H^+. The review is focused on mechanism of action of these metalloenzymes and artificial electrocatalysts and discusses general principles that guide the rates and product selectivity of these reactions. The importance of the 2nd sphere interactions in both enzymatic and artificial molecular catalysis is discussed in detail.

Received 3rd November 2020

DOI: 10.1039/d0cs01405b

rsc.li/chem-soc-rev

Introduction

Human activity over the last century has resulted in an increased distribution of oxidized forms of carbon, nitrogen and sulfur in the environment.[1] Occam's razor would suggest that much of this is derived from the use of fossil fuel for energy to drive industrial and technological developments.[2] Obtention of the energy stored in the C–H and C–C bonds of carbon-based fuels by oxidizing them with O_2 has, expectedly, released large amounts of CO_2 in the atmosphere; much beyond the capacity

School of Chemical Sciences, Indian Association for the Cultivation of Science, 2A & 2B Raja SC Mullick Road, Kolkata, 700032, India. E-mail: icad@iacs.res.in

Sk Amanullah

Sk Amanullah received his BSc (2012) from Presidency College, Kolkata and MSc (2014) from Indian Institute of Technology, Kharagpur. He joined Prof. Dey's group as a PhD scholar in 2014. His thesis is focused to understand nature's choice of macrocyclic porphyrinoids for diverse reactivity.

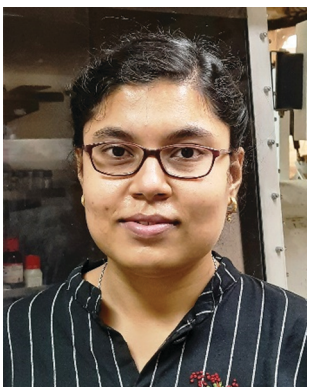

Paramita Saha

Paramita Saha received her BSc (2015) and MSc (2017) from Jadavpur University. She joined Prof. Dey's group as a PhD scholar in 2017. Her thesis is focused to the synthesis of metallo-clusters for catalysis relevant to sustainable energy and environment.

of the natural carbon fixation mechanism.[3] This has led to rising concerns regarding the sustainability of our current lifestyles and industrial activities. Logically, this has spurred research activites to find new methods of fixing these oxides and oxoanions of carbon, nitrogen and sulfur. These include both chemical and electrochemical methods. And inevitably a switch to non-fossil energy sources, such as wind, solar, nuclear, geothermal, etc is being advocated.[4]

Atmospheric CO_2 could be captured and converted into value added chemicals such as formic acid, carbon monoxide, methanol, ethylene, *etc.*[5–9] Over the last few decades, extensive research has been conducted resulting in a number of homogeneous[10,11] and heterogeneous[12–14] electrochemical and photochemical[15,16] pathways to achieve the same. Alternatively, the reduction of CO_2 to various C-based products is a part of the geochemical Carbon cycle which fixes 250 gigatonnes of CO_2 every year. Several earth abundant metal-based metalloenzymes are involved in this process which occurs under ambient conditions. The reduction of CO_2 follows fundamentally different mechanisms in these enzymes. In photosynthetic carbondioxide reduction, the CO_2, post capture, is reduced by hydride, more specifically *via* NADPH, by two electrons.[17] In the reductive acetyl CoA pathway, CO_2 is reduced to CO using H^+ and e^- derived from H_2. In methanogens, however, the pathway to produce CH_4 from CO_2 involves reduction with hydride, molecular H_2 as well as H^+ and e^- derived from H_2 *via* hydrogenases.[18]

Similarly, reduction of oxides and oxoanions of nitrogen poses challenges and heralds promises. Emission of NO_x and SO_x have same sources as CO_x *i.e.*, fossil fuels. The atmospheric concentration of these oxides has been steadily increasing over the last decade and their detrimental effects is not limited to acid rain anymore but include long term damage to human health as well as the ozone layer.[19] Like CO_2, there are different routes of biochemical nitrogen cycle involve interconversion of various oxides of nitrogen (N_xO_y) each of which has prominent roles in biology. Nitrite, in particular, is a pivotal entity in the nitrogen cycle, mediating conversion of inorganic nitrates to ammonia or nitric oxide (NO). The NO generated is eventually recycled back to biological nitrogen pool. Nitrite reduction may be an assimilatory, respiratory or dissimilatory process. Assimilatory nitrite reduction by siroheme containing nitrite reductase produces ammonia which participates in biosynthetic pathways utilised for cell growth in bacteria. Some bacteria also exploit respiratory nitrite ammonification, involving cytochrome *c* containing nitrite reductase, as a process where nitrite acts as the terminal electron acceptor of the respiratory chain. This is a dissimilatory mode of energy conservation in lower living organisms. A contrasting route of nitrite reduction is denitrification. Denitrification involves the anaerobic nitrate reduction to molecular dinitrogen. Dissimilatory nitrite reductases, a heme or a Cu-containing enzyme, in denitrifiers converts nitrite to nitric oxide.

Diminishing fossil fuel and increasing global energy demand has encouraged the investigation into means of storing energy in the form of value added chemicals which can be obtained by the reduction of CO_2 as well as oxonions of nitrogen like NO_2^-.[20,21] In nature, the reduction of CO_2 and NO_2^- proceeds through electron transfer from proteins like ferredoxin which are also involved in the reduction of proton from H_2O to H_2 *i.e.,* the reduction potentials for CO_2, NO_2^- and H^+ reduction

Abhijit Nayek

Abhijit Nayek received his BSc (2015) from Midnapore College and MSc (2017) from Ramakrishna Mission Residential College, Narendrapur. He joined Prof. Dey's group as a PhD scholar in 2017. His current research focuses on understanding synthesis of active site mimics of [FeFe]-hydrogenases and the mechanism of H_2–H^+ interconversion.

Md Estak Ahmed

Md Estak Ahmed received his BSc (2012) from Ramakrishna Mission Residential College, Narendrapur and MSc (2014) from Indian Institute of Technology, Kanpur. He joined Prof. Dey's group as a PhD scholar in 2014. His thesis was focused to bio-inspired models of metalloenzymes involved in low-valent transformations. Currently he is a postdoctoral researcher at Georgetown University, USA.

Abhishek Dey

Abhishek Dey received his BSc (1999) from Presidency College, Kolkata and MSc (2001) from Indian Institute of Technology, Kanpur and PhD (2007) from Stanford University, CA, USA. After postdoctoral stay at Stanford University, he moved to Indian Association for the Cultivation of Science (IACS), Kolkata as an Assistant professor (2009). Currently, he is a professor at the same department. His primary research interests include inorganic reaction mechanisms relevant to renewable energy and clean environment.

are similar. Hence, while protons, H^+, are necessary to reduce both CO_2 and NO_2^-, its reduction to H_2 competes with reduction of CO_2 and NO_2^- itself. At the same time H_2 itself is a convenient carier of energy and this energy can be extracted from it either by combustion or electrochemically. This, along with the drive to generate fuel from CO_2, NO_2^- *etc.*, has automatically brought to focus the storage of energy in the form of hydrogen itself. Hydrogen can be generated *via* reduction of H^+ by e^- and these, including H_2, are components essential to reduction of CO_2 and NO_2^- discussed above.

In this review, we focus on the reduction of CO_2, NO_2^- and H^+. We present an electronic structure-based approach for the activation and reduction of these species using mononuclear 1st row transition metal species. Thereon an overview of the natural enzymes involved in these reductions will be used followed by a review of artificial catalysts reported in the literature. In particular, the mechanism of action of these enzymes and complexes and the roles played by 2nd sphere residues will be stressed upon to understand the structure function correlations necessary for the design of efficient and selective catalysts.

Electronic structure and catalyst design

Molecular orbital (MO) theory considerations can be crucial when designing catalysts for the activation of small molecules. An analysis of the MO of the small molecule and possible ligand fields around a metal can narrow down the search for a metal-based catalyst and its ligand. CO_2, for example, is a linear triatomic molecule. While its HOMO is localized on the more electronegative oxygen atoms, the LUMO is a C–O σ* (Scheme 1) orbital. The LUMO+1 is the degenerate set of in-plane and out-of-plane C–O π* orbitals (Scheme 1). Reduction of CO_2 will entail population of these orbitals and the electrons required must be obtained from the metal center(s) of the catalyst used; a mononuclear complex having axial symmetry ($x = y$) is considered here. For efficient activation, it is desirable that the metal donor orbitals are poised to overlap with the CO_2 acceptor orbitals. The contours of the orbitals involved suggest that a d_{z^2} orbital is suitable for generous overlap with the C–O σ* and the $d_{xz/yz}$ orbitals are suitable to overlap with the C–O π* orbitals. Thus, it would seem that a metal center with occupied d_{z^2} and $d_{xz/yz}$ would provide ideal configurational interaction for the initial activation and eventual final reduction of CO_2.

Considering the relative orbital energies of the d-orbitals in different trigonal and tetragonal ligand fields, two geometric dispositions of the metal catalyst appear attractive for CO_2 activation *i.e.,* occupied d_{z^2} and $d_{xz/yz}$ orbitals (Scheme 2). A triaonal ligand field with no or weak ligand along the *Z*-axis can achieve the desired occupation of the d_{z^2} and the $d_{xz/yz}$ orbitals with a d^4, d^5 and d^6 (as demonstrated below) occupation to activate a CO_2 molecule approaching along the *Z*-axis. For maximum activation of CO_2, a low spin d^6 cofiguration is required at least and further occupation of the higher energy $d_{x^2-y^2}$ and d_{xy} orbitals will not offer further advantage. This electronic structure automatically requires strong field ligands or

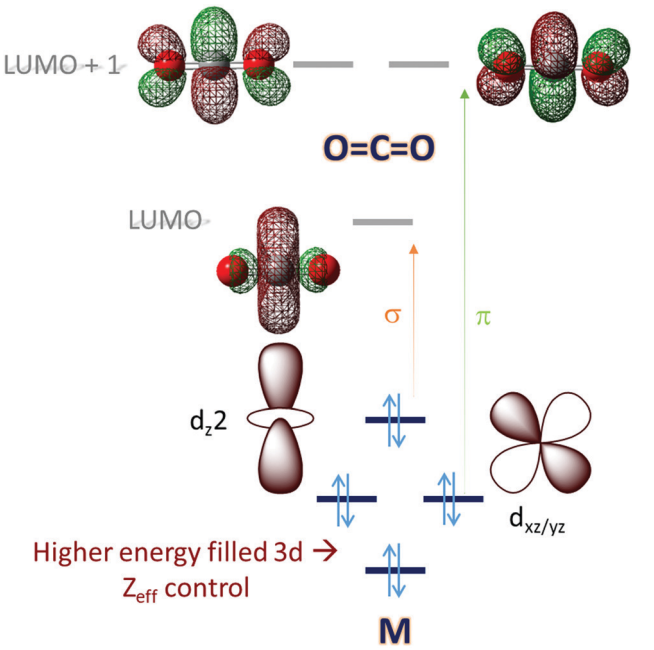

Scheme 1 An electronic structure consideration of CO_2 activation and reduction using a 3d metal active site.

2nd or 3rd row transition metals to ensure low spin state at the metal as high spin configuration will lead to depopulation of the active d_{z^2} and $d_{xz/yz}$ orbital and population of the inactive $d_{x^2-y^2}/d_{xy}$ orbital. Similarly, a low spin d^8 tetragonal ligand field is well equipped to activate a CO_2 approaching along the *Z*-axis. Since the inactive d_{xy} orbital is lower in energy in this ligand field than the active orbitals, additional two electrons will be required in this catalyst architecture than the trigonal architecture described earlier.

The electronic structure considerations allow narrowing down the choices for metals and ligands required for CO_2 activation as well as the oxidation states required which are eventually important for lowering the overpotential for the electrochemical reduction of CO_2. For example, the analysis above suggests that for 2nd and 3rd row transition metal complexes, which tend to result in low spin

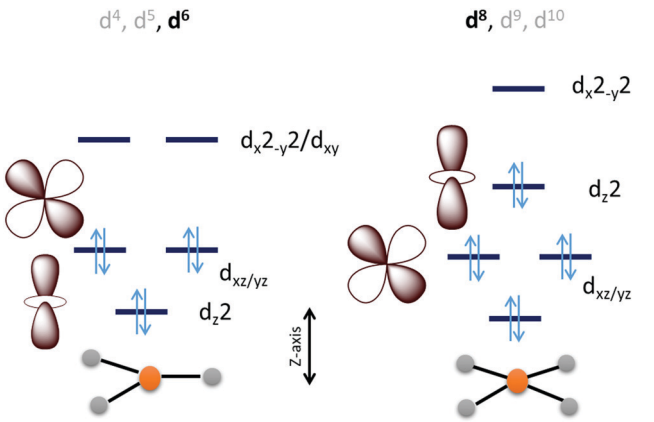

Scheme 2 An electronic structure consideration of CO_2 activation and reduction using a 3d metal active site having trigonal (left) and tetragonal (right) ligand field.

states, the trigonal geometry can result in efficient CO_2 activation and reduction with 6 d-electrons. Attempting to install low spin in a first-row metal in a trigonal geometry will require the use of π-acid ligands which would drain out the electron density from these metal donor orbitals compromising the activation of CO_2. Obtention of stable three co-ordinate metal complexes (or with weak axial ligands) may be a synthetic challenge depending on the metal chosen. The second tetragonal option is more feasible with abundant examples in reported literature which inherently employed this design. A tetragonal ligand field will optimally require a low-spin d^8 configuration. A reasonably strong σ donor ligand in the *XY*-plane will elevate the energy of the $d_{x^2-y^2}$ orbital ensuring the occupation of the active d_{z^2} orbital. As a result, metal centers like Fe^0, Co^I and Ni^{II} in tetragonal ligand field can, in principle, be able to activate CO_2 efficiently. Of course, effective nuclear charge of Ni(II) may be prohibitive of the back donation from its occupied orbital and its further reduction to Ni(I) or Ni(0) states may be necessary. It is likely that CO_2 activation can be achieved by a half-filled d_{z^2} (*e.g.* Fe^I, Co^{II}) in the tertragonal geometry but it should be less effective than a filled d_{z^2} orbital. Complexes of the 2nd and 3rd row transition metal neighbours of Fe and Co, having tetragonal ligand field, should be active as well.

Finally, the activation of CO_2 results in shift of electron density from the metal center to the bound CO_2. The shift of electron density to the bound CO_2 can be stabilized by suitably placed non-covalent 2nd sphere interactions. These may include secondary Lewis acidic metal center, hydrogen bonding and electrostatic interactions. Of these hydrogen bonding is particularly attractive as apart from stabilizing the charge transfer, it can facilitate proton transfer to the bound CO_2 as well which is required for the reaction to proceed. Thus, the insight obtained from ligand field theory and MO theory (an electronic retrosynthesis of catalyst) suggests that Fe(0) and Co(I) square planar or square pyramidal complexes with weak axial ligands and 2nd sphere hydrogen bonding residues (which can also act as proton transfer residues) should be ideal for the activation and the ensuing reduction of CO_2. The same approach can be used to design catalysts for NO_x and SO_x reduction as well.

In the case of NO_2^- the HOMO is in-plane and localized substantially on the nitrogen while the LUMO is a N–O π* (Scheme 3). To cleave the N–O bond one needs to bind the NO_2^- and populate the anti-bonding N–O π* orbital. The HOMO being delocalized over both N and O centers of NO_2^- can bind a metal center both η-N as well as η-O. An empty d_{z^2} orbital can for a σ bond with the HOMO of the NO_2^- while a populated $d_{xz/yz}$ can assist in cleaving the N–O bond by back bonding into the N–O π*. Considering the MO of the HOMO and LUMO of a free NO_2^- it appears reasonable to assume that a η-N co-ordination to a metal center would lend it to better backbonding, essential for N–O bond cleavage, from the metal center as well. The electronic structure configurations that allow such bonding possibilities in trigonal and tetragonal ligand fields are d^4 (Scheme 3) and d^6 (Scheme 3), respectively. Considering the motivation of using a first-row transition metal complex with optimal Z_{eff} to actuate the balance between forming a σ bond with the NO_2^- and backbonding to it, a d^6 low spin configuration

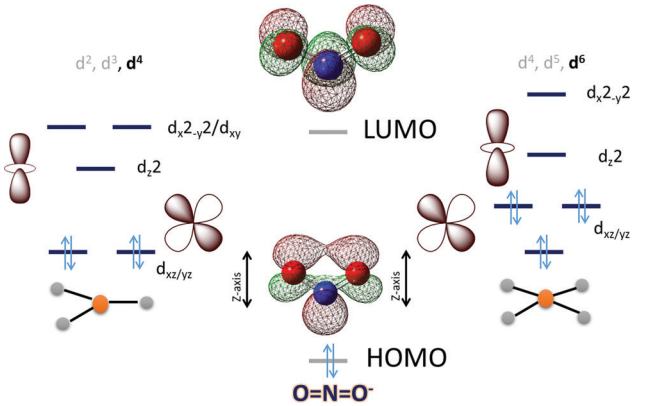

Scheme 3 An electronic structure consideration of NO_2^- activation and reduction using a 3d metal active site having trigonal (left) and tetragonal (right) ligand field.

would be suitable for the purpose *i.e.*, Fe^{II}, Co^I *etc.* Similar to the case of CO_2 the electron density shift of the metal center to the bound NO_2^- needs stabilization and the reaction forward requires protons. Thus, a hydrogen bonding from a group capable of proton transfer in the 2nd sphere would assist the reaction. Additionally, H-bonding interaction with the O atoms will also aid binding the NO_2^- *via* the N atom by restricting the electron density on the O atoms from participating in bonding.

Having considered a straight-forward and intuitive MO theory-based expectations for a monometallic molecular complex likely to be suitable for the reduction of CO_2 and NO_2^-, the natural metalloenzymes doing the same is now discussed.

CO_2 reduction

Introduction

CO_2 is a linear molecule with a high C–O bond enthalpy of ~191 kcal mol^{-1}. The one electron reduction of CO_2 to its corresponding anion radical ($CO_2^{-\bullet}$) is associated with a large re-organization energy due a change in geometry from linear to bent. This is reflected in the requirement of highly negative potential to reduce CO_2 by one electron (−1.97 V and −1.90 V *vs.* NHE in an aprotic solvent, *N*,*N*-dimethylformamide (DMF)[22] and in water,[23] respectively). However, it is desirable to conduct these reactions involving multiple protons and electrons at relatively modest potentials (eqn (2)–(5)). Hence, catalytic strategies have been developed to avoid the high energy steps.[3,24]

$$CO_2(aq) + e \rightarrow CO_2^{-\bullet}(aq), \quad E^\circ = -1.90\ V \qquad (1)$$

$$CO_2(g) + 2H^+ + 2e \rightarrow CO(g) + 2H_2O, \quad E^\circ = -0.52\ V \qquad (2)$$

$$CO_2(g) + H^+ + 2e \rightarrow HCO_2^-(aq), \quad E^\circ = -0.43\ V \qquad (3)$$

$$CO_2(g) + 6H^+ + 6e \rightarrow CH_3OH(aq) + H_2O, \quad E^\circ = -0.38\ V \qquad (4)$$

$$CO_2(g) + 8H^+ + 8e \rightarrow CH_4(aq) + 2H_2O, \quad E^\circ = -0.24\ V \qquad (5)$$

In this section, we have attempted to summarize the conceptual development in the design of catalysts for electrocatalytic CO_2 reduction. Several strategies have been devised considering

the primary as well as the secondary coordination sphere and a wide variety of metal–ligand combinations. However, the central theme of this review is the contribution of the second sphere to catalysis. A bio-inspired approach is a good way of designing catalysts as metallo-enzymes have evolved over billions of years optimizing the rates and selectivity of specific reactions they catalyze using elegant 2nd sphere interactions. Enzymes have evolved to use amino acid residues, additional metal centres and well-defined substrate/product channels to regulate and optimize their reactivity. This allows catalyzing reactions with precise thermodynamic and kinetic control. Therefore, prior understanding about the enzymatic machinery is very important before designing molecular catalysts for the same purpose.

Lessons from nature

Six pathways are known for the fixation of inorganic carbon into organic materials to be incorporated into biomass: (i) reductive pentose phosphate (Calvin–Benson–Bassham cycle)[25] (ii) reductive acetyl-CoA pathway (Wood–Ljungdahl pathway)[26] (iii) reductive citric acid cycle (TCA and Arnon–Buchanan cycle)[27,28] (iv) decarboxylate/4-hydroxybutyrate cycle (v) 3-hydroxypropionate/4-hydroxybutyrate cycle and (vi) 3-hydroxypropionate cycle. These processes have been discussed in detail in the previous reviews.[3,29] In this review we will discuss about the second inorganic pathway which contains two CO_2 reduction steps: (a) carbon monoxide dehydrogenase (CODHs) catalysed CO_2 to CO interconversion and (b) formate dehydrogenase catalysed reduction of CO_2 to formic acid.

CO dehydrogenases (CODHs)

There are two types of CODHs participating in CO_2 to CO interconversion. Oxygen-sensitive enzyme from obligate anaerobes like *Moorella thermoacetica*, *Carboxythermus hydrogenoformas* and *Methanosarcina bakerii* use the [NiFe]CODH active site for reversible conversion of CO_2 to CO. These enzymes have turnover frequency (TOF) of $\sim$40 000 s^{-1} for CO oxidation (at 70 °C using methyl viologen) and 45 s^{-1} for CO_2 reduction and operate with almost zero over-potential, *i.e.*, close to the thermodynamic potential of the CO_2/CO couple, at −0.52 V *vs.* SHE at pH 7.[30] The second class of CODHs are air-stable [MoSCu]-containing enzymes which are found in aerobes such as *Oligotropha carboxidovorans*. These enzymes show lower CO oxidation activity (TOF $\sim$ 100 s^{-1}) and their NiFe analogues and do not show any CO_2 reduction activity. We will not discuss about this class of CODHs in this review which has been reviewed elsewhere.[31,32]

[NiFe]CO dehyrogenases

Enzyme architecture. These are dimeric enzyme, contain a distinctive Ni–Fe–S centre termed the C-cluster. Early spectroscopic studies prior to the crystal structure had suggested that the C-cluster is composed of a [4Fe–4S]cubane with a unique Ni site nearby.[33–35] CODH structures revealed an unprecedented metallocluster consists of [Ni–3Fe–4S] containing distorted cubane which is coordinated with a unique Fe site, also called ferrous component II, FCII (Fig. 1A).[36] The Ni-centre is

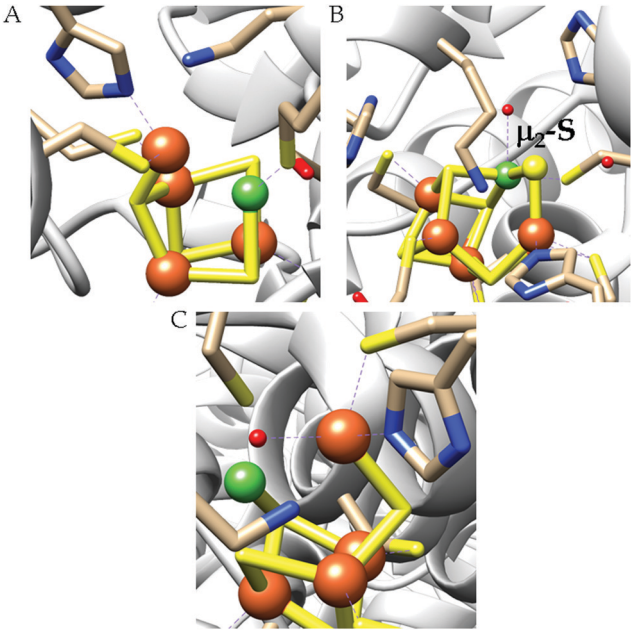

Fig. 1 The active site structure of the [NiFe]CODHs at resting state; (A) from *Moorella thermoacetica* (pdb: 1MJG);[36] (B) from *Carboxythermus hydrogenoformas* (pdb: 1SU8);[37] (C) from *Moorella thermoacetica* (pdb: 3I01).[38] The figures are redrawn using the software package Chimera 1.12rc.

coordinatively unsaturated as it is bound to three sulfur ligands and the unique Fe centre is coordinated by a His, a Cys, and a H_2O/OH^- ligand. In some cases, such as in *Carboxythermus hydrogenoformas* CODHs (*Ch*CODH), C-cluster contains an additional sulfide ligand (μ_2-sulfido) bridging Ni of the distorted cubane and the unique Fe (Fig. 1B).[37] The role of this bridging sulfido-ligand in catalysis is still unknown. However, many crystal structures have been solved where a water molecule is bound to the unique Fe site in an identical fashion, completing a distorted tetrahedral geometry (Fig. 1C).[38,39] None of these structures contain the μ_2-sulfide bridge, because the sulphide coordination site of the Fe version is occupied by the water molecule. These crystallographic data were consistent with the previous spectroscopic analyses suggesting a water molecule bound to the Fe.[40] It is still unknown how the protons exchange with the bulk solvent during catalysis. It has been suggested that a network of histidine residues which link the buried C-cluster with the solvent exterior could be a possible route for proton transfer.[41,42] Additional [4Fe–4S] clusters are present in all CODH structures, which are believed to be the electron transfer centers.[35]

General mechanism. X-ray structures of the enzymes with different substrates and inhibitors and extensive spectroscopic investigations have provided the key mechanistic insights into the CO_2 reduction by [NiFe]CODHs. Treating the enzyme crystals with bicarbonate in the presence of appropriate reducing agents, the CO_2 adduct of the enzyme has been trapped and structurally characterized (Fig. 2).[39] The CO_2 binds with the Ni^{II}-centre (with a Ni–C distance of 1.96 Å) completing square planar coordination geometry of Ni^{II}-centre. Upon CO_2 binding, the Fe-centre releases

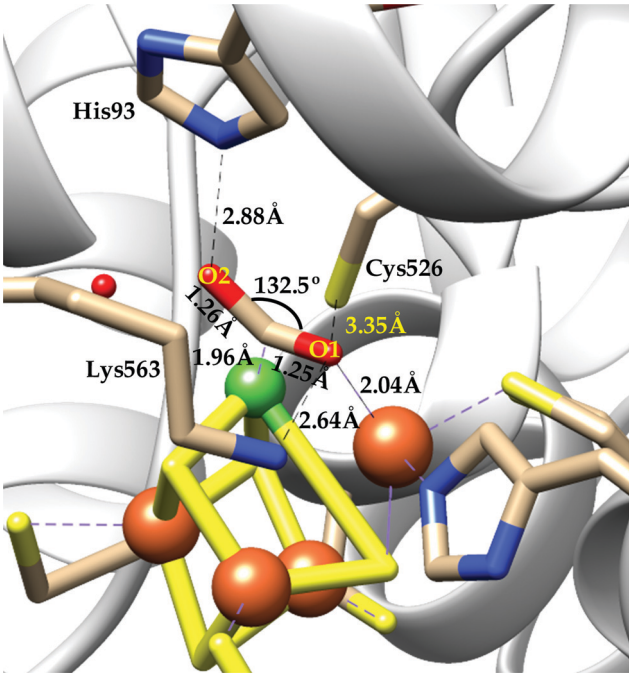

Fig. 2 The structure of *Ch*CODH with CO_2 (−600 mV + CO_2 state; pdb: 3B52).[39]

the H_2O/OH^- ligand and coordinates with one of "O" atom of CO_2 (O1, Fe–O1 distance = ∼2.04 Å). The same "O" atom (O1) of CO_2 is also H-bonded to a Lys residue (Lys563) and the other (O2) is within the H-bonding distance to a protonated His (His93). The CO_2 ligand is sufficiently bent (∠C–O–C = ∼132.5°) and C–O bonds are substantially elongated to ∼1.26 Å, suggesting substantial charge transfer to the CO_2 antibonding orbitals *via* back-bonding and hence the activated CO_2 may be viewed as a $CO_2^{-\bullet}$ which is obtained here at a much higher potential (−0.6 V *vs.* NHE) than the thermodynamic potential of free CO_2.[43] Overall, the reaction is proposed to be initiated by electron transfer to the C-cluster generating a low-valent Ni-center (Ni^I/Ni^0), followed by CO_2 binding (Scheme 4). After that proton-assisted C–O bond cleavage yields an oxidized Ni^{II}–CO intermediate and finally CO release completes the catalytic cycle. Therefore, the overall process involves a "push–pull" activation of CO_2;[43] where the Ni^0 centre acts as a Lewis base to "push" the electron density to the Lewis acid, CO_2 to form the CO_2-adduct while the optimally oriented Fe-centre acts as a Lewis acid which should aid the charge transfer from the Ni to CO_2. Therefore, the iron-centre acts a "metal activator" during the CO_2 binding to the Ni-centre. The protonated peptide residues stabilize the negatively charged bound $CO_2^{-\bullet}$ species by coulombic and H-bonding interaction. This "2nd sphere interaction" ultimately allows access to high-energy intermediate exerting the "pull"-effect to facilitate the electron transfer from Ni to CO_2 and as well as C–O bond cleavage.

Formate dehydrogenases (FDHs)

There are two types of formate dehydrogenases, metal independent NAD^+ dependent and Mo/W containing formate dehydrogenases. The most abundant class of formate dehydrogenases are $NAD(P)^+$ dependent. They are the major source of energy conversion in methylotrophic aerobic bacteria, fungi and plants.[44,45] This class of enzymes have a characteristic property of transferring both proton and electron together in the form of a hydride, from one site to another. More specifically, from the formate to the C_4-atom of the pyridine ring of $NAD(P)^+$ for the oxidation of formate to CO_2. It is difficult to drive the reaction in reverse direction, *i.e.*, to reduce CO_2 to formate, because the reduction potential of $NAD(P)^+$ is more positive than that of CO_2.[46] Hence, this has not been included in this review. The Mo/W-containing formate dehydrogenases on the other hand, can catalyze the reduction of CO_2 to formate (with rate ∼280 s^{-1}) as well as formate oxidation (with rate ∼3400 s^{-1}).[47]

Mo and W-containing formate dehydrogenase. This second class of formate dehydrogenases are extremely oxygen-sensitive and use Mo or W-atoms in their active site.[48,50] The crystal structures of several enzymes of this class have been reported.[48,51] In the oxidized form, the W^{VI} or Mo^{VI} ions possess a distorted trigonal prismatic geometry with four "S" atoms from

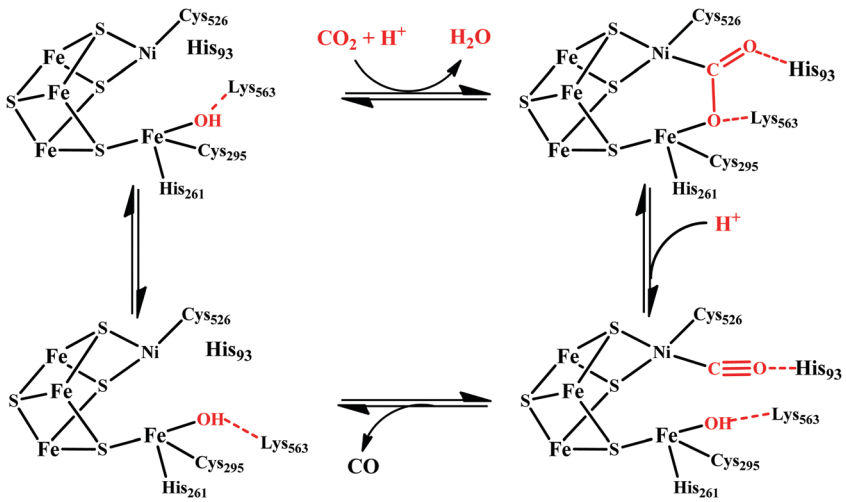

Scheme 4 Proposed mechanistic cycle of CO_2 reduction to CO by [NiFe]CODHs.

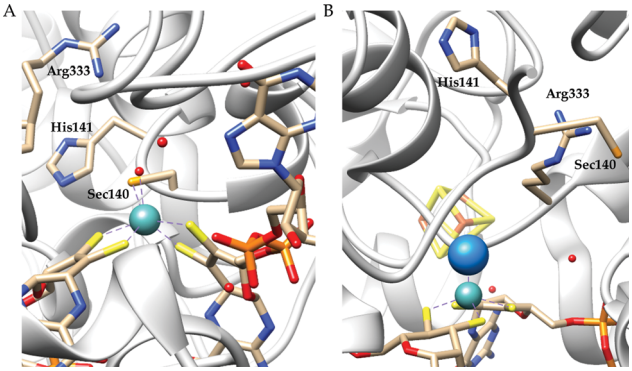

Fig. 3 The active site structure of the formate dehydrogenase H from *E. coli*; (A) oxidized state (pdb: 1FDO);[48] (B) reduced state (pdb: 2IV2).[49] The figures are redrawn using the software package Chimera 1.12rc.

two pyranopterin moiety (Fig. 3A). A sulphur-atom from a cysteine or a selenium-atom from a selenocysteine residue is attached with the metal centre. Either a sulphur or an oxygen (water) is also proposed to bind the metal centre. Two conserved arginine and histidine residues are present in the close vicinity of the metal centre and are anticipated to influence the course of the reaction. In the reduced state the central Mo or W atom possess a square pyramidal geometry with four sulphur from the two pyranopterin ligands in the equatorial plane (Fig. 3B). In the axial position, a sulphur atom is thought to be present. However, in the reduced structure, the selenocysteine ligand is no longer bound to the metal-centre and is located ~12.2 Å away from the central metal centre.[49] Based on the structural, spectroscopic and kinetic data a plausible mechanism has been proposed where the hydride transfer for the formation of C–H bond was proposed to be the rate-determining step (Scheme 5).[52–55]

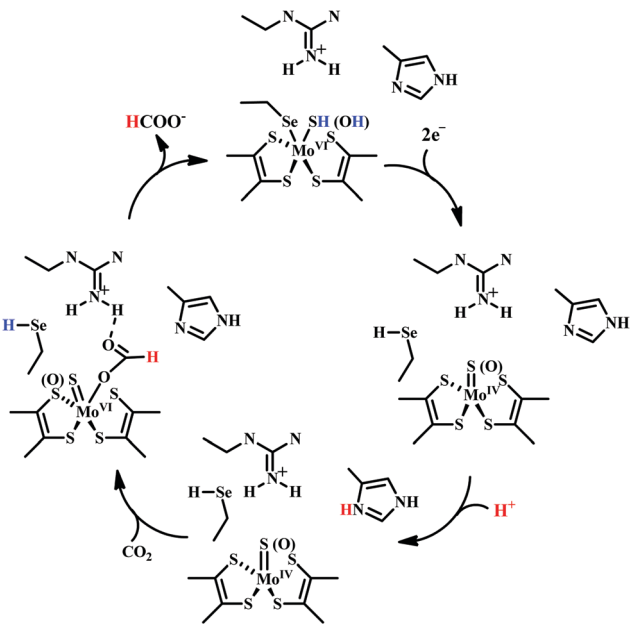

Scheme 5 Proposed mechanistic cycle of CO_2 reduction to formate by selenium and molybdenum dependent formate dehydrogenase.

Challenges and general outlook

Efficient carbon dioxide reduction to useful molecules such as carbon monoxide, formic acid, methanol, methane *etc.*, is an important challenge and provides a great opportunity to convert waste to valuable commodities. Although, the field of transition metal catalyzed CO_2 reduction is relatively new, it has expanded substantially in the recent years. However, the major challenges associated with CO_2 economy are: (i) capturing the pure CO_2 from the atmosphere, which is quite difficult because the scarcity of CO_2 in the atmosphere and (ii) reducing CO_2 selectively as separation of mixture of products is undesirable. The reduction of CO_2 competes wth the reduction of H^+ which is another reactant in electrochemical CO_2 reduction and strategies are needed to avoid competing H^+ reduction. Similarly, practicable CO_2 reduction systems need to be O_2 tolerant or selective towards CO_2 even in the presence of a strong oxidant as O_2.

In this section a review of the molecular electrocatalysts is presented with a focus on the effects of 2nd sphere interactions on the efficiency of ctalysis. These interations include the effect of hydrogen bonding, redox-active metal or ligands, additional metals, *etc.* A combination of suitable design or the primary coordination sphere and inclusion of 2nd sphere residues have been found to have a profound impact on CO_2 reduction helping address some of the challenges discussed above.

Molecular catalysts

The idea that transition metals can activate CO_2 dates back to the work by Aresta and Nobile, where a bent CO_2 was attached in a η^2-mode (through C and O atoms) with a Ni-centre.[56] Meshitsuka reported electrochemical CO_2 reduction with Co and Ni-phthalocyanines, but lacked product chracterization, TON, *etc.*[57] Later in the 1980s, Eisenberg and co-workers reported electrochemical reduction of CO_2 to CO (along with H_2 production) with tetraaza-macrocycles of Co and Ni.[58] It was likely one of the first report of electrochemical CO_2 reduction with high current density and turn-over numbers (TON). In the following years, a number of electrocatalysts have been developed with high TONs and selectivity. We have divided this section in two major categories depending on the ligand type: (i) non-heme catalysts and (ii) heme or other macrocycle catalysts. It should be noted that in this review, we have discussed electrocatalytic reduction of carbon dioxide under homogeneous conditions only.

Non-heme system

Metal–bipyridine complexes. In 1984, Lehn and co-workers reported electrocatalytic CO_2 reduction in the presence of a $Re(bpy)(CO)_3Cl$ (bpy = 2,2′-bipyridine) catalyst.[59] They found selective reduction of CO_2 to CO at −1.25 V *vs.* NHE in a 9 : 1 DMF : water solution. It was later proposed that CO_2 binds to the Re^0 centre and after reductive decarbonylation generating a carboxylato-rhenium intermediate.[60] Upon protonation it eliminates a molecule of water and generates $[Re^{II}(bpy)(CO)_3Cl]^+$ complex which upon further reduction

regenerates the starting molecule. Tanaka and co-workers did a remarkable study in electrocatalytic CO_2 reduction with similar Ru-based catalysts ($[Ru(bpy)_2(CO)_2]^{2+}$ or $[Ru(bpy)_2(CO)Cl]^{+}$).[61] They showed a pH dependent product selectivity. Controlled potential electrolysis (at −1.25 V *vs.* NHE) at pH 6 generated a mixture of CO and H_2. Alternatively, at pH 9 it generated CO and H_2 along with $HCOO^-$. The reaction was proposed to be initiated by the generation of an unstable penta-coordinated Ru^0 intermediate ($[Ru(bpy)_2(CO)_2]^{2+}$ or $[Ru(bpy)_2(CO)Cl]^{+}$). In the presence of CO_2, both likely generated $[Ru(bpy)_2(CO)(COO^-)]^{+}$ intermediate, which upon protonation should generate $[Ru(bpy)_2(CO)(COOH)]^{+}$ intermediate. Under acidic condition (pH 6), further protonation releases a molecule of water to regenerate the catalyst. Under weakly alkaline condition (pH 9), it may undergo a $2e^-/1H^+$ process to regenerate the penta-coordinated Ru^0 intermediate releasing $HCOO^-$.

Meyer and co-workers reported electrocatalytic CO_2 reduction by similar 2,2′-bipyridyl-complex of Rh and Ir.[62] They reported selective reduction of CO_2 to formate (without formation any CO during electrocatalytic condition) by *cis*-$[Rh(bpy)_2X_2]^{+}$ (where, X is Cl^- or OTf^-) at −1.30 V *vs.* NHE. They also found $[M(bpy)_2(CO)H]^{+}$ (where M = Os, Ru) can reduce CO_2 to CO as major product in anhydrous acetonitrile medium.[63] However, up to 25% formate was observed upon addition of water into the solution. Later, Kubiak and co-workers developed a series of 2,2′-bipyridyl-complex of Re, Re(bpy-R)$(CO)_3Cl$ (where R = H/4,4′-dicarboxyl/4,4′-dimethyl/4,4′-di-*tert*-butyl/4,4′-dimethoxy) for electrocatalytic CO_2 reduction (Fig. 4a).[64] The Re(bpy-*t*Bu)$(CO)_3Cl$ was found to be most effective to selectively reduce CO_2 to CO at ∼100% faradaic efficiencies at −1.60 V *vs.* NHE. The observed high selectivity over competitive proton reduction was explained using extensive kinetic investigations, which suggests that under same condition, the reaction with CO_2 is ∼25 times faster than that of water or methanol.[65]

Bourrez *et al.* reported earth abundant Mn-based catalysts, $[Mn(L)(CO)_3Br]$ complexes (where, L = 2,2′-bipyridine or 4,4′-dimethyl-2,2′-bipyridine, Fig. 4a), which can catalyze the electrochemical reduction of CO_2 to CO at relatively lower overpotential (at −1.10 V *vs.* NHE).[66] However, in comparison with the Re catalysts, there was one distinct difference in the corresponding Mn-catalysts, which is the tendency for dimerization after the first reduction. The irreversible loss of X (where, Cl^-, Br^- or OTf^-) is responsible for such dimer formation (eqn (6)). This is in contrast to the Re counterparts, where the first reduction is reversible (no loss of X). Such a behaviour explains lower activity by Mn-bpy based electrocatalysts.[67]

$$[Mn^{I}(bpy\text{-}R)(CO)_3X] + e \rightarrow \frac{1}{2}[Mn^{0}(bpy\text{-}R)(CO)_3]_2 + X \quad (6)$$

To eliminate this dimerization pathway, Kubiak and co-workers developed a strategy using a bulky bipyridyl ligand, 6,6′-dimesityl-2,2′-bipyridine (mesbpy), instead of 2,2′-bipyridine (Fig. 4b). The Mn(mesbpy)$(CO)_3Br$ and $[Mn(mesbpy)(CO)_3(MeCN)](OTf)$ were shown to generate single 2e reduction wave without formation of any dimeric species. However, spectroelectrochemistry coupled with IR (IR-SEC) data suggested the formation of a Mn^I–CO_2H catalytic intermediate during reduction of the catalyst in presence of CO_2 and a weak Brønsted acid source. This intermediate requires unusual ∼400 mV higher overpotential to initiate the reaction.[68] However, in the presence of Lewis acidic cations such as Mg^{2+}, not only the over-potential of the reaction could be reduced to as less as 300–450 mV but the rate of the reaction can also be increased by ∼10 fold.[69] With Mg^{2+}, the reaction proceeds *via* the reductive disproportionation of CO_2 to CO and

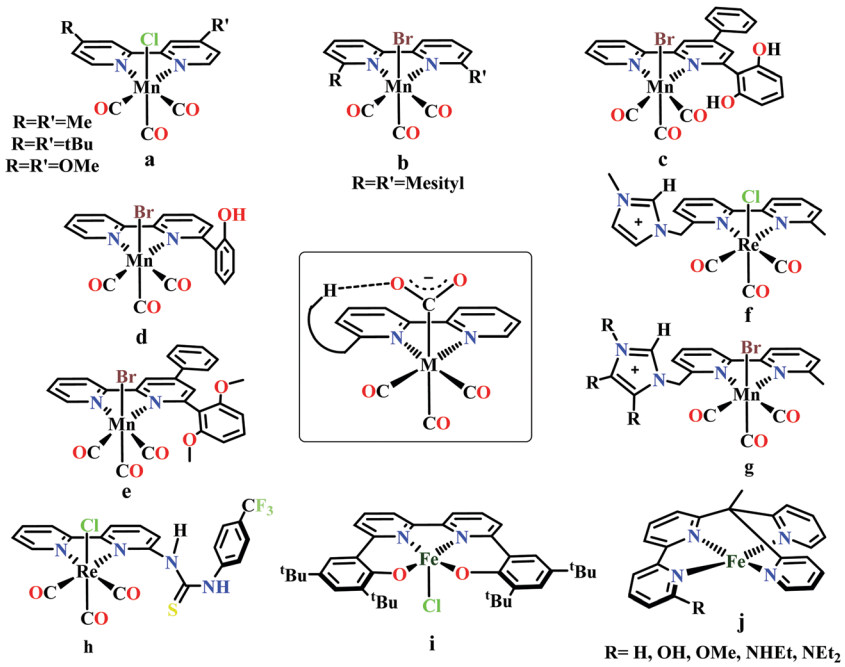

Fig. 4 Representative molecules for bipyridine-based metal-complexes for CO_2 reduction.

CO_3^{2-}. The catalytic activity was further improved by using the catalyst as a soluble Lewis acid adduct of Zn^{II}(cyclam), as a co-catalyst coupled with Mn(Mesbpy)$(CO)_3$Br. With this approach the usage of sacrificial additives can be avoided and the formation of insoluble products such as $MgCO_3$ or $ZnCO_3$ (which can change the thermodynamics of CO_2 reduction) can be prevented.[70]

Tetracarbonyl Mo and W complex of bpy or bpy-*t*Bu, M(bpy-R)$(CO)_4$ (where, M = Mo/W; R = H/*t*Bu in 4,4′-positions) were developed which has been shown to undergo electrocatalytic CO_2 reduction.[71] N-Heterocyclic carbene based Mn-complexes, MnBr(*N*-methyl-*N*′-2-pyridylbenzimidazol-2-ylidine)$(CO)_3$ and MnBr-(*N*-methyl-*N*′-2-pyridylimidazol-2-ylidine)$(CO)_3$ were reported to catalyze electrochemical conversion of CO_2 to CO.[72]

Gobetto and co-workers introduced a pendant 2,6-dihydroxyphenyl group in a [*fac*-Mn(dhbpy)$(CO)_3$Br] (where, dhbpy = 4-phenyl-6-(1,3-dihydroxybenzen-2-yl)2,2′-bipyridine, Fig. 4c).[73] The catalyst can undergo electrochemical CO_2 reduction upon controlled potential electrolysis in anhydrous acetonitrile to CO (70%) and formic acid (22%), even in the absence of any external proton source. Later, Bocarsly and co-workers studied the effect of pendant phenol group in a similar model, Mn(hbpy)$(CO)_3$Br (where, hbpy = 6-(2-hydroxyphenyl)-2,2′-bipyridine, Fig. 4d).[74] The presence of phenol group in the second coordination sphere, the catalyst showed more than seven times higher current density with 86% faradaic efficiency for CO evolution in a 5% water–acetonitrile solution relative to Mn(bpy)$(CO)_3$Br (Fig. 4b) at similar over-potential. An intramolecular proton-assisted dehydration of Mn(hbpy)$(CO)_3$COOH with lower entropy of activation was proposed to be the reason for the enhanced catalytic activity. The effect of a H-bond acceptor anisole group instead of a phenolic –OH group was invesigated by Rochford and co-workers. They synthesized {*fac*-Mn^{I}([$(MeO)_2$Ph]$_2$bpy)$(CO)_3(CH_3CN)$}(OTf) (where, [$(MeO)_2$Ph]$_2$bpy = 6,6′-bis(2,6-dimethoxyphenyl)-2,2′-bipyridine), which contained four pendant methoxy groups attached with the benzene (Fig. 4e).[75] In the presence of external proton source, the catalyst was shown to reduce CO_2 to CO at remarkably lower over-potential. The [$(MeO)_2$Ph]$_2$bpy ligand exerts an additional electronic influence along with a weak allosteric hydrogen-bonding interaction which was proposed to be responsible for lowering down the activation barrier for C–OH bond cleavage from the metallocarboxylic acid intermediate. A schematic diagram depicting the influence of the second sphere residues with the bound CO_2-adduct is shown in the inset in Fig. 4.

Nippe and co-workers have introduced a series of Lehn-type Re and Mn-complexes with pendant imidazolium moiety attached to the bipyridyl-ligand (Fig. 4f and g).[76,77] The results obtained with Re complexes, {Re[bpyMe(ImMe)]$(CO)_3$Cl}PF_6 and {Re[bpyMe($ImMe_2$)]$(CO)_3$Cl}PF_6 suggested that the positively charged imidazolium group lowers the over-potential of CO_2 reduction (Fig. 4f). The C_2–H group from the imidazolium moiety facilitates the release of Cl^- during reduction. Similarly, an extensive study was conducted on a series of Mn-complexes: {Mn[bpyMe(ImMe)]$(CO)_3$Br}PF_6; {Mn[bpyMe($ImMe_2$)]$(CO)_3$Br}PF_6; {Mn[bpyMe($ImMe_4$)]$(CO)_3$Br}PF_6 and {Mn[bpyMe(Im^{t}Bu)]$(CO)_3$Br}PF_6 (Fig. 4g).[77] All of them could catalyze the electrochemical reduction of CO_2 to CO in presence of water at much lower over-potential, suggesting a strong synergistic interaction between the imidazolium groups and the water molecules. This interaction resulted in local hydration and facilitate the CO_2 reduction. Like the previous Re-system, here also the 2nd sphere C_2–H of the imidazolium moiety was proposed to play a crucial role.

Neumann and co-workers modified the *fac*-[Re(bpy)$(CO)_3$Cl] complex and tethered a thiourea-moiety in the second coordination sphere (Fig. 4h).[78] The thiourea moiety may act both as hydrogen bond promoter and a proton donor. Hence, it not only stabilized the carboxylic acid intermediate but also act as local proton source to accelerate the C–O bond cleavage step of the catalytic cycle. This resulted the catalyst to undergo selective reduction of CO_2 to CO at a TOF as high as 3040 h^{-1}. Machan and co-workers have reported an iron(III) chloride (Fig. 4i), [Fe^{III}(tbudhbpy)]Cl (where, tbudhbpy = 6,6′-di(3,5-di-*tert*-butyl-2-hydroxybenzene)-2,2′-bipyridine) which can catalyze the disproportionation of CO_2 to CO and carbonate in anhydrous DMF.[79] However, in the presence of an external acid source like phenol it was shown to generated formate as major product (FE ∼ 68%) with H_2 (FE ∼ 30%) and CO (FE ∼ 1%) as minor products. Recently, Marinescu and co-workers have modified rhenium tricarbonyl bipyridine moiety with pendant secondary and tertiary amines in the 6- and 6′-positions of the bipyridine group.[80] These catalysts have shown to reduce CO_2 to CO with moderate faradaic efficiencies (51–73%).

Despite tremendous development in the CO_2 reduction electrocatalysts with bipyridine-backbone, fewer studies have been carried out using first-row transition metals, except Mn. For example, no such report was present with iron, until recently, Long and co-workers have introduced a series of iron–bipyridine complexes with general formula, [(bpy^RPY2Me)Fe^{II}]$^{n+}$ (where, bpy^RPY2Me = 6-(1,1-bis(pyridin-2-yl)ethyl)-2,2′-bipyridine) and R = H, OH, OMe, NHEt, NEt_2, Fig. 4j.[81] These complexes can undergo electrocatalytic CO_2 reduction with different product selectivity depending upon the pendant protic functional groups of different acid strengths in the second coordination sphere. [(bpy^{NHEt}PY2Me)Fe^{II}]$^{2+}$ appeared to be the most efficient catalyst amongst them reducing CO_2 to CO. The pendant NH group was proposed to facilitate the C–O bond cleavage by acting as a local proton source. In contrast, the more acidic OH group favors the generation of H_2 over CO.

Metal–phosphine complexes. Phosphine based electrocatalytic CO_2 reduction was reported by Wagenknecht and co-worker in 1984.[82] They proposed a Rh$(dppe)_2$Cl catalyst (where dppe = 1,2-bis(diphenylphosphino)ethane) catalyze the reduction of CO_2 to formate with trace amount of cyanoacetate at −1.30 V *vs.* NHE. Although mechanistic analysis was not carried out, it was postulated that a proton abstraction from the solvent acetonitrile was involved. Szymaszek *et al.* reported an IrCl$(CO)(PPh_3)_2$ catalyst, which can efficiently reduce CO_2 to a mixture of CO and formic acid.[83] They proposed the formation of Ir^{I}-hydride and hydroxo complexes during the reduction of IrCl$(CO)(PPh_3)_2$. The hydroxo complex coordinates with CO_2 while the hydrido complex assist the insertion of CO_2 into the Ir–H bond to generate formic acid. In the subsequent years,

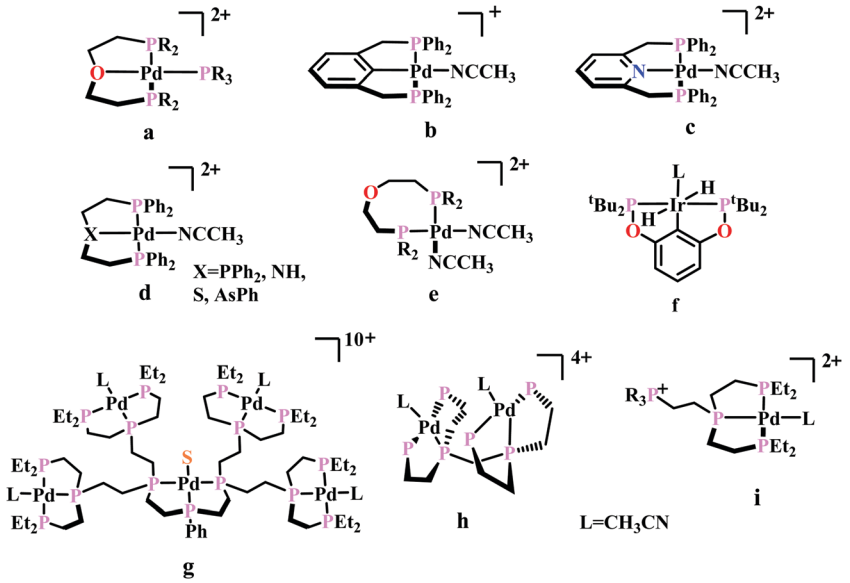

Fig. 5 Representative molecules for phosphine-based metal-complexes for CO_2 reduction.

Dubois and co-workers have made remarkable advancements in phosphine based CO_2 reduction catalysis.[11,84] They introduced a series of triphosphine based metal complexes with a general formula $[M(triphos)(solvent)](BF_4)_n$. Fe, Co, and Ni were selected for initial screening for electrocatalytic CO_2 reduction anticipating that they are not very oxyphilic in their usual oxidation states.[84] However, they showed poor catalytic activity in terms of over-potential and catalytic turnover. Nonetheless the redox properties of the Ni complexes were quite fascinating, which drove them to study the corresponding Pd-complexes. The Pd-complexes with general formula $[Pd(triphos)PR_3]$ $(BF_4)_2$ (where R = Et, Ph, OMe, CH_2OH, Fig. 5a) had shown electrochemical conversion of CO_2 to CO in acidic acetonitrile solution. Further studies suggested dissociation of the monodetate PR_3 ligand with concomitant binding of solvent (acetonitrile). This labile ligand or solvent is required for the catalysis. For example, $[Pd(etpC)(CH_3CN)](BF_4)_2$ (where, etpC = bis(2-dicyclohexylphosphinoethyl)phenylphosphine) was shown to catalyze CO_2 reduction, while $[Pd(dppe)_2](BF_4)_2$ does not because the dissociation of the phosphine is not facile. Therefore, the active catalyst was proposed to be $[Pd(triphos)(solvent)]$ $(BF_4)_2$, where CO_2 replaces the labile solvent molecule.[85] These series of $[LPd(S)]^{2+}$ catalysts (where L = triphosphine ligands; S = solvent, Fig. 5a–e) were proposed to follow a general mechanistic pathway (Scheme 6). Initial reduction to Pd^I is followed by the reaction with CO_2 to generate $[LPd(S)(CO_2)]^+$ intermediate. Based on the 1st order dependence on the concentration of CO_2 as well as the catalyst under high acid concentrations, it was proposed that the reaction of Pd^I with CO_2 is the rate determining step at high acid concentrations. Next, protonatio, followed by second electron transfer and solvent dissociation leading to the formation of a $[LPd(COOH)]^+$ intermediate. Further protonation at one of O-atoms of CO_2 generates a "dihydroxy carbene" intermediate. A C–O bond cleavage, releasing a molecule of water, generates the CO-bound intermediate, $[LPd(CO)]^{2+}$. In solutions with low acid concentration, this C–O bond cleavage is proposed to be the rate limiting step. Rapid CO dissociation from the Pd^{II}-species and solvent association completes the catalytic cycle.

To understand the effect of ligand donor strength on Pd, a series of square-planar palladium complexes containing tridentate ligands of type PXP (where X = C, N, O, S, and As) were synthesized. None of them were as effective as the triphosphine complex. During electrocatalysis, they were found to generate H_2 instead of CO. The selectivity for producing H_2 or CO appears to depend on the basicity or the redox potential of the complexes. Complexes with more negative redox potential, increases the basicity of the Pd-atom favouring the formation of Pd-hydride,

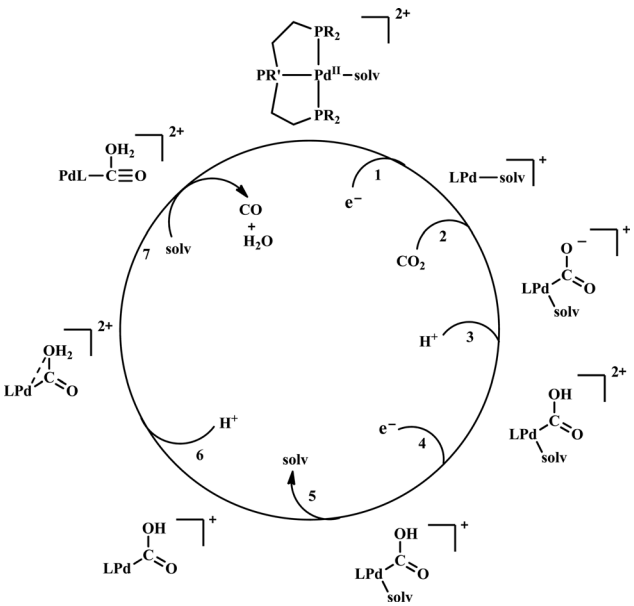

Scheme 6 General mechanistic scheme for the electrocatalytic CO_2 reduction by $[Pd(triphosphine)(S)]^{2+}$ catalysts.

which eventually generates H_2. While, with less negative redox potentials or a less basic Pd-atom favours protonation of the "O"-atom of the coordinated CO_2 to generate CO.[86] An Ir-pincer complex, Ir(PCP)–H_2(MeCN), was developed (Fig. 5f) which catalyzed electrochemical CO_2 reduction to generate formate, selectively.[87] Only a small amount of H_2 and CO was detected.

A unique dendritic complex was synthesized (Fig. 5g) where the central-Pd is surrounded by four Pd-atoms linked to the terminal phosphorus *via* an ethylene linkage.[88] The idea was to enhance the rate and/or decreasing the overpotential of CO_2 reduction by co-operative binding of CO_2. But the complex failed to show greater catalytic activity, instead it appeared to be a poor catalyst relative to its monomeric analogue. Later, a bimetallic complex was synthesized (Fig. 5h) which can be viewed as two $[Pd(triphos)(solvent)]^{2+}$ units linked through a methylene bridge.[89] This complex could reduce CO_2 to CO at relatively lower potential (−1.05 V *vs.* NHE) with ∼1000 times enhancement in rate relative to the monomer. At higher acid concentration, the reaction was 1st order with respect to [catalyst] and 1st order in $[CO_2]$, indicating involvement of two Pd-atoms per one molecule of CO_2. In contrast with the monomer (*vide supra*), at lower acid concentration, the reaction is 1st order with respect to [acid] instead of a 2nd order dependence. This clearly indicates the second Pd-atom binds with the "O-atom" of the bound CO_2 at the transition state instead of a proton proton. However, formation of Pd–Pd bond deactivated the catalyst and only a TON of 10 could be obtained. As an extension of the logic flow, a pendant phosphonium ion was introduced (Fig. 5i) which can stabilize the negatively charged "O^-"-atom of CO_2 at the transition state *via* coulombic interaction.[90] Although, the rate of CO_2 binding was doubled, no catalytic rate enhancement was observed.

Previously, Kubiak and co-workers reported a binuclear "cradle"-type complex, $[Ni_2(\mu\text{-CNMe})(CNMe)_2(dppm)_2](PF_6)_2$, (where dppm = bis(diphenylphosphino)methane, Fig. 6a) to catalyze the reduction of CO_2 with quite low overpotential, −0.67 V *vs.* NHE. But, with time it ultimately undergoes complete carbonylation to afford $Ni_2(CO)_3(dppm)_2$.[91] A series of alkyl isocyanide bridged binuclear Ni^0-clusters with the general formula $[Ni_2(\mu\text{-dppa})_2(\mu\text{-CNR})(CNR)_2]$ (where, dppa = bis(diphenylphosphine)amine; R = Me, *n*-Bu, 2,6-$Me_2C_6H_3$, Fig. 6b) were reported to undergo reductive disproportionation of CO_2 to CO and carbonate ion.[92] Formate was produced in the presence of proton (from residual water). During catalysis the generated CO was found to be trapped by the catalyst. An interesting binuclear copper catalyst was developed (Fig. 6a), $[Cu_2(\mu\text{-}PPh_2bpy)_2(MeCN)_2][PF_6]_2$ (where PPh_2bpy = 6-(diphenylphosphino)-2,2′-bipyridyl, Fig. 6c).[93] It was shown to undergo electrochemical CO_2 reduction to CO and CO_3^{2-} at −1.35 V *vs.* NHE. The unique bipyridine based ligand scaffold acts as an electron reservoir for these systems, where the electrons are localized in the π*-orbitals of the bipyridine-fragment. A turnover frequency (TOF) of $>2\ h^{-1}$ was maintained throughout an experiment for 24 h and recovered quantitatively in its original form after the electrolysis.

As an extension of the concept of co-operative CO_2 binding and reduction, a series of isocyanide and CO bound and halide capped trinuclear-nickel clusters were developed (Fig. 6d) with the general formula, $[Ni_3(\mu_3\text{-L})(\mu_3\text{-X})(\mu_2\text{-dppm})_3]^{n+}$ (where L = I^-, Br^-, CO, CNR; X = I^-, Br^-; *n* = 0, 1).[94] They were reported to undergo reductive disproportionation of CO_2 to CO and CO_3^{2-} at relatively lower overpotential indicating co-operativity due to the presence of a trinuclear Nickel cluster. Although the reduction potentials of these molecules fall into a relatively narrow range of −0.84 V to −0.94 V *vs.* NHE, the slight difference in redox potentials affect the rate of CO_2 reduction dramatically. This clearly invokes the influence of the substituents of the capping ligand.

Artero and co-workers reported a series of Co-diphosphine electrocatalysts (Fig. 6e–h) to convert selectively CO_2 to formate in DMF–water system with high faradaic efficiency (>90%) and at moderate overpotential (500–700 mV in DMF).[95] The catalysts

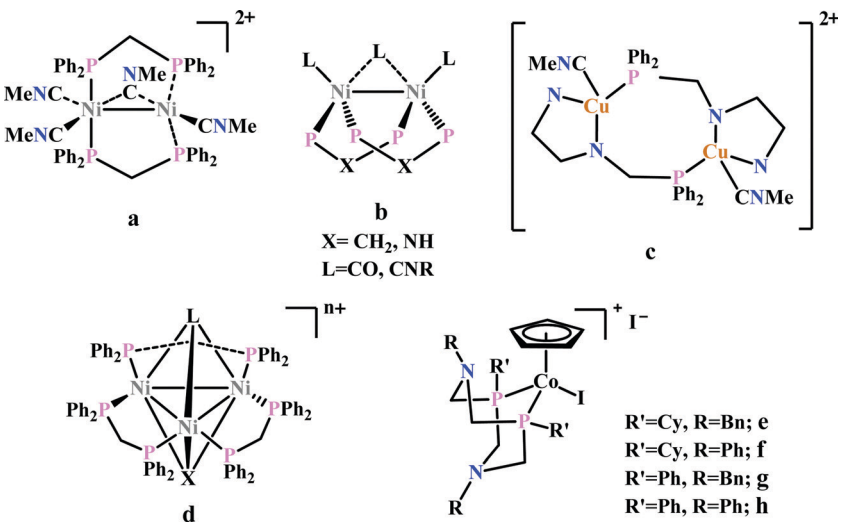

Fig. 6 Representative non-heme molecules for electrocatalytic CO_2 reduction with influence from second coordination sphere.

had a general formula, [CpCo($P^R_2N^{R'}_2$)I]I (where, $P^R_2N^{R'}_2$ = 1,5-diaza-3,7-diphosphacyclooctane). Cyclohexyl or phenyl substituents on P and benzyl or phenyl substituents on N were employed, to tune the donor ability of P and basicity of the N. Similar Ni-complexes were known for efficient formate oxidation.[96–98] The high selectivity for formate (instead of CO or H_2 formation) was postulated to be due to higher hydricity of the $CpCo^{II}$(diphosphine)–H intermediate, they undergo hydride transfer to CO_2. However, the pendant amine groups are not directly involved in proton transfer, but they stabilize the intermediates through H-bonding with the water molecules during hydride transfer. With the most electron-donating phosphine ligand and the most basic amine group, the catalyst could show an excellent TOF of $>1000\ s^{-1}$ which is much higher than other formate reducing catalysts.[87,99–101]

Heme and other macrocyclic system

Metalloporphyrin complexes. Initially Fe^0-porphyrins were anticipated to participate in outer-sphere electron transfer due to its fast conversion to the corresponding Fe^I-porphyrins and the redox process is reversible. But it reacted with the aliphatic halides or vicinal dibromides at much faster rate than that expected for undergoing an outer-sphere electron transfer process. Hence, an inner-sphere process was anticipated through the bond formation between iron and electrophilic centre, such as CO_2.[102–106] In the presence of CO_2, an increment of electrocatalytic current at the $Fe^{I/0}$ potential signalled electrocatalytic CO_2 reduction by iron porphyrins.[107] Fe^0-Porphyrins have shown selective reduction of CO_2 to CO at -1.55 V *vs.* NHE. However, in the presence of tetraalkylammonium salts as supporting electrolytes in DMF, the porphyrin undergoes carboxylation and/or hydrogenation after a few cycles. Savéant and co-workers introduced a hard electrophile such as Mg^{2+} ion, which not only improved stability of the catalyst, but also improved the rate of CO production.[108] The reaction was believed to proceed with the binding of one CO_2 molecule to the Fe^0-porphyrin. Another molecule of CO_2, being a Lewis acid assisted the cleavage of one of the C–O bond generating Fe^{II}–CO and $MgCO_3$. The order of reactivity is proportional to the ionic potential of the metal, *i.e.*, $Mg^{2+} \cong Ca^{2+} > Ba^{2+} > Li^+ > Na^+$.[109] Now, the mechanism of the synergistic effect should be of the same nature as with weak Brønsted acids, where ion-pairing will be replaced by hydrogen bonding.[110] It had been demonstrated using weak acids, such as 1-propanol, 2-pyrrolidone, and CF_3CH_2OH could improve both efficiency and life time of the catalyst without significant H_2 generation.[109] A 350 h^{-1} TON could be achieved. The major canonical form of the initial CO_2-adduct was proposed to be Fe^{II}–CO_2^{2-}, stabilized by H-bonding with two acid synergist molecules. Stronger acids (such as CF_3CH_2OH) could catalyze the transformation selectively to CO, while weaker acids (like 1-propanol) generates formic acid to some extent. A minor resonant structure of the initial CO_2-adduct, Fe^I–CO_2^- was proposed to be responsible for the release of formic acid in presence of weaker acids.

The mode of activation relies on the ion-pairing with the negatively charged ''O''-atoms of the Fe bound-CO_2. This invokes a ''push–pull'' mechanism, *i.e.*, an electron pair is pushed from the Fe^0 into the CO_2 molecule. This process is temperature dependent and at -40 °C, the reaction proceeds with the involvement of two CO_2 molecules, while at room temperature only one CO_2 was proposed to be present in the iron-coordination sphere. It required either one divalent cation or two mono-valent cations for the activation. This is an example of a bimetallic catalysis, where an electron-rich Fe^0-center initiates the reaction with CO_2 and an electron-deficient metal-centre assists the C–O bond cleavage to accelerate the reaction, mimicking the natural process catalyzed by enzyme, [NiFe]-CODH. Naruta and co-workers reported a series of bio-inspired cofacial iron-porphyrin dimer (*o*-Fe_2DTPP, Fig. 7g and h) with the Fe···Fe separation of 3.4–4 Å, anticipating easy access and co-operative binding of the linear CO_2 molecule (2.32 Å) in between.[111] The high selectivity for CO (with 95% faradaic efficiency) at a considerably higher rate (TOF $\sim$ 4300 s^{-1}) was attributed to the influence of second iron, which is absent in FeTPP or *m*-Fe_2DTPP (Fig. 7h).

The reaction of CO_2 with Fe^0-porphyrin was proposed to be proceed through the formation of CO_2 adduct (Scheme 7). The adduct is stabilized in presence of external acid source (AH). A second molecule of AH is involved in generation of a precursor complex, where a H-bond is being formed between one of the ''O'' of CO_2 and the external proton source. Heterolysis of the C–O bond followed by reductive decarbonylation regenerates the catalyst. The rate-determining step is proposed to be the cleavage of the C–O bond, where an electron transfer (ET) from the central iron-atom is concerted with proton transfer (PT). Therefore, invoking an intramolecular concerted proton electron transfer with bond cleavage mechanism operated in the rate-determining step.[112]

Based on the observed role of proton donors, it was anticipated that tethering acid functionality with the catalyst should accelerate the reduction process by increasing the local proton concentration, which is otherwise impossible to attain in such high amount considering bimolecular reaction condition. A series of *meso*-phenyl substituted iron-porphyrins were synthesized with varying tethered phenol groups (Fig. 7a–c).[113] The eight phenolic protons in CAT (Fig. 7a) was estimated to operate with phenol concentration as high as 150 M and it could efficiently converted CO_2 to CO with high rate and faradaic efficiency. On the contrary, the octa-methoxy analogue, Fe^0TDMPP (Fig. 7b) was a poor catalyst with large over-potential and low TOF, invoking the importance of the intramolecular proton source in catalysis.[114] On an effort to lowering down the over-potential, a fluorinated analogue of CAT was considered, FCAT (Fig. 7c), anticipating the electron withdrawing inductive effect of the F-atoms. Despite lowering down the electron density over iron-centre, this catalyst was found to be one of the best electrocatalysts to convert CO_2 to CO, selectively.[115] The effect of solvent in electrocatalytic CO_2 reduction was reported by Warren and co-workers using a 2-hydroxyphenyl substituted TPP (TPOH, simpler version of CAT,

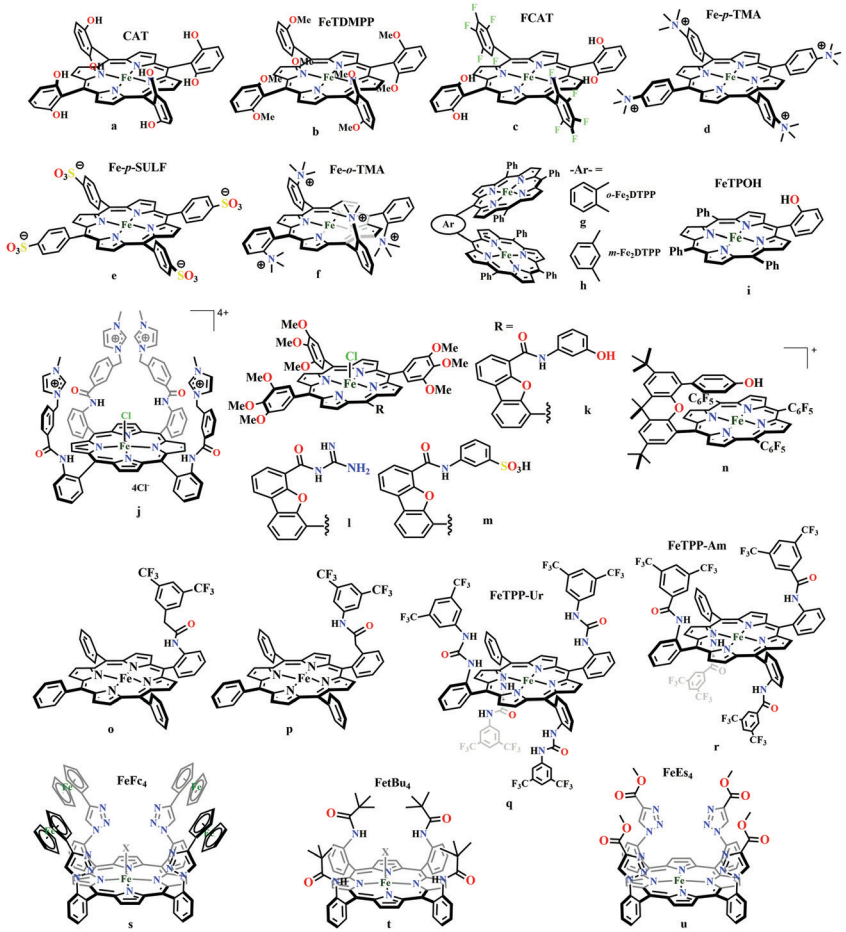

Fig. 7 Representative molecules for electrocatalytic CO_2 reduction by porphyrin-based catalysts.

Fig. 7i).[116] The Fe-TPOH complex was shown to reduce CO_2 to CO (96% FE) at TOF $\sim$ 4500 s^{-1} in acetonitrile in presence of weak Brønsted acids (1 M water or 8 mM phenol). In contrast, the catalyst was found to be very poor in DMF. Based of Abraham's H-bond acidity[117] and basicity[118] as metrics, it has been suggested that DMF being a strong H-bond acceptor, plays a detrimental role in catalysis, where H-bonding is very crucial in accelerating the rate. Substituting the four *meso-p*-hydrogens of FeTPP by trimethylammonium groups (WSCAT) could afford formation of a water-soluble porphyrin (Fig. 7d). Under neutral pH, it catalyzes the reduction of CO_2 to CO, selectively.[119]

The enhanced catalytic activity in CAT and FCAT was a direct proof of participation of pendant OH-functionalities installed in the catalysts. Appearance of a distinct pre-wave in front of the catalytic wave was suggestive of protonation of the Fe^0–CO_2 adduct prior to further reduction.[120] Therefore, the stabilization of the Fe^0–CO_2 adduct through H-bonding with the pendant OH-groups is likely the main reason for such efficient catalysis (Scheme 8). The protonation is conducted from the pendant phenol groups, while the re-protonation of the phenoxide occurs from the externally added phenol. Hence, the role of the pre-positioned phenol groups was proposed to be as H-bond stabilizers and maintaining high concentration proton donor. The next step is concerted electron transfer and proton transfer with the cleavage of one of the two C–O bonds (CPETBC) of the bound CO_2. However, the intermediates proposed were based on simulation of electochemical parameters, no such intermediate was isolated or spectroscopically characterized.

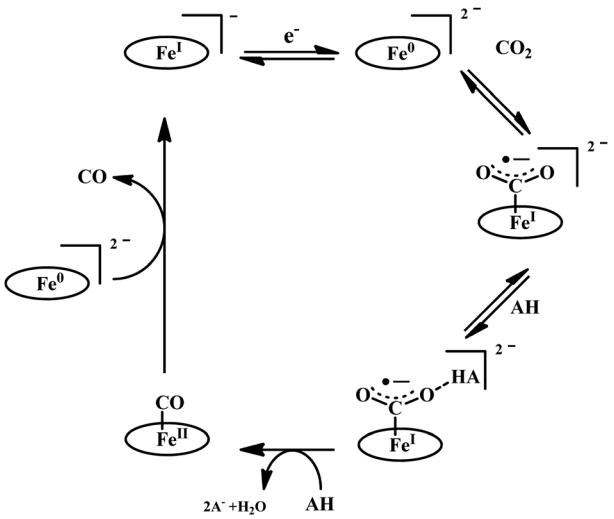

Scheme 7 Proposed mechanistic pathway for the reduction of CO_2 to CO by Fe-porphyrin electrocatalysts.

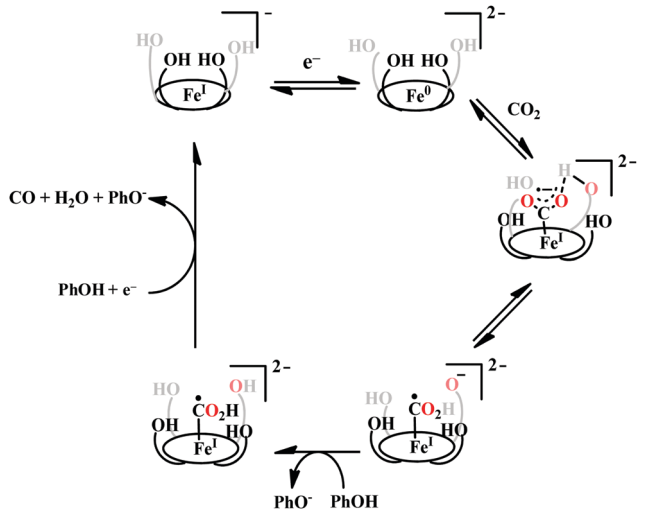

Scheme 8 Proposed mechanistic pathway for the reduction of CO_2 to CO by Fe-porphyrin electrocatalysts with pendant acid functionality, $(OH)_4$.

The reaction intermediate was probed by trapping reaction intermediates taking advantage of porphyrins bearing hydrogen bonding residues.[121–123] At least two intermediates were observed using resonance Raman spectroscopy in an iron-porphyrin complex bearing a distal H-bonding pocket (Fig. 7u) involved in the homogeneous chemical reduction of CO_2 (Scheme 9).[124] The first intermediate (intermediate I), which could only be stabilized at −95 °C, was found to be a Fe^{II}–CO_2^{2-} adduct. Warming up the solution to −80 °C lead to the protonation in presence of weak acid (methanol) to give rise to another intermediate; intermediate II. The intermediate II was established to be a Fe^{II}–COOH species (using labelled CO_2 and proton). In the presence of phenol as acid source, only intermediate II could observed even at −95 °C and no intermediate I could be isolated. On the contrary, in presence of strong acid like *p*-toluenesulfonic acid the product, Fe^{II}–CO, species was generated rapidly at −95 °C. Intermediate I being very basic can abstract proton rapidly even from MeOH while intermediate II requires a strong acid to cleave the C–O bond to eliminate water. In the absence of strong acid, intermediate II gradually released formic acid. This investigation realized the definitive role of the M-COOH species in determining the selectivity of CO_2 reduction; a C-protonation leads to HCOOH while an –OH protonation releases CO.

The pendant OH-groups can stabilize the negatively charged $[porphyrin\text{-}Fe^{0}\text{–}CO_2]^{2-}$ adduct through the formation of H-bond. However, this intermediate may also be stabilized by coulombic interactions with positively charged groups attached to the porphyrin. For example, the WSCAT (or Fe-*p*-TMA, Fig. 7d) can boost the catalysis, while replacing trimethylammonium with sulfonate (Fe-*p*-SULF, Fig. 7e) shows reduced catalytic effect. However, replacing four-*ortho* hydrogens by trimethylammonium group (Fe-*o*-TMA, Fig. 7f), can catalyze the reduction of CO_2 to CO almost exclusively and that too with a TOF of 10^6 s^{-1} and very low over-potential (~200 mV).[125]

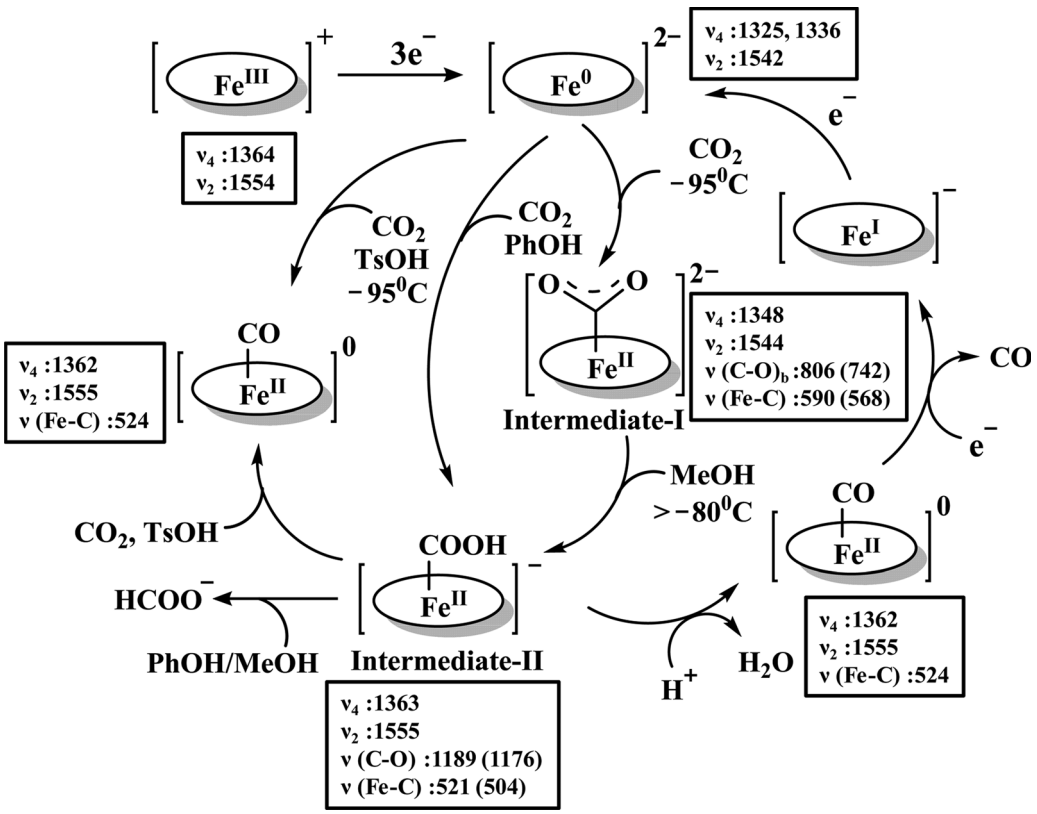

Scheme 9 Proposed mechanistic cycle for the reduction of CO_2 by a distal-triazole containing Fe-porphyrin. The vibrations (in cm^{-1}) are given in the boxes.

Aukauloo and co-workers have attached methylimidazolium fragments as ionic liquid units, modifying the α_4-tetra-aminophenylporphyrin (Fig. 7j).[126] The cationic pendant methylimidazolium was introduced to stabilize the negatively charged Fe–CO_2 adduct. The catalyst was shown to be very active electrocatalyst to reduce CO_2 to CO at only 418 mV over-potential in water with 91% faradaic efficiency and higher TOF, TON values of 14 986 s^{-1} and 1.08×10^8, respectively. Nocera and co-workers have shown the proton-relay in iron hangman porphyrins with phenol (HPDFe-PhOH, Fig. 7k), guanidinium (HPDFe-GND, Fig. 7l), and sulfonic acid (HPDFe-3SA, Fig. 7m) proton donor groups.[127] Selective reduction of CO_2 to CO with $>93\%$ faradaic efficiencies were described where the CO_2 binding within the hangman-cleft was proposed to determine the rate of the reaction. Deprotonation of the hanging sulfonate group was responsible for exhibiting lower TOF due to unfavourable electrostatic interaction with the negatively charged CO_2-adduct. Despite tremendous rate acceleration by the hanging phenolic group, often improper alignment of the activating group may exert ill-defined results. For example, in the case of complex **7n** (Fig. 7n), the axial Cl^-, forming a H-bond with the phenolic-OH group renders an inefficient CO_2 reduction, compared to the same complex with triflate ion.[128] Therefore, distal H-bonding interaction plays a key role in determining the stability of the intermediates affecting the product selectivity as well as the rate of the reaction as suggested by the solution mechanistic investigation. Hence, a proper estimation about the role of distal residues was warranted.

Recalling the role of His and Lys in the activation of CO_2 in [NiFe]CODHs, Chang and co-workers have synthesized a series of *ortho*- and *para*-substituted amide pendants at different positions from the porphyrin-plane (*e.g.*, complex **7o–p** in Fig. 7).[129] The *ortho*-functionalized positional isomers (unlike *para*-functionalized) were found to engage in through-space interactions to enhance the rate of the electrochemical conversion of CO_2 to CO. The complex with a distal amide, **7p** was involved in greater enhancement over **7o**, demonstrating the importance of precise geometric orientation of 2nd sphere pendants for designing effective catalyst. A series of iron-porphyrins with different distal environment spanning from amide (Fe picket-fence porphyrin) to triazole-with different substituents (complex **7t** and **7u** in Fig. 7).[130] They exhibit TOFs ranging from 1–1000 s^{-1} without changing the pK_a of the external acid source used (phenol). Theoretical calculations (DFT) suggested the intermediate-I (Fe–CO_2^-) is better stabilized by coulombic interactions, while the C–OH bond cleavage from the intermediate-II (Fe–COOH) is greatly influenced by the distal hydrogen bonding interactions. H-bonding alone could tune the rate of the CO_2 reduction by as much as 1000-fold without change of overpotential or proton source. On a similar note, Aukauloo and co-workers pointed out the influence of multi-point H-bonding in the super-structured iron-porphyrin bearing urea (FeTPP-Ur, **7q**) and amide (FeTPP-Am, **7r**) functionalities in comparison with FeTPP.[131] In comparison with FeTPP and FeTPP-Am (can make single-point H-bond), the pendant urea-functionalized FeTPP-Ur can reduce the over-potential of CO_2 to CO electroreduction by $\sim$300 mV while retaining high TOFs. Also, the entrapped water molecules within the molecular clefts were found to be sufficient as a proton source.

Therefore, the Fe^0-porphyrins are generally found to be biased for catalysing the reduction of CO_2 to CO, where "pull-effect" from the secondary coordination sphere boosts up the rate of C–O bond cleavage up to 10^6 s^{-1}. In absence of activators (such as external/internal acid source), the rate is relatively slow and formate is produced as a by-product likely *via* C-protonation of the Fe^{II}–COOH intermediate as demonstrated by Mondal *et al.*[124] However, the reduction can be directed for the production of formate by the introduction of tertiary amines.[132] Greater catalytic activity is attributed with the higher basicity of the tertiary amine. The axial amine appears to push the electron density over the bound "C"-atom (recalling *trans*-effect), thereby increasing the basicity on the C-atom of the Fe–COOH intermedate to allow the protonation and facilitate dissociation of formate (Scheme 10). The use of a weaker acid is warranted to avoid the formation of metal-hydride to undergo HER.

Conceptual development of a suitable electrocatalysts for efficient CO_2 reduction (in terms of over-potential, rate, stability, *etc.*) is quite fascinating for academic interests but its practical implementation is seriously deterred by the requirement of pure CO_2.[133] Considering the abundance of O_2 over CO_2 in the atmosphere and in flue gases (8–15% CO_2), one of the major challenges in practical CO_2 reduction is the O_2-sensitivity of the low-valent metals. Note, O_2 (0.83 V *vs.* NHE at pH 7)[134] has much higher reduction potential in comparison with CO_2. However, due to kinetic limitations, reduction of O_2 to water is also very challenging, leading to the generation of partially reduced oxygenated species (PROS) such as superoxide, peroxide, *etc.*, which are very reactive often responsible for irreversible catalyst degradation.[135–137] Hence, an O_2-tolarrant catalyst scheme is warranted. Successful technologies from hydrogen-evolving catalysts suggests three ways this can be achieved:[138–145] (a) using a co-catalyst, which can scavenge any PROS; (b) the catalyst by itself can reduce O_2 to water without releasing PROS and (c) choosing appropriate catalyst which can react selectively with CO_2 over O_2. The $FeFc_4$ (Fig. 7s) complex has been known to catalyze the 4e/4H^+ reduction of O_2 to water over a wide range of pH.[146] The three of the four appended ferrocene-moieties and the central Fe^{II}-atom give the required four electrons, while protons are derived from water.[123] Hence this bi-functional catalyst was chosen to device an O_2-tolarant CO_2 catalyst, where the Fe^0-state was activated for selective CO_2 reduction (kinetic advantage) to CO, while Fe^{II}-state was activated for fast and selective O_2 reduction to water (Scheme 11).[147] Furthermore the Fe^0-porphyrins was found to react with CO_2 with $\sim$500 times faster rate relative to O_2 offering selective CO_2 reduction even in

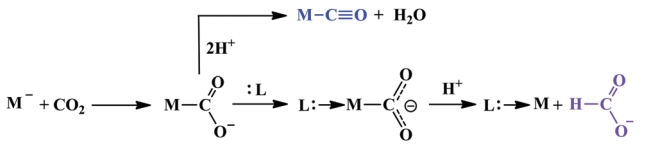

Scheme 10 Contrasting pathways in CO_2 reduction.

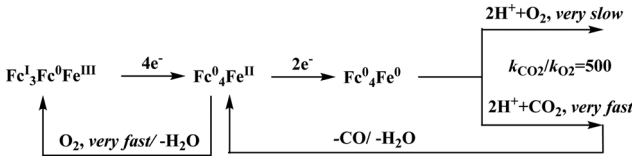

Scheme 11 General reaction scheme of O_2-tolerant electrocatalytic CO_2 reduction by $FeFc_4$.

3 : 1 mixture of O_2 : CO_2. This was the first, and till date the only, report of any O_2-tolarant low-valent transition metal-based CO_2 reduction catalyst.

Macrocyclic complexes other than porphyrin. Mehitsuka and co-workers identified for the first time that the transition metals can catalyze electrochemical CO_2 reduction using Co amd Ni-phthalocyanine complexes.[148] Eisenberg and co-workers reported electrocatalytic CO_2 reduction to CO or a mixture of CO and H_2 at a potential range of (1.05–1.35 V) *vs.* NHE employing a series of Co and Ni-bound tetra-aza macrocyclic ligands.[58] Sauvage and co-workers have studied the electrochemical CO_2 reduction in [Ni^{II}(cyclam)] (where, cyclam = 1,4,8,11-tetraazacyclotetradecane) complexes (Fig. 8a and b).[149–151] The complexes appeared to be extremely stable, highly selective (with faradaic efficiency up to 96% for CO production) and operated at very low over-potential (−0.62 V *vs.* NHE) even under aqueous conditions. In dry DMF, the catalyst was biased to the formation of formate. The intermolecular H-bonding with the solvent molecules along with the intramolecular H-bonding with the cyclam-NH was proposed to be key reason for such high reactivity and selectivity.[150] Similar moieties with unsaturated or open-chain forms were shown to have poor catalytic response relative to the cyclam complexes. However, these macrocycles were found to be very pH sensitive and also required mercury electrodes for turnover. Later, Anson and co-workers suggested the high electrocatalytic activity originated from the [Ni^{I}(cyclam)] complex adsorbed on the mercury surface.[152] Also, during long term electrolysis without stirring the catalyst was found to react with CO to form a CO-bound insoluble complex, [Ni^{0}(cyclam)(CO)].[153] The N–H groups attached to the cyclam were found to be essential for their stability over mercury-surface. Replacing N–H with *N*-methyl not only enhanced the tendency to adsorb over mercury-surface but also destabilized the corresponding Ni^{I}-complexes.[154] Fujita and co-workers reported similar cyclam-like 14 membered N_4-macrocycles, [Ni^{II}(HTIM)] (where, HTIM = C-RRSS-2,3,9,10-tetramethyl-1,4,8,11-tetraazacyclotetradecane, Fig. 8c and d) and [Ni^{II}(DMC)] (where, DMC = *C-meso*-5,12-dimethyl-1,4,8,11-tetraazacyclotetradecane), which were shown to be excellent catalysts for selective reduction of CO_2 to CO.[155] With time several other catalysts have been developed whereby by simply changing the pH of the solution the product selectivity could be manipulated. A series of other Ni-macrocycles were developed, [Ni^{II}(MTC)] (where, MTC = 2,3-trans-cyclohexano-1,4,8,11-tetraazacyclotetradecane,

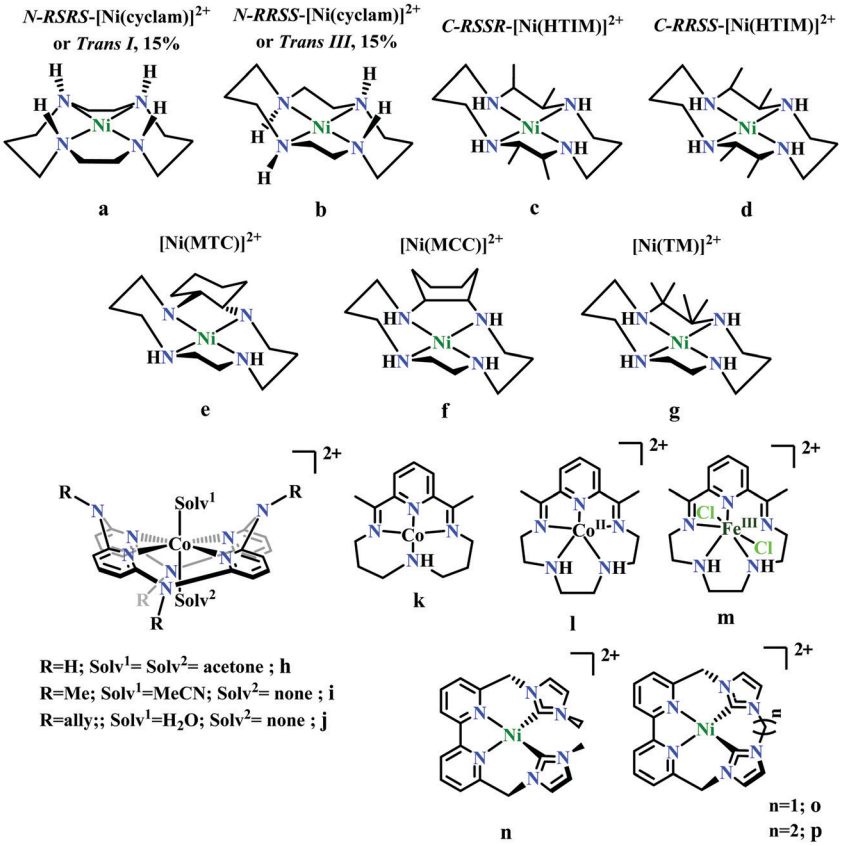

Fig. 8 Representative macrocyclic complexes for electrocatalytic CO_2 reduction.

Fig. 8e), [Ni^{II}(MCC)] (where, MCC = 2,3-ciscyclohexano-1,4,8,11-tetraazacyclotetradecane, Fig. 8f) and [Ni^{II}(TM)] (where, TM = 2,3-tetramethyl-1,4,8,11-tetraazacyclotetradecane, Fig. 8g).[156] [Ni^{II}(HTIM)] and [Ni^{II}(MTC)] were shown to be more efficient over [Ni^{II}(cyclam)] and at pH 5, they were found to reduce CO_2 to CO selectively with 88 ± 7% faradaic efficiency and with ~550 mV over-potential. When the pH was lowered to 2, the competitive HER was started to occur at 750 mV over-potential and at 870 mV over-potential, the catalysts was completely biased for H_2 evolution. It is well established that among the five possible planar conformational isomers, in aqueous solution, [Ni^{II}(cyclam)] predominantly exists in the *trans*-III (~85%) and *trans*-I (~15%) configuration (Fig. 8a and b).[157] However, the CO_2 binding with the *trans*-I was proposed to be more favourable in comparison with *trans*-III.[156,158]

Based on the initial work from Sauvage followed by Anson, Kubiak and Ye, a plausible mechanistic cycle has been proposed (Scheme 12).[150,152,153,159–161] Initial electron-transfer to [Ni^{II}(cyclam)] generates the one electron reduced species, [Ni^{I}(cyclam)], which gets adsorbed on the electrode surface. In the presence of CO_2, the adsorbed [Ni^{I}(cyclam)] likely forms an adduct with CO_2, which gets stabilized by H-bonding to the adjacent N–H groups. Further, reduction and protonation lead to the formation of [Ni^{I}(cyclam)(COOH)] intermediate, which upon protonation generates [Ni^{II}(cyclam)(CO)] releasing a molecule of water. Reductive decarbonylation regenerates the active-catalyst, [Ni^{I}(cyclam)]. The facile and faster formation of [Ni^{I}(cyclam)(CO)] limits the rate of the process. Kubiak and co-workers have used an efficient CO-scavenger, [Ni^{II}(TMC)] (where, TMC = 1,4,8,11-tetramethyl-1,4,8,11-tetraazacyclotetradecane) to prevent from the catalyst deactivation.[160] Shafaat and co-workers used a semi-enzymatic model by introducing [Ni^{II}(cyclam)] into a Cu-containing biological scaffold, azurin, which can provide a well-defined secondary coordination sphere to modulate catalytic efficiency and selectivity.[161] Chang and co-workers have realized the effect of additives which can stabilize the CO_2-adduct in [Ni^{I}(cyclam)] through H-bonding of different strength.[162] A bis(aryl)urea additive could afford an enhanced current increment relative to isostructural amide additive. A co-operative multi-point H-bonding in urea-additive was proposed for such augmented catalytic activity.

Marinescu and co-workers have introduced cobalt-bound azacalix[4](2,6)-pyridine framework with different substitutions on the pendant secondary and tertiary (methyl and allyl) amines (Fig. 8h–j).[163] In the presence of weak Brønsted acid, the complex with N–H pendant can catalyze the reduction of CO_2 to CO with ~98% faradaic efficiency. While the other pendant *N*-alkyl variants were found to have poor catalytic rates which were lower by at least two order of magnitude. The pendant N–H groups were proposed to stabilize the Co^0–CO_2 adduct (through intramolecular H-bonding) as well as promote the C–OH bond cleavage to release CO (Scheme 13). Also, the N–H groups were proposed to decrease the over-potential by increasing the $Co^{I/0}$ reduction potential. Unlike cyclam, this macrocycle is unique because here the pendant amines lie completely outside the primary coordination sphere of the metal-centre which allows discrete control over the number and configuration of the pendant proton donors in the outer sphere of the metal-centre without interfering in its primary coordination sphere.[164] To discern the roles of the first and second coordination spheres in CO_2 reduction catalysis, a series of cobalt complexes were synthesized with varying pendant secondary and tertiary amines. The theoretical calculations suggested that the N–H group was not transferring the proton directly to the bound CO_2, in contrast, they bind acid molecules from the solution. Hence, in the rate-determining step each pendant amine was proposed to bind an acid molecule non-cooperatively which eventually activate and enhance the local concentration of proton donors around the COOH adduct.

Peters and co-workers made a macrocyclic-cobalt complex with redox non-innocent ligand, $[Co^{III}N_4H(Br)_2]^+$ (where, N_4H = 2,12-dimethyl-3,7,11,17-tetraazabicyclo-[11.3.1]-heptadeca1(7),2,11,13,15-pentaene) (Fig. 8k).[165] This complex was shown to undergo

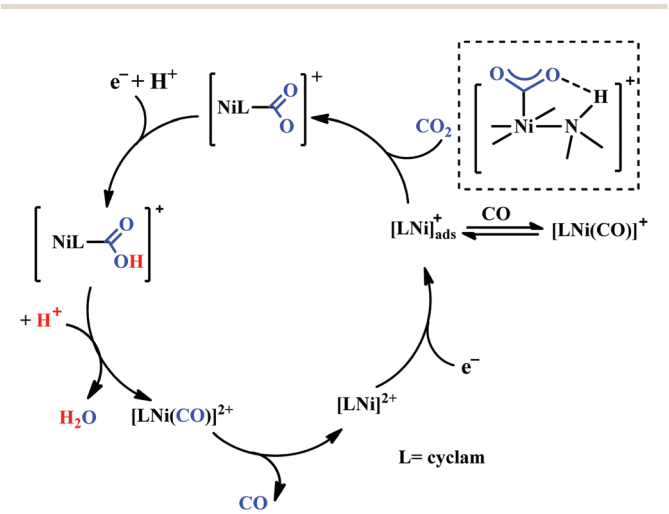

Scheme 12 Proposed mechanistic pathway of electrocatalytic CO_2 reduction to CO by [Ni^{II}(cyclam)]-based macrocycles.

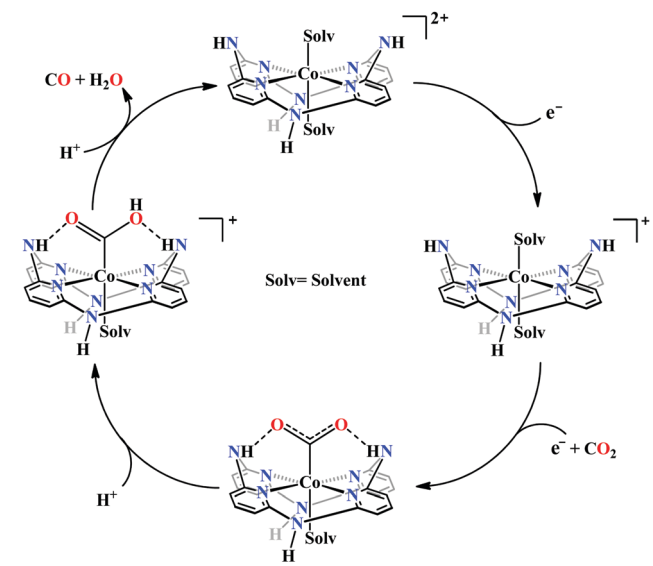

Scheme 13 Proposed mechanistic pathway for electrocatalytic CO_2 reduction to CO by azacalix-pyridine based macrocycles.

electrocatalytic CO_2 reduction to CO (FE ~ 45%) with concomitant generation of H_2 (~30%) in wet acetonitrile medium. In the same ligand framework, just by changing the metal, the CO_2 reduction can be biased for either CO or formate. This phenomenon was shown by Robert and co-workers in a unique pentadentate ligand system, 2,13-dimethyl-3,6,9,12,18-pentaazabicyclo-[12.3.1]octadeca-1(18),2,12,14,16-pentaene (Fig. 8m).[99] The Co^{II}-complex is biased to generate CO with faradaic efficiency as high as 82%. In contrast, the Fe^{III}-complex was shown to generate formate (FE ~ 75–80%, with no detectable H_2 or CO). This unusual change in product selectivity was explained considering the electronic structure of the M-COOH intermediate. In the case of Co-complex, there is greater π-back-bonding to the π*-orbitals of CO_2 from the formal Co^{II}-centre rendering the C–O bond weak to facilitate CO release upon C–O bond cleavage. On the contrary, the Fe-complex passes through a formal Fe^{III}–COOH intermediate. Poor π-back-bonding from Fe^{III} renders lower charge density over "O", favouring the isomerization to Fe–OCOH intermediate, which leads to the generation of formate (Scheme 14). Jurss and co-workers have developed a series of nickel complexes with tetradentate chelating ligands comprised of a redox-active 2,2′-bipyridyl core and electron-rich N-heterocyclic carbene (NHC) donors (Fig. 8n–p).[166] During electrocatalytic CO_2 reduction, the complexes showed a drastic change in product selectivity from H_2 to CO on transitioning from an open-chain to macrocyclic conformation with increasing linker size.

Over the years, several bio-inspired model of [NiFe]-CODHs have been developed involving several different ligand-framework, such as phosphine, bipyridine, porphyrin, cyclam, *etc.* It has been observed that second coordination sphere greatly influence the product selectivity as well as the tuning the rate of the reaction. Irrespective of the ligand frameworks, the initial CO_2 activation was shown to be happen through the nucleophilic attack from the electron-rich metal centre. This implies, an electron-rich late transition metal should be more useful. The negatively charged metal–CO_2 complex is stabilized either by protonated basic residues or any Lewis acidic metal. The C–O bond cleavage is proposed to be the rate-determining step, where an intramolecular basic residue (such as amines) are shown to play a pivotal role in shuttling the protons to the

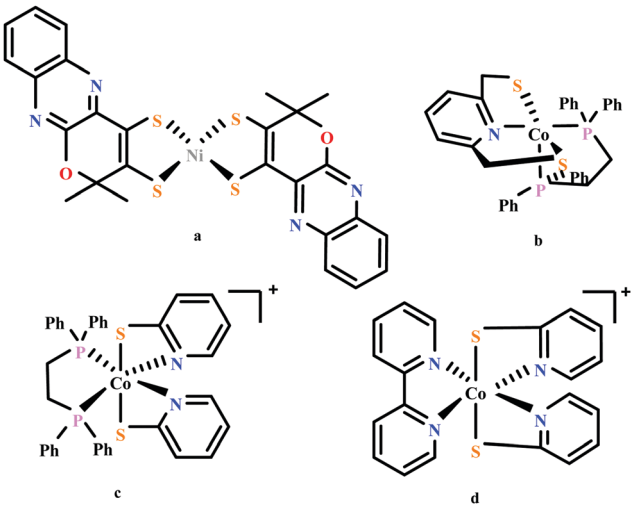

Fig. 9 Representative metal–thiolate based electrocatalysts for CO_2 reduction.

metal–COOH species. However, the role of thiols is not well explored. A nickel–tetrathiolate complex, mimicking molybdopterin (Fig. 9a), was reported to reduce CO_2 to formate (with minor amounts of CO and H_2) with 340 mV over-potential.[167] To understand the effect of metal–thiolates in CO_2 reduction, electron-rich late transition metal (cobalt) bound pyridine-dithiolate complex, 2,6-dithiomethylpyridinocobalt(dppe) (Fig. 9b) was synthesized.[168] The catalyst was shown to reduce CO_2 to CO (>95% faradaic efficiency) with an unprecedented <100 mV over-potential and that too with a TOF of 1559 ± 8 s^{-1}. The electron-rich thiolates play a dual role. Firstly, on getting protonated under the experimental conditions (H_2O + CO_2), increases the formal potential of the $Co^{II/I}$ process, which in turn lowers down over-potential of CO_2 reduction, and secondly, the other thiolate increases the electron density over Co^{I}-state (through back-bonding) activating it to bind CO_2 (Scheme 15A). The strong covalent bonding in a Co^{III}–COOH intermediate develops large negative charge-density over the "O"-atoms, preventing "C-protonation" and the generation formate. On the contrary, the thiolate mediates the proton relay to the "OH" group of

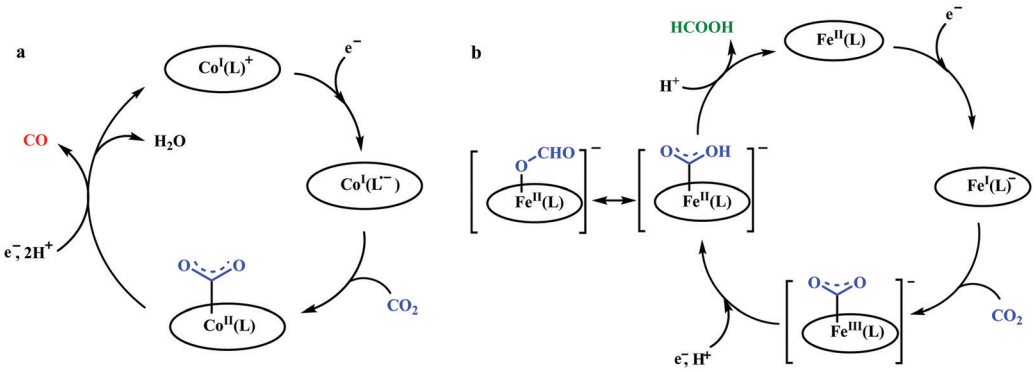

Scheme 14 Proposed mechanistic pathway for electrocatalytic CO_2 reduction to CO *vs.* formic acid; catalyzed by same ligand framework but with different metals: (a) cobalt and (b) iron.

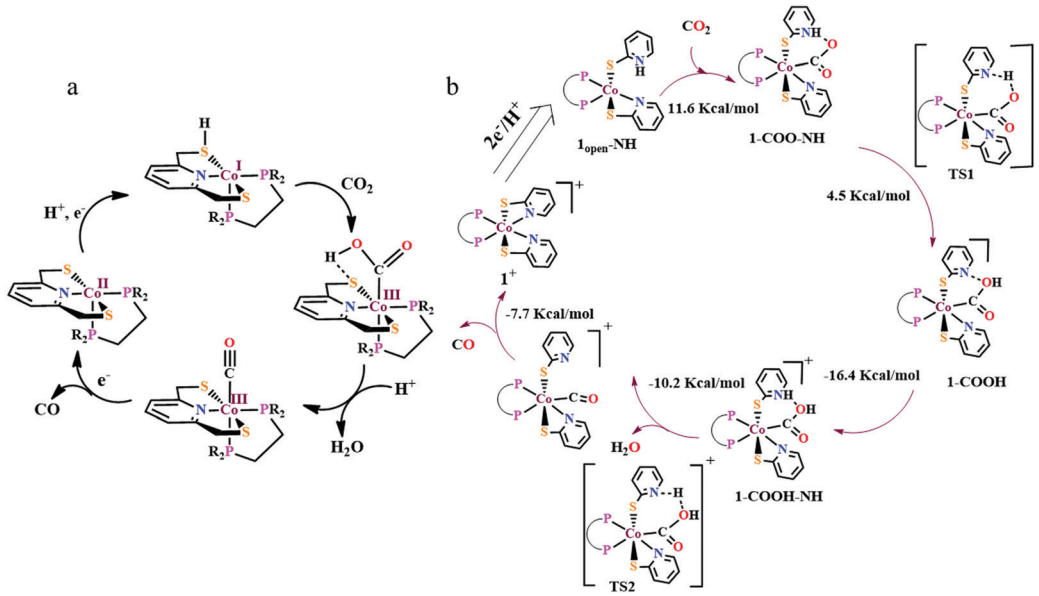

Scheme 15 Proposed mechanistic cycle for the selective reduction of CO_2 to CO through the influence of (a) a thiol-protonation; (b) a hemilabile-pyridine protonation.

Co^{III}–COOH intermediate in the rate-determining process of C–O bond cleavage leading to selective generation of CO. Hence, a dithiolate ligand framework can lead to the development of efficient CO_2 reducing catalyst operative at low over-potential with high turnover rate. As an extension of the concept, a thio-pyridinato complex, cobalt^{III}-bis(2-thiopyridinato)-diphenyl-phosphenoethane chloride (Fig. 9c) was synthesized. This complex can also catalyze the reduction of CO_2 to CO from the Co^{I}-state.[169] Unlike thiol-protonation, the hemilability of the pyridine arn on protonation mediates the proton-relay (Scheme 15B). Whereas, both thiolates being bound to the cobalt-centre, stabilizes the Co^{I}-state for CO_2 binding. Less energy demanding proton-transfer from the pyridine moiety selectively to the "OH" results in facile C–OH bond cleavage to form CO. Recently, Mougel and co-workers have reported a pyridinethiolate bound cobalt complex, bipyridine-bis-(2-pyridinethiolato)-cobalt(III)-hexaflurophosphate (**9d**).[170] The catalyst can convert CO_2 to formate selectively with a very low overpotential of110 mV and a TOF of 10 s^{-1}.

To provide a comprehensive overview, the catalysts which were found to convert CO_2 to CO or formate with >90% product selectivity are summerized in Table 1. The TOF numbers were not included because they were determined under a variety of different experimental conditions using different mathematic equations. Each mathematical equation is derived considering different boundary conditions, hence benchmarking the catalysts in terms of TOF does not really help their comparability.

Mechanistic consideration of CO_2 reduction and rational design

A major challenge in CO_2 reduction is control of competitive proton reduction process (hydrogen evolution reaction, HER, Scheme 16c), which is more favourable than CO_2 reduction both thermodynamically and kinetically. Similarly, selectivity over the C-based product is desirable *i.e.* CO, HCOOH or CH_4. The initial step of CO_2 activation is the nucleophilic attack of the electron-rich metal centre on the electrophilic C-atom of CO_2 (Scheme 16a). The CO_2 reduction will result in a M^{n+2}–CO_2^{2-} species which is very basic and will pick a proton easily to M^{n+2}–COOH species. Irrespective of the ligand framework used, the reaction generally proceeds *via* this metal–COOH species. The bound –COOH species bears a formal charge of −1. A C-protonation (g) will lead to the release of HCOOH while an O-protonation (f) will lead to CO (Scheme 16). The competing reaction involves the protonation of the metal to form the corresponding hydride (Scheme 16b). The resulting M^{n+2}–H species can either be protonated again (c) to release H_2 or attack the CO_2 as a nucleophile to produce formate (d).

Production of CO from CO_2 requires the reaction to move along a → f. Two key factors need to be controlled to achieve selectivity i. avoiding protonation of the metal centre (b) and ii. protonation of the O-centre of the M^{n+2}–COOH species (g).

i. Avoiding protonation of the metal centre:

The electronic structure of the metal centre may be tuned by judicious choice of ligands to restrain its basicity and avoid protonation. A good example of this is demonstrated in the Ni-cyclams. The CO_2 binds the Ni-centre at its formal +1 state displacing a bound CO, the second electron required to reduce the CO_2 further is provided to a $[Ni–CO_2]^+$ species.[158,160,174] This avoids starting the reaction at a formal Ni(0) state which, apart from concerns of dissociation from the ligand, would be more prone to protonation and thereby loose selectivity.

Another approach to avoid metal protonation is the use of reductive disproportionation of CO_2 to CO and CO_3^{2-} which rescinds the requirement of proton all together and is inherently

Table 1 Homogeneous electrocatalysts for the reduction of CO_2 to CO or formate

Complex	Conditions	Overpotential	Product	TON	Ref.
$Re(bpy)(CO)_3Cl$	DMF (+ H_2O), 0.1 M NEt_4Cl, GC electrode	0.56 V	90% CO		59
$Re(bpy\text{-}tBu)(CO)_3Cl$	CH_3CN (+ H_2O), 0.1 M NBu_4PF_6, GC electrode	0.74 V	100% CO		64
$Mn(bpy)(CO)_3Br$ (**4a**)	CH_3CN (+ H_2O), 0.1 M NBu_4ClO_4, GC electrode	0.24 V	90% CO		66
$Re(bpy\text{-}thiourea)(CO)_3Cl$ (**4h**)	CH_3CN (+ H_2O), 0.1 M NBu_4PF_6, GC electrode	$\sim$0.47 V[a]	89% CO		78
$[(bpy^{NHEt}PY2Me)Fe^{II}]^{2+}$	CH_3CN (+ H_2O), 0.1 M NBu_4PF_6, GC electrode	$\sim$0.36 V[a]	81 $\pm$ 11% CO		81
o-Fe_2DTPP (**7g**)	DMF (+ H_2O), 0.1 M NBu_4PF_6, GC electrode	0.66 V	95% CO	1.58×10^8	111
CAT (**7a**)	DMF (+ H_2O), 0.1 M NBu_4PF_6, GC electrode	0.46 V	>90% CO	5×10^7	113
FCAT (**7c**)	DMF (+ PhOH), 0.1 M NBu_4PF_6, GC electrode	0.39 V	$\sim$100% CO		115
Fe-*o*-TMA (**7f**)	DMF (+ H_2O + PhOH), 0.1 M NBu_4PF_6, GC/Hg electrode	0.22 V	$\sim$100% CO		125
FeTPOH (**7i**)	CH_3CN (+ H_2O), 0.1 M NBu_4PF_6, BPG electrode	0.36 V	96% CO	4000	116
(**7j**)	DMF (+ H_2O), 0.1 M NBu_4PF_6, GC electrode	0.42 V	91% CO	1.08×10^8	126
Fe-*ortho*-2-amide (**7p**)	DMF (+ PhOH), 0.1 M NBu_4PF_6, GC electrode	$\sim$0.54 V[b]	92% CO		129
FeTPP-Ur (**7q**)	DMF (+ H_2O), 0.1 M NBu_4PF_6, GC electrode	0.43 V	91% CO	3.28×10^6	131
6e–h	DMF (+ H_2O), 0.1 M NBu_4PF_6, GC electrode	0.50–0.70 V	>90% formate	15–23	95
$[Pt(dmpe)_2](PF_6)_2$	CH_3CN (+ PhOH), 0.1 M NEt_4PF_6, GC electrode	<0.10 V	>90% formate		171
$(Ph_4P)[Ni^{III}(qpdt)_2]$ (**6m**)	CH_3CN (+ CF_3CH_2OH), 0.1 M NBu_4ClO_4, Hg/Au amalgam electrode	0.34 V	$\sim$90% formate (trace CO, H_2)		167
Nickel cyclam (**8a–b**)	H_2O (pH 4.1), 0.1 KNO_3, electrode	$\sim$0.2 V	Up to 96% CO	$\sim 10^2$	149–151
$[Ni^{II}(HTIM)]$ and $[Ni^{II}(MTC)]$	H_2O (pH 5), 0.1 $NaClO_4$, Hg electrode	$\sim$0.55 V	88 $\pm$ 7% CO		156
Cobalt aminopyridines (**8h–j**)	DMF (+ MeOH/CF_3CH_2OH), 0.1 M NBu_4PF_6, GC electrode	0.35–0.68 V	$\sim$98% CO	1.22×10^6	163
2,6-Dithiolatomethylpyridine-dppe cobalt(II) (**9b**)	CH_3CN (+ H_2O), 0.1 M NBu_4ClO_4, GC electrode	0.05–0.07 V	95% CO	1×10^6	168
$[Co(dppe)(2\text{-}PyS)_2]Cl$ (**9c**)	CH_3CN (+ H_2O), 0.1 M NBu_4ClO_4, GC electrode	0.18 V	92% CO	1×10^5	169

[a] Calculated from the equation: $E = E^\circ - 0.059pK_a$; assuming $E^\circ_{CO_2/CO,1\ M\ H_2O} = -1.54$ V[172] *vs.* $Fc^{+/0}$ in CH_3CN. [b] Assuming $E^\circ_{CO_2/CO,PhOH} = -1.64$ V *vs.* $Fc^{+/0}$ in DMF, pK_a of PhOH was considered to be 15.4.[173]

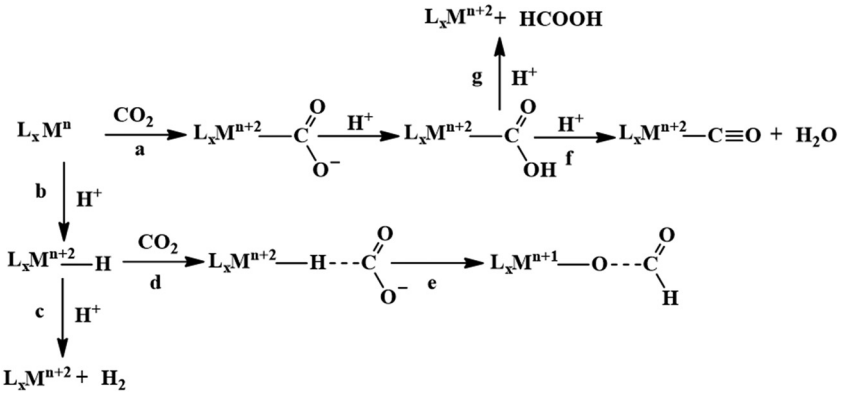

Scheme 16 Controlling the competitive pathways in CO_2 reduction.

selective for CO by design. This is demonstrated in a series of copper and nickel-phosphine as well as manganese-bipyridine complexes.[69,92–94]

Finally, a bio-inspired approach is to use bound thiolate ligand or 2nd sphere pendant amine groups to act as the site of protonation keeping the metal centre free for CO_2 reduction. This has been demonstrated in the cobalt thiolate complexes where the thiolate ligand is protonated.[168] This protonation helps shift the reduction potential of the metal centre more positive reducing the over potential of the process and the protonated thiol ligand is later utilized to stabilize the M^{n+2}–CO_2^{2-} intermediate and protonate it to M^{n+2}–COOH species.

ii. Protonation of the O-centre in the M^{n+2}–COOH species.

To selectively protonate the O-centre, several complexes have been developed with pendant groups which can help the proton transfer to this intermediate. Hydrogen bonding from these pendant groups helps in both facilitating the reduction of CO_2 as well as the following proton transfer to the M^{n+2}–COO^{2-} and M^{n+2}–COOH intermediate species. These include cyclam-NH,[150,154,158] phenols,[114] water,[124,147] amide,[129,130] thiols,[168] azacalix-pyridine[163] and pyridinium.[169] The stabilization of the M^{n+2}–CO_2^{2-} can also be attained by electrostatic field.[125]

Although the focus has been installing proton transfer and hydrogen bonding groups, an often-unappreciated fact is the possibility to control the charge density at the C-center by tuning the covalency of the metal carbon bond of the M^{n+2}–COOH species.[169] This was suggested when analysing the selectivity for CO observed for a Cobalt dithiolate complex. The Co^{III}–COOH intermediate had a fairly covalent Co–C bond resulting in depletion of the negative charge on the C-centre of

the –COOH$^-$ species and the negative charge was localized on the O-atom. This automatically biased the system for O protonation to release CO and no HCOOH could be thus be formed.

Nitrite reduction

Introduction

This section is focussed primarily on the heme-containing nitrite reductases. An attempt has been made to explicitly discuss different structural and functional aspects, focussing on enzymatic architecture and detailed mechanism emphasizing the roles of the basic residues within the active site of different enzymes involved in nitrite reduction. The later part of the review focusses on the recent investigations with 'model systems', directed towards understanding the mechanisms of these enzymes and the discussions concentrates on the factors which distinguishes the three non-identical nitrite reduction pathways. This review mainly concentrates on heme based enzymes and hence discussions on model systems will also be limited to heme related porphyrinoid complexes.

Lesson from Nature

Nitrite reduction to ammonium

The conversion of nitrite to ammonium ion is accomplished in two different pathways, one involves assimilation of nitrite and the other is a dissimilatory process (Scheme 17). In each of the pathways, nitrite is reduced by six electrons to ammonium and the process is catalyzed using enzymes containing iron-based porphyrinoid cofactors, skipping the release of any detectable intermediates.[175,176] The metal involved relates to the prebiotic ammonia formation from nitrite by reduced iron in the early earth.[177] However, these two routes of nitrite reduction involve discrete cellular mechanism and occur in different cellular compartments: assimilation in cytoplasm/chloroplasts and dissimilation in periplasm. The enzymes involved in catalysis are structurally distinct with different physiological redox partners.[176]

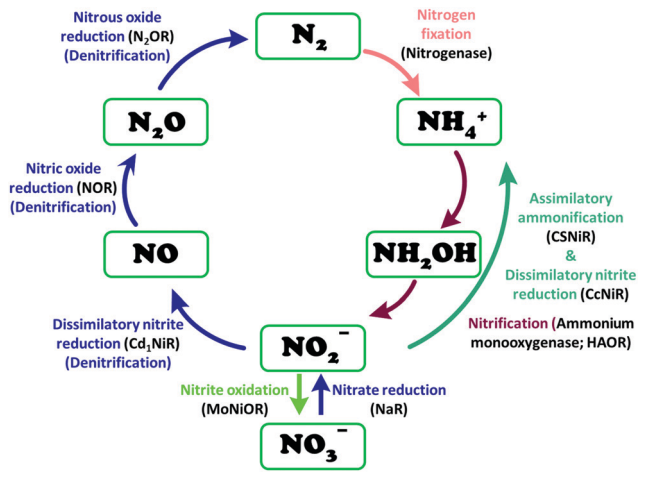

Scheme 17 Biochemical nitrogen cycle. Different pathways of interconversion of various oxides of nitrogen, dinitrogen and ammonium are highlighted. The enzymes catalysing the conversions are written in black inside parenthesis.

Dissimilatory nitrite reduction to ammonium. This process is better known as respiratory nitrite ammonification and is catalysed by heme c of multiheme cytochrome *c* nitrite reductase (CcNiR) (EC 1.7.2.2). CcNiR plays a crucial role catalysing the final step of dissimilatory nitrate reduction to ammonia. This process is utilised by several bacteria where nitrate is used as terminal electron acceptor of anaerobic respiratory chain for energy conservation. Initial step involves reduction of nitrate to nitrite by molybdenum-containing nitrate reductases (NaR). In the final step CcNiR efficiently reduces the nitrite to ammonia (6 elecrtron-7 proton reduction) bypassing release of any intermediates.[178]

Electron source. Inside the periplasm CcNiR (also known as NrfA: after the name of the encoding gene nrf, nitrite reduction with formate) forms stable membrane associated complex with multiheme quinol oxidase which provides electron from membrane quinone pool to the electron chain.[175,179,180]

Enzyme architecture. CcNiR from several bacteria *viz. Escherichia coli*,[181] *Wolinella succinogenes*,[182,183] *Sulfurospirillum deleyianum*,[184] *Desuldomonas desulfuricans*,[185,186] *Desulfovibrio vulgaris*,[187] *Shewanella oneidensis*[188,189] and *Thioalkalivibrio nitratireducens*[190] were structurally characterised using X-ray crystallography.

All cystallographically characterised enzymes (except *T. nitratireducens*) have homodimers of penta heme (labelled heme 1–5, Fig. 10b) subunits with extensive interaction between the monomers.[189] Each monomer contains five heme c and arranged in near-parallel and near-perpendicular heme pairs (Fig. 10b). Hemes 2–4 are axially bis-histidine ligated with a CysXXCysHis binding motif and heme 1 constitute the enzyme active site coordinated by water/hydroxyl group in the distal position and lysine (Lys_{134}) in the proximal position (belonging to a CysXXCysLys$_{134}$ binding motif).[178,191] The bis-histidine ligated hemes participate in electron relay during the catalysis.[192,193] The active site is surrounded by conserved histidine (His_{277}), tyrosine (Tyr_{218}), arginine (Arg_{114}) and glutamine (Gln_{276}) residues (Fig. 10c, *Wolinella succinogenes* CcNiR sequence numbering). It also hosts two hexacoordinated calcium ions which have substantial structural and functional roles.[178,194] Mutation studies revealed that Gln_{276} calcium ion pair stabilises the distal ligand binding to iron centre through a network of hydrogen bonding and in turn regulated the substrate affinity of the active site.[195,196] The His_{277}, Tyr_{218} and Arg_{114} residues play central roles in nitrite reduction through extensive hydrogen bonding to the substrate.[175,197,198] Electron transfer from physiological redox partner to the active site is facilitated by adjacent hemes which is also evident from the redox potentials of the hemes which are compatible to the potential of NO_2^- reduction.[192,198] In addition, an inlet channel with positive electrostatic surface potential assist approach of nitrite to the active site (also helps in proton supply) and an outlet channel with negative electrostatic surface potential facilitating ammonia release has also been identified.[182,184,185] A novel octaheme cytochrome *c* nitrite reductase (TvNiR) from *Thioalkalivibrio nitratireducens* has also been structurally characterised. It exists as a homo-hexamer with eight hemes per monomer. Each monomer consists of two domains:

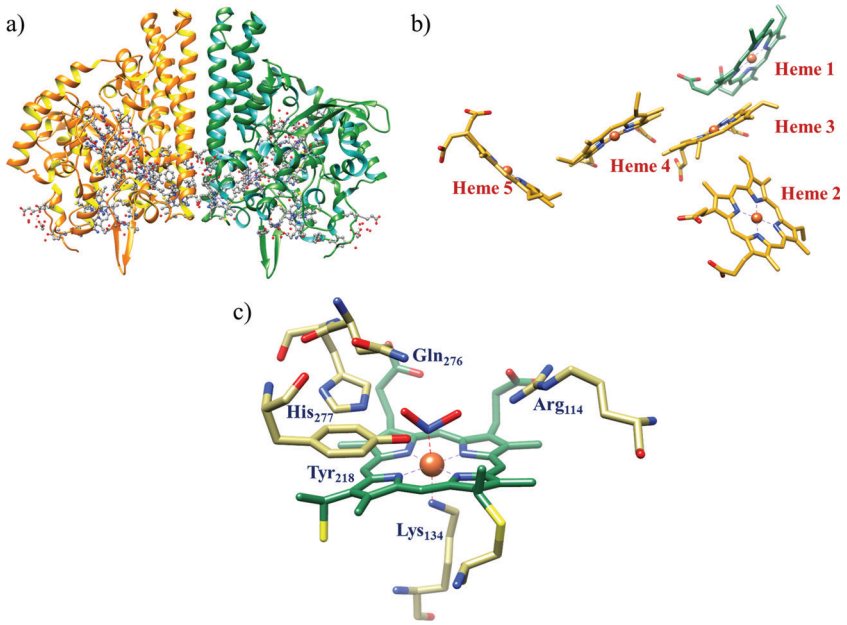

Fig. 10 (a) Three-dimensional structure of the *Wolinella succinogenes* CcNiR homodimer, the momomers are shown in different colours (with yellow and green ribbon colour), (b) arrangement of hemes (1–5) in the monomer with green ribbons; the five heme c are numbered according to their attachment to the protein chain. Heme 1 contitutes the enzyme active site. (c) Nitrite bound active site structure. (a) and (b) are based on PDB file 1FS7[182] and (c) is based on PDB file 2E80.[175]

in the N-terminal domain resides three hemes with a unique fold and C-terminal domain has five hemes which structurally and functionally conform with CcNiR.[190]

Mechanism of nitrite reduction. CcNiR catalyses six-electron, seven-proton nitrite reduction to ammonia avoiding the release of any intermediates. The mechanism of this reaction has been under investigation using structural,[181,182,184,186,187,190] electrochemical,[189,192,199,200] theoretical[195,201–203] and spectroscopic[181,194,204] tools for nearly two decades.[175,202] A summary of the findings is presented with particular stress on the role of 2nd sphere residues.

The overall reaction can be split up into five episodes:

(a) The first episode deals with substrate binding to the active site and subsequent heterolytic N–O bond cleavage. The enzyme resting state is a high spin Fe^{III}–OH_2 (Scheme 18a), confirmed on the basis of Fe–O bond length of 2.1 Å.[175] It undergoes reduction to Fe^{II}–OH_2 which results in the weakening of Fe–O bond (2.39 Å) (Scheme 18b). The substrate nitrite then displaces the water molecule to bind to Fe^{II} in 'nitro' mode (through N-atom)[175,197] and a low spin nitrite bound Fe^{II} is formed (Scheme 18c).[205] The extensive back-bonding from Fe^{II} d_{xz} orbital (HOMO) to nitrite π*-orbital (LUMO), results in strong Fe–N bond (1.9 Å) and a simultaneous weakening of N–O bond.[175] Additionally, formation of hydrogen bonds from the protein residues to the oxygen atoms of the bound nitrite molecule contributes to N–O bond heterolysis.[193,197] The structure of the nitrite bound states reveal that the two oxygen atoms of nitrite are at hydrogen bonding distances to the protonated His_{277} (2.6 Å) and positively charged Arg_{114} (2.8 Å).[175] The N–O bond is cleaved through double protonation on one of the O-atom (Scheme 18d and e). At pH < 7, His_{277} is protonated and is found to facilitate initial protonation and the second protonation (after endothermic reprotonation). But at higher pH, the first proton transfer (PT) occurs from Tyr_{218} and the second PT is also mediated by the same residue after exothermic reprotonation.[178,194] Hence, these two consecutive PT steps results in heterolytic N–O bond cleavage[204] to form $\{FeNO\}^6$ intermediate (Scheme 18f) and the first water molecule is released.[197,206]

All iron-nitrosyl intermediates in this review will be represented by Enemark–Feltham notation. In the Enemark–Feltham notation, $\{M(NO)_x\}^n$, the index x indicates the number of coordinated NO molecules to metal M, and the exponent n counts the number of valence electrons, which is the summation of the number of electrons in the metal(d) and NO(π*) orbitals.[207]

(b) The second episode of the mechanism comprises two proton-coupled electron-transfer (PCET) steps (PCET1 and PCET2), leading to an Fe-HNO intermediate. The electronic structure of $\{FeNO\}^6$ is best described as a Fe^{II} metal centre bound to a NO^+ ligand.[208] $\{FeNO\}^6$ are strong electrophiles[209] while $\{FeNO\}^7$ intermediate (Scheme 18g) is highly stable and represent a thermodynamic sink.[210–212] So, to escape the formation of this intermediate two rapid consecutive PCET steps occur to the $\{FeNO\}^6$ species to form an $\{Fe(HNO)\}^8$ intermediate (Scheme 18h). Also, the reduction of $\{FeNO\}^6$ to $\{FeNO\}^7$ involves linear to bent transition of Fe–NO unit. The two consecutive electron transfer can be rationalised by the fact that $\{FeNO\}^8$ is formed before this reorganisation of Fe–NO bond takes place.[175] Conformational and electron structure studies reveal both the reductions to be ligand centred. Proton from PCET1 (**f** → **g**, Scheme 18) recharges the enzyme active site, with protonation of Arg_{114} and that from PCET2 (**g** → **h**, Scheme 18) does an electrophilic attack at the N-centre of NO forming $\{Fe(HNO)\}^8$ (as shown in Scheme 18f–h).[206]

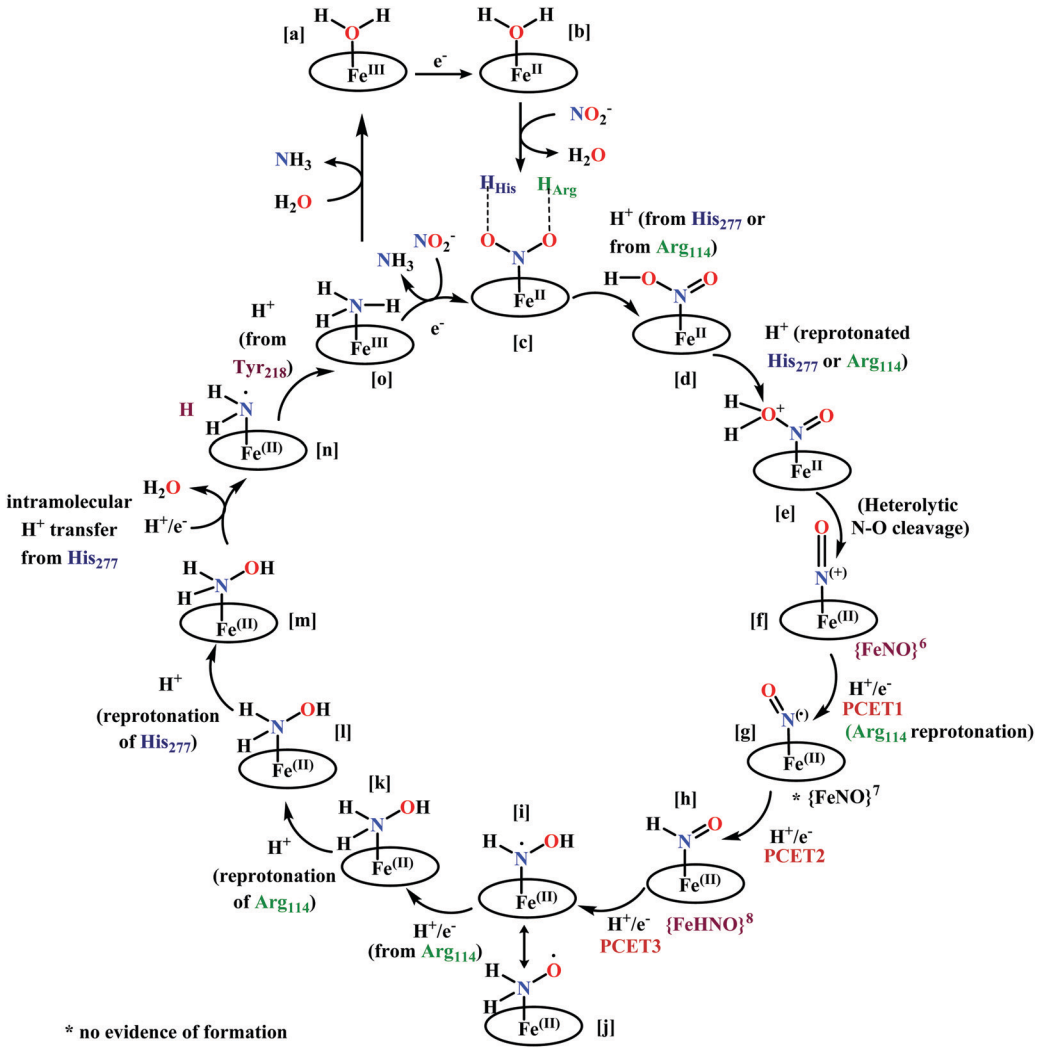

Scheme 18 Mechanism of nitrite reduction to ammonia catalyzed by cytochrome *c*-containing nitrite reductase.

(c) In the third episode a hydroxylamine intermediate is formed and the necessary proton required is found to be supplied *via* Arg_{114}. Initially a PCET step (PCET3) protonates His_{277} endothermically which then transfers the proton to $\{Fe(HNO)\}^8$ with an electron forming two elusive isomeric intermediates (Scheme 18i and j). Next an intramolecular PT from Arg_{114} to this intermediate followed by exothermic 1-electron reduction leads to the hydroxylamine intermediate (Scheme 18k).[202]

(d) Second N–O bond cleavage occurs in the fourth episode of this catalytic cycle aided by a PT from His_{277}. After the formation of hydroxylamine intermediate, the reaction proceeds through two protonation steps. This is the rate limiting step of the catalytic cycle.[198,205] Two consecutive protonations of Arg_{114} and His_{277} occurs respectively (Scheme 18k–m). The fully protonated active site then undergoes an intramolecular PT from His_{277} resulting in another N–O bond cleavage with release of a water molecule (Scheme 18m and n).[202,203]

(e) In the fifth and final episode, the $(H_2N^+)Fe$ intermediate formed previously undergoes reduction being highly electrophilic. The radical intermediate $(H_2N^{+\bullet})Fe$ (Scheme 18n) formed is also very reactive and theoretical and site-directed mutation investigations revealed that at this stage Tyr_{218} can participate in a PT step.[198] The electronic structure of the radical intermediate explains stabilization by Tyr_{218} residue due to electron delocalisation from the radical to the aromatic ring.[203] The issue of product dissociation was addressed by Neese by conducting a relaxed surface scans of the Fe–N(NH_3) distance in two model complexes: $(H_3N^{+\bullet})H_{Arg}$ and $(H_3N^{+\bullet})H_{Arg}$ H_{Tyr}. A spin change likely occur during the dissociation of ammonia from $(H_3N^{+\bullet})H_{Arg}$ H_{Tyr} potential energy surface. Here, elongation of the Fe–N(NH_3) bond results in switching from low to high spin surface. Due to this spin state change, dissociation step becomes much less energy demanding. Thus, ammonia is released from the active site in high spin Fe^{III} state (Scheme 18o).[203] The open coordination site is then occupied by another nitrite molecule available in the vicinity to initiate another cycle or by a water molecule resulting to the resting state.

Assimilatory nitrite reduction. Oxygenic phototrophs assimilate nitrogen by capturing nitrate ions from the soil. Nitrate is then reduced to ammonia, a more assimilable form of nitrogen.

This results in the conversion of inorganic nitrogen to organic nitrogen. Nitrate is reduced to ammonia in two steps, with sequential utilisation of two enzymes. The first step involves reduction of nitrate to nitrite, catalysed by molybdenum containing assimilatory nitrate reductases (aNR). The second step deals with reduction of nitrite to ammonia by assimilatory nitrite reductases (aNiR).[213] The later step involves nitrite reduction using six electrons and eight protons and none of the intermediates are released during the total catalytic cycle. aNirR are siroheme containing nitrite reductase (CSNiR).

Electron source. There are two types of assimilatory nitrite reductase depending upon the source of the electrons used in reduction process: (a) in photosynthetic organisms, photosynthetically reduced ferredoxin (cyanobacteria and chloroplasts of photosynthetic eukaryotes) are the electron source. These are ferredoxin:nitrite oxidoreductase (EC 1.7.7.1), commonly known as ferredoxin dependent nitrite reductase;[214–216] and (b) in most heterotrophs, source of electrons is reduced pyridine nucleotide. These are NAD(P)H dependent nitrite reductase.[217] In this review we will mainly focus on ferredoxin dependent nitrite reductase.

Enzyme architecture. Structure of CSNiR have been studied from various phototrophs such as higher plants, alga[218] and cyanobacteria.[214] Of all these spinach chloroplast enzyme (Fig. 11a)[214,219] has been most extensively studied one. CSNiR is a product of nasB, nirB and Nii genes in *Paracoccus denitrificans*,[220] *Escherichia coli*[221] and tobacco[222,223] respectively. CSNiR is composed of a single polypeptide chain[219] with three domains folded around the prosthetic groups. All classes of assimilatory nitrite reductases contain two prosthetic groups, a siroheme (Fe isobacteriochlorin unit)[224] and an iron–sulphur cluster (Fe_4S_4 cluster).[222]

From crystallographic structure analysis (spinach chloroplast enzyme), it is quite evident that siroheme and Fe_4S_4 cluster are in very close proximity to one another and are directly linked through a bridging sulphur atom from the Cys_{486} residue. The cluster is coordinated to four Cys–S atoms (Cys_{441}, Cys_{447}, Cys_{482} and Cys_{486}) which are essential for cofactor binding[219] and also facilitates efficient electron transfer to the siroheme centre from reduced ferredoxin. The active site also contains conserved Arg_{109}, Arg_{179} and Lys_{224} which forms a large pocket suitable for nitrite binding and reduction (Fig. 11b).[219,222,225] There are several other Arg and Lys residues surrounding the active site which aids in the overall reduction process. These positively charged residues are also essential for stabilising the eight carboxylate groups present in the siroheme backbone. Electrostatic potential energy surface of NiR reveal the presence of a tapered tunnel (approx. diameter 8 Å) from the protein surface to the active site. Several positively charged basic residues surround the active site resulting in a positively charged electrostatic surface which promotes nitrite binding/stabilisation and induces expulsion of ammonium formed as the product (Fig. 12).[219]

NiR has only one ferredoxin (Fd) binding site.[215] Modelling studies and site directed mutagenesis studies suggests electrostatically stabilised 1 : 1 complex formation between NiR and Fd wherein the acidic residues are supplied by Fd and NiR contributes the basic residues.[225] From crystallographic data it was also revealed that the distance of Fe_2S_2 cluster of Fd to Fe_4S_4 cluster is shorter than distance between Fe_2S_2 cluster and siroheme. The shorter distance suggests that electron transfer (ET) should be significantly faster from Fd to Fe_4S_4 cluster than to siroheme. Using different electrochemical techniques, midpoint redox potential (E_m) of the cofactors were determined. E_m for siroheme (−290 mV) was found to be 75 mV more positive than E_m Fe_4S_4 cluster (−370 mV).[226] This result also agrees with the previous observation that Fe_4S_4 cluster is reduced prior to siroheme Fe-center.[226]

Mechanism of nitrite reduction. Theoretical modelling of NiR revealed that the enzyme catalyses nitrite reduction to ammonia coupling the transfer of eight protons and two water molecules along with six electrons for the overall process. All the residues present near the active site are unlikely to be protonated at the same time due to electrostatic repulsive

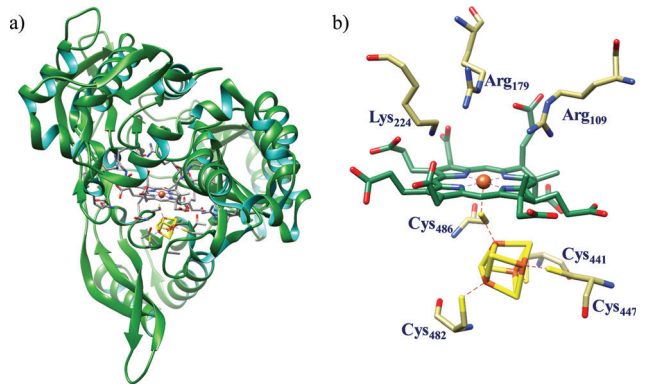

Fig. 11 (a) Three dimensional structure of spinach nitrite reductase (ferredoxin dependent nitrite reductase) and (b) active site structure of CSNiR. Both structures are based on PDB 2AKJ.[219]

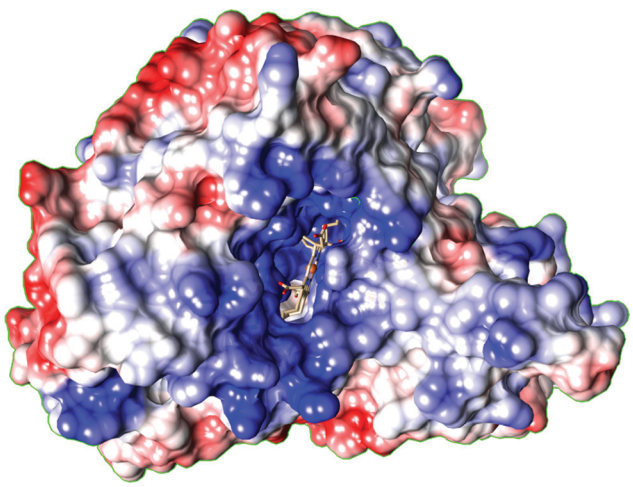

Fig. 12 Electrostatic surface of CSNiR showing the presence of an open tunnel from the surface of the protein to the siroheme and iron–sulfur cluster. Positive regions are shown as blue, and negative regions are shown as red. Many Lys and Arg are found in this region as shown by blue colouration (based on PDB 2AKJ).

interactions between the closely placed residues. In addition, ferredoxin binding to the active site closes the channel connecting protein surface to the active site, thus solvent access to the active site is lost. This is assumed to decrease the pK_a values of the nearby residues. Thus, electron transfer from Fd is coupled with proton transfer from the protonated residues. On completion of one reduction step, oxidised Fd is released, pK_a of the residues are restored causing protonation from the bulk solvent to which the channel gets exposed again.[219]

The enzyme nitrite reductase in its resting state is fully oxidised with the cluster in $(Fe_4S_4)^{2+}$ state and siroheme iron in high spin Fe^{III} state (Scheme 19a). Conversion of nitrite to ammonia by aNiR also involves five steps and the mechanism is almost same as that of CcNiR. The exact role of each of the active site residues are not clear yet and require more extensive investigations. Till date the proposed reaction mechanism involves assumption of the proton donating sites infered from ligand bound crystal structural data. The enzyme initially undergoes one electron reduction, and upon substrate binding, resulting in nitrite bound low spin Fe^{II} coordinated siroheme.[176,219] Alternatively, several spectroscopic and kinetic data revealed that nitrite binds to Fe^{III}–siroheme forming a low spin Fe^{III}–siroheme–nitrite complex (Scheme 19b). Several Nitrite bound crystal structure of the active site reveals that nitrite is bound in 'nitro' mode and the oxygen atoms are at hydrogen bond forming distances to Lys_{224}, Arg_{179} and Arg_{109}.[219,223] The shortest possible hydrogen bond around NO_2 was with Lys_{224} and thus $O(NO_2)$ may be protonated. The Arg_{179} is assumed to be the second proton donor from structual data. The first N–O bond is cleaved with proton from Lys_{224} side conforming a similar S–O bond cleavage in siroheme containing dissimilatory sulphite reductases.[227] After the N–O bond cleavage, a second electron is transferred and a NO-bound ferrosiroheme species with $(Fe_4S_4)^{2+}$ state (Scheme 19c). The candidates for proton donor to this intermediate were Arg_{179} and Arg_{109} as elucidated from structural data.[223] Addition of two more electrons coupled with the proton transfer results in reduction of NO to result in a hydroxylamine-bound siroheme (Scheme 19d). Crystal structures of Nii3–NO and Nii3–NH_2OH were solved.[223] Finally, two more electrons donated resulted in an ammonia bound siroheme (Scheme 19e), from where the ammonium ion was readily released out through the positively charged substrate channel. The protonations were assisted by the active site residues, the ultimate sources of these protons being the solvent within the channel. The enzyme receives the six electrons required in single steps from the reduced ferredoxin, which is quite challenging. Although recent efforts attempted to understand the complex mechanism of nitrite reduction by aNiR,[225,228] there remains considerable uncertainity about exact pathways of reaction where an enzyme capable of storing two electrons at a time is involved. It is quite likely that the six-electron reduction proceeds by a series of three 2-electron steps.[218]

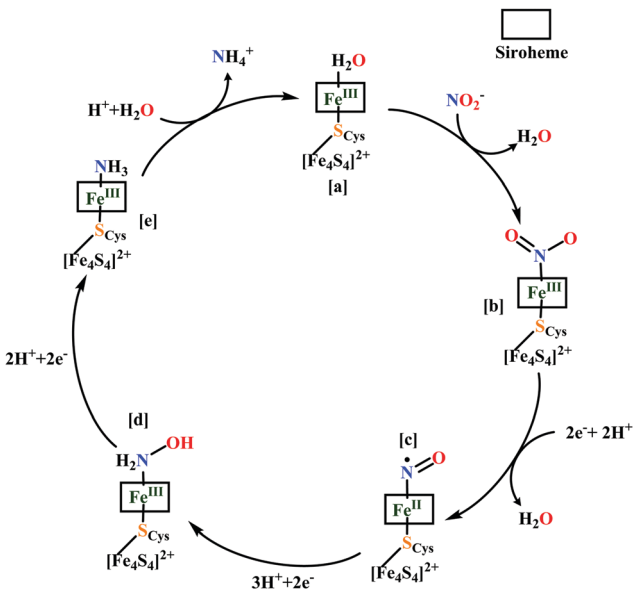

Scheme 19 Proposed reaction mechanism of aNiR. Since the basic residues involved in the protonation steps are not extensively proved yet, informations about the residues are not included.

After elucidation of reaction mechanism in both these type of nitrite reductases, an obvious question that comes to mind is that why nature implemented two very different heme cofactors varying widely in structure for catalysing the same reaction. A very recent theoretical investigation on electron transfer pathway of siroheme *vs.* heme in sulphite reductases suggested that siroheme prefers electron transfer *via* a bridging cysteine–S atom from the proximal Fe_4S_4 cluster more than heme. In contrast, heme prefers direct mode of electron transfer *via* porphyrin ring. This may lead to unwanted side reactions involving attack of radicals on heme. In siroheme, there is an interrupted π-conjugated system due to presence of sp^3-carbons direct mode of electron transfer is disfavoured. Hence, nature might have implemented such a unique macrocycle for this reaction to protect the cofactor from undesired radical attack.[229]

Nitrite reduction to nitric oxide

Dissimilatory denitrification. In nature, denitrification is the part of biological nitrogen cycle which involves transformation of nitrate to nitrogen gas. Denitrification is defined as the loss of fixed nitrogen (product of nitrification process by nitrifying bacteria) to maintain biological N balance, *i.e.*, respiratory reduction of nitrate to dinitrogen contributing to biological N_2 formation. Reduction of nitrate occurs in four stages, each catalysed by specific metalloenzyme according to the scheme shown below.[180,230,231]

$$NO_3^- \xrightarrow{NaR} NO_2^- \xrightarrow{NiR} NO \xrightarrow{NOR} N_2O \xrightarrow{N_2OR} N_2$$

Denitrification is the major metabolic process in facultative anaerobes under low oxygen tension where N-oxides serves as terminal electron acceptor. Molybdenum containing nitrate reductase (NaR) catalyses the first step, *i.e.*, nitrate reduction to nitrite. Nitrite reductase (NiR) catalyse the reduction of nitrite to gaseous product nitric oxide (NO). This is thus considered as a major source of NO in bacteria. Purification and characterisation of NiR from several bacterial sources

reveal that there are two distinct classes dissimilatory nitrite reductase which yield NO as the sole product. These could be either have copper (CuNiR) or heme (Cd_1NiR) as cofactor; later being more abundant[232] will be discussed here in details.

Dissimilatory nitrite reduction to nitric oxide (by heme cofactor). The heme containing dissimilatory nitrite reductase, Cd_1NiR, as the name suggests, is composed of a heme-c and a heme d_1 cofactor (EC 1.7.2.1).

Enzyme architecture. Cd_1NiR (expressed from *nirS* genes)[176] is a homodimeric enzyme of the bacterial periplasm with each monomer being folded into two domains: (a) one α-helical N-terminal domain with a covalently attached heme c, and (b) one eight bladed β-propellar C-terminal domain containing heme d_1 in its core. Structures of Cd_1NiR from *Pseudomonas aeruginosa* (Fig. 13a)[233–235] and *Paracoccus pantotrophus*[236–239] have been extensively studied and their catalytic mechanism have also been probed using different theoretical and spectroscopic techniques. The heme-c moiety functions as electron acceptor from soluble electron carriers such as c-type cytochromes (cyt c_{550}, cyt c_{551} and cyt c_{554}) or copper proteins such as azurin or pseudoazurin[240–243] and transfers the electron to the heme d_1 which constitutes the enzyme active site (site of nitrite binding and reduction).[233,239] Heme d_1 (3,8-dioxo-17-acrylateporphyrindione) is unique to this class of enzyme distinguished from usual heme moieties by the presence of a partially saturated macrocycle and a set of oxo and acrylate substituents.[244]

P. aeruginosa Cd_1NiR (Pa-Cd_1NiR) in oxidised form (resting state) has the heme-c axially coordinated by His_{51}/Met_{88}, whereas heme d_1 is coordinated by His_{182} in the proximal position and by a hydroxyl group in the distal position. Distal site of the active site pocket constitutes residues such as Tyr_{10} (from the N-terminal arm of the adjacent partner monomer), two conserved histidines-His_{327} and His_{369}. Crystal structure of the oxidised form revealed that Tyr_{10} remains hydrogen bonded to the distal hydroxyl ligand of heme d_1. These distal residues presumably are involved in substrate binding and/or protonation.[234,246] Reduction of heme d_1 iron centre stimulates hydroxyl ligand release[245] which further induces a series of conformational changes. Displacement of a loop in heme c domain is followed by rotation of Tyr_{10} away from heme d_1 distal site and hydrogen bond formation between Thr_{59} and Gln_{11}.[233] All these changes in heme c domain of adjacent partner monomer exposes the heme d_1 active site for nitrite binding.[233,246]

In *P. pantotrophus* Cd_1NiR (formerly known as *Thisophaera pantotropha*) (Pp-Cd_1NiR), the oxidised state (as isolated form) has bis-histidine coordinated heme c (His_{17}/His_{69}) and heme d_1 is coordinated by His_{200} in the proximal position and by Tyr_{25} (from the same domain) at the distal site. Thus, the active site has closed coordination which implies that this as-isolated form is the 'inactive form' of the enzyme and is catalytically inert. Reduction of this enzyme results in movement of the N-domain loop causing structural rearrangement at both the heme centres. At heme c, His_{17} ligand is replaced by Met_{106} and the Tyr_{25} dissociates from the heme d_1 thus leaving the active site open for nitrite binding. Conserved His_{345} and His_{388} completes the active site.[236,239,247,248] Hence, redox energy driven conformational changes regulates the catalytic process. These conformational changes are very essential for the enzyme to transform into its 'active form' to perform its reductase activity. Thus, there is an 'on/off' mechanism for the regulation of the enzyme activity. Pa-Cd_1NiR Tyr_{10}Phe mutant is spectroscopically and functionally indistinguishable from the wild type enzyme.[249,250] The Pp-Cd_1NiR Tyr_{25}Ser mutant, has a coordination environment of the active site similar to that in steady-state catalytic condition, *i.e.*, its 'active form'.[240,251] These experimental findings suggest that the tyrosine residue, though do not have any role in catalysis may have been an intentional inclusion to regulate the 'on/off' mechanism.[176] The structural changes were also governed by the protonation states of the conserved histidine residues in the enzyme active site. It was found that the structure of reduced Pp-Cd_1NiR grown at pH 9.0[251] where the histidines are likely to be deprotonated were electrostatically analogous to the structure of oxidised Pa-Cd_1NiR with His–Ala mutants at pH 5.5–6.5.[234] This gave rise to another hypothesis that the structural conformation of the enzyme is guided by the overall charge in the active site pocket rather than the oxidation states of the heme centres only.[251]

Mechanism of nitrite reduction. The catalytic cycle of nitrite reduction by Cd_1NiR initiates with the reductive activation of the 'inactive form' (Scheme 20a and b). Initially, heme c of cFe^{III}–d_1Fe^{III} form (Scheme 20a) is rapidly reduced by external electron donors (such as cyt c_{551} or azurin) to cFe^{II}–d_1Fe^{III} form (Scheme 20b). In Pp-Cd_1NiR potentiometric titration potential

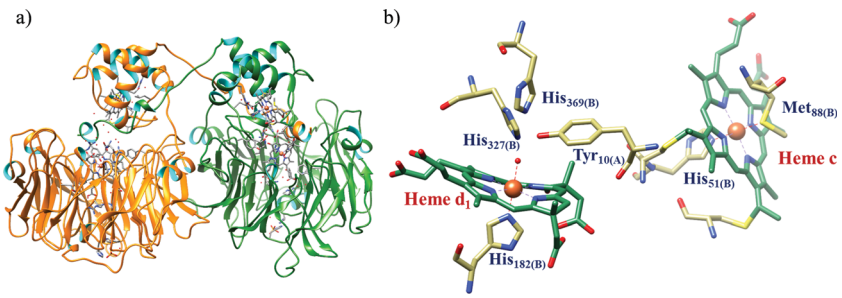

Fig. 13 (a) 3D ribbon representation of Cd_1NiR from *Pseudomonas aeruginosa* showing the homodimers and (b) active site structure of *P. aeruginosa* Cd_1NiR in oxidised form, heme c is also included participating in electron transfer to the active site. Both (a) and (b) are based on PDB 1NIR.[245]

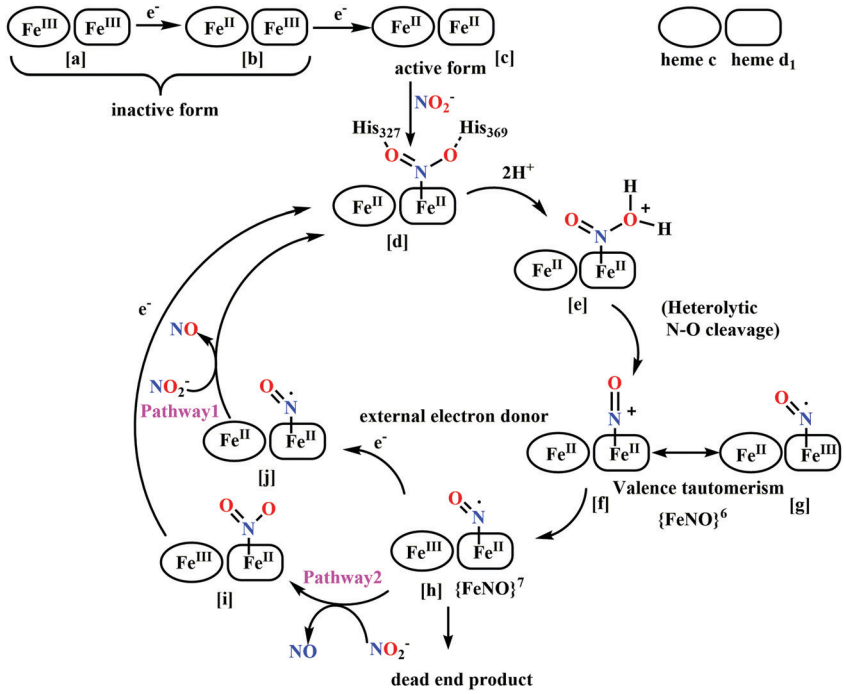

Scheme 20 Proposed reaction mechanism of Cd_1NiR.

in the reductive as well as oxidative directions (+60 mV and +210 mV, respectively) revealed hysteresis and cooperativity between the two heme centres.[248] The external electron donors have redox titration potential in the range of +250 mV,[252] hence electron transfer process *in vivo* is not clear. It was proposed that there may be some activation factor in bacterial periplasm or alternatively, the enzyme may function only when the ratio of reduced to oxidized electron donor proteins is very high.[253] Electron transfer from heme c to heme d_1 is coupled with conformational changes, generating the 'active form' of the enzyme. Heme c is replenished with electron from external electron donors resulting in fully reduced form: cFe^{II}–d_1Fe^{II} (Scheme 20c) which binds to the substrate.[254]

In Cd_1NiR, nitrite binds to the d_1Fe^{II} with high affinity.[234] Although nitrite shows 'nitrito' mode of binding in haemoglobin and myoglobin,[255–257] it exhibits a 'nitro' mode of binding in heme d_1 (Scheme 20d).[239] This mode of binding is also supported by proposed mechanism responsible for NO released. High affinity for nitrite can be explained by two factors (a) presence of two electron withdrawing oxo substituent in heme d_1 ring moiety and (b) electrostatic interactions with two protonated conserved histidine residues in the active site pocket.[246] Cyanide (an inhibitor ion) binding has been useful as a probe of the affinity of ferrous heme d_1 for anions and role of the protein residues in controlling ligand binding. It has been observed that in Pa-Cd_1NiR His_{369}Ala mutant, affinity for cyanide binding is 10-fold reduced. Due to reduced steric hindrance in the active site, CO binds to the mutant much faster than the wild type (WT) enzyme than the His_{369}Ala mutant.[235] Thus, overall positive electrostatic potential of the distal site is the dominant factor affecting the affinity of anionic ligand (CN^-, NO_2^-) which compensates for relatively weak affinity of ferrous heme iron towards anionic ligands.

The next step involves protonation at the oxygen atom and heterolytic N–O bond cleavage, resulting in release of a water molecule and $d_1\{FeNO\}^6$ formation (Scheme 20f and g). The two protonated histidine residues at the active site are well positioned to serve as the proton donors during catalysis[233–239,258,259] and their role has been verified by site directed mutational studies[234] and theoretical calculations.[260] It has been observed that both Pa-Cd_1NiR His_{369}Ala mutant and His_{327}Ala mutant lost nitrite reductase activity. However, effect of two residues are not equivalent. The His_{369} being at a shorter distance to both the oxygen atoms, play a more important role in stabilising the nitrite bound complex through hydrogen bonding.[234,235,260]

The last step of the catalytic cycle is NO dissociation which has been the subject of much debate over several decades. Earlier, the $d_1\{FeNO\}^6$ complex was considered to be a 'dead end' product supporting the fact that NO has very high association constants for binding to ferrous hemoproteins such as myoglobin and haemoglobin ($K_a \sim 10^{11}$–10^{12} M^{-1})[261] and cyt aa_3 oxidase ($K_a \sim 10^{10}$ M^{-1}).[262] So, NO was thought to be released from d_1Fe^{III}–•NO complex formed by intramolecular electron transfer from Fe^{II} to π*-orbital of NO (valence tautomerism) (Scheme 20f and g).[233,234,263] However, this hypothesis was never proven. Indeed, spectroscopic evidence of a long lived Pp-Cd_1NiR d_1Fe^{III}–NO exists in absence of excess reducing equivalents. Also, this NO dissociation from this adduct is not observed.[263,264] In addition, it was shown that NO is dissociated rapidly from reduced Pa-Cd_1NiR (k_{off} = 71 s^{-1}),[259,265] thus suggesting a reduced affinity of the ferrous heme d_1 towards NO ($K_a \sim 10^7$ M^{-1}) in contrary to other hemoproteins. These

conclusions on Pa-Cd_1NiR are also supported by the results of ultra-fast kinetic studies on Pp-Cd_1NiR which showed that intramolecular electron transfer from heme c to heme d_1 triggers NO release (Scheme 20, pathway 1).[254] Investigation of the reduction process of Pa-Cd_1NiR by pulse radiolysis technique provided kinetic evidence for negative cooperativity between two $d_1$heme sites of the dimeric enzyme and also suggested that intramolecular electron transfer from heme c to heme d_1 is highly regulated by an allosteric mechanism.[258,266,267] This can explain the requirement for two redox centres for Cd_1NiR functioning.[268] Hence, NO most likely is released from $d_1\{FeNO\}^7$. It is also established experimentally that nitrite reacts with reduced NO-bound Pa-Cd_1NiR and has NO dissociation at rates much faster than the catalytic turnover (Scheme 20, pathway 2).[265] Hence it can be concluded that Cd_1NiR efficiently catalyses nitrite reduction and NO release only in presence of substrate and electron donors on the vicinity of the active site. In absence of reductants, NO release is sluggish.[248,269–272]

A combination of very high field electron-nuclear double resonance (ENDOR) techniques and theoretical calculations on Pa-Cd_1NiR suggested that a dynamic and co-operative network of hydrogen bonds in the active site is also responsible for NO release. The structure obtained theoretically in best agreement with experimental findings reveal that the conserved His_{327} has no hydrogen bonds to the NO. Thus, the role of this residue is limited to maintaining positive electrostatic potential in the distal side of the active site. The d_1Fe–NO complex is hydrogen bonded to OH from Tyr_{10} and the protonated His_{369} residues. In Tyr_{10}Phe mutant-NO complex, the His_{369} residue moves closer to the NO, whereas mutation of both distal histidine residues with alanine displaces Tyr_{10} preventing hydrogen bond formation. This suggests cooperative behaviour for Tyr_{10} and His_{369}. Hence, these observations suggest that hydrogen bonding network in the distal active site is dynamic and the position and strength of the hydrogen bonds are closely dependent on each other.[273] All these factors act cooperatively along with the crucial contribution from unique electronic properties of heme d_1 cofactor.[237,274] Sperm whale apomyoglobin reconstituted with heme d_1 also releases NO at 4 orders of magnitude greater rate than common heme b myoglobin ($4\ s^{-1}$ *vs.* $2 \times 10^{-4}\ s^{-1}$).[268] Hence, the fast NO release is likely controlled by properties of heme d_1. Two spectroscopic evidences point to this. The magnetic data revealed that ferric heme d_1 has unusual low spin $(d_{xz,yz})^4(d_{xy})^1$ electronic ground state, completely different from the usual $(d_{xy})^2(d_{xz},d_{yz})^3$ protoheme ground state. This peculiar ground state results in the unpaired electron (HOMO) residing in the heme plane, whereas the filled orbitals (d_{xy} and d_{yz}) residing at the axial planes resulting in very weak π-interaction with NO π*-orbital forming weak Fe–NO bond as compared to NO bond with heme b.[237] Secondly, presence of the two electron withdrawing keto substituent and saturation at two pyrrolic centres, contributes to NO dissociation and tunes the reduction potential of iron in heme d_1 such that NO formed is not reduced further differentiating it from CcNiR. An important insight of the catalytic mechanism is the assignment of the rate determining step. In steady state turnover of nitrite, catalytic rate constant (k_{cat}) for Pp-Cd_1NiR is $72\ s^{-1}$,[269] which shows a higher value compared to $6\ s^{-1}$ in Pa-Cd_1NiR[259] at pH 7.0. Therate of intramolecular electron transfer, which triggers NO dissociation from heme c to heme d_1, is $\sim 1000\ s^{-1}$ in Pp-Cd_1NiR[263,275] and $3–6\ s^{-1}$ in Pa-Cd_1NiR.[266] Dissociation rate constant of NO (k_{off}) in Pp-Cd_1NiR is $65–200\ s^{-1}$ (ref. 268) and $6–35\ s^{-1}$ in Pa-Cd_1NiR.[259] Analysis of these kinetic parameters clearly indicate that in Pp-Cd_1NiR, k_{cat} is comparable to k_{off} of $\{[FeNO]\}^7$, hence probably NO dissociation is rate limiting step, whereas in Pa-Cd_1NiR k_{cat} corresponds to intramolecular electron transfer rate. Thus, in Pa-Cd_1NiR, d_1Fe(II) formation step is rate limiting followed by fast NO release.

Nitrite reductase activity of other metalloproteins. Several studies revealed that both haemoglobin (Hb) and myoglobin (Mb) have nitrite reductase activity with the capability to generate NO.[276–278] Such heme based nitrite reduction generally proceeds through N-bound nitrite complex as the starting point, similar to that observed for bacterial NiRs. Mechanistic studies revealed that such reduction pathway proceeds to the formation of $\{FeNO\}^7$ complexes of Hb or Mb (eqn (7) and (8)).[277]

An alternative possible reduction pathway through O-bound complex was first explored by Radu Silaghi–Dumitrescu in Cd_1NiR.[279] Theoretical calculations suggested that this reaction proceeded through a protonation from distal histidine residue leading to formation of hydroxo–Fe(III) complex and NO. Similar mechanism is also suggested for nitrite reduction by Mb^{II} and Hb^{II} (Scheme 21).[276] Several other instances of metalloprotein-based nitrite reduction to NO have been reported in recent years.[278,280–287]

$$Mb^{II} + NO_2^- + H^+ \rightarrow NO + Mb^{III} + OH^- \quad (7)$$

$$Mb^{II} + NO \rightarrow Mb^{II}\text{–}NO \quad (8)$$

Challenges and general outlook. A single reaction (nitrite reduction) has been handled in nature by three different pathways utilising three completely different heme architectures. The chemistry behind the functioning of any enzyme active site is governed by both the primary coordination environment of the cofactors as well as the protein amino acid residues constituting the secondary environment. This chemistry is difficult to mimic in model complexes as it is difficult to design the exact protein ambiance outside a protein matrix. While selective roles of some of the residues can be probed, recreating the overall catalytically relevant protein architecture in a synthetic construct is a dauntic task. Detailed investigation of the synthetic analogues mimicking the cofactor structure, can however be equally important in predicting and/or reproducing the fundamental aspects of structure, spectroscopy, magnetic and electronic structure and chemical reactivity of the biological systems. These are discussed in he following sections.

Nitrite reductase model complexes

First generation models comprise iron-porphyrin complexes which could rationally explain oxidation states, coordination

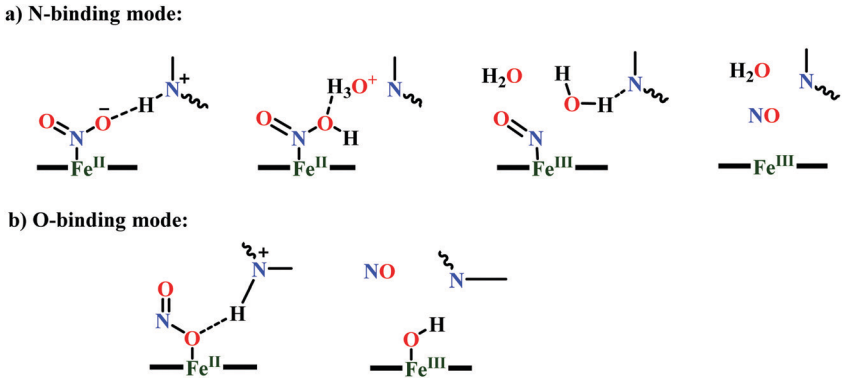

Scheme 21 Proposed NO generation mechanisms catalysed by Hb.

nature, identity of donor ligands, the ligation alternatives at the active site. Structural, spectroscopic and electrochemical characterisation of these led to logical designing of second-generation models to incorporate some feature of the enzyme, as has been understood from enzymatic studies. Blueprint of a third-generation model systems must include the consideration of the roles of basic residues residing in the enzyme active site.

Solution chemistry of nitrite

Nitrite is the conjugate base of nitrous acid having pK_a of 3.16 at 25 °C.[288] This implies that at physiological pH, nitrite exists completely in its ionic form. The aqueous chemistry of nitrite is highly pH dependent, same has been observed in enzyme systems. One electron reduction of nitrite to NO requires two equivalents of acid, hence nitrous acid is oxidising in nature at very low pH, whereas reduction potential of nitrite to NO drops to 0.37 V at pH 7.0 and becomes energetically uphill at higher pH.[289]

$$HNO_2 + H^+ + e^- \rightarrow NO + H_2O \text{ (at pH} < 3) \quad E^\circ = 0.99 \text{ V (}vs.\text{ NHE)} \quad (9)$$

$$NO_2^- + 2H^+ + e^- \rightarrow NO + H_2O \text{ (at pH} = 7) \quad E^\circ = 0.37 \text{ V (}vs.\text{ NHE)} \quad (10)$$

$$NO_2^- + H_2O + e^- \rightarrow NO + 2OH^- \text{ (at pH} > 7) \quad E^\circ = 0.46 \text{ V (}vs.\text{ NHE)} \quad (11)$$

NiR model complexes

Several metalloporphyrin complexes having coordinated nitrite ion have been characterised. We addressed the model complexes developed and characterised in a chronological order and based on their relevance in the catalytic cycle of nitrite reduction reaction.

Nitrite binding. Three linkage isomers are possible for nitrite binding to mononuclear metal complexes (Fig. 14). When NO_2^- coordinates *via* N-atom, M–NO_2^- is called 'nitro' mode of binding while coordination through a single O-atom, M–ONO^- is termed as 'nitrito' complex. Alternatively, NO_2^- can be coordinated in a bidentate fashion *via* both the oxygens.[290]

The structures reported for heme containing nitrite reductases have been limited to 'nitro' binding mode despite the differences in proximal ligation to heme (*e.g.*, Lys for CcNiR, μ-SCys for CSNiR and His for cyt cd_1NiR), nature of macrocycle (heme c *vs.* siroheme *vs.* heme d_1) and different basic residues in distal heme pocket.[175,239,291] It is also interesting to find from the crystal structures of nitrite ligated synthetic iron porphyrin complexes that both Fe^{II} (ref. 292) and Fe^{III} (ref. 293–295) binds *via* N-atom (Fig. 15).[209,296] [(TpivPP)Fe(NO_2)(NO)]$^-$ has been an exceptional complex where both nitro and nitrito mode of binding have been observed in same crystal due to disorder in nitrito group.[297]

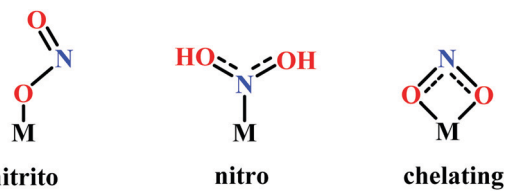

Fig. 14 Nitrite ligand binding modes in monomeric complexes.

Photoirradiation of (TPP)Fe(NO)(NO_2) resulted in linkage isomerism of nitrite to its nitrito form.[298,299] Such nitrito binding has also been observed in crystal structures of other metalloporphyrin nitrite complexes of Mn,[300] Ru[301,302] and Os.[303,304] First instance of nitrito mode of binding to a heme protein was for horse heart Fe^{III}–Mb (Mb^{III}) and its derivatives[256,257,305] and Fe^{III}–Hb or deoxy–Hb(Hb^{III}).[255] Once bound to nitrite, all these complexes form low spin iron centres. When a crystal structure is not available, differentiation of the binding modes can be easily done by infrared vibrational spectroscopy. For nitro complexes, the antisymmetric and symmetric stretching modes are ν_a (NO_2) = 1470–1370 cm^{-1} and ν_s (NO_2) = 1340–1290 cm^{-1}, respectively and for nitrito mode, ν_a (NO_2) = 1510–1400 cm^{-1} and ν_s (NO_2) = 1100–900 cm^{-1}.[290,306]

Reductions in the presence of protons and electrons. If we consider nitrite reduction in biology, both CcNiR and CSNiR

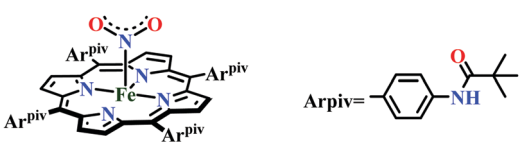

Fig. 15 Molecular structure [(TpivPP)Fe(NO_2)]$^-$.

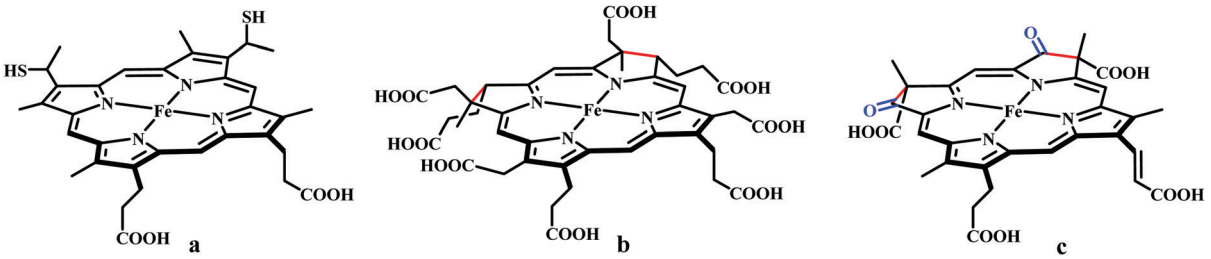

Fig. 16 Structure of (a) heme c in CcNiR, (b) siroheme in CSNiR and (c) heme d_1 in Cd_1NiR. The saturated pyrrolic centres and electron withdrawing groups are highlighted in red and blue respectively.

reduces nitrite to ammonium ion (NH_4^+) directly without involving the release of any intermediate in both dissimilatory and assimilatory pathways. However, Cd_1NiR reduces nitrite to NO, which is then released as a part of dissimilatory denitrification reaction. In all these enzymes, the substrate is reduced after binding to the iron centres of different heme cofactors (heme c in CcNiR (Fig. 16a), siroheme in CSNiR (Fig. 16b) and heme d_1 in Cd_1NiR (Fig. 16c)) in their active site, all of them involving heme c (except Fe_4S_4 in CSNiR) as their electron transfer partners. The peptide residues in the distal site has a steering role in directing the substrate to the active site, stabilising it by hydrogen bonding interactions and then assist in protonation of the substrate and subsequent release of a molecule of water. This is common to all the three enzymes, resulting in $\{FeNO\}^6$ intermediate. From this point on the further reaction both in CSNiR and CcNiR takes up electrons and protons to result in ammonium ion formation whereas Cd_1NiR forms $\{FeNO\}^7$ through an electron transfer from heme c, resulting in NO release with concomitant nitrite binding thus proceeding to another cycle of nitrite reduction. While detailed protonation and electron transfer steps of CSNiR $\{FeNO\}^6$ have not yet been explored, for CcNiR, $\{FeNO\}^7$ formation is avoided through two consecutive PCET steps generating $\{FeHNO\}^8$.

Several iron porphyrin-based nitrite reductase model complexes have been synthesised and their structural, spectroscopic, magnetic and electronic properties have been explored. Electrochemical investigations also gave some interesting results. The first area of focus was the differences in the heme backbone structure (Fig. 16) *i.e.*, (a) heme c in CcNiR which is a substituted porphyrin macrocycle (Fig. 16a), (b) siroheme in CSNiR which has isobacteriochlorin unit with two saturated β-pyrroles (four sp^3 hybridized peripheral carbons)[224] (Fig. 16b) and (c) heme d_1 in Cd_1NiR which has an isobacteriochlorin macrocycle with two electron withdrawing oxo substituent and two saturated β-pyrroles (two sp^3 hybridized peripheral carbons)[307] (Fig. 16b). Hence, the divergent reactivity may stem from differences in structures of Fe-porphyrinoid macrocycles. To explore this possibility, several model complexes were synthesized (Fig. 17), characterized and electrochemistry of those complexes were investigated by several groups.[296,308–316]

It was observed that nitrite bound complexes of these models were unstable to examine its transformation to $\{FeNO\}^6$.[292,294] But ferrous-nitrosyl adducts $\{FeNO\}^7$ of these complexes were stable and thus $\{FeNO\}^6$ could be prepared by one electron oxidation of $\{FeNO\}^7$. Hence, the electrochemistry of nitrosyl adducts have also been explored as well (Table 2).[210,211,317–320]

Under coulometric conditions, reduction of nitrosyl adducts of most iron porphyrins proceeded exclusively to ammonia, mediated by hydroxylamine bound species.[212,321–327] This was verified from reduction reaction of bis(hydroxylamine) complexes which yield ammonia in presence of excess hydroxylamine (eqn (16)). The rate of hydroxylamine formation was related directly to the basicity of $\{FeNO\}^8$ complexes (eqn (12) and (13)). Changes in macrocycle moiety had a vast influence on the rate and was accelerated in hydroporphyrins and were slower in oxoporphyrins. $Fe(P)(NH_2O^+)$ (eqn (14)) was readily formed in siroheme model Fe(2,4 DMOEiBC) (Fig. 17k) whereas its formation was least favourable in heme d_1 model Fe(2,4-dioxoOEiBC) (Fig. 17l). It produces NO/N_2O rather than ammonia.[327]

$$Fe(P)(NO) + e^- \rightarrow Fe(P)(NO)^-, \quad \text{where } [Fe(P)(NO) = \{FeNO\}^7] \tag{12}$$

$$Fe(P)(NO)^- + H^+ \rightarrow Fe(P)(HNO) \tag{13}$$

$$Fe(P)(HNO) + H^+ \rightarrow Fe(P)(H_2NO^+) \tag{14}$$

$$Fe(P)(H_2NO^+) + H^+ \rightarrow Fe(P)(NH_2OH) \tag{15}$$

$$2Fe(P)(NH_2OH)_2 + NH_2OH \rightarrow Fe(P)(NO) + 3NH_3 + 3H_2O \tag{16}$$

Fe(OEP)(HNO) complex can be chemically generated by protonation of $\{FeNO\}^8$ with weak acids such as chloro-substituted phenol which is stable over few hours.[326] Since $\{FeHNO\}^8$ is highly reactive, earlier it could only be transiently observed in protected environments as in proteins,[323,324] bis-picket fence porphyrins.[325] Thus $\{FeHNO\}^8$ intermediates could also be stabilised in electron rich porphyrin-nitrosyl complexes.

Reaction pathways of $\{FeHNO\}^8$ hence formed may also include disproportionation to $\{FeNO\}^7$ and H_2 (eqn (17)) observed for FeTPP[212] (Fig. 17a) or a cross reaction involving reduction of $\{FeHNO\}^8$ (eqn (18)). Reduction of $Fe^{II}(TFPPBr_8)NO$ ($TFPPBr_8$ = 2,3,7,8,12,13,17,18-octabromo-5,10,15,2-tetrakis-(pentafluorophenyl)porphyrin, Fig. 18) with cobaltocene yields a stable $\{FeNO\}^8$ complex $[Co(C_5H_5)_2]^+[Fe(TFPPBr_8)NO]^-$. This complex was isolated and characterised, giving an exclusive example of stabilised $\{FeNO\}^8$ intermediate, which is otherwise elusive. In the presence of strong acid such as triflic acid, it disproportionated to $\{FeNO\}^7$ and H_2, in a pathway observed earlier, without any direct evidence of mediation by a $\{FeHNO\}^8$

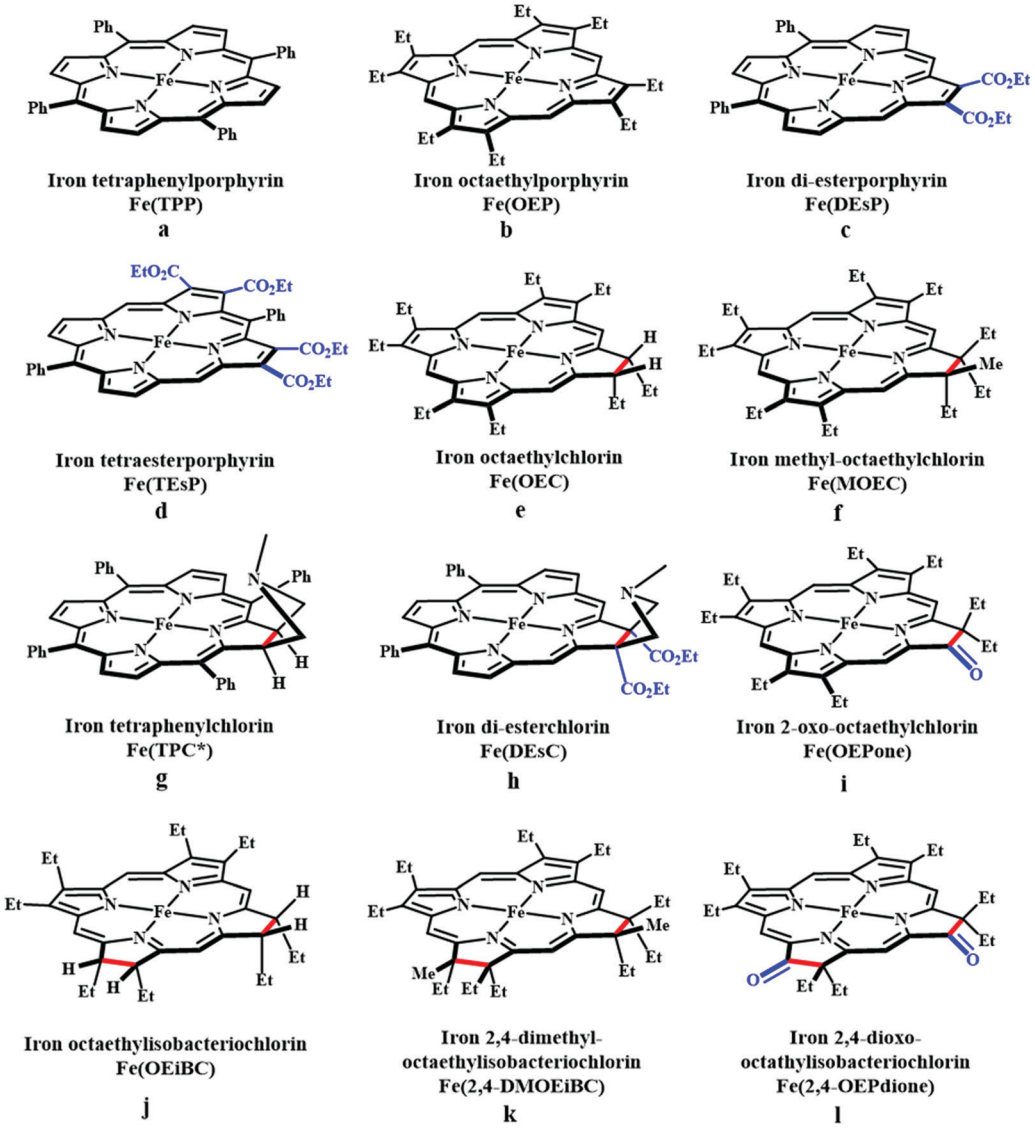

Fig. 17 Molecular structures of heme based nitrite reductase model complexes. The saturated pyrrolic centres and electron withdrawing groups are highlighted in red and blue respectively. (j) and (k) Closely resembles siroheme structure and (l) resembles heme d_1 structure.

species (eqn (19)).[328] Electrochemistry of the reported heme-nitrosyl adducts also helped in understanding the electronic structure of the various heme model complexes.

$$2Fe(P)(HNO) \rightarrow 2Fe(P)(NO) + H_2 \quad (17)$$

$$Fe(P)(HNO) + Fe(P)(NO)^- \rightarrow Fe(P)(HNO)^- + Fe(P)(NO) \quad (18)$$

$$2[Co(C_5H_5)_2]^+[Fe(TFPPBr_8)(NO)]^- + 2CF_3SO_3H \rightarrow 2[Fe(TFPPBr_8)(NO)] + H_2 + 2CF_3SO_3^- + 2Co(Cp)_3^+ \quad (19)$$

A closer look at Table 2 reveal a clear trend observed in reduction potential of both the oxidation process ($\{FeNO\}^{6/7}$ couple) and reduction process ($\{FeNO\}^{7/8}$ couple). Insertion of EWGs to the β-pyrrolic position shifted the redox couples to higher potential (for Fig. 17c and d). Conversely, saturating the pyrroles, *i.e.*, making β-pyrrolic carbons sp^3-hybridised had a reverse effect, shifting the redox couples to lower potentials (for Fig. 17e–h, j and k). Oxidation of $\{FeNO\}^7$ complexes of oxoOEC and dioxoOEiBC resultes in a porphyrin π-cation radical generation whereas in OEP, the oxidation is metal centered.[319] A very interesting work was done by Meyer and co-workers, who employed a water soluble porphyrin $[Fe(III)(H_2O)(TPPS)]^{3-}$ (TPPS = (*meso*-tetrakis(*p*-sulfonatophenyl)porphyrin)), Fig. 19 in mildly aqueous acidic solution to electro-reduce nitrite to ammonia (eqn (20)–(22)), with N_2O and hydroxylamine as side product. This reaction was highly pH dependent. Although, comprehensive mechanism of the reaction is not understood clearly, this may be considered as a structural and functional model of CcNiR.[321,330]

$$[Fe(H_2O)(TPPS)]^{4-} + HONO + H^+ \rightarrow [Fe(TPPS)(NO^+)]^{3-} + 2H_2O \quad (20)$$

Table 2 Reduction potentials of reported heme-nitrosyl adducts in various solvents

Complex	Solvent	$E\{FeNO\}^{6/7}$ (V) *vs.* SCE	$E\{FeNO\}^{7/8}$ (V) *vs.* SCE	Ref.
Fe(TPP)(NO)	DCM	0.74	−0.93	211
Fe(OEP)(NO)	DCM	0.71	−1.02	320
	THF	0.66	−1.07	320
	Butyronitrile	0.63	−1.08	317
Fe(DEsP)(NO)	DCM	0.83	−0.75	329
Fe(TEsP)(NO)	DCM	0.87	−0.65	329
Fe(TPC*)(NO)	DCM	0.45	−1.02	329
Fe(OEC)(NO)	Butyronitrile	0.48	−1.08	317
Fe(MOEC)(NO)	DCM	0.59	−1.02	320
	THF	0.64	−1.06	
Fe(OEPone)(NO)	DCM	0.76	−0.81	319 and 320
	THF	0.76	−0.86	320
Fe(DEsC)(NO)	DCM	0.59	−0.93	329
Fe(OEiBC)(NO)	Butyronitrile	0.22	−1.11	317
Fe(2,4-DMOEiBC)(NO)	DCM	0.34	−1.17	320
	THF	0.38	−1.16	
Fe(2,4-OEPdione)(NO)	DCM	0.74	−0.69	319 and 320
	THF	0.80	−0.80	

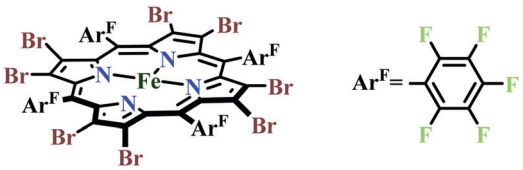

Fig. 18 Molecular structure of Fe(TFPPBr$_8$).

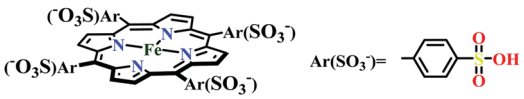

Fig. 19 Molecular structure of $[Fe(III)(TPPS)]^{3-}$.

$$[Fe(TPPS)(NO^{+})]^{3-} + 2e^{-} \rightarrow [Fe(TPPS)(NO^{-})]^{5-} \quad (21)$$

$$[Fe(TPPS)(NO^{-})]^{5-} + 4e^{-} + 5H^{+} \rightarrow [Fe(TPPS)(NH_3)]^{4-} + H_2O \quad (22)$$

In another related investigation the binding constants for NO to pyridine bound ferrous porphyrins (Table 3) to form $\{FeNO\}^7$ for porphyrins and hydroporphyrins was substantially small compared to very high values for oxoporphinone and porphinedione. Hence, enhanced histidine coordination to heme d_1 may play a role in NO release.[320]

Fe(III)-porphyrin complexes with NH_3 as a ligand has been reported but not structurally characterised, magnetic studies reveal Fe^{III} low spin state. Ammonia as is weakly bound and have a strong tendency to hydrolyse. This observation is relevant with release of NH_3 during the turnover of nitrite reductase catalytic cycle.[332]

Table 3 Formation constants for pyridine coordination to $\{FeNO\}^7$

Complex	Solvent	$K_{(complex)(py)}$	Ref.
Fe(TPP)(NO)	Ethylene chloride	0.7	331
Fe(OEP)(NO)	THF	~0.3	320
Fe(MOEC)(NO)	THF	1.1–0.1	320
Fe(OEPone)(NO)	THF	4.8 ± 0.2	320
Fe(2,4-DMOEiBC)(NO)	THF	~0.3	320
Fe(2,4-OEPdione)	THF	88 ± 3.0	320

It has been recently reported that presence of EWGs on the periphery of porphyrin macrocycle (Fig. 17c, d and h) lowers the energy of porphyrin π*-orbitals. This results in competitive back-bonding from filled dπ-orbitals of iron between porphyrin π*-orbitals and NO π*-orbitals, weakening the Fe–NO adduct formation.[333] This observation is evident from the analyses of the NO stretching frequencies (Table 4) (ν_{NO}) reported for $\{FeNO\}^7$ complexes reported till date.

Complexes having higher ν_{NO} for $\{FeNO\}^7$ systems tend to release NO easily owing to weaker Fe–N bond (Fig. 20 and 21). This can be rationalised by the fact that stronger backbonding with porphyrin π* will reduce backbonding to NO π*. This effect also tunes the pK_a and coherently affect the thermodynamics of the next reaction; NO release or a PCET step to $\{FeHNO\}^8$. In heme c, ν_{NO} for $\{FeNO\}^7$ is lower (1651–1671 cm^{-1}), suggestive of disfavoured NO release, as has been the case in CcNiR.[339] Aspects of facile PCET at this step has been recently reported for a series of model complexes where the effect of saturating the pyrroles and role of EGW were systematically investigated.[329] It has been discussed that for PCET to be facile, the bond dissociation free energy (BDFE) of the N–H bond on $\{FeHNO\}^8$ should be high. This report was first to evaluate the N–H BDFE involved in the PCET to $\{FeNO\}^7$ species.[340] The BDFE of N–H bond in $\{FeHNO\}^8$ can be calculated using the following equation:[341]

$$BDFE_{NH} = 1.38pK_a + 23.06E^{\circ} + C \quad (23)$$

where the pK_a was that of $\{FeNO\}^8$ species, which was calculated from the change in Gibb's free energy, ΔG° of the protonation equilibrium step. E° represents the one-electron reduction potential of the $\{FeNO\}^{7/8}$ redox process, which was directly obtained from the cyclic voltammogram. C is a constant which depends on the solvent.[341]

The ΔG° of protonation was computed using DFT calculations. The calculated $BDFE_{NH}$ values revealed that the protonation of $\{FeNO\}^8$ species gradually became less favorable from FeOEP to FeOEPone to Fe(2,4-OEPdione). This was consistent with the previously reported trend for nitrite reduction to ammonia, using moderately strong acids like phenols, under controlled potential electrolysis, *i.e.*, the rate of the reaction:

Table 4 N–O bond stretching frequency (ν_{NO}) in cm^{-1}

Complex	$\{FeNO\}^6$ (6C)	$\{FeNO\}^7$ (6C)	$\{FeNO\}^8$	Ref.
Fe(TPP)(NO)	1844 (1914)	1676 (1626)	1496	329 and 338
Fe(OEP)(NO)	1862	1670	1441	338
Fe(DEsP)(NO)	(1923)	1686 (1641)		329
Fe(TEsP)(NO)	(1927)	1688 (1646)	1550	329
Fe(TPC*)(NO)	—	1680 (1635)	—	329
Fe(OEC)(NO)	—	1670	—	317
Fe(OEPone)(NO)	1720	1662 (1916)	1442	318, 319 and 338
Fe(DEsC)(NO)	—	1691 (1633)	1537	329
Fe(OEiBC)(NO)	—	1670	—	317
Fe(2,4-OEPdione)	1700	1665 (1916)	1442	318, 319 and 338
Fe(TFPPBr$_8$)(NO)	—	1726	1547	328

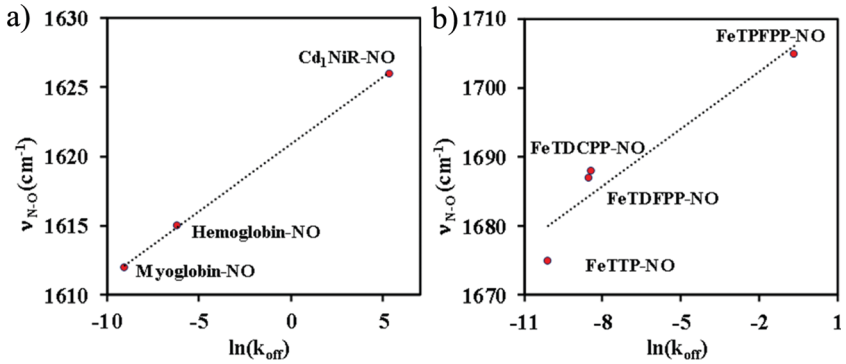

Fig. 20 Correlation between N–O stretching frequency and rate of NO dissociation: (a) in six-coordinate heme nitrosyls in enzyme systems;[334–336] (b) in synthetic Fe-porphyrin nitrosyl complexes, TTP (*p*-tolyl), TDFPP (2,6-difluorophenyl), TDCPP (2,6-dichlorophenyl), TPFPP (pentafluorophenyl).[337]

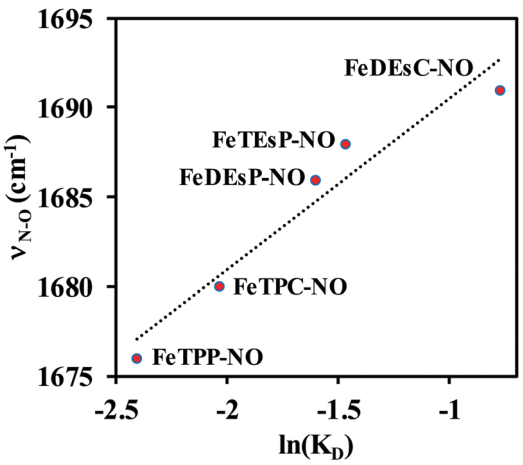

Fig. 21 Correlation between experimentally measured N–O stretching frequency and NO dissociation constant in model complexes.

FeOEP > FeOEPone > Fe(2,4-OEPdione), where the protonation of {FeNO}^{8} species was proposed to be the rate-limiting step.[327]

Hence, it can be concluded that the E° and pK_a of the {FeNO}^{7} species determine the thermodynamics of the PCET step or those of the competitive NO dissociation step. The presence of EWGs along with saturated pyrrolic centres result in weak BDFE$_{NH}$; probably explaining the role of heme d_1 in Cd_1NiR. On the contrary, higher values of BDFE$_{NH}$ resulting from balance between E° and pK_a is responsible for facile PCET to {FeNO}^{7} producing {FeHNO}^{8} which eventually proceeds to NH_4^+ formation and release relevant to CcNiR mechanism.

In this section, heme containing nitrite reductase enzymes and their structural and mechanistic aspects were discussed. The role of basic residues was highlighted, which has already been explored in details in the enzymes. Next, the different results based on synthetic model complexes were discussed. It is observed from the literature that main focus till now has been on the understanding of the role played by the different macrocyles employed by nature for nitrite reduction reaction. In the future more studies with reconstituted enzyme active site needs to be done. This may give a holistic view of the observed differences in the mechanistic pathways. Also, synthesis of tailor-made model complexes with a secondary structure is necessary for a deeper understanding of the roles played by proton transfer and electron transfer residues in nitrite reduction reaction to get more control of the fate of this reaction in an artificial setting. While the large structural changes responsible for the on–off switch may be difficult (or impossible) to mimic in artificial systems, the roles played by tyrosine, arginine, lysine and hstidines can definitely be understood better.

H_2 and H^+ interconversion

Introduction

Hydrogen is the most abundant element in the Universe but in Earth it is in the tenth position, as molecular H_2 being a light gas escapes easily into space.[342] Most of the hydrogen is fixed in the form of strong bonds with other elements like C, N and O. For example, the reaction of H_2 with O_2 releases substantial energy.

$$2H_2(g) + O_2(g) \rightarrow 2H_2O(l), \quad \Delta H^\circ = -286 \text{ kJ mol}^{-1} \quad (24)$$

Hydrogen can be used as a fuel, due to its high enthalpy of combustion (-143 kJ mol^{-1}) or as an energy vector in a fuel cell and heralds a potential and much sought-after eco-friendly alternative to the conventional fuels.[343,344] Furthermore, if H_2 can be obtained *via* electrochemical splitting of H_2O the resulting renewable energy cycle can be sustainable. But H_2 also has some notable disadvantages when practical implementation is considered, such as (i) low solubility in water limits its availability as an energy source in an aqueous medium, (ii) H_2 gas being very light is difficult to store.[345] The reverse of the above reaction (eqn (24)) *i.e.*, water splitting, occurs extremely rapid through a radical chain mechanism but the reaction is energetically uphill with a high ΔG° value of 237 kJ mol^{-1} and also associated with a large kinetic barrier.[346,347] Thus, it is not easy to reduce H_2O to form H_2 without a catalyst. A potential hydrogen fuel economy is suffering from the availability of efficient and robust catalysts that can generate hydrogen from easily available water source.[348–350] Metallic platinum and its alloys can efficiently produce H_2 from the water with very low overpotential,[351] but those are rarely available[352] and very expensive. The scarcity and cost of the platinum, has attracted immense interest to search for cheap alternative catalysts for hydrogen evolution.[142,352,353]

Lessons from Nature

In nature, many lower microorganisms *e.g.* algae and bacteria[354–357] have the capability either to pull out electrons from hydrogen molecules to carry out their metabolic processes or to reduce protons to hydrogen by removing electrons. In these microorganisms, the inter-conversion between hydrogen uptake and release is efficiently mediated by a class of enzymes, known as hydrogenases. Hydrogenases are class of a metalloenzyme[354,355,358] that can efficiently convert proton to hydrogen reversibly with minimum overpotential with a turnover rates of 10^2–10^4 mol s^{-1} for per mole of the enzyme.[345,359–362] Hydrogenases are widespread in nature and they occur in bacteria, archaea, and some eukarya.[354–357] These enzymes catalyse the interconversion of H_2 to H^+ and participate in various physiological processes *e.g.* sulfate reduction, nitrate reduction, carbon dioxide reduction, *etc.*[363]

$$\frac{1}{2}H_2 \rightarrow H^+ + e, \quad E = -0.059pH \qquad (25)$$

It is believed that initially the atmosphere of Earth was hydrogen rich. So, it was expected that hydrogenases were matured to produce energy as a form of molecular H_2. Thus, hydrogenases can either assist the lower microorganisms to survive under such conditions or to organise the ecosystem where energy transfer was mediated by H_2.[355] These molecular H_2 driven microorganisms have been found mainly in deep-sea levels where the other sources of energy (*e.g.* photosynthesis) are unavailable. Based on these the main role of hydrogenases is thought to be energy production, and this can be enough to sustain an entire ecosystem. In O_2-poor wetland soil and submerged sediments, H^+ ions are important electron acceptors and H_2 is produced by hydrogenase action in fermentative bacteria.[364] Hydrogen is also produced by algae and cyanobacteria that under certain conditions use hydrogenases to consume electrons produced by photosynthesis.[365,366]

Types of hydrogenases

Based on their metal content, hydrogenases are classified into three classes namely [FeFe]-hydrogenase (Fig. 22), [NiFe]-hydrogenase (Fig. 23), and [Fe]-hydrogenase (Fig. 24).[345,367–369] Among them [NiFe]-hydrogenases are the most abundant in nature and biased towards hydrogen oxidation whereas [FeFe]-hydrogenases are most selective towards proton reduction.[355,363,368] The third class, [Fe]-hydrogenase or 5,10-methenyltetrahydromethanopterin dehydrogenase (Hmd) is mainly found in methanogens. Only in the presence of a hydride acceptor/donor substrate it reacts with H_2 or produce H_2.[367,370,371]

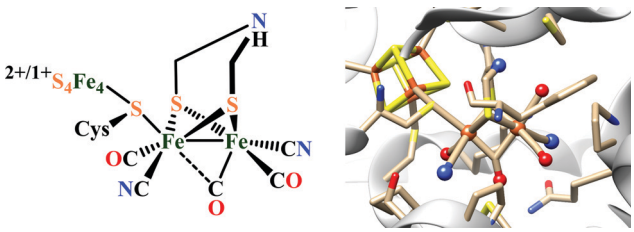

Fig. 22 Schematic representation (left) and X-ray crystal structure (right) of the'H-cluster' in the H_{ox} state, found in [FeFe]-hydrogenase (PDB ID: 3C8Y[386] with modification of the bridgehead atom from oxygen to nitrogen).

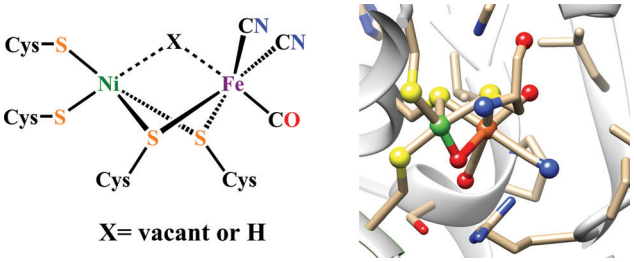

Fig. 23 Schematic representation (left) and X-ray crystal structure (right) of the [NiFe]-hydrogenase (PDB ID: 1WUJ[402]) active site.

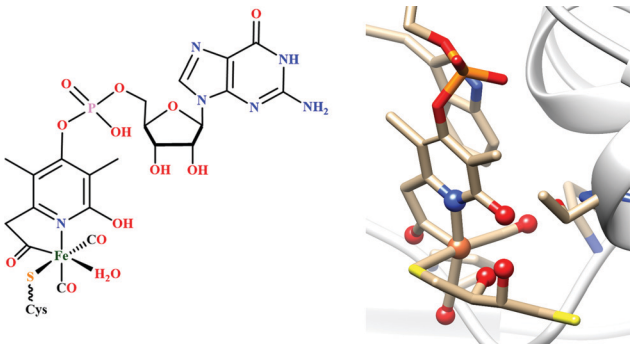

Fig. 24 Schematic representation (left) of the [Fe]-hydrogenase active site with the Hmd cofactor, and the X-ray crystal structure (right) of the mono-iron complex obtained from the cysteine 176 mutant (PDB ID: 3H65[406]).

Structure and activity of [FeFe]-Hydrogenases

The X-ray crystal structures of the [FeFe]-hydrogenases, particularly from *Clostridium pasteurianum* and *Desulfovibrio desulfuricans*, reveal the structure of this class of enzymes.[372,373] The active site of [FeFe]-hydrogenase contains a unique dinuclear [2Fe] sub-cluster which is covalently linked by a cysteine sulphur to a [4Fe–4S]-cluster, thus forming the H-cluster. The Fe_4S_4 cluster acts as a source of electrons required for H^+ reduction. Both X-ray crystallographic[372,373] and infrared spectroscopic[374,375] investigations confirmed that each of the two Fe centre contains one CN^- and one CO ligand, both in a terminal binding mode. Whereas, an additional CO ligand is found to be bridging between both Fe atoms, in the oxidised H_{ox} state of the H-cluster. The H_{ox} state can be described as low spin Fe(II)Fe(I) state with spin state $S = 1/2$[376,377] and a Fe_4S_4 cluster in the oxidized and diamagnetic $[4Fe–4S]^{2+}$ state.[378] The strong π acidic CO and CN^- ligand stabilizes the low oxidation states of Fe by metal to ligand backbonding. The two diiron cores bridged by a dithiolate ligand, whose composition is matter of debate. From X-ray crystallographic data it is proposed to be $–SCH_2XCH_2S–$, where X can be nitrogen (–NH, adt), oxygen (O, odt), carbon (C, pdt) and a azadithiolate bridge is considered as the most likely.[379] Furthermore,[14]N quadruple analysis and EPR spectroscopy support this hypothesis.[380–382] The proximal

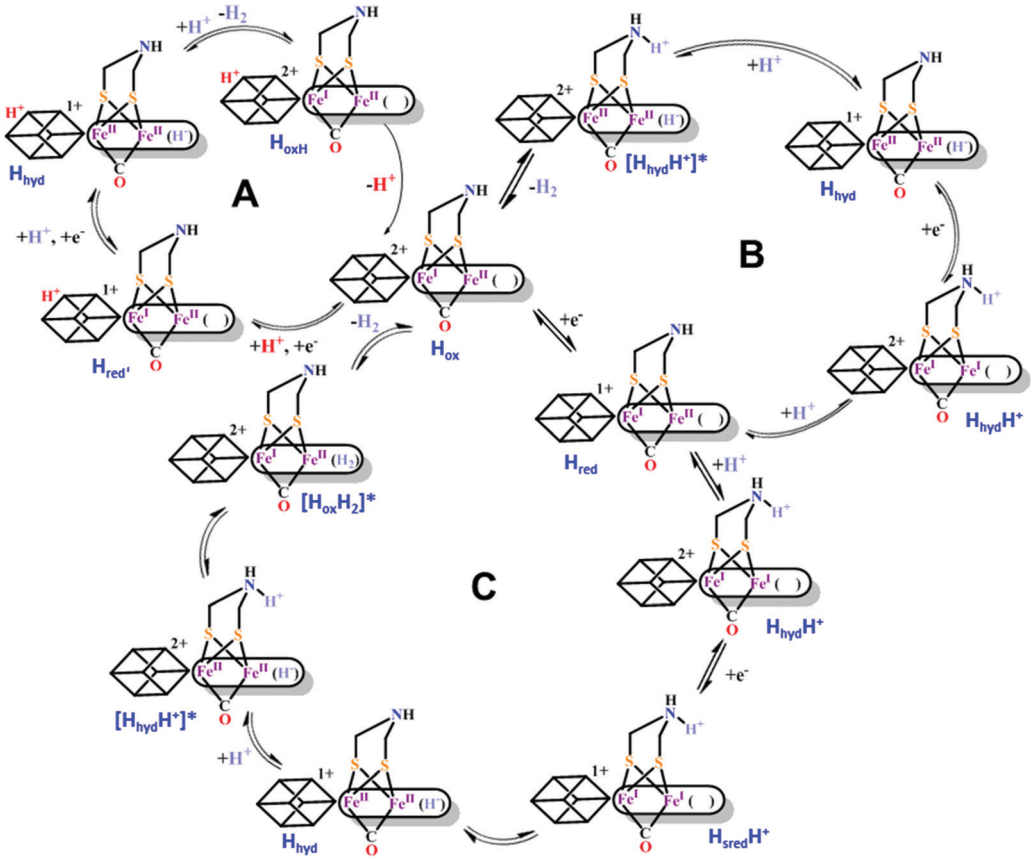

Scheme 22 Proposed catalytic cycles for reversible H^+ reduction by [FeFe]-hydrogenases.[387–390]

iron (Fe_p) is directly bound to the [4Fe–4S] cluster and is coordinatively saturated. Whereas the distal iron (Fe_d) has a vacant coordination site where the substrate (H_2 or H^+) may bind as well as inhibitors like O_2 and CO. Recent spectroelectrochemical investigations reveal that the Fe(I)Fe(I) state of the enzyme binds the first proton at the bridgehead nitrogen atom.[383,384] Then successive reduction and proton rearrangement results in the formation of Fe(II)Fe(II)–H^- species.[385] At the bridgehead nitrogen atom, the second protonation occurs, which is well oriented to couple with the hydride, to release H_2 (Scheme 22).

Structure and activity of [NiFe]-Hydrogenases

Structural characterization of the [NiFe]-hydrogenases disclosed that these enzymes consist of a large subunit containing the [NiFe] active site and a small subunit containing three FeS clusters,[391,392] which connects the active site of the enzyme to the surface of the protein and acts as an electron transport chain from the [NiFe] site to the electron acceptor cytochrome c_3.[393] Crystal structures of the hydrogenase show a [3Fe–4S] cluster in the centre of the chain, a [4Fe–4S] cluster close to the surface of the protein and a [4Fe–4S] cluster located approximately 13 Å away from the active site.[394] The dinuclear active site contains two metal ions, Ni and Fe, bridged by two cysteine thiolates. Ni has two additional thiolates as terminal ligands and Fe is coordinated by one CO and two CN^- ligands.[391,392,395] Electron paramagnetic resonance spectroscopy and infrared spectroscopic techniques has revealed different possible redox states of the active site.[396] Previously it was believed that only three intermediate species are involved in the catalytic cycle. The resting diamagnetic Ni-SI_a species ($Ni^{II}Fe^{II}$) takes up one electron and one proton to give the paramagnetic Ni-C state ($Ni^{III}\mu(H)Fe^{II}$).[397,398] The diamagnetic Ni-R state ($Ni^{III}\mu(H)$-Fe^{II})[399,400] is generated from the Ni-C state upon one electron reduction. Ni-R undergoes protonation at the hydride to produce H_2, which eliminates to regenerate the resting Ni-SI_a state. But recent studies established that Ni-C state upon low temperature photolysis produces new EPR active states, jointly called as Ni-L state, that are assigned to migration of the bridging hydride as proton.[367,401] In both Ni-C state and Ni-R state the hydride bridges the two metallic centres (Scheme 23). Throughout this whole catalytic cycle, the Fe centre remains in the low spin Fe^{II} state, a configuration favoured by the two strong field CO and CN^- ligands, whereas the Ni centre changes its oxidation states between the Ni^{III} (in Ni-C) and Ni^{II} (in Ni-R and Ni-SI_a).

Structure and activity of [Fe]-Hydrogenases

In some methanogenic archaea, there is a third type of hydrogenase, which had long been believed to be purely bio-organic and they were initially called metal free hydrogenases.[403] But it is now a well-known fact that these enzymes contain a iron in their active site and do not contain any nickel or iron–sulfur

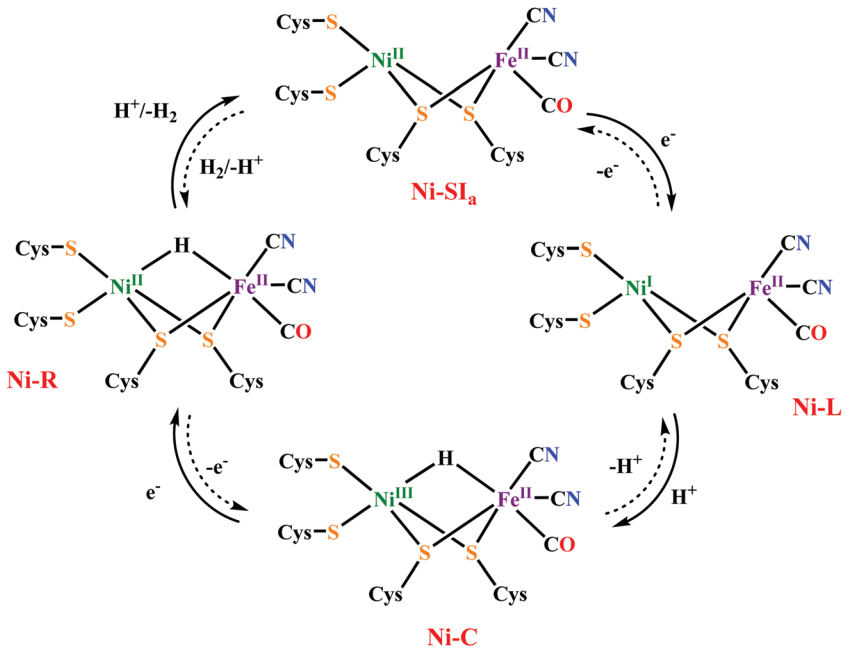

Scheme 23 Proposed catalytic mechanism for reversible H_2 oxidation by [NiFe]-hydrogenases.[367,400]

clusters. So, they are now referred as iron–sulfur cluster free hydrogenase and abbreviated as [Fe]-hydrogenase or Hmd. [Fe]-hydrogenases heterolytically split hydrogen into a proton (H^+) and a hydride (H^-), where the H^- transferred to the substrate containing the carbocation, methenyl-tetrahydromethanopterin (methenyl-H_4MPT$^+$). Thus, it catalyzes the reversible reduction of methenyl-H_4MPT$^+$ with H_2 to methylene-H_4MPT and a H^+ (Scheme 24).[404,405] This reduction is a key intermediary step in the biological conversion of carbon dioxide to methane.

Role of cyanide and carbon monoxide as ligands in hydrogenase active site. The CO and CN^- ligands that are bound to the active site metal centres of the hydrogenases are important in tuning chemical reactivity of the coordinated iron or nickel. Both the ligands are strong π-acidic with vacant π* orbitals that allow for substantial back-bonding with low-valent metal centres such as the Fe in hydrogenase active sites. When bound to a low-valent metal, these ligands accept electron density from a filled metal d orbital into an empty antibonding orbital of the C–N or C–O bond. While the negative charge of the CN^- ion decreases its π-bonding ability relative to CO, hydrogen bonding mitigates the negative charge effect of CN^- and increases its π-bonding. Thus, the π-acceptor CO and CN^- ligands in hydrogenases serve to increase the electrophilicity (Lewis acidity) of the metal. The elevated Lewis acidity of the active site also supports heterolytic cleavage of H_2.[407] The CO-containing ligand set on hydrogenases may tune the acidity of bound H_2 (possibly to more physiological pH values) to facilitate proton transfer between bound H_2 to a basic site *i.e.* adt (–NH).

Dihydrogen coordination chemistry and hydrogenases. Dihydrogen is the simplest molecule, but it has limited metal coordination complexes. H_2 molecule has a very strong σ bond and without having any nonbonded electrons to hold onto metals its difficult for H_2 to form stable complexes. But the unexpected discovery of H_2 coordination to zero-valent tungsten supported by three CO and two organophosphine groups[408–410] produced a new type of complexes termed as σ complexes.[408,411–413] In the σ-bond coordinated H_2 complexes $M_{d\pi} \rightarrow H_2$ back-bonding from filled metal d orbitals to the H_2 σ* orbital is present that greatly strengthens the coordination (Scheme 25). The back-donation component is quite analogous to

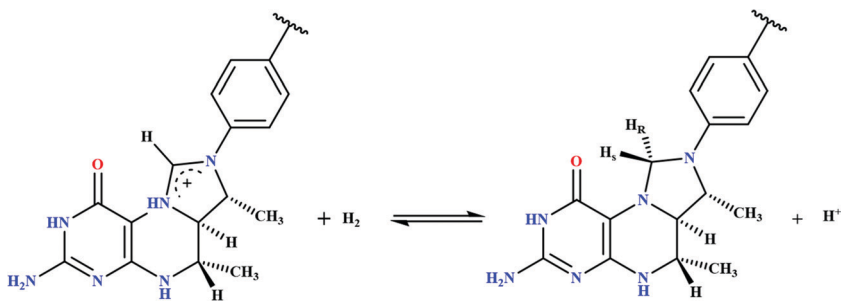

Scheme 24 Scheme of the reversible heterolytic splitting of H_2 by Hmd, showing a hydride stereospecifically transferred into the pro-R site of methenyl-H_4MPT$^+$ to yield methylene-H_4MPT and a proton.

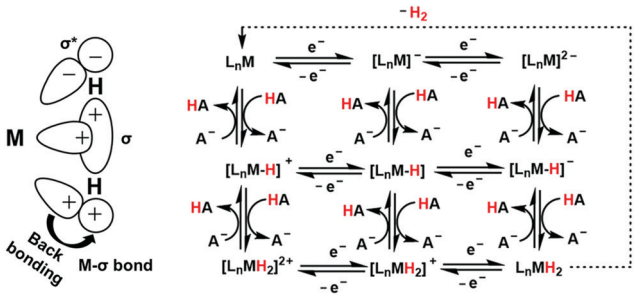

Scheme 25 Schematic presentation of the formation of M–H_2 σ bond and $M_{d\pi} \rightarrow H_2$ backdonation (left). Possible mechanistic pathways for catalytic reduction of proton to hydrogen in the natural hydrogenases or synthetic catalysts (right).

that in metal-olefin π coordination in the Classic Dewar–Chatt–Duncanson model.[414,415] H_2 does not stably bind to highly Lewis acidic d^6 metal centers (*e.g.*, cationic systems with electron-withdrawing ligands) or to d^9 or d^{10} Lewis acids because the backdonation is much weaker (electron-poor metal centers) than in electron-rich metal centers. Substantial backdonation can lead to H–H bond splitting and oxidative addition to form a dihydride complex. The nature of the L_5M ligand set is important, electron-donating L ligands increase the back-bonding, which eventually ruptures the H–H bond as a result of over-population of the H_2 σ* orbitals. Alternatively, strongly electron withdrawing CO ligands compete for back-bonding, especially when trans to the ligand of interest (*i.e.*, H_2), This limits $M_{d\pi} \rightarrow H_2$ back-bonding and favours molecular H_2 coordination over cleavage to dihydride moieties. Strongly Lewis acidic cationic complexes disfavour homolytic H_2 splitting but favour heterolytic splitting. However, if all ligands are π acidic like CO, the complexes are thermally unstable. For such electron-poor centers, loss in backdonation offsets H_2 binding to some extent by increased donation from H_2 to the electron-poor center. The back-bonding stabilizes the H_2 binding, yet it is not quite strong enough to cause H–H bond scission. In bioactivation of H_2 by hydrogenases, the finely tuned stabilization of molecular H_2 coordination rather than dihydride formation is crucial to the function of the enzyme. Here, the unprecedented biological presence of CO ligands in the active site of hydrogenases is a key feature utilized by nature to ensure that the activation of H_2 involves reversible molecular bonding instead of irreversible oxidative addition to form a dihydride. Molecular binding of H_2 is beneficial in hydrogenases for several reasons. It is a surprisingly versatile ligand because it is effectively amphoteric like CO, binding to virtually every unsaturated metal fragment. The balance between its good donor/acceptor abilities and natural stability of CO is considered as an excellent, ubiquitous ligand. H_2 also can have steric (small size) and its low solubility in water offers solvation and entropic advantages over other ligands. H_2 binding can be completely reversible, and H_2 ligands formed by protonation steps can readily eliminate as free H_2. All are important for the understanding of the activation of H_2 in metalloenzymes and are among the many organometallic principles relevant to the structure and function of hydrogenases. An heterolytic cleavage of H_2 is more relevant to biological activation of H_2 than the above described homolytic splitting. The H–H bond can be effectively split into H^+ and H^- fragments. Here neither the metal oxidation state nor the coordination number changes, whereas in homolytic splitting, the oxidation state of the metal increases by 2 and the coordination number also increases.

As pointed out by DuBois, the heterolytic cleavage of H_2 should be at or near equilibrium to avoid high energy intermediates.[416–420] This implies the hydride (H^-) acceptor ability of the metal and the proton (H^+) acceptor ability of the base (either external or internal) must be energetically matched to provide enough energy to drive the heterolysis of H_2, but this reaction should not be strongly exergonic to offer reversibility in catalysis.

Challenges and general outlook. Hydrogen is heralded by many as a "fuel of the future", but more accurately, it is a form of stored energy and a transportable fuel. Three major challenges in H_2 energy economy are, (a) how to obtain H_2 in large amounts, (b) how to store it and (c) how to release its energy. The latter is the best developed because of the availability of fuel cells, albeit expensive, and is slowly becoming an accepted technology. At present H_2 is stored by compression or liquefaction, although there is an intense interest in finding low-cost lightweight materials that, like Pd, can reversibly absorb high volumes of H_2 but without the disadvantages of cost and prohibitive weight (for transport). Hydrogen can be produced by electrolysis of water using these enzymes as cathodes by protein thin film voltammetry. Using the enzymes directly[421] to produce H_2 is, no doubt, a big jump towards green fuel but the rate of hydrogen production is very slow and obtained current densities are very small (typically 2–4 mA/1 mM hydrogenase).[345] On the other hand, protein film voltammetry[422] is a powerful tool for understanding the mechanism of hydrogen production by these enzymes and provides valuable insights to design/tune artificial catalysts. The purification cost of enzymes is high, in particular, considering the fact that hydrogenases require strictly anaerobic conditions. Thus, commercial H_2 production by this route is challenging. Decades of effort by the synthetic inorganic and organometallic chemistry community has resulted in several artificial small molecules resembling the active site of [FeFe]- and [NiFe]-hydrogenases. But the natural enzymes as well as the model complexes are known to operate under strictly anaerobic conditions because it will be difficult to substitute the "supramolecular" protection that is provided by the protein environment to filter or neutralize attacks by this aggressor. If hydrogen has to be familiarized as an alternative energy source, then the cost of production should be cheap and the hydrogen producing catalyst must function under aerobic conditions also in the aqueous medium using abundant water sources without purification.

Synthetic model systems for HER

[FeFe]-Hydrogenase mimics

The number of structural and functional models of diiron dithiolate and related systems of the active site of the [FeFe]-hydrogenase has grown steadily since the first structures of the

enzyme were reported some 20 years ago. Substantial progress has been made in producing stable mixed-valent species with bridging CO. Nonetheless many of the model systems that are similar to the enzyme in their oxidation state and valency of the iron and these consists of abiological phosphine or carbene ligands. On the functional side, mostly diiron hexacarbonyls have been explored. These systems generally reduce proton with large overpotentials and the catalytic cycle passes through the Fe(I)–Fe(I)/Fe(0)–Fe(0) levels as opposed to that of the natural Fe^{II}–Fe^{I} states in the enzymatic systems.

Proton reduction by [FeFe]-Hydrogenase mimics in organic medium

In 1929, synthesis of $[Fe_2(CO)_6(\mu\text{-SEt})_2]$ was reported by Reihlen *et al.*[423] When the protein crystal structure of [FeFe]-hydrogenase was available in 1998–1999,[372,373] the striking resemblance of the diiron subsite of the H-cluster to the $[(\mu\text{-pdt})Fe_2(CO)_6]$ (pdt = propanedithiolate), formerly described by Seyferth,[424] became evident. The electrochemical reduction of proton to hydrogen has been investigated in substantial details using this diiron ditiolate bridged complexes by several groups previously.[425–428] These complexes were classified based on the nature of the bridge, terminal ligands. In most cases the evolution of hydrogen has been confirmed by the use of gas chromatography (GC) and the faradaic yields are generally above 80%.

In their resting state diiron model complexes are mainly in their Fe^{I}–Fe^{I} form and undergoes stepwise reversible or quasi-reversible reductions to produce Fe^{0}–Fe^{0} state. In this section the focus is on the inclusion of 2nd here residues and their effect on proton reduction activity of diiron model complexes. Substituting the dithiolate bridge has little impact on the redox potentials of the model complexes. Replacing the CO ligands by electron donating ligands shifts the reduction towards more negative value. However, when the tereminal –CO ligands are replaced by electron donating ligands (*e.g.* phosphines, carbenes, CN^{-}), the basicity of the iron centre increses and subsequently they are pronated by the proton source directly[429–432] to produce the hydride intermediate. But when the diiron is not basic enough to undergo direct protonation they undergo one- or two-electron reduction to produce the $Fe^{I}Fe^{0}$ or the $Fe^{I}Fe^{0}$ state, which are enough basic to undergo protonation even in the presence of a weak proton source to produce the hydride intermediates.[430,433–437] A second protonation of the hydride intermediates then produces the dihydride intermediates and which then releases H_2 regenerating the starting species. Iron hexacarbonyl complexes, in presence of weak acids undergo reduction before protonation, due to their lower basicity. When a basic residue is present in the model complex, in presence of a suitable proton source, the electrocatalytic cycle is initiated by the protonation of the basic residue. Introduction of a redox active ligand in the model complex results a double reduction, one at the iron centre and other at the ligand. When a bidentate ligand is attached at the Fe centre, the chelating isomer is reported to be more efficient for H_2 production than the symmetrically substituted bridging isomer both in terms of i_{cat}/i_p value and turn over number (TON). Based electrochemical analysis various mechanisms (*e.g.*, EECC, ECEC, ECCE, CECE, CEEC; E means an electron transfer step and C means a chemical step here protonation) are reported for the proton reduction activity in acidic medium.

Diiron model complexes with monothiolate bridge. Sun and coworkers reported the electrocatlytic proton reduction by a diiron complex with a nonbridging aromatic group; $[(\mu\text{-}S\text{-}2\text{-}RCONHC_6H_4)_2Fe_2(CO)_6]$ [R = 4-FC_6H_4] (Fig. 25a).[438] They showed that complex **a** (Fig. 25) is electrocatalytic active at the second reduction potential (−1.7 V *vs.* Fc^{+}/Fc) for reduction of protons from Acetic acid (AcOH) in Acetonitrile (CH_3CN) medium with an overpotential of −0.2 V.

Diiron complexes of the type $Fe_2(CO)_6(\mu\text{-R})_2$ were developed by Si *et al.*, where [R = C_6H_4-*o*-OMe (Fig. 25b); C_6H_4-*p*-OMe (Fig. 25c); C_6H_4-*p*-Cl (Fig. 25d)].[439] They showed that all these complexes reduces proton at their second reduction event in presence of AcOH. The complex **b** (Fig. 25) in presence of excess PMe_3 was transformed to $Fe_2(CO)_4(\mu\text{-}SC_6H_4\text{-}o\text{-}CH_3O)_2(PMe_3)_2$ (Fig. 25e), which was catalytically active at −2.08 V in CH_3CN medium in presence of AcOH.

Diiron model complexes with substituted dithiolato bridge. Various diiron model complexes with different –R groups in $SCH_2CH(R)CH_2S$ bridge has been synthesized and their electrocatlytic proton reduction activity has been studied by different groups. Due to the π acidity of the carbonyl ligands in the $Fe_2S_2(CO)_6$ derivatives the formation of hydride species *via* protonation requires either the use of very strong acids or electrochemical reduction earlier to protonation. The second process needs high driving force which increases the overpotential for HER. However, substitution of CO ligands by strong σ donor CN^{-} ligands increases the charge density of the cluster but the use of cyanide ligands outside the protective protein environment creates inherent stability issues under acidic conditions. To avoid this thioether groups, isocyanides,

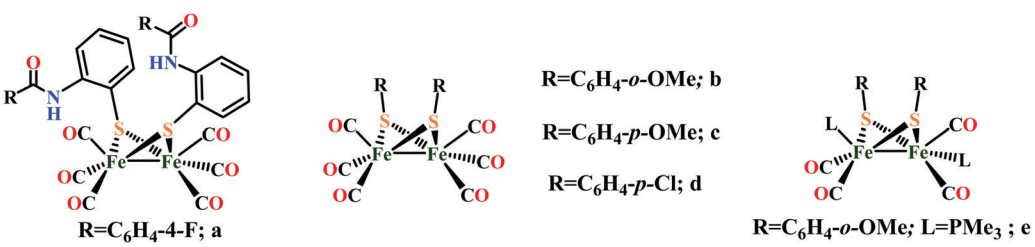

Fig. 25 Diiron model complexes with nonbridging group with all carbon atoms.

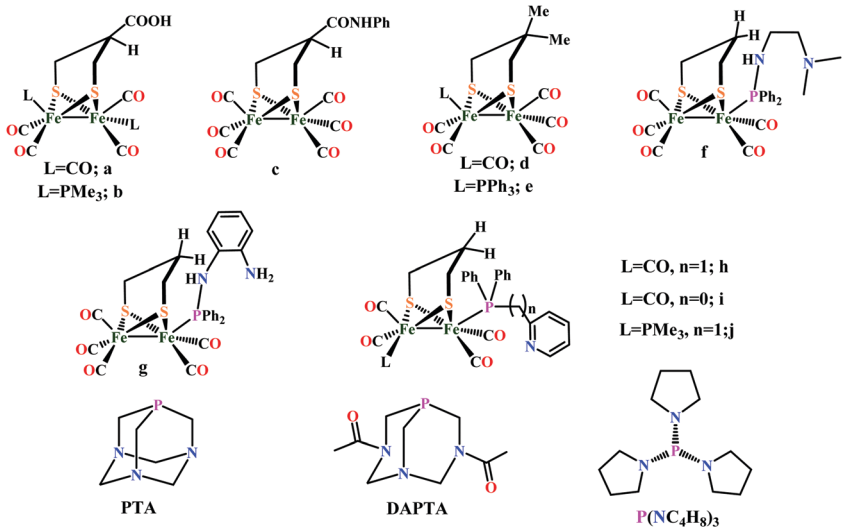

Fig. 26 Diiron model complexes with various –R groups in $SCH_2CH(R)CH_2S$ bridge.

carbenes, isonitriles, amines and phosphines have been used widely. By replacing –CO with phosphine or phosphites causes a 0.2–0.3 V lowering of reduction potential of the model complexes and replacement of a second –CO by phosphine causes nearly an identical additional shift revealing the additivity of the enhanced σ donation on increasing the potential and further substituion of the phosphines only lowers the potential further more. Thus, eletron defficient phosphine like PTA (1,3,5-triaza-7-phosphaadamantane, Fig. 26) and itsacetylated derivative DAPTA (3,7-diacetyl-1,3,7-triaza-5-phosphabicyclo[3.3.1]-nonane, Fig. 26) has been used. Similarly, tris(*N*-pyrrolyl)phosphine, ($P(NC_4H_8)_3$) (Fig. 26) causes a small shift, 30 mV per phosphine ligand reflecting the fact that it is an exceptionally weak donor ligand.[440]

Darensbourg and coworkers developed a series of diiron model complexes bearing carboxylic acid functionalities [(R_1 = COOH, R_2 = H; Fig. 26a and R_1 = CONHPh, R_2 = H Fig. 2c)].[441] They reported that complex (μ-$(SCH_2)_2$CHCOOH)$[Fe(CO)_3]_2$ (Fig. 26a) and (μ-$(SCH_2)_2$CHCONHPh)$[Fe(CO)_3]_2$ (Fig. 26c) reduces proton in presence of AcOH in CH_3CN at their Fe(I)–Fe(I)/Fe(I)–Fe(0) redox levels at −2.51, and −2.43 V *vs.* Fc^+/Fc, respectively whereas the $–PMe_3$ substituted complex (μ-$(SCH_2)_2$-CHCOOH)$[Fe(CO)_2(PMe_3)]_2$ (Fig. 26b) catalyzes H_2 production from AcOH at its formal Fe^I–Fe^0 state. Singleton *et al.* showed that when both R_1 = R_2 = Me and L = PPh_3 (Fig. 26e) the Fe^0–Fe^0 species of the complex was active towards electrocatalytic H_2 production, whereas the Fe^0–Fe^I species is not.[442] Apparently the weak donor ability of triphenylphosphine renders iron insufficiently electron rich to accommodate the oxidative addition of a proton.

Wang *et al.* reported electrocatlytic proton reduction by similar diiron model complexes (Here R_1 = R_2 = H) containing pendant nitrogen bases in phosphine ligands (μ-pdt)-$[Fe_2(CO)_5PPh_2NH(CH_2)_2N(CH_3)_2]$ (Fig. 26f) and (μ-pdt)-$[Fe_2(CO)_5PPh_2NH(2\text{-}NH_2C_6H_4)]$ (Fig. 26g) in the presence of trifluoromethanesulfonic acid (CF_3SO_3H) in CH_3CN medium.[443] They reported that the secondary amine in complex (μ-pdt)-$[Fe_2(CO)_5PPh_2NH(2\text{-}NH_2C_6H_4)]$ (Fig. 26g) has a weak intramolecular hydrogen bonding with both the terminal nitrogen and sulfur atom. They suggested that a proton transfer pathway from amine in phosphine ligand to the sulfur atom of active site. Protonation of complexes (μ-pdt)$[Fe_2(CO)_5PPh_2NH(CH_2)_2N(CH_3)_2]$ (Fig. 26f) and (μ-pdt)$[Fe_2(CO)_5PPh_2NH(2\text{-}NH_2C_6H_4)]$ (Fig. 26g) only occurred at the terminal nitrogen atom. Similarly Li *et al.* introduced pyridyl groups to the phosphine ligands of the diiron complex as a pendant basic site.[444] The electrocatalytic proton reduction activity of (μ-pdt)$[Fe_2(CO)_5(Ph_2PCH_2Py)]$ (Fig. 26h), (μ-pdt)$[Fe_2(CO)_5(Ph_2PPy)]$ (Fig. 26i) and (μ-pdt)$[Fe(CO)_2(PMe_3)][Fe(CO)_2(Ph_2PCH_2Py)]$ (Fig. 26j) was investigated in the prsesence of AcOH in CH_3CN medium. The catalytic efficiency of complex (μ-pdt)$[Fe_2(CO)_5(Ph_2PCH_2Py)]$ (Fig. 26h) and (μ-pdt)$[Fe_2(CO)_5(Ph_2PPy)]$ (Fig. 26i) was found to be relatively low. The overpotentials for the electrocatalytic reduction of protons from AcOH are 400 mV *vs.* Fc^+/Fc for (μ-pdt)$[Fe_2(CO)_5(Ph_2PCH_2Py)]$ (Fig. 26h) and 370 mV *vs.* Fc^+/Fc for (μ-pdt)$[Fe_2(CO)_5(Ph_2PPy)]$ (Fig. 26i). The effect of water on the proton reduction activity of (μ-pdt)$[Fe(CO)_2(PMe_3)][Fe(CO)_2(Ph_2PCH_2Py)]$ (Fig. 26j) was probed in CH_3CN and in CH_3CN–H_2O (50 : 1, v/v). The electrocatalytic current for proton reduction was considerably enhanced in CH_3CN–H_2O (50 : 1, v/v). The electrocatalytic efficiency for proton reduction by (μ-pdt)$[Fe(CO)_2(PMe_3)]$-$[Fe(CO)_2(Ph_2PCH_2Py)]$ (Fig. 26j) in CH_3CN–H_2O (50 : 1, v/v) increases 5 times than that of in pure CH_3CN. Just like the secondary amine in the azadithiolate bridged diiron complexes, here the pyridyl group in the phosphine ligand of diiron complexes can serve as a proton relay in the presence of strong acid, resulting to the decrease of the overpotential for electrocatalytic proton reduction by 360–490 mV.[444] Also, the hydrophilicity of the pyridyl group in these diiron complexes renders the electrocatalytic efficiency more susceptible to water.

Diiron model complexes with μ-arenedithiolato bridges. One strategy for designing diiron model complexes with redox

properties closer to the thermodynamic potential for proton reduction is inclusion of a suitably substituted aromatic dithiolato bridgehead, as showed by Felton and co-workers.[445] The benzene dithiolate (bdt^{2-}) ligand assists to adjust the redox reactions of the catalyst by lowering the potential difference between the successive reduction states. This has been described by an interaction of the metal d-orbitals with a combination of the filled sulfur pπ orbitals and the arene pπ orbitals, which shields the change in electron density at the iron center as the oxidation state is changed, thus minimizing the changes in electron energies upon reduction.

On substituting the benzene ring with increasing number of electron withdrawing –Cl groups leads to an anodic shift in reduction potential and a associated lowering of the overpotential of hydrogen evolution was observed.[445] A same ECEC mechanism (E corresponds to an electron transfer step, and C, to a chemical reaction, here protonation) is also suggested for the catalytic proton reduction from weak acids by compound **b**, **c** and **d** (Fig. 27).[445] As the number of electrons withdrawing groups is increased in the complexes **b** to **d** (Fig. 27) 250 mV improvement of the overpotential of AcOH reduction was observed but compromises the catalytic efficiency in terms of TOF.[445] The analogous methyl substituted complex $[Fe_2(CO)_6\{\mu\text{-}SC_6H_3(CH_3)S\}]$ (Fig. 27e) produces H_2 at −2.10 V in presence of AcOH with a overpotential of 0.64.[445]

Chen *et al.* reported a series of Fe_2S_2 complexes containing phenolic –OH groups and –OMe groups adjacent to the sulfur centers.[446] They showed that phenolic –OH groups adjacent to the sulfur centers in complexes **f**, **h**, **i**, **j** and **k** (Fig. 27) modestly render their reduction potentials less negative and hence lowered the catalytic overpotential compared to the unsubstituted complex $[(\mu\text{-bdt})Fe_2(CO)_6]$ (Fig. 27a) due to internal hydrogen bonding. Spectroscopic investigations suggested the presence of intramolecular hydrogen bonding between the phenolic –OH groups and the adjacent sulfur atoms. However these hydroquinone complexes **f**, **h**, **i**, **j** and **k** (Fig. 27) is less effective catalyst for proton production from weak acids compared to $[(\mu\text{-bdt})Fe_2(CO)_6]$ (Fig. 27a) because of the internal hydrogen bonding. The internal hydrogen bonding in these complexes lowered the basicity of the dianionic $[Catalyst]^{2-}$ species of the rate-determining step. Whereas the dimethoxy derivative **g** (Fig. 27), in which hydrogen bonding is absent, is a better catalyst compared to $[(\mu\text{-bdt})Fe_2(CO)_6]$ (Fig. 27a) due to the increased basicity of the corresponding dianion. These results further indicate that the pK_a value of the $[CatalystH]^-$ species is the most important factor for catalytic activity for this family of catalysts.[446]

Lin and coworkers reported phosphine derivatives (Fig. 27l–o) of $[Fe_2(CO)_6\{\mu\text{-}SC_6H_3(CH_3)S\}]$ (Fig. 27e) complex and examined their proton reduction activites in CH_3CN medium in presence of AcOH.[447] The reduction potential of the parent complex $[Fe_2(CO)_6\{\mu\text{-}SC_6H_3(CH_3)S\}]$ (Fig. 27e) is more positive than those of complexes **l–o** (Fig. 27) due to the fact that phosphine ligands are more electron-donating than CO.

Durgaprasad *et al.* reported a series of diiron model complexes by incorporating 1,2-ethylene-dithiolate on the benzenedithiolato bridgehead.[448] They showed that compounds $[Fe_2\{\mu\text{-diph-6,7-qdt}\}(CO)_6]$ (Fig. 27p) and $[Fe_2\{\mu\text{-btdt}\}(CO)_6]$ (Fig. 27q) exhibit electrocatalytic proton reduction in presence of a strong acid TsOH. For the electrocatalytic proton reduction catalysed by compound $[Fe_2\{\mu\text{-diph-6,7-qdt}\}(CO)_6]$ (Fig. 27p), they proposed a CEEC mechanism. Whereas, the hexa carbonyl compound $[Fe_2\{\mu\text{-btdt}\}(CO)_6]$ (Fig. 27q) did not undergo protonation in presence of *p*-toluenesulfonic acid in its Fe^I–Fe^I oxidation state,may be due to the involvement or delocalization of lone pair of electrons of ring nitrogen with ring sulfur pi-electrons. Accordingly an EC electrocatalytic reduction mechanism is proposed for compound $[Fe_2\{\mu\text{-btdt}\}(CO)_6]$ (Fig. 27q).

Diiron model complexes with azadithiolato bridges $[SCH_2N(R)CH_2S]$. In [FeFe]-hydrogenase the Fe(I)Fe(I) form of the enzyme is suggested to undergo protonation or tautomerization to provide a terminal hydride. However, comparing the HER mechanism of enzyme system and the hexacarbonyl synthetic models it can be speculated that electron poor models like complexes containing six CO ligands first undergoes reduction below Fe^I–Fe^I state before the protonation. However, a model complex bearing Brønsted basic sites in the second coordination sphere, can have a strong impact on the electrocatalytic HER mechanism and potential where catalysis occurs.[449] In acidic media the basic residues are generally protonated and reduce the electron density on the catalytic

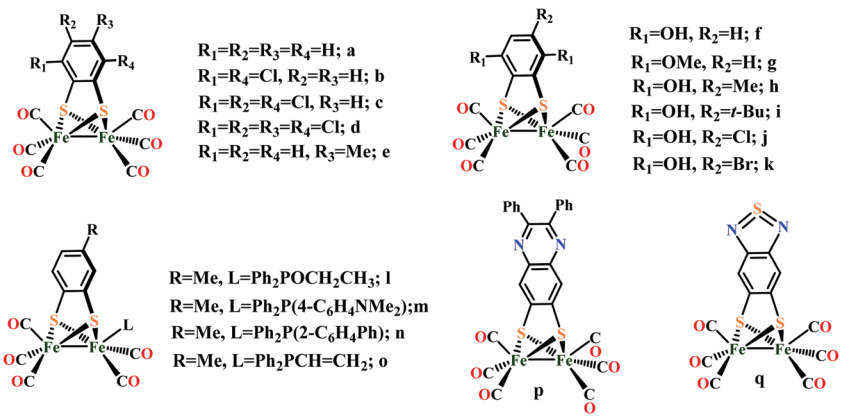

Fig. 27 Diiron model complexes containing μ-arenedithiolato bridges.

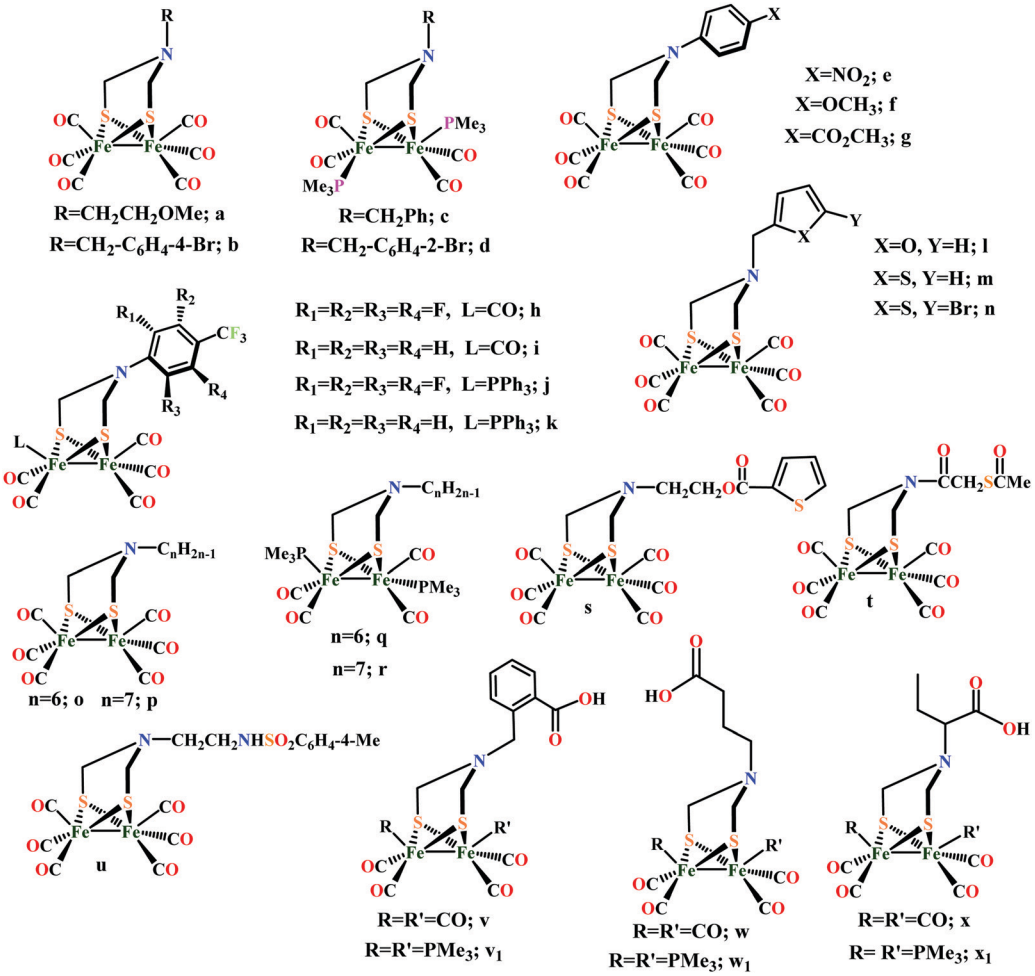

Fig. 28 Diiron model complexes with azadithiolato bridges [$SCH_2N(R)CH_2S$].

center causing milder reductions compared to those of more anionic species.[428] For example, proton reduction catalyzed by $[Fe_2(CO)_6\{\mu\text{-}SCH_2NH(R)CH_2S\}]$ derivatives having different R substituent [R = CH_2CH_2OMe (Fig. 28a),[426,450] R = $CH_2C_6H_4$-4-Br (Fig. 28b)[451]] was investigated.[426] For the $[Fe_2(CO)_6\{\mu\text{-}SCH_2NH(R)CH_2S\}]$ (R = CH_2CH_2OMe) (Fig. 28a) complex, in the presence of a strong acid like TsOH in CH_3CN, the protonation of the amino group takes place first to produce $\mathbf{aH^+}$ (Scheme 26) then the first protonation occurs at −1.2 V *vs.* Fc^+/Fc to produce aH (Scheme 26) which then undergoes protonation to produce a mixed valent ammonium hydride-[a(μ-H)H^+] (Scheme 26). Then second reduction of this hydride below −1.2 V *vs.* Fc^+/Fc takes place to generate a-2H (Scheme 26), which then slowly release H_2 (Scheme 26, pathway A). When a stronger acid $HBF_4{\cdot}Et_2O$ is used, it protonates a-2H to generate a-3H^+ which then reduces by one electron at −1.4 V *vs.* Fc^+/Fc to produce H_2 at a faster rate (Scheme 26, pathway B). In CH_3CN solvent $[Fe_2(CO)_6\{\mu\text{-}SCH_2NH(R)CH_2S\}]$ (R = $CH_2C_6H_4$-4-Br, Fig. 28b) complex follows a similar type of mechanism.[426,451] In presence of weak acid like AcOH neither protonation of the bridged-N atom nor formation of bridged hydride at Fe–Fe bond takes place in in CH_3CN.

Proton reduction by $[\{Fe(CO)_2(PMe_3)\}_2\{\mu\text{-}SCH_2N(R)CH_2S\}]$ (Fig. 28c and d) was also monitored in the presence of a weak and of a strong acid.[430,432,452] Weak acid like AcOH neither protonate the bridged-N atom nor the Fe–Fe site.[432,452] In presence of a stronger acid (TfOH, pK_a = 2.6 in CH_3CN), catalysis takes place at around −1.5 V *vs.* Fc^+/Fc, which is a potential assigned to the reduction of the protonated amino species (Fig. 28c, R = CH_2Ph[430]) or of the bridging hydride (Fig. 28d, R = $CH_2C_6H_4$-2-Br[432]). When R = CH_2Ph (Fig. 28c), no catalysis was observed at −1.1 V *vs.* Fc^+/Fc, at which the reduction of Fe(μ-H)Fe isomer takes place or at −1.0 V *vs.* Fc^+/Fc at which the doubly protonated species get reduced.[430] However on prolonged controlled potential electrolysis, slow catalysis is observed at these potentials.[430] For the $[\{(\mu\text{-}SCH_2)_2\text{-}N(4\text{-}NO_2C_6H_4)\}Fe_2(CO)_6]$ (Fig. 28e) complex a CECE mechanism was suggested in presence of AcOH (0–10 mM) in CH_3CN by Liu *et al.*[453] But in case of the –OMe substituted complex **f** (Fig. 28) an EECC mechanism was proposed in presence of AcOH (0–10 mM) in CH_3CN medium.[454] Here the bridged N atom of **f** (Fig. 28) was not protonated by weak acid AcOH. From the Bulk electrolysis of a CH_3CN solution of complex **f** (0.33 mM) with excess AcOH (6.6 mM) at −2.18 V showed hydrogen formation with

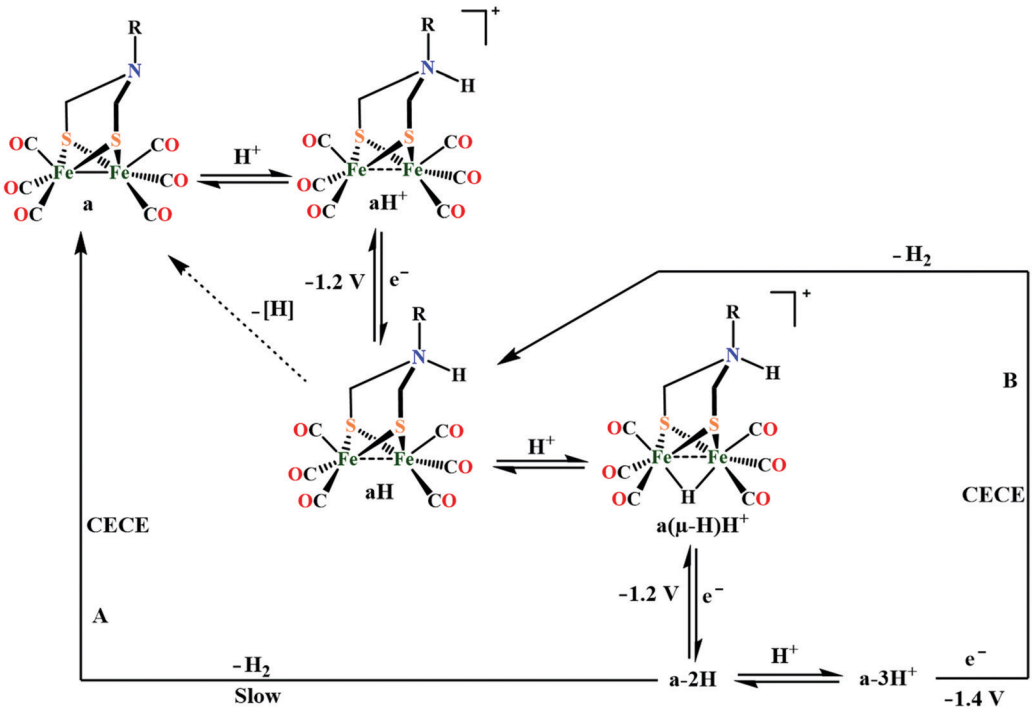

Scheme 26 Proposed mechanisms of proton reduction catalysed by $[Fe_2(CO)_6\{\mu\text{-}SCH_2NH(R)CH_2S\}]$ complexes (R = CH_2CH_2OMe, Fig. 28a) in MeCN.[426]

~5 turnovers. Similarly for the complex **g** (Fig. 28) in presence of weak AcOH a EECC mechanism was also proposed.[455] Bulk electrolysis experiment of the CH_3CN solution of complex **g** (Fig. 28) (0.33 mM) with excess AcOH (6.6 mM) revealed that the initial rate of electrolysis was five times greater than that of in absence of the catalyst. In the presence of a strong acid like CF_3CO_2H an ECCE mechanism was proposed for the electrocatalytic proton reduction catalysed by complex **g** (Fig. 28).[455]

Wang *et al.* reported a set of adt-bridged fluorophenyl-substituted diiron active site models of [Fe–Fe] hydrogenase, $[(\mu\text{-adt})C_6F_4CF_3\text{-}p]Fe_2(CO)_6$ (Fig. 28h), $[(\mu\text{-adt})C_6H_4CF_3\text{-}p]Fe_2(CO)_6$ (Fig. 28i), $[(\mu\text{-adt})C_6F_4CF_3\text{-}p]Fe_2(CO)_5PPh_3$ (Fig. 28j), $[(\mu\text{-adt})\text{-}C_6H_4CF_3\text{-}p]Fe_2(CO)_5PPh_3$ (Fig. 28k).[456] They demonstrated that the electrocatalytic proton reduction by these complexes is mostly dependent on the strength of the proton source used. When weak AcOH is used as the proton source, the electrocatalytic proton reduction process starts off with two consecutive one-electron reduction processes to produce H_2 *via* the Fe^0–Fe^0 state whereas in the presence of strong acid, $HBF_4{\cdot}Et_2O$, the catalytic process commenced by the protonation of the bridgehead N atom followed by reduction of the bridgehead protonated N atom around −1.29 V *vs.* Fc^+/Fc, to generate H_2 *via* the Fe^0–Fe^I state. Thus, by altering the strength of the acid triggers the initial electron-transfer step from the reduction of the bridgehead protonated N atom to the active site of $[Fe^I\text{–}Fe^I]$.

Sun and coworkers prepared three heterocycle-containing diiron azadithiolate hexacarbonyl model complexes, $[\{(\mu\text{-}SCH_2)_2\text{-}NCH_2(2\text{-}C_4H_3O)\}](Fe_2(CO)_6)$ (Fig. 28l), $[\{(\mu\text{-}SCH_2)_2NCH_2(2\text{-}C_4H_3S)\}]\text{-}(Fe_2(CO)_6)$ (Fig. 28m) and $[\{(\mu\text{-}SCH_2)_2NCH_2(5\text{-}Br\text{-}2\text{-}C_4H_2S)\}Fe_2(CO)_6]$ (Fig. 28n).[457] They proposed that the methyl group near the heterocycle might increase the electron density in the π system by donating electrons by hyperconjugation (σ conjugation), and slightly decrease the nuclear electron density of the Fe atom through the three atoms (N, C, S). Such an effect can be increased by the oxygen atom in furan and bromine atom on the thiophene, resulting in less negative reduction potentials. The catalytic proton reduction for these complexes were studied in CH_3CN in presence of 0–8 mM $HClO_4$ under CO atmosphere. They showed that the furan-containing model complex $[\{(\mu\text{-}SCH_2)_2NCH_2(2\text{-}C_4H_3O)\}]\text{-}(Fe_2(CO)_6)$ (Fig. 28l), displayed electrocatalytic proton reduction at −1.13 V *vs.* Fc^+/Fc whereas the thiophene-containing analogues **m** and **n** (Fig. 28) exhibit catalytic proton reduction at −1.20 and −1.09 V *vs.* Fc^+/Fc, respectively in presence of $HClO_4$. Along the same lines Si *et al.* reported a series of a novel class of $(N\text{–}C_nH_{2n-1})$-1,3-azapropanedithiolate-bridged [Fe–Fe] hydrogenase model complexes $[Fe_2(CO)_6(CH_2S)_2N\text{–}C_nH_{2n-1}]$ (n = 6, 7) and their PMe_3-disubstituted complexes $[Fe_2(CO)_4(PMe_3)_2(CH_2S)_2N\text{–}C_nH_{2n-1}]$ (n = 6, 7) and investigated their electrochemical behaviour in presence of AcOH.[452] They proposed an ECEC mechanism for electrocatalytic proton reduction of the complexes **o–r** (Fig. 28) in presence of AcOH. From the bulk electrolysis experiment of 1 mM solution of complex $[Fe_2(CO)_4(PMe_3)_2(CH_2S)_2N\text{–}C_nH_{2n-1}]$ (n = 6) (Fig. 28q) (5 ml, 5 mM) with excess AcOH (20 mM) at −2.3 V *vs.* Fc^+/Fc it was observed that the initial rate of electrolysis was approximately 1.8 times that without the catalyst. 12 F charge per mole of **q** (Fig. 28) was passed over the course of 20 min, which corresponds to 6 turnovers.

Eletrocatalytic proton reduction by the $[(\mu\text{-}SCH_2)_2NCH_2CH_2\text{-}O_2CC_4H_3S\text{-}2]Fe_2(CO)_6$ complex (Fig. 28s) in presence of AcOH in CH_3CN medium was proposed to proceed *via* EECC mechanism.[458]

Similarly, Song *et al.* reported a *N*-acylated diiron azadithiolate complex $[\{(\mu\text{-}SCH_2)_2\text{-}NC(O)CH_2SC(O)Me\}Fe_2(CO)_6]$ (Fig. 28t) which had the ability to to undergo proton reduction to generate hydrogen gas in the presence of weak acid AcOH *via* an EECC mechanism.[459] The bulk electrolysis of AcOH (25 mM) catalyzed by **t** (Fig. 28t) (0.50 mM) in CH_3CN medium at −2.34 V *vs.* Fc^+/Fc indicated a total of 12.3 F per mol of **t** (Fig. 28) to be passed during half an hour. This corresponds to 6.1 turnovers. Complex **u** (Fig. 28) was reported to display proton reduction activity in presence of a strong acid CF_3SO_3H in CH_3CN medium.[460] Based on the electrochemical measurement a CECE mechanism was proposed for the proton reduction by **u** (Fig. 28).

A series of model complexes bearing aryl and alkyl carboxylic acid groups to the dithiolate bridge of diiron unit, $[Fe_2(CO)_6\{(\mu\text{-}SCH_2)_2\text{-}NCH_2C_6H_4\text{-}2\text{-}COOH\}]$ (Fig. 28v), $[Fe_2(CO)_6\{(\mu SCH_2)_2NCH_2CH_2\text{-}CH_2COOH\}]$ (Fig. 28w) and $[Fe_2(CO)_6\{(\mu\text{-}SCH_2)_2NCH(CH_2CH_3)COOH\}]$ (Fig. 28x) have been synthesized with the aim of decreasing the potential for reduction of protons to hydrogen and their proton reduction activity in presence of TfOH is studied by Gao *et al.*[461] They proposed that in the case of complex $[Fe_2(CO)_6\{(\mu SCH_2)_2NCH_2\text{-}CH_2CH_2COOH\}]$ (Fig. 28w) the carbon chain is long enough to allow interaction between the carboxyl group and the diiron cluster. A CECE mechanism is suggested for the complex **v**, **w** and **x** (Fig. 28) for electrocatalytic proton reduction in accordance with a previous report.[462] It was observed that the increase of catalytic current against amount of added acid (TfOH) for PMe_3 substituted complex $\mathbf{w_1}$ and $\mathbf{x_1}$ is greater (200 μA for adding of 4 eq. of TfOH) than that for $\mathbf{v_1}$ (50 μA for adding of 4 eq. of TfOH). A CECE mechanism was proposed for the formation of hydrogen with $\mathbf{v_1}$, $\mathbf{w_1}$ and $\mathbf{x_1}$ (Fig. 28). In complex $\mathbf{v_1}$ (Fig. 28) the first protonation occurs at the bridging N atom whereas the in complex $\mathbf{w_1}$ and $\mathbf{x_1}$ (Fig. 28) the first protonation occurs at Fe–Fe bond. However, complexes $\mathbf{w_1}$ and $\mathbf{x_1}$ (Fig. 28) proved to be electrochemically active upon the addition of water alone, suggesting that the carboxyl group can provide H_3O^+ protons to the amino bridge thus catalyse proton reduction under neutral conditions (Scheme 27).

Most of the above complexes have been investigated to test their ability to catalyze the reduction of acids to form hydrogen and the results are summarized in Table 5. The solvent used (mostly acetonitrile), the acid source, the peak potentials for the catalytic process, the standard potential for reduction of the acid in the used solvent, the overpotential and catalytic efficiency (C.E.) were tabulated. In a few instances, the overpotential is not reported either because the standard potential is not known in the solvent used (THF or CH_2Cl_2) or because the catalytic current may in fact not be due to reduction of the acid but to further reduction of the catalyst in the presence of acid. Potentials are referenced with respect to Fc^+/Fc in acetonitrile and correspond to the peak of the catalytic process. Standard potentials are for the couple in acetonitrile. These were calculated as shown in previously reported literature.[463] The pK_a-values were used from the literature. Overpotentials are the catalytic peak potential minus the standard reduction potential of the acid used. The ratio of the catalytic current and the current for reduction of the catalyst in the absence of acid is examined. This ratio is divided by the ratio of the acid concentration, to the catalyst concentration to give catalytic efficiency (C.E.).

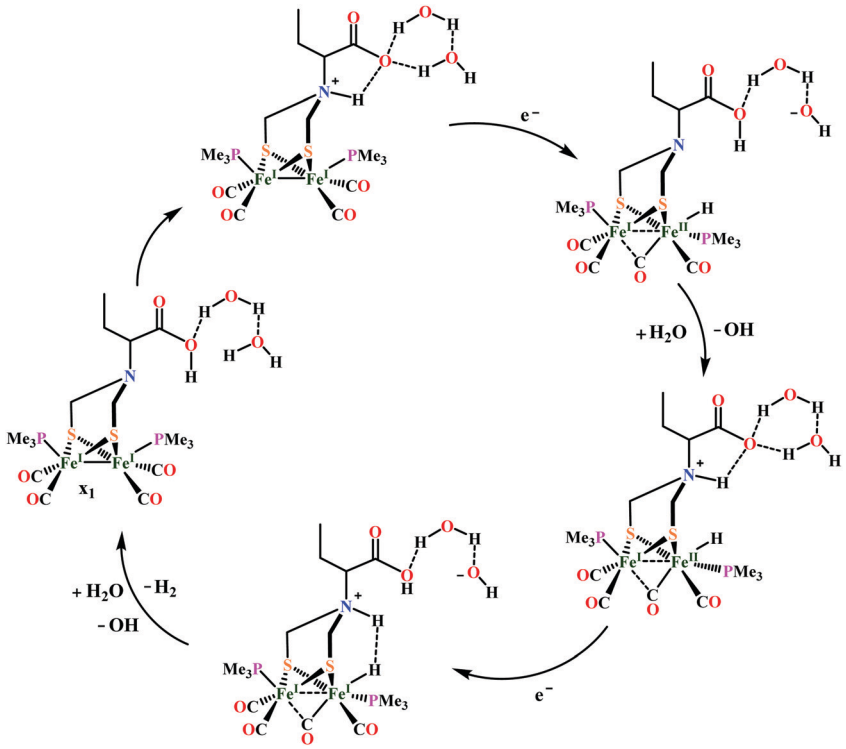

Scheme 27 Proposed mechanism for the electrocatalytic proton reduction mediated by $[Fe_2(CO)_4(PMe_3)_2\{(\mu\text{-}SCH_2)_2NCH(CH_2CH_3)COOH\}]$ (Fig. 28x_1) in aqueous medium, explaining the role of the −COOH group as a proton transfer relay.[461]

Table 5 Summary of electrochemical proton reduction data in organic medium for [FeFe]-hydrogenase model complexes

Complex	Solvent used	Acid used	Catalytic peak potential (V) *vs.* Fc^+/Fc	Standard reduction potential of the acid used (V) *vs.* Fc^+/Fc	Overpotential (V)	Catalytic efficiency (CE)	Ref.
25d	CH_3CN	AcOH	−1.7	−1.46	−0.2	0.09	438
25i	CH_3CN	AcOH	−2.08	−1.46	−0.62	—	439
26a	CH_3CN	AcOH	−2.5	−1.46	−1.0	0.27	441
26b	CH_3CN	AcOH	−2.3	−1.46	−0.8	0.28	441
26b	CH_3CN	HCl	−1.45	−0.67	−0.78	0.06	441
26c	CH_3CN	AcOH	−2.4	−1.46	−0.9	0.19	441
26e	CH_3CN	AcOH	−2.3	−1.46	−0.8	0.40	442
26f	CH_3CN	CF_3SO_3H	−1.75	−0.29	−1.46	1.0	443
26g	CH_3CN	CF_3SO_3H	−1.7	−0.29	−1.4	0.88	443
27a	CH_3CN	AcOH	−2.06	−1.46	−0.60	0.31	446
27a	CH_2Cl_2	HBF_4	−1.4	−0.28	−1.1	0.38	464
27a	CH_3CN	TsOH	−1.25	−0.65	−0.60	0.23	465
27b	CH_3CN	AcOH	−1.97	−1.46	−0.51	0.32	445
27c	CH_3CN	AcOH	−1.88	−1.46	−0.42	0.31	445
27d	CH_3CN	AcOH	−1.85	−1.46	−0.39	0.23	445
27e	CH_3CN	AcOH	−2.10	−1.46	−0.64	0.44	445
27f	CH_3CN	AcOH	−2.05	−1.46	−0.59	0.12	446
27g	CH_3CN	AcOH	−2.10	−1.46	−0.64	0.38	446
27h	CH_3CN	AcOH	−2.05	−1.46	−0.59	0.12	446
27i	CH_3CN	AcOH	−2.05	−1.46	−0.59	0.12	446
27j	CH_3CN	AcOH	−2.10	−1.46	−0.6	0.09	446
27k	CH_3CN	AcOH	−2.10	−1.46	−0.6	0.09	446
28a	CH_3CN	HBF_4	−1.3	−0.28	−1.0	0.52	450
28a	CH_3CN	TsOH	−1.3	−0.65	−0.6	0.29	450
28e	CH_3CN	AcOH	−1.73	−1.46	−0.27	0.16	453
28f	CH_3CN	AcOH	−2.20	−1.46	−0.7	0.19	454
28g	CH_3CN	CF_3CO_2H	−1.60	−0.89	−0.7	0.34	455
28h	CH_3CN	AcOH	−2.2	−1.46	−0.7	0.36	456
28h	CH_3CN	HBF_4	−1.5	−0.28	−1.2	0.37	456
28i	CH_3CN	AcOH	−2.1	−1.46	−0.6	0.23	456
28i	CH_3CN	HBF_4	−1.5	−0.28	−1.2	0.22	456
28j	CH_3CN	AcOH	−2.2	−1.46	−0.7	0.31	456
28j	CH_3CN	HBF_4	−1.6	−0.28	−1.3	0.18	456
28k	CH_3CN	AcOH	−2.3	−1.46	−0.8	0.60	456
28k	CH_3CN	HBF_4	−1.6	−0.28	−1.3	0.80	456
28l	CH_3CN	$HClO_4$	−1.2	−0.26	−0.9	0.32	466
28m	CH_3CN	$HClO_4$	−1.45	−0.26	−1.19	0.50	457
28n	CH_3CN	$HClO_4$	−1.25	−0.26	−0.99	0.43	457
28o	CH_3CN	AcOH	−2.1	−1.46	−0.60	—	452
28p	CH_3CN	AcOH	−2.2	−1.46	−0.70	—	452
28q	CH_3CN	AcOH	−2.15	−1.46	−0.69	—	452
28r	CH_3CN	AcOH	−2.1	−1.46	−0.60	—	452
28s	CH_3CN	AcOH	−2.2	−1.46	−0.7	0.22	458
28t	CH_3CN	AcOH	−2.2	−1.46	−0.7	0.50	459

Proton reduction by [FeFe]-mimics in aqueous medium. Numerous synthetic structural and functional hydrogenases model systems[345,467,468] and their electrocatalytic proton reduction activity in organic medium has been investigated[426,428,469] and some of them are reported above. Lately electrocatalytic and photocatalytic of some [Fe–Fe] hydrogenase model systems have been reported in aqueous medium.[469–472] Since these complexes are generally insoluble in water, their reactivity in aqueous medium has been investigated either under heterogeneous conditions or *via* miscelle formation.

The $[(\mu\text{-bdt})Fe_2(CO)_6]$ (Fig. 27a) complex displays electrocatalytic proton reduction at −0.66 V *vs.* SHE in an aqueous sodium dodecyl sulphate (SDS) solution at pH 3.[473] Bulk electrolysis experiment at −0.66 V *vs.* SHE of the complex at pH 3 confirms the production of H_2 with faradaic efficiency close to 100%. In its catalytic cycle the complex first undergoes $2e^-$ reduction to produce the active Fe^0–Fe^0 state followed by a PCET step to produce a hydride intermediate $[Fe^0–Fe^{II}(H)]^-$ (Scheme 28), which then reacts with protons to produce H_2 and regenerate the Fe^I–Fe^I form. However, in organic solvents, this $[Fe^0–Fe^{II}(H)]^-$ (Scheme 28), intermediate is very hard to protonate by strong acids, which explains the poor activity of this for H_2 production in acetonitrile.

Several azadithiolate (ADT) bridged [FeFe]-hydrogenase model complexes are reported to produce H_2 in aqueous medium.[474,475] Complex $BrC_6H_4N(CH_2S)_2Fe_2(CO)_6$ (Fig. 29a) when physiadsorbed on edge plane graphite surface, has been demonstrated to display electrocatalytic proton reduction at pH < 3.[474] While these catalysts are found to reduce proton at very negative potentials in organic medium, in aqueous medium the potential of proton reduction is shifted towards more positive value due to enhanced solvation of the anionic reduced states. The catalyst shows a TOF of 6400 s^{-1} at a potential of −0.5 V *vs.* SHE in 0.5 N H_2SO_4. Long term controlled potential electrolysis of the complex at −0.5 V indicates the TON of the catalyst is

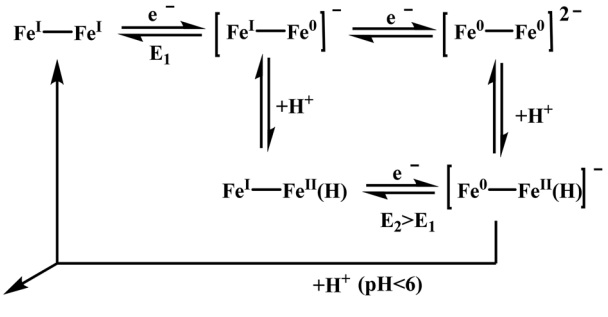

Scheme 28 Proposed mechanism for the catalysis of electrochemical H_2 production mediated by [(μ-bdt)$Fe_2(CO)_6$] (Fig. 27a).

$\gg 10^8$ and the faradaic efficiency $>95\%$. The HER proceeds *via* the Fe(0)Fe(0) state under weakly acidic conditions and *via* the Fe(I)Fe(0) state in strongly acidic conditions. Complex $BrC_6H_4N(CH_2S)_2Fe_2(CO)_6$ (Fig. 29a) and some other molecular catalysts which efficiently produces H_2 in water, are directly adsorbed or deposited on various electrode surface. However, a very few electrocatalysts are reported which are covalently attached onto the electrode surfaces in a site-specific manner.[441,476–479] Covalent attachment of the catalyst solves the problem which appears in physiadsorption like excess catalyst loading, slower electron transfer between catalyst and the electrode, leaching of the catalyst.[480] An azadithiolate bridged [Fe–Fe] hydrogenase mimic containing terminal alkyne group (Fig. 29b) is developed to covalently attach the complex on the modified electrode surface using click chemistry.[475] The complex reduces proton electrocatalytically in presence of dil. H_2SO_4 medium with a high TON and TOF. The covalent attachment offers two orders of magnitude greater catalyst coverage without compromising the inherent catalytic properties of the complex. However, these catalysts need strongly acidic medium and substantial overpotential to be operative. Recently a series of *N*-aryl substituted azadithiolate (ADT) bridged [FeFe]-hydrogenase model complexes (Fig. 29c–e) have been reported in which the bridgehead N lone pair is fixed towards the one of the metal centres by *ortho* substitution of the aryl groups.[145] Heterogeneous electrochemistry of these complexes physiadsorbed on edge plane graphite electrode reveals that the overpotential of proton reduction can be reduced to 160–180 mV in pH 5.5 water (Table 6).

Hydrogen activation by [FeFe]-mimics. Mimicking the catalytic activity of [FeFe]-hydrogenases demands a synthetic diiron complex to catalyse not only the evolution of H_2, but also its oxidation. Such a conversion is of great interest particularly as cheaper alternatives to Pt electrodes in fuel cells. However H_2 heterolysis is very much challenging because free H_2 is weakly acidic (pK_a(THF)[481] ≈ pK_a(MeCN) ≈ 50[482]). This problem can be solved by its binding to a cationic metal like Fe(II). Many [Fe–Fe] hydrogenase models including the above-described ones, can catalyse the hydrogen evolution reaction, but very few of them can mediate or catalyse the reverse reaction, the hydrogen activation. An ideal model system should mimic the H_{ox} (Fe^I–Fe^{II}) state of the enzyme where H_2 binds and cleaved.

Complex (μ-pdt)$[Fe(CO)_2(PMe_3)_2]_2$ (Scheme 29a) on treatment with concentrated HCl produces a stable bridging hydride complex **b**[483] (Scheme 29). Complex **b** (Scheme 29) mediates H/D exchange from H_2/D_2 and from H_2/D_2O. This reaction is inhibited by CO but promoted by sunlight suggesting a vacant coordination site for D_2 binding. In the catalytic cycle D_2 binding takes place prior to D–D cleavage. A series of similar complexes, $(\mu\text{-L})_2[Fe(CO)_2(PMe_3)]_2$, (L = SEt,$SCH_2CH_2S$, $SCH_2C_6H_4CH_2S$) and their protonated derivatives was also evaluated.[484] The different thiolate ligands however has no effect on H/D exchange. Therefore, the sulphur ligands are unlikely proton acceptors in H_2 splitting. Two mechanisms were proposed for the H/D exchange by **b** (Scheme 29).[484] The (μ-pdt)$[Fe(CO)_2(PMe_3)_2]_2$ (Scheme 29a) complex also reacts with SMe^+ to form **c**,[485] which can take up H_2 and catalyses the photolytic H/D exchange in D_2/H_2O. Complex (Scheme 29) **c** does not catalyse H_2/D_2 exchange under anhydrous conditions. Here the H_2/D_2 binding site is trans to the (μ-SMe) and H/D exchange is facilitated by H_2O, the external base. So there is a need of a pentacoordinate Fe(II) Lewis acidic centre for $(H/D)_2$ binding and an Brønsted base for deprotonation of the

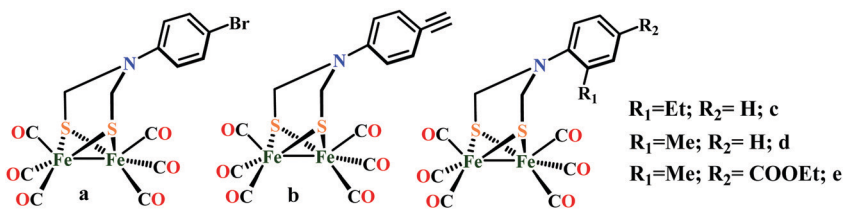

Fig. 29 Proton reducing [FeFe]-hydrogenase model complexes in aqueous medium.

Table 6 Summary of electrochemical proton reduction data for complexes **a–e** (Fig. 29)

Complex	Medium	*E* (V)	TON	TOF (s^{-1})	Overpotential (V)
a	Aqueous medium (pH < 3)	−0.5 V *vs.* SHE	10^8	6400	0.18
c–e	Aqueous medium (pH 5.5)	−0.6 to −0.8 V *vs.* SHE	—	11–50	0.16–0.18
c	Organic medium (proton source TFA)	−1.8 V *vs.* Fc^+/Fc	0.15 ± 0.01	65	1.27
d	Organic medium (proton source TFA)	−1.8 V *vs.* Fc^+/Fc	0.32 ± 0.05	32	1.31
e	Organic medium (proton source TFA)	−1.8 V *vs.* Fc^+/Fc	0.35 ± 0.05	79	1.06

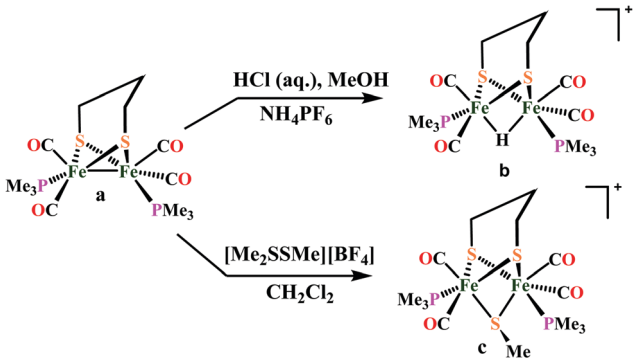

Scheme 29 Preparation of complex **b** and **c**.

coordinated $(H/D)_2$. Complexes **b** and **c** (Scheme 29) can catalytically cleavage H_2 but cannot oxidize H_2 into protons.

Initial attempts at activating and oxidizing H_2 with synthetic [FeFe]-hydrogenase models utilized compounds in their Fe(I)Fe(I) or Fe(II)Fe(II) forms, neither of which is relevant to the biological mechanism, which proceeds through an Fe(I)Fe(II) state. The mixed-valent core of H_{ox} exhibits a rotated Fe_d coordination geometry exposing a site on an electrophilic Fe center to bind H_2 (or the inhibitor CO). Model complexes mimicking the H_{ox} model with an azadithiolate ligand $[Fe_2[((SCH_2)_2N)(CO)_3(PMe)_3(dppv)]^+]$ can react with H_2, in a stoichiometric manner, to produce corresponding hydride complexes.[486] But The related propanedithiolate complex $[Fe_2[((SCH_2)_2CH_2)(CO)_3(PMe)_3(dppv)]^+]$ and oxadithiolate complex $[Fe_2[((SCH_2)_2O)(CO)_3(PMe)_3(dppv)]^+]$ analogues are inactive.[487,488] These results suggest that heterolytic hydrogen activation is assisted by the azadithiolate ligand.

Complex $[Me_3P(CO)_2Fe(N^{Bn})Fe(CO)(dppv)]$ (Fig. 30d) is the first model which slowly (>26 h, 25 °C) activates H_2 and yields a bridging hydride at very high pressure (Scheme 30). But in presence of 1 eq. of a mild oxidant, $[Fe(C_5Me_5)_2]BAr^F{}_4[Ar^F = 3.5\text{-}C_6H_3(CF_3)_2]([Fc]BAr^F{}_4)$, and a weak base at 25 °C it reacts faster under 2 atm of H_2 to produce $[d(\mu\text{-}H)]^+$ species (Scheme 30).[489] However the more electrophilic model $[Fe_2[(SCH_2)_2N^{Bn}](CO)_4(dppn)]^+$ [dppn = 1,8-bis(diphenylphosphino)naphthalene] (Fig. 30e), in presence of 1 eq. of $[Fe(C_5Me_5)_2]BAr^F{}_4$ reacts even more rapidly ($t_{1/2}$ < 13 min at 20 °C) with 1 atm of H_2 compared to $[Me_3P(CO)_2\text{-}Fe(N^{Bn})Fe(CO)(dppv)]$ (Fig. 30d). $[Fe_2[(SCH_2)_2N^{Bn}](CO)_4(dppn)]^+$ (Fig. 30e) heterolyzes {in presence of $[Fe(C_5Me_5)_2]BAr^F{}_4$} H_2 which is 20 times faster than $[Me_3P(CO)_2Fe(N^{Bn})Fe(CO)(dppv)]$ (Fig. 30d) {in presence of $[Fe(C_5Me_5)_2]BAr^F{}_4$} and 10^4 times faster than that by complex $[Me_3P(CO)_2Fe(N^{Bn})Fe(CO)(dppv)]$ (Fig. 30d) in the absence of an oxidant. The kinetic isotopic measurement studies indicate that H_2 binding is the rate-determining step in these reactions.

Thus, for H_2 activation the systems require a Lewis acidic Fe centre, a basic azadithiolate ligand and an electron sink. In the enzyme system these roles are beautifully served by the distal Fe atom, the azadithiolate group and the Fe_4S_4 cluster. To mimic the Fe_4S_4 cluster a redox active FcP* ligand is introduced to the complex $[Me_3P(CO)_2Fe(N^{Bn})Fe(CO)(dppv)]^+$ (Fig. 30d) by Rauchfuss and co-workers.[490] The dicationic form of complex **f** (Fig. 30) (**f**$^{2+}$) reacts with H_2 in a PCET pathway to produce the bridging hydride complex. The FcP* ligand is reduced by one electron in a heterolytic H_2 cleavage pathway. Only a 2-fold increase is observed here compared to **d** (Fig. 30) in presence of external oxidant. Complex **d** (Fig. 30) can only stoichiometrically activate H_2, while the dication **f**$^{2+}$ oxidises H_2 in the presence of excess

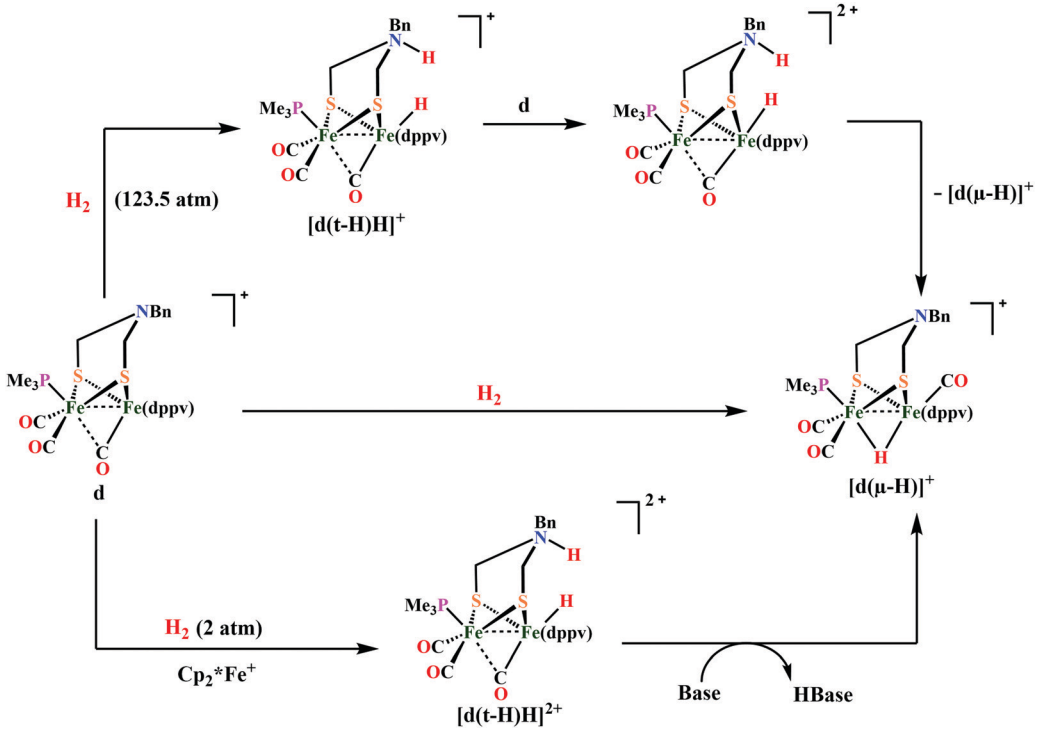

Scheme 30 Stoichiometric activation of H_2 with $[Me_3P(CO)_2Fe(N^{Bn})Fe(CO)(dppv)]$ (Fig. 30d) in the presence[489] and absence of an external oxidant.[487]

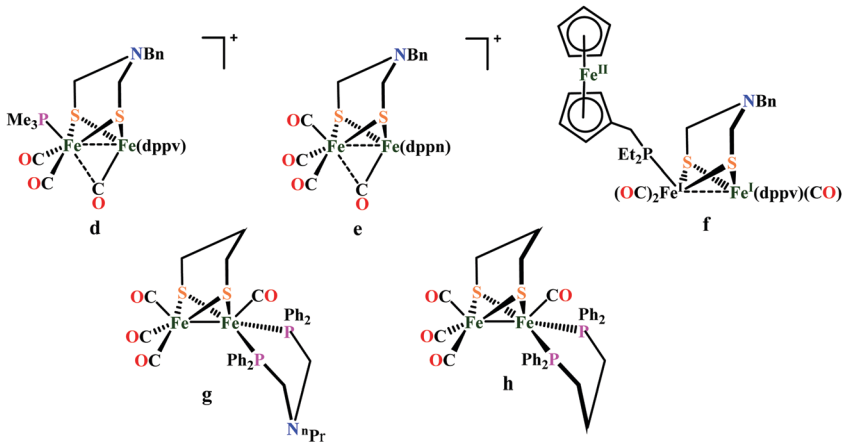

Fig. 30 Hydrogen activating [FeFe]-hydrogenase model complexes **d**, **e**, **f**, **g** and the catalytically inactive complex **h**.

oxidant and excess base, but the rate is extremely slow (TOF = 0.4 h^{-1}). Complex $[(OC)_3Fe(pdt)(\mu\text{-dppf})Fe(CO)]$ [dppf = 1,1-bis(diphenylphosphino)ferrocene][491,492] (Fig. 30g) catalyses H_2 oxidation in presence pyridine at the surface of an electrode.[493] It catalytically oxidises H_2 in presence of excess oxidant $FcBAr^F{}_4$ and base P(*o*-tolyl)$_3$,[494] demonstrating that the redox active group need not to be directly attached to the diiron core to attain the catalytic turnover.[494] Analogous complex $[(CO)_3Fe(pdt)(\mu\text{-dppp})Fe(CO)]$ {dppp = 1,2-bis(diphenylphosphanyl)propane} (Fig. 30h) lacking an internal base moiety on the phosphine ligand does not react with 1 atm H_2 under similar conditions, illustrating the necessity of proton relay.

O_2-Tolerant proton reduction by [FeFe]-mimics. Oxygen sensitivity arises from the generation of reactive oxygen species due to partial reduction of molecular oxygen by the reduced metal clusters involved in proton reduction.[495] Oxygen contamination is unavoidable for proton reducing systems in spite of the fact that the cathode is generally in a strictly anaerobic environment due to fact that the diffusion of the gaseous oxygen produced at the anode cannot be avoided during prolonged electrolysis.[142] Again the standard reduction potential of oxygen is higher than that of proton. So, a catalyst which can reduce protons can always reduce oxygen. However, the active site of a proton reducing catalyst is designed in such a way that it can perform $2H^+/2e^-$ transformation. Whereas four protons and four electrons are required to completely reduce oxygen to water. Logically the proton reducing catalysts may lack of the electrons required to reduce oxygen to water. The partially reduced oxygenated species (PROS) thus generated (*e.g.* O_2^- and H_2O_2)[496,497] can rupture the nearby Fe–S clusters involved in transporting the electrons necessary for proton reduction and/or remain bound to the cluster after electron transfer from the 2Fe2S cluster.[498] Computational studies have proposed that the thermodynamics of O_2 binding to the cluster is in fact favourable, and gas channels are available for O_2 to enter into the active site.[499–501] Since the [FeFe]-hydrogenase and its synthetic analogues are intolerant towards oxygen during catalysis, their use as a practical water splitting catalyst is greatly compromised.[502,503] An investigation of oxygen reduction by azadithiolate bridged diiron complexes (Fig. 29) shows that these complexes irrespective of the nature of the bridging atom, reduce O_2 in their single reduced state [Fe(0.5)Fe(0.5)] producing considerable amount of H_2O_2 (>50%) above pH 5 leading to catalyst decay during proton reduction under aerobic conditions.[497] However, at acidic pH the extent of H_2O_2 production is significantly lowered and is reduced by the nature of the bridging ligand (*N*-alkyl adt bridged complex produces the lowest amount of PROS).[497] A hydrogen bonding interaction from the protonated bridgehead N atom stabilises a metal-bound hydroperoxo intermediate formed during O_2 reduction and reduces H_2O_2 production at lower pH (Scheme 31).

To enhance this hydrogen bonding stability of the peroxide intermediate, to stall its hydrolysis, a series of [FeFe]-hydrogenase mimics with *ortho* substituted arenes attached to bridgehead N atoms is reported (Fig. 29c–e) where the phenyl ring is rotated off the nitrogen lone pair. These complexes reduce proton at very low overpotential in the presence of O_2 near neutral pH (pH 5.5).[145] This class of 2Fe subsite mimics produces almost no H_2O_2 during competitive O_2 reduction; rather they reduce O_2 to H_2O. These complexes are the first examples of synthetic models of hydrogenases that can operate unabated in the presence of O_2.

[NiFe]-Hydrogenase mimics

In the past two and half decades, after the first crystallographic structure of a [NiFe]-hydrogenase was reported in 1995, there has been attempts to structurally and functionally mimic the active site structures of [NiFe]-hydrogenases.[392] For many years it has been a key challenge for synthetic chemists to reproducing the structure and function of the active site of [NiFe]-hydrogenase in artificial mimics motivated by its original dissymmetric structure and its atypical reactivity. Though there are several NiFe model complexes reported in the literature,[394,468,469,504–507] only a few could accurately mimics the structure, function and reactivity of the active site of [NiFe]-hydrogenase.[508] The major limitation of most active site mimics is, unlike enzyme, their chemistry is mainly centred on the Fe site[505] or on M (M = Mn, Ru) in heterodinuclear NiM models.[509–513] The NiFe model complexes reported so far show the hydride ligand is either bridging[511,513–518]

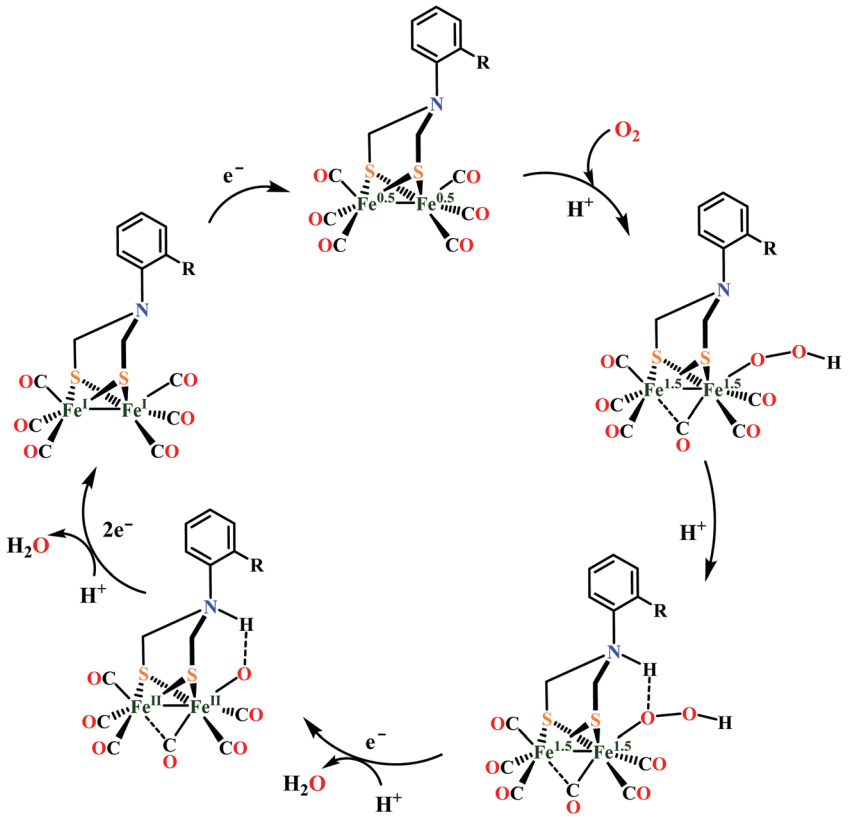

Scheme 31 Proposed mechanism for O_2 reduction by *ortho* substituted ADT bridged Fe–Fe mimics (Fig. 29c–e).

but displaced toward the Fe site, or terminaly bound to the Fe centre.[519–521] Rauchfuss and co-workers have reported a NiFe mimic displaying redox activity at the Ni site with the formation of a $Ni^{I}Fe^{II}$ species. However, DFT calculations showed that in the corresponding protonated species the hydride ligand is bound to iron.[522] Recently, Artero, Duboc and co-workers reported a heterodinuclear NiFe complex, $L^{N2S2}Ni^{II}Fe^{II}$ which shows nickel-centred proton reduction. They were also able to isolate two derivatives that are involved as intermediates in the catalytic cycle that reproduce the structure and spectroscopic signatures of the Ni-R and Ni-L states.[508]

Proton reduction by [NiFe]-mimics in organic medium. After successful modelling of the [NiFe]-H_2ase active site, focus shifted to develop functional models of the same. Rauchfuss and co-workers synthesized a dinuclear NiFe-bridging hydride complex $[(dppe)Ni(\mu\text{-}H)(\mu\text{-}pdt)Fe(CO)_3]^+$ (Fig. 31a), through the apparently facile protonation of $[(dppe)Ni(\mu\text{-}pdt)Fe(CO)_3]$, initially reported by Schröder,[419] with HBF_4.[515] Complex **31a** produces H_2 from trifluoroacetic acid (TFA) in CH_2Cl_2. Substitution of two CO ligands through phosphites (Fig. 31b), phosphines (Fig. 31c and d)[514] or diphosphines,[515] led to a series of derivatives. All these dinuclear bridging hydride derivatives are also active for proton reduction in organic medium in presence of TFA. Comparing the H_2 evolution in CH_2Cl_2 and DMF at a platinum electrode,[523] the overpotential of H_2 evolution from TFA catalyzed by **31a** could be obtained 1 V. Despite of low stability of the phosphine derivatives (Fig. 31b–d) in CH_3CN, proton reduction were further performed which yielded lower overpotential values in the range of 260–430 mV.[514]

In 2010, Fontecave, Artero and co-workers reported another functional model of [NiFe]-H_2ase, with a S_4 ligands framework around the nickel, like the enzyme and a cyclopentadienyl ligand on the iron center. The reaction of [Ni(xbsms)] with $[CpFe(CO)_2(thf)](BF_4)$ in CH_2Cl_2 cleanly and rapidly yields $[(xbsms)Ni^{II}Fe^{II}(CO)_2Cp]^+$. Upon exposure to light $[(xbsms)Ni^{II}Fe^{II}(CO)_2Cp]^+$ loses one CO to form monocarbonyl species $[(xbsms)Ni^{II}Fe^{II}(CO)Cp]^+$ (Fig. 31e). Complex **31e** was shown to catalyze H_2 evolution from TFA in DMF with a 730 mV overpotential requirement. DFT calculations proposed that possible formation of a bridging hydride could occur through protonation at the CO ligand in the one-electron reduced state, followed by rearrangement and elimination of the CO ligand.[523] A year later, the same group synthesized a dinuclear nickel–manganese complex $[Ni(xbsms)Mn(CO)_3(H_2O)]^+$ (Fig. 31f) with the same ligand backbone around the nickel centre.[513] **31f** catalysed hydrogen evolution from TFA in DMF with an overpotential requirement of 860 mV, similar to complex **31e**. Song *et al.* reported another series of Ni–Mn complexes, two of them (Fig. 31g) are active for H_2 evolution from acetic acid in CH_3CN[512] with low catalytic current enhancement but reduced overpotential requirement (~480 mV).

Weber *et al.* reported a structural and functional mimic of [NiFe]-H_2ase with an unusual $\{S_2Ni(\mu\text{-}S)(\mu\text{-}CO)Fe(CO)_2S\}$-coordination environment around the metals (Fig. 31h).

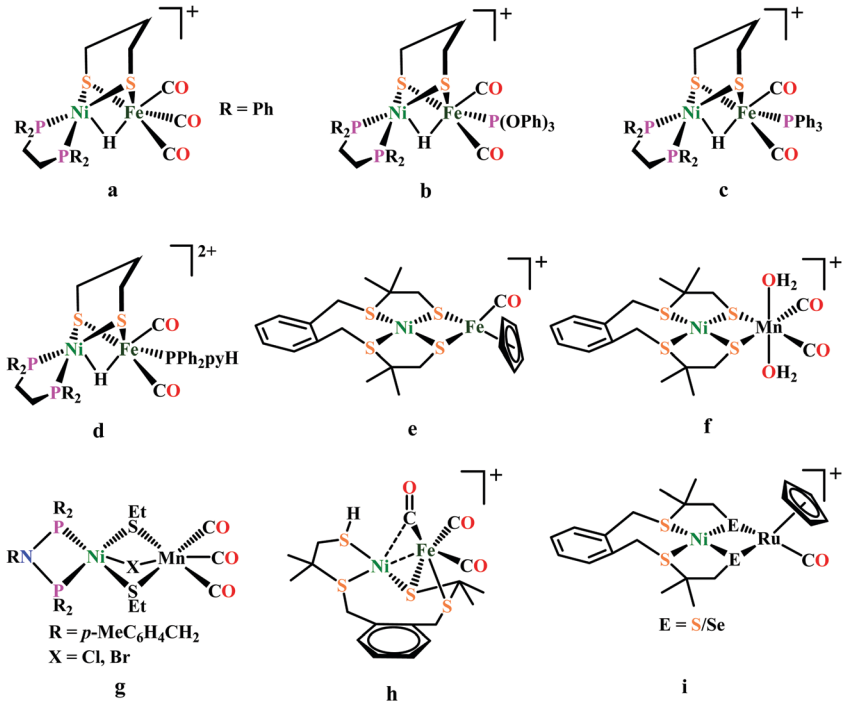

Fig. 31 Structurally relevant, selected [NiFe]-hydrogenase mimics, active for electrocatalytic proton reduction. The only known [NiMn] systems (f and g) shows electrocatalytic proton reduction.

Interestingly, upon addition of 1 equivalent HBF_4 to **31h**, protonation took place at the terminal thiolate sulfur atom, that is coordinated to nickel, in a reversible way to produce protonated species [**31**H][BF_4].[523] This was the first experimental evidence of thiolate protonation, mimicking the postulated catalytic intermediates of [NiFe]-hydrogenases with a Cys-SH protonation.[524–526] Both protonated and un-protonated species does proton reduction reaction from TFA in CH_3CN at 540–570 mV overpotential.[527] Using the analogous strategy, recently, Bouwman and co-workers reported two heterodinuclear NiRu complexes (Fig. 31i) one with bridging sulfur and another with bridging selenium. This complexes catalyze hydrogen evolution in the presence of acetic acid in acetonitrile solution with a overpotentials requirement of 810–830 mV.[528] The same group also reported a NiFeSe complex with same ligand framework but here CO is ligated instead of PPh_3. This complex was found to be active for hydrogen evolution from acetic acid in DMF solution.[529] Ogo and co-workers reported a NiFe-mimic which was able to mediate both hydrogen evolution as well as oxidation in organic medium (CH_3CN/CH_3OH). This complex heterolytically activated H_2 at atmospheric pressure and room temperature in presence of strong base, sodium methoxide, to form a hydride-bearing complex $[Ni^{II}(X')(\mu\text{-}H)Fe^{II}\{P(OEt)_3\}_3]^+$ (Fig. 32a). The new hydride species thus formed is active for hydrogen evolution in presence of strong acid. So, this system shows promise as a catalyst for hydrogen evolution with a quite large overpotentials requirement.[521]

Recently, Artero, Duboc and co-workers described a heterodinuclear NiFe complex, $[L^{N2S2}Ni^{II}Fe^{II}cp(CO)]^+$ (Fig. 32b) that shows 'Ni'-centred proton reduction from [Et_3NH][BF_4] in CH_3CN.[508] In contrast to the NiFe complex containing terminal Fe(II)-hydride, reduction of **32b**, with $NaBH_4$ afforded a hydride complex, $L^{N2S2}Ni^{II}(H)Fe^{II}$. Based on experimental evidences and theoretical calculations, it was proposed that $L^{N2S2}Ni^{II}Fe^{II}$ first undergoes a one-electron reduction to generate $L^{N2S2}Ni^{I}Fe^{II}$. This active species is further reduced to afford a bipyridine based redical anion, $L^{N2S2}{\cdot}Ni^{I}Fe^{II}$, which reacts with protons to yield a metal hydride intermediate akin to the metalloenzyme, $L^{N2S2}Ni^{II}(H)Fe^{II}$. This metal hydride species further reacts with another equivalent of proton to produce H_2 and regenerate the initial $L^{N2S2}Ni^{II}Fe^{II}$ state (Scheme 32).[400] **32b** displays significant catalytic activity at a 500 mV overpotential from Et_3NHBF_4 in CH_3CN solution. The second-order rate constant of proton reduction by this mimic is 2.5×10^4 M^{-1} s^{-1}, which translates into a TOF of 250 s^{-1} at a concentration of 10 mM H^+.[508] Based on extensive DFT calculations, a year later, Tang *et al.* proposed that **32b** does proton reduction following a much lower energy route *via* an E[ECEC] mechanism through an Fe-centred hydride intermediate.[530] The same group in collaboration with others, synthesized a hybrid material NiFe@PCN-777 by incorporating the complex **32b** into the Zr-based MOF PCN-777. FTO supported thin films of the NiFe@PCN-777 composite is active for proton reduction from Et_3NHBF_4 in CH_3CN medium, inside the MOF cavities.[531] The doubly reduced species of complex **32b** is active for proton reduction in presence of weak acid like [Et_3NH][BF_4] while Ahmed *et al.* shown that in presence of strong acid like HBF_4 singly reduced species is the active form for proton reduction in CH_3CN medium.[531]

To finely tune the reactivity of the [NiFe]-hydrogenase mimics Brazzolotto *et al.* modified the ligand environment, exclusively at the Fe site of complex **32b**. Substitution of the

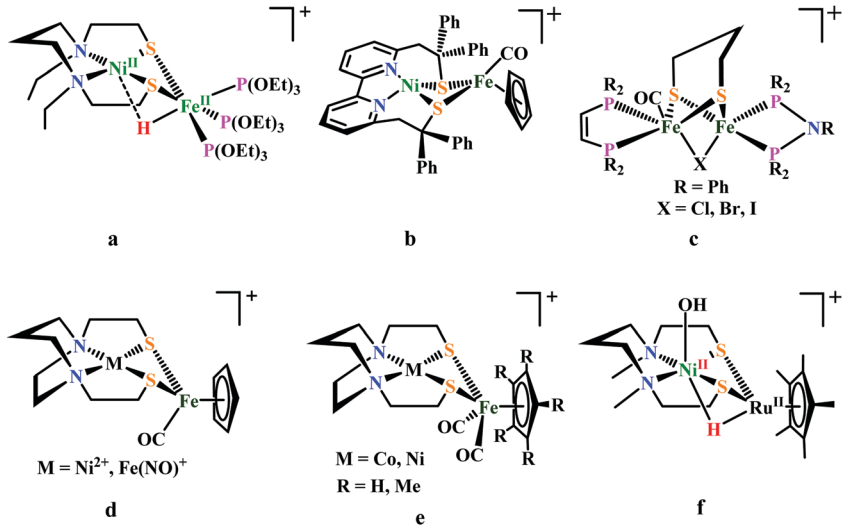

Fig. 32 Selected NiFe-complexes as functional models of [NiFe]-hydrogenases (b–f); a is the NiFe-mimic active for the bidirectional conversion of protons and electrons into dihydrogen.

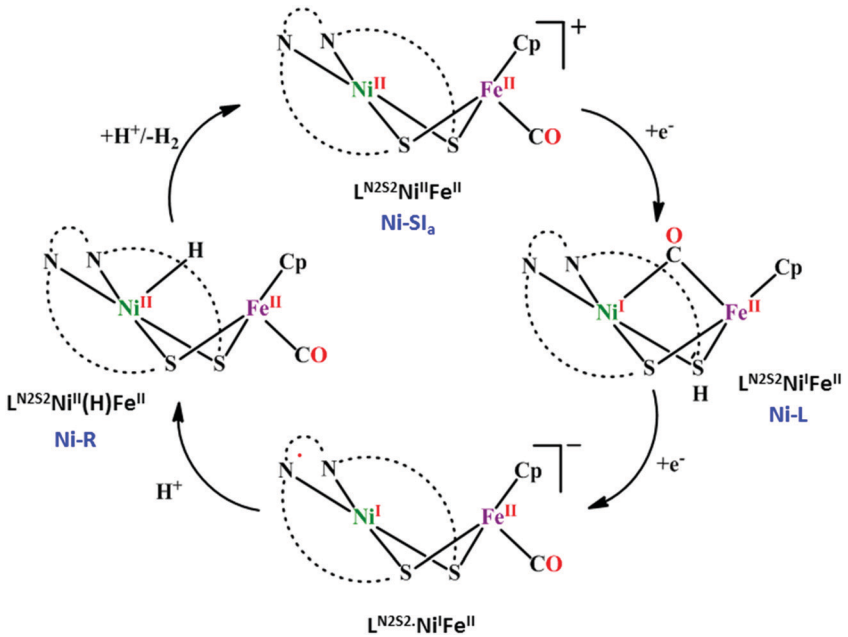

Scheme 32 Proposed mechanistic cycle of proton reduction in complex $[L^{N2S2}Ni^{II}Fe^{II}cp(CO)]^+$ (Fig. 32b).

Cp^- (cyclopentadienyl) ligand by Cp^{*-} (pentamethylcyclopentadienyl) to synthesize $[L^{N2S2}Ni^{II}Fe^{II}cp^*(CO)]^+$ leads to remarkable modifications in its structural properties. Especially for the {Ni(μ-S)$_2$Fe} core with a butterfly structure in $[L^{N2S2}Ni^{II}Fe^{II}cp(CO)]^+$ changes to a quasi-diamond structure in $[L^{N2S2}Ni^{II}Fe^{II}cp^*(CO)]^+$. This new complex thus formed is also active for proton reduction in CH_3CN medium in presence of $[Et_3NH][BF_4]$ as a proton source. In the presence of CO, the electrocatalytic proton reduction activity of cp* species inhibits up to 90% while in case of complex **32b** the inhibition is only 30%.[532] A new series of the structural and functional models, $[RN(PPh_2)_2Ni(\mu\text{-pdt})(\mu\text{-X})Fe(CO)(dppv)][BF_4]$ (Fig. 32c) (R = *p*-$MeC_6H_4CH_2$, EtO_2CCH_2 and X = Cl, Br, I) for the active site of [NiFe]-hydrogenases has been reported by Song and co-workers. These halogenido-bridged model complexes are active for H_2 evolution from Cl_2CHCO_2H in CH_3CN with an overpotential requirement of 530–570 mV. It was seen that the analogous chloro-bridged complexes are catalytically more active than bromo- or iodo-bridged.[533]

Recent electrochemical as well as theoretical studies by Hall, Darensbourg and co-workers of MN_2S_2 (M = Ni^{2+}, $Fe(NO)^{2+}$) bound to $[(\eta^5\text{-}C_5H_5)Fe(CO)]^+$ as electrocatalyst (Fig. 32d) demonstrated that in the electrochemical proton reduction process, reduction-induced hemi-lability of the bridging *cis*-dithiolates is a key step.[534,535] For tuning the electronic character of the M(μ-S_2)Fe core, the $MN_2S_2{\cdot}Fe(\eta^5\text{-}C_5R_5)(CO)$ platform offers numerous possibilities. Modifying M within

the metallodithiolate ligand, as well as replacing H by CH_3 at the η^5-C_5R_5 moiety increases the electron density at the Fe center, which might facilitate the reductive Fe–S bond cleavage. Although release of a free thiolate in these hemi-labile ligands creates a needed internal pendant base, this benefit might be countered by the increase in over-potential for addition of the first electron. Analogous study on MN_2S_2·$[Fe(\eta^5\text{-}C_5R_5)(CO)]^+$ (M = Ni^{2+}, Co^{2+} and R = H, CH_3) (Fig. 32e) complexes by Ghosh *et al.* shows that these catalysts are active for proton reduction in CH_3CN medium in presence of TFA acid source. The over-potentials for the HER by these complexes are in the range of 1–1.3 V. The theoretical modelling suggests that the bridging thiol acts as a proton shuttle during catalysis.[536] Different nitrosyl derivatives of NiFe complexes have also been synthesized to finely tune their catalytic hydrogen evolution activity in terms of TOF and overpotential.[537]

Proton reduction by [NiFe]-mimics in aqueous medium. Most of the [NiFe]-hydrogenase model complexes have been studied in non-aqueous medium while a very few have been studied in aqueous medium under heterogeneous conditions. Recently, Ahmed *et al.* reported that complex **32b** is active for proton reduction in aqueous acidic medium under heterogeneous conditions. This complex shows 'Ni'-centred proton reduction as observed in organic medium.[508] The one electron reduced species, Ni^IFe^{II} directly reacts with protons to formed a metal-hydride, which parallels the mechanism at play at the [NiFe]-hydrogenase active site. Controlled potential electrolysis performed at −0.85 V *vs.* NHE in pH 3 phosphate buffer resulted in electrocatalytic production of H_2 with faradaic yields of 83%. Turnover number and turnover frequency was determined from the long-term (10 h) controlled potential electrolysis data to be 7.2×10^6, and 200 s^{-1}, respectively.[538] Ogo and co-workers reported a μ-hydrido $Ni^{II}Ru^{II}$ complex, $[Ni^{II}L(H_2O)(\mu\text{-}H)Ru^{II}(\eta^6\text{-}C_6Me_6)]^+$ (Fig. 32f) as a [NiFe]-hydrogenase mimics, reacts with one equivalent of HCOONa in water to produce a (μ-hydrido)(formato) $Ni^{II}Ru^{II}$ complex. The (μ-hydrido)(formato) $Ni^{II}Ru^{II}$ complex acts as an effective catalyst for hydrogen evolution from HCOOH and the maximum TON obtained in one hour at pH 3.5 at 60 °C was 857.[539] The catalytic cycle is shown in Scheme 33 where the μ-hydrido $Ni^{II}Ru^{II}$ complex reacts with $HCOO^-$ to form a (μ-hydrido)(formato) $Ni^{II}Ru^{II}$ complex, and after CO_2 liberation a dihydrido intermediate is produced. The reductive elimination of H_2 from the dihydrido intermediate proceeds, leading to the formation of the Ni^IRu^I complex, which reacts with proton to regenerate the μ-hydrido $Ni^{II}Ru^{II}$ complex.[539]

Hydrogen activation by [NiFe]-mimics. Although there are many structural and functional mimics of [NiFe]-hydrogenases reported in the literature a few can activates H_2 homiletically or heterolytically.[486,511,520,521,540,541] It should be noted that among all the NiFe-mimics, most of them only activate H_2 in a stoichiometric or sub-stoichiometric manner. Only a few complexes can activate H_2 catalytically.[511,540,542] Ogo and co-workers synthesized and isolated a paramagnetic Ni(μ-H)Ru complex $[(Ni^{II}L)(H_2O)(\mu\text{-}H)Ru^{II}(\eta^6\text{-}C_6Me_6)]^+$ (Fig. 32f). A diamagnetic dinuclear NiRu aqua complex $[(Ni^{II}L)Ru^{II}(H_2O)(\eta^6\text{-}C_6Me_6)](NO_3)_2$ reacts with H_2 at ambient conditions in water to form the intermediated species **32f**. The introduction of an aqua ligand to the $Ni(\mu\text{-}S)_2Ru$ unit was not only to increase water solubility but also to act as a base to form the $Ni(\mu\text{-}S)_2$-(μ-H)Ru species in water. Because in the hydrogenases the X ligand (H_2O, OH^-, or O^{2-}) present in the resting state is act as a base to activate H_2 in aqueous media as shown this study.[511] A breakthrough was made by the same group when they reported a NiFe-mimic which was able to mediate both hydrogen evolution and oxidation, thus reproducing the bidirectional activity of the [NiFe]-hydrogenases for the first time at a binuclear core.

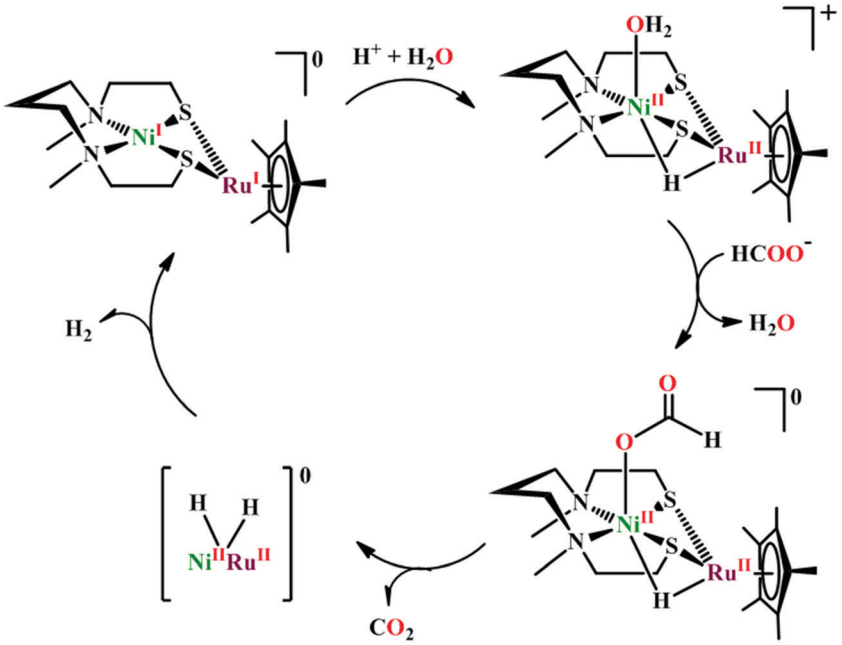

Scheme 33 Proposed mechanism for proton reduction from formic acid catalyzed by NiRu complexes in acidic aqueous media.

The main strategy of the synthesis was using three triethylphosphite ($P(OEt)_3$) ligands to modulate the electronic properties of the iron centre to promote coordination of H_2 as a first step towards its activation. Heterolytic spiltting of H_2 is promoted in presence of a strong base, sodium methoxide which capture the proton, while the hydride ligand is still coordinated to a Fe-centre in a terminal way (Fig. 32a). This hydride species can be oxidized using mild oxidant like methylviologen (MV^{2+}). Release of a proton from this hydride species regenerates the starting complex and thus completing the catalytic cycle (Scheme 34).[521] Compared to **32f**, **32a** is more similar to the active site of [NiFe]-hydrogenase because Ru is replaced by Fe. Recently, Isegawa, Ogo and co-workers performed a detailed mechanistic study by DFT calculation to see the electron/hydride transfer from a NiFe-complex and the corresponding changes in the redox states.[543] Rauchfuss and co-workers synthesized two NiFe-model complexes $(CO)_2(CNBAr^F{}_3)_2Fe(\mu\text{-pdt})Ni(dxpe)$ (dxpe = dppe, **33a**; dxpe = dcpe, **33b**), each with two CO and two $BAr^F{}_3$ protected cyanide ligands on Fe site.[543] To make the iron-centre more electrophilic, introduction of $BAr^F{}_3$ ligands is essential. In presence of H_2 both complexes form terminally bound metal-hydride at the Fe-centre. When a weak acid was added to these terminal-hydride species, dihydrogen-bridging products were formed. Catalytic extraction of electrons from H_2 was achieved by use of the low-valent Ni^IRu^I complex **33c** with Cu^{2+} as oxidant at pH 4–6.[540] $[(cymene)Ru(\mu\text{-pdt})Ni(dppe)](BAr^F{}_4)$ (Fig. 33d) reacted with 1 atm of H_2 to give $[(cymene)Ru(\text{-pdt})(\mu\text{-H})\text{-}Ni(dppe)](BAr^F{}_4)$.[541] In this case, H_2 was reduced to two H^-, while the metal ion was oxidized.

Oxygen-tolerant [NiFe]-mimics. Most of the hydrogenases and their synthetic mimics are either inhibited or even irreversibly damaged by molecular oxygen.[142,368,544] The first S-oxygenated NiFe-complex (Fig. 34a) was reported by Driess's lab as a model for sulfonate intermediates in O_2-tolerant hydrogenase; it was

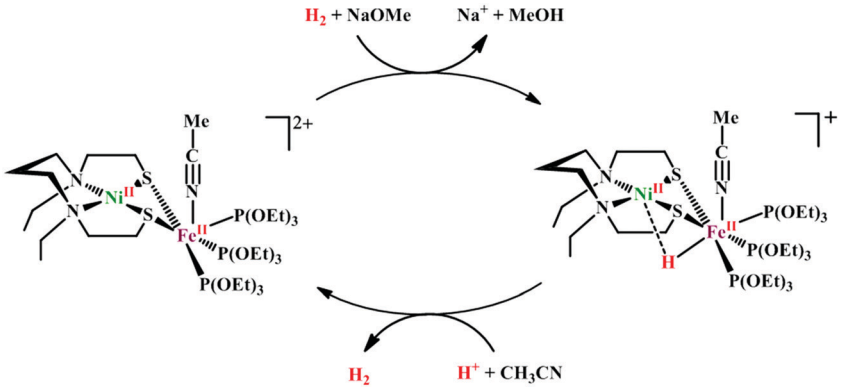

Scheme 34 Proposed mechanism of heterolytic H_2 activation by complex **31a**.

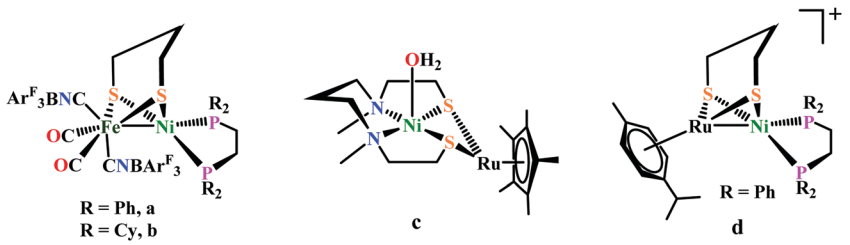

Fig. 33 Selected examples of [NiFe]-hydrogenase mimics active for H_2 activation.

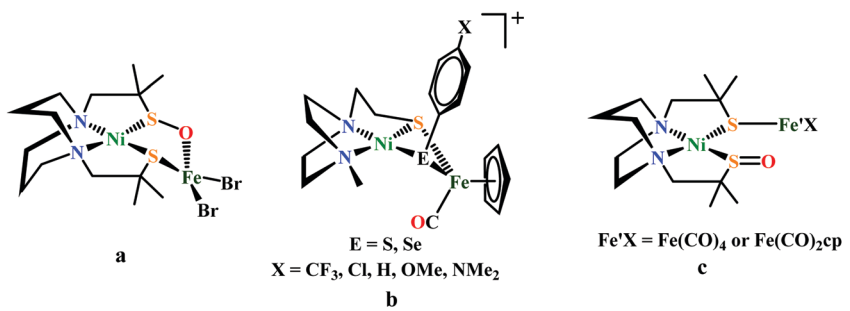

Fig. 34 Only known NiFe-complexes studied as a O_2-tolerarent [NiFe]-hydrogenase mimics.

synthesized from $FeBr_2$ and the pre-formed sulfenato nickel complex rather than direct oxygenation.[545]

Under aerobic conditions, the affinity of oxygen for sulfur and selenium, in [NiFeS]- and [NiFeSe]-hydrogenase, yields oxygenated chalcogens, and delays an inevitable and irreversible oxygen damage at the metals by maintaining the NiFe core structures. To identify the controlling features of S-site oxygen uptake, recently Darensbourg *et al.* synthesized a series of $Ni(\mu\text{-}E_{PhX})(\mu\text{-}S'_{N_2})Fe$ (E = S or Se, Fe = $(\eta^5\text{-}C_5H_5)Fe^{II}(CO)$) (Fig. 34b) complexes and tuned them electronically by changing the *para*-substituent on μ-EPhX (X = CF_3, Cl, H, OMe, NMe_2). DFT analysis suggests that the more electron-rich sulfurs are more O_2 responsive in the SPhX series; the selenium analogues were even more reactive with O_2.[545] In another study the same group described a biomimetic study for S/Se oxygenation in $Ni(\mu\text{-}EPh)(\mu\text{-}SN_2)Fe$, (E = S or Se); Fe = $(\eta^5\text{-}C_5H_5)Fe^{II}(CO)$ complexes related to the oxygen-damaged active sites of [NiFeS]/[NiFeSe]-hydrogenases. Upon O_2 exposure, it forms monooxygenated and dioxygenated species, and treatment with O-abstraction agents such as P(*o*-tolyl)$_3$ or PMe_3 reversed the oxygenation of the S/Se atoms. Although, $NiE_{Ph}Fe^+$ complex differs from the [NiFeSe]-hydrogenase active site as the selenium in the model is in a bridging position, rather than terminal as nature has adopted, the relative reactivities are consistent with what is found in nature.[546]

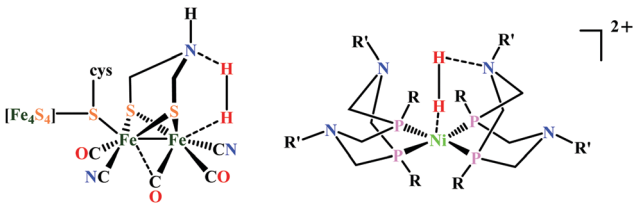

Fig. 35 [FeFe]-hydrogenase active site (left) and $[Ni(P^R{}_2N^{R'}{}_2)_2]^{2+}$ molecular catalyst (right), H_2 bound in each case in the active site.

Very recently, Song and co-workers reported two S-oxygenated intermediate [(mmp-sulfeno-dach)Ni][Fe′X] (Fe′X = $Fe(CO)_4$, $Fe(CO)_2$cp) (Fig. 34c) of an O_2-tolerant [NiFe]-hydrogenase mimics analogues to Driess's system. Reactivity study on both complexes indicates that they undergo the ligand dissociation reactions in the presence of Me_3NO to give their precursor complex, while complex with cp ligand undergoes a complicated sequential reaction in the presence of organometallic oxidant $FcBF_4$ to afford the trinuclear Ni(II) complex, unexpectedly.[546]

Other functional models

Ni(II) complexes. Inspired by the pendant azadithiolate ligand in the active site of [FeFe]-hydrogenase, a series of functional models of mononuclear nickel complexes based on bis diphosphine ligands with pendent amines $[Ni(P^R{}_2N^{R'}{}_2)_2]^{2+}$have been synthesized.[547–549] This mononuclear Ni complexes having beneficial acid–base and redox qualities permits mediation of both H_2 oxidation and production (Fig. 35).[547–550]

Catalytic oxidation of H_2 by Ni complexes. A Ni complex without proton relays, $[Ni(depp)_2]^{2+}$ {depp = 1,2-bis(diethylphosphanyl) propane} (Fig. 36a) slowly catalyses the oxidation of H_2 in the presence of Et_3N.[417] The Ni^{II} hydride complex $[HNi(depp)_2]^{2+}$, without proton relay, shows an irreversible oxidation peak at 0.0 V. But introducing a proton relay into the ligand by the form of a PNP (PNP = $Et_2PCH_2NMeCH_2PEt_2$) ligand $[Ni(PNP)_2]^{2+}$ (Fig. 36b) is obtained. The oxidation peak of $[HNi(PNP)_2]^{2+}$ is shifted to negative potential (−0.62 V). So, by introducing a PNP ligand as a proton relay leads to a much lower energy pathway for oxidation of H_2. The $[Ni(PNP)_2]^{2+}$ complex has an overpotential of about 100 mV, that is 600 mV less than that observed with $[Ni(depp)_2]^{2+}$ for electrocatalytic H_2 oxidation. But rate of catalysis was still slow. The incorporation of a pendant amine group into the PNP ligand triggers a notable decrease in the overpotential for the electrocatalytic H_2 oxidation. Like the cyclohexane here the six-

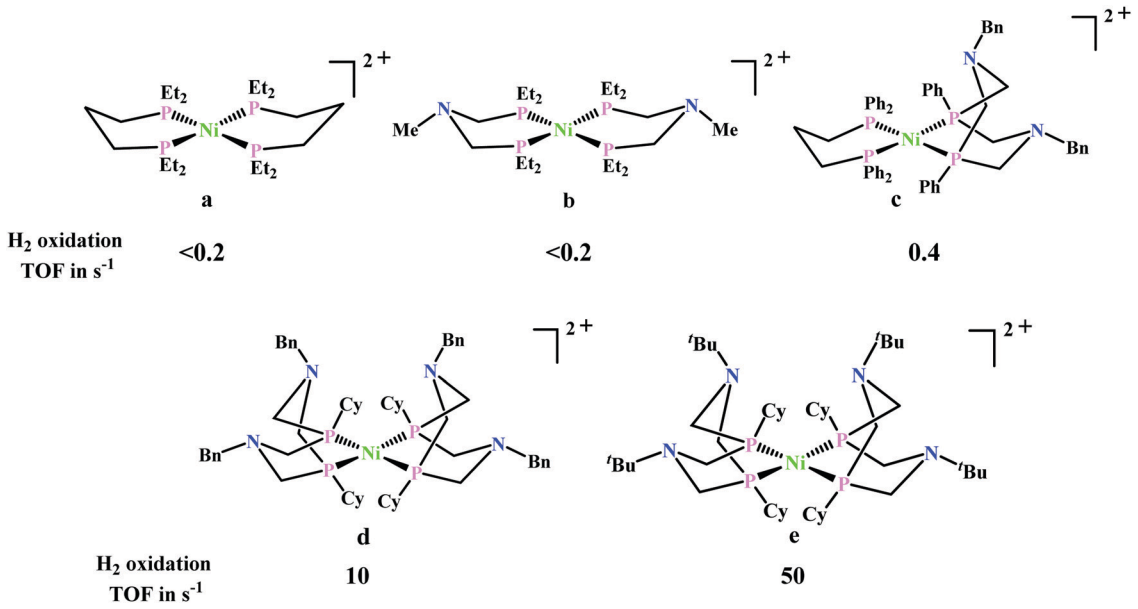

Fig. 36 Ni(II) molecular complexes catalysing H_2 oxidation.

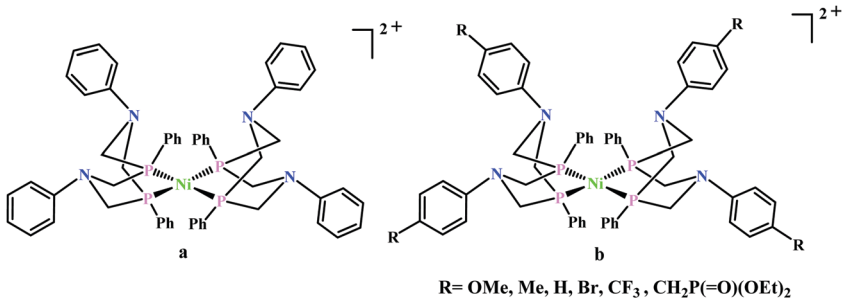

Fig. 37 Proton reducing Ni(II) catalysts.

membered ring Ni–PNP go through chair/boat conformational transitions. But only in the boat conformation the pendant amine is well positioned to interact with a Ni–H bond. But from a crystal structure of $[Ni(PNP)_2]^{2+}$ derivative (with an ^{n}Bu group on each N, Fig. 36c) it is seen that the both six-membered rings are in the chair form. So the energy of conversion of the chair form to the boat form contributes to the kinetic barrier for oxidation of H_2 by $[Ni(PNP)_2]^{2+}$. At least one of the pendant amines adopts boat conformation when a second six-membered ring into the cyclic "P_2N_2" ligand structure of $Ni(P_2N_2)$ complexes is added. By virtue of this the pendent amine becomes properly positioned to interact with a H^- or H_2 ligand on the metal.[417] By varying the alkyl or aryl group bound to P or N atoms in $Ni(P_2N_2)$ the steric and electronic properties can be tuned so that certain reactions are favoured. The calculated TOF of $[Ni(P^{Cy}{}_2N^{Bn}{}_2)_2]^{2+}$(Cy = cyclohexyl; Bn = benzyl) (Fig. 36d) complex for electrocatalytic H_2 (1 atm) oxidation is about 10 s^{-1}, which is much higher than that observed with $[Ni(PNP)_2]^{2+}$. A similar complex containing one P_2N_2 ligand, $[Ni(P^{Cy}{}_2N^{Bn}{}_2)$-(dppp)]$^{2+}${dppp = 1,2-bis(diphenylphosphanyl)propane} catalyses the H_2 oxidation of with a TOF of 0.4 s^{-1} which much

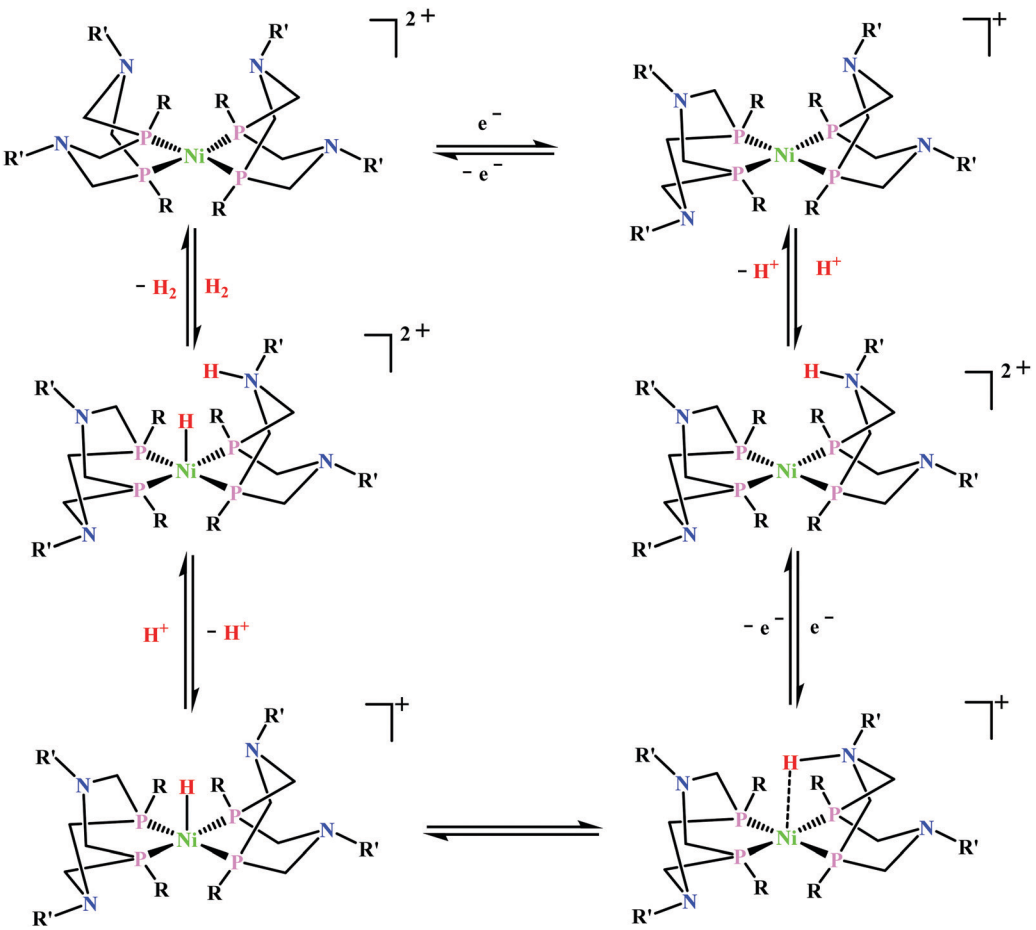

Scheme 35 H_2 oxidation (counter-clockwise) and evolution (clockwise) cycle mediated by $[Ni(P^R{}_2N^{R'}{}_2)_2]^{2+}$ molecular catalysts.[548] This cycle is a simplification that neglects certain side reaction pathways, and the order of the steps depends on the identities of substituents R and R′.[428]

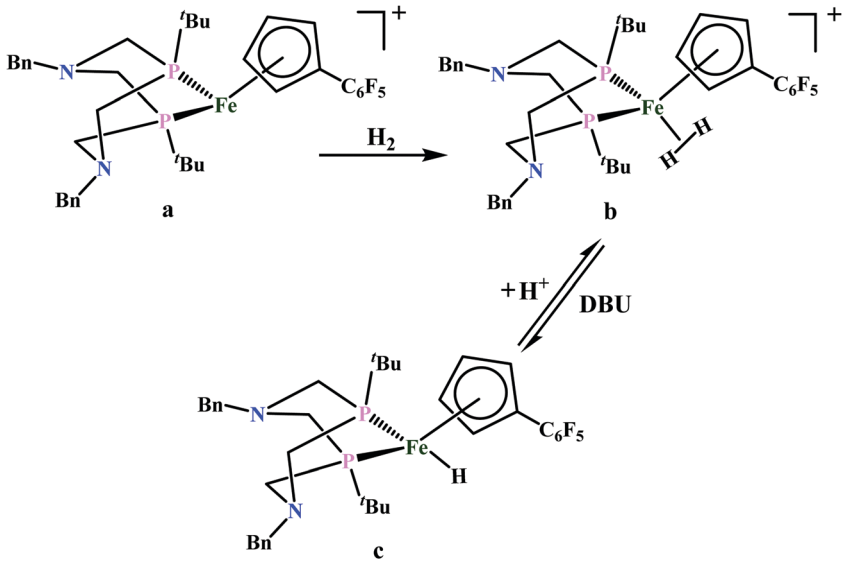

Scheme 36 Reaction of $[(CpC_6F_5)Fe(P^{tBu}{}_2N^{Bn}{}_2)]^+$ with H_2.

less than that compared to the $[Ni(P^{Cy}{}_2N^{Bn}{}_2)_2]^{2+}$ due to with two well positioned pendant amines in later complex.[417] The TOF increases with the number of well positioned pendant amines, indicating that the pendant amines facilitate the binding of H_2. However theoretical studies on $[Ni(P^{Me}{}_2N^{Me}{}_2)_2]^{2+}$, reveals that only one pendant amine is directly associated in the heterolytic binding or cleavage of H_2.[417] The calculated TOF for the Oxidation of H_2 (1 atm) by $[Ni(P^{Cy}{}_2N^{tBu}{}_2)_2]^{2+}$ (^{t}Bu = *tert*-butyl) (Fig. 36e) Complex is 50 s^{-1} at −0.77V *vs.* Fc^+/Fc in presence of Et_3N.[551,552] The higher TOF value for this complex compared to that for $[Ni(P^{Cy}{}_2N^{Bn}{}_2)_2]^{2+}$ is because of the higher basicity of nitrogen atoms attached with *tert*-butyl groups than those of benzyl groups.

Ni-Catalysts for production of H_2 by proton reduction. A series of $[Ni(P^{Ph}{}_2N^{R}{}_2)_2]^{2+}$ complexes containing aryl groups on both the P and N atoms are reported to electrochemically reduce protons.[552,553] When R = Ph, the $[Ni(P^{Ph}{}_2N^{Ph}{}_2)_2]^{2+}$ complex (Fig. 37a) electrochemically reduces buffered solution of protonated dimethylformamide ($H–DMF^+$) in CH_3CN medium with a TOF of 350 s^{-1} at 22 °C and with a overpotential of approximately 0.3 V.[416,420] A series of related complexes $[Ni(P^{Ph}{}_2N^{C_6H_4R}{}_2)_2]^{2+}$ (Fig. 37b) are reported by varying the substituent R group on the *para* position of the aromatic ring of the pendent amine.[554] The substituent-R group is changed from electron-withdrawing groups (–CF_3 and –Br) to –H to electron-donating groups (–Me and –OMe) to examine the effect of basicity of pendent amine group. The $E_{1/2}$ values for the Ni(II/I) couple varies from −0.74 V for R = –CF_3 to −0.88 V for R = OMe and for the Ni(I/0) couple the $E_{1/2}$ values varies from −1.07 V (for R = OMe) to −0.89 V (for R = CF_3). The TOF values calculated for the electrochemical proton reduction from protonated DMF ($H–DMF^+$) in presence of CH_3CN is 740 s^{-1} (for R = Br), 590 s^{-1} (for R = H), 310 s^{-1} (for R = OMe) and 95 s^{-1} (for R = –CF_3). The most electron donating –OMe substituent makes the pendent amine most basic among these, so making the elimination of H_2 difficult. But the strong electron donating group –CF_3 withdraws too much electron density from the pendent amine thus lowering its basicity too much so that it is protonated easily. For this series of Ni complexes the addition of H_2O permits higher TOF. Addition of 0.1–0.3 (M) H_2O in presence of $H–DMF^+$ the catalytic rates become typically 20–50% faster compared to that in absence of H_2O.[554] The added water facilitates the conversion of a catalytically inferior *exo* isomer to catalytically superior endo isomer. For the $[Ni(P^{Ph}{}_2N^{C_6H_4R}{}_2)_2]^{2+}$ complex when [R = $CH_2P(=O)(OEt)_2$, phosphonate] the fastest rates are observed in presence of water. The rate of H_2 production from $H–DMF^+$ for this complex is 500 s^{-1} without added water. But in presence of H_2O it displays a much higher rate of 1850 s^{-1}. Due to the presence of four phosphonate groups, this complex encounter additional H-bonding interactions with H_2O.[553]

A bi-directional catalyst for production and oxidation of H_2. The Ni(II) complex $[Ni(P^{Ph}{}_2N^{CH_2CH_2OMe}{}_2)_2]^{2+}$ containing CH_2CH_2OMe substituents on the pendant amine, reacts reversibly with 1 atm H_2 to give a to give a mixture of the three isomers.[428] Catalytic production of H_2 is observed at −0.55 V when *p*-cyanoanilinium is used as a proton source. A PCET pathway is expected in this case.[555,556] The TOF calculated for the catalytic H_2 production is very low <0.5 s^{-1}. The complex

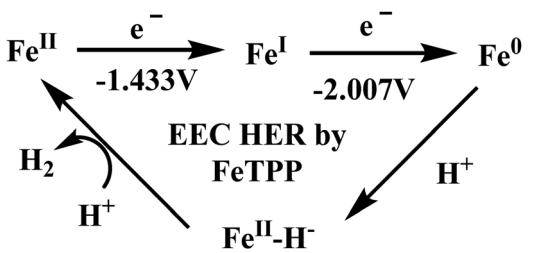

Scheme 37 Probable mechanism of the HER catalysed by FeTPP.

$[Ni(P^{Ph}{}_2N^{CH_2CH_2OMe}{}_2)_2]^{2+}$ is found to be a bidirectional catalyst, indicating that it also slowly catalyses the H_2 oxidation with a low overpotential.[548] A similar type of complex $[Ni(P^{Cy}{}_2N^{Gly}{}_2)]$ exhibits similar bidirectional functions also in water (Scheme 35).[557]

Ni-Complexes containing P_2N ligand. It is observed that by using a seven membered $(7P^{Ph}{}_2N^{Ph})(7P^{Ph}{}_2N^{Ph}$ = 1,3,6-triphenyl-1-aza-3,6-diphosphacycloheptane) ligand instead of $(P^R{}_2N^{R'}{}_2)$ ligands the HER activity of these Ni(II) complexes can be greatly enhanced. Complex $[Ni(7P^{Ph}{}_2N^{Ph})]^{2+}$ electrocatalytically reduces H–DMF^+ at −1.13 V *vs.* Fc^+/Fc to produce H_2. In presence of 0.2(M) acid concentration the calculated overpotential for the catalytic proton reductionof complex **9** is 625 mV.[557] However in presence of 0.43(M) H–DMF^+ the calculated TOF is 33 000 s^{-1} for complex **9**. With the addition of water the catalytic current increases. In presence of 1.2 M water the TOF for the catalytic proton reduction catalysed by complex **9** is found to be 106 000 s^{-1}, which exceeds the value those reported for [Fe–Fe] hydrogenase enzyme (TOF = 9000 s^{-1} at 30 °C).[557]

Fe-Based complexes containing P_2N_2 ligand. Iron based diphosphine containing pendent amines are also reported.[558–560] The complex at room temperature $[(CpC_6F_5)Fe(P^{tBu}{}_2N^{Bn}{}_2)]^+$ (Scheme 36a) reacts with 1 atm H_2 to generate complex $[(CpC_6F_5)Fe(P^{tBu}{}_2N^{Bn}{}_2)(H_2)]^+$ (Scheme 36b) which then reacts with DBU to form complex $[(CpC_6F_5)Fe(P^{tBu}{}_2N^{Bn}{}_2)(H)]$ (Scheme 36c).[559] $[(CpC_6F_5)Fe(P^{tBu}{}_2N^{Bn}{}_2)(H)]$ (Scheme 36c) catalyses H_2 oxidation with TOF of 0.66–2 s^{-1} and a overpotential of 160–220 mV.

Fe-Porphyrins. The importance of the pendant base in hydrogen production is a well-established fact not only in hydrogenases but also in its molecular complexes.[547,560–570] The same is also true in case Iron porphyrins. Iron porphyrin complexes containing second-sphere distal triazole residues in both organic and aqueous medium display a hydrogen evolu-

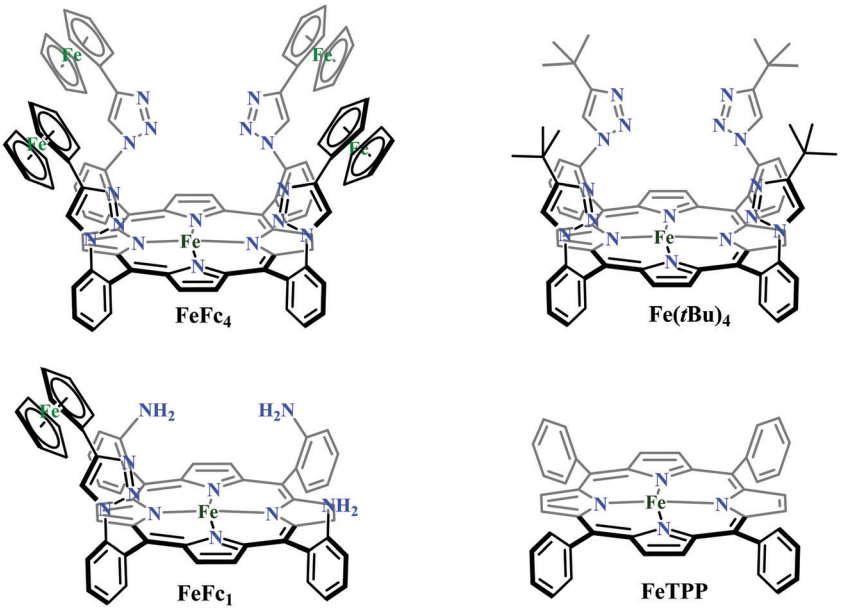

Fig. 38 Structures of Fe porphyrins complexes showing HER.

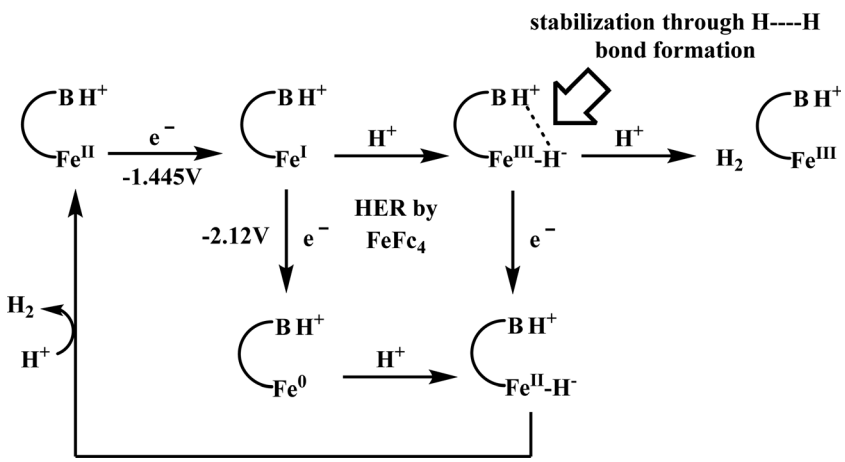

Scheme 38 Probable mechanism of the HER catalysed by Fe porphyrins containing distal triazole basic residues.

tion reaction (HER) catalyzed by the Fe(I) state whereas an analogous iron porphyrin complex without the distal residues catalyzes the HER in the formal Fe(0) state (Scheme 37).[571]

Three iron porphyrins namely $FeFc_4$, $FeFc_1$, and $Fe(tBu)_4$ (where Fc and *t*Bu represent bulky and hydrophobic ferrocene and *tert*-butyl substituents on the triazole ring, respectively, Fig. 38) with second sphere distal triazole residues are reported to show hydrogen evolution reaction in their Fe(I) state in both CH_3CN medium in presence of TsOH (proton source) and in aqueous buffer solution when the catalyst is physiadsorbed on EPG and the pH of the buffer solution is below the pK_a of triazole with the increase in the acid concentration the catalytic current at −1.44 V saturates.[560] While Iron porphyrins without any such secondary structure (FeTPP) can catalyse HER only in their Fe(0) state in both organic and aqueous medium. But with increasing acid concentration the catalytic current increases instead of saturation. The Fe(I) state of FeTPP can catalyse HER under homogeneous condition only in presence of PPh_3. The distal triazole residues of $FeFc_4$, $FeFc_1$, and $Fe(tBu)_4$ complexes gets protonated in presence of TsOH. DFT calculations suggests that upon protonation the Fe(I) center produces an Fe^{III}–H^- species which gets stabilized by these protonated triazoles through dihydrogen bond formation. Thus, only after the protonation of the distal triazole(s) HER can be catalysed by the Fe(I) state. Based on these results it can be concluded that having a pendant base in the second sphere in iron porphyrins provide a thermodynamic advantage by increasing the pK_a of the metal by enhancing the proton affinity by forming dihydrogen bonding (Scheme 38).[560]

General conclusion and outlook

The natural systems have evolved to maximize efficiency for a given catalytic transformation and they exhibit high rates without compromising the selectivity. One needs to look deeper than the immediate structural disposition of a naturally occurring enzymatic active site, keeping in mind the function its primed for, to identify additional attributes that allow these metallo enzymes to access the efficiency they display. Often, for the small molecule reductions discussed here, this includes spatial and temporal control of delivery of protons and electrons to the active site. The metalloenzymes discussed here provide abundant examples of how the control over proton and electron transfer is crucial to maintain product selectivity in these transformations. The prevalent approach in developing small molecule catalysts for the activation of CO_2 relies heavily on past accomplishments in organometallic chemistry.[572] While this has resulted in several 2nd and 3rd row transition metal-based systems with encouraging rates and selectivity, recent developments have highlighted how high rates and selectivities can be accessed by being bio-inspired. Although there are several examples of establishing well-designed proton conduits in the catalysts, electron transfer rates are yet to be controlled to yield tangible advantages to the overall catalysis process.

A thorough understanding of the mechanism of the metalloenzymes along with electronic structure function correlations can lead to the development of efficient 1st row transition metal catalysts for these tasks of contemporary importance. This requires detailed understanding and integration of the 2nd sphere effects in the design of the artificial catalysts. This is beautifully demonstrated in hydrogen evolution catalyzed by synthetic mimics and bio-inspired models of hydrogenases where bi-directional catalysis with practicable rates have been demonstrated.[425] Gradually such approaches are increasingly being deployed to handle CO_2 and NO_2^- reduction. The inclusion of hydrogen bonding residues in CO_2 reduction has resulted not only in facile catalysis but also in much desired selectivity. This is demonstrated in the work by Saveant, Dey, Marinescu, Machan and others. Similarly, while there have been remarkable developments in the understanding of 2nd sphere residues in O_2 reduction by iron porphyrins, these effects are yet to be realized in NO_2^- reduction.[136,329] However, progress has been slow primarily because of the difficulty involved in designing the ligand. The electronic retrosynthesis approach discussed in this review may aid such design.

Selectivity is crucial for controlling the desired product from the reduction of these species. For example, CO_2 can be reduced to CO, HCOOH, H_2CO, CH_3OH or CH_4. Similarly, NO_2^- can be reduced to NO, HNO, N_2, N_2H_4 and N_2. Logically, selectivity over these processes are desirable. Here too, understanding the mechanism of the metalloenzymes can provide solutions as discussed in this review. Going forward one needs to address means to handle competing reactions. For example, the reduction of proton to hydrogen competes with the reduction of CO_2. Similarly, the reduction of O_2 competes with the reduction of protons, CO_2 as well as NO_2^- as the reduction of O_2 is thermodynamically more favourable than the reduction of the rest. While the competition between CO_2 reduction and proton reduction has received some attention, the literature is scanty in the area of O_2 tolerance, with a few rare instances of such selecitivity. Yet, practical application of any of these technologies will require maintaining catalytic performance in the presence of O_2 which is abundant in the atmosphere and its removal will only increase the cost of any catalytic process. For instance, direct reduction of CO_2 is severely limited by the cost of capturing CO_2 from atmosphere. Alternatively, if CO_2 present in the flue gas (8–15%) can be reduced, the cost of CO_2 capture can be subverted. This will require the catalyst to be tolerant to O_2. Unfortunately, the sensitivity to O_2 is a limitation of the natural enzymes as well as many of them are inhibited by O_2 albeit reversibly in some handful cases. Thus, this is an area that will require creative solutions above and beyond what exists and can be learnt from naturally occurring enzymes. The Dey group has established a few examples of O_2 tolerant H^+ and CO_2 reduction catalysts.[145,147,573] Finally, it is fair enough to assume that robust catalysts for these important multi-proton and multi-electron reactions are likely to be based on heterogeneous materials. Thus, a transition of the building knowledge in the area of bio-inspired molecular catalysts to smart materials is warranted.

Conflicts of interest

There are no conflicts to declare.

References

1 A. P. Ballantyne, C. B. Alden, J. B. Miller, P. P. Tans and J. W. C. White, *Nature*, 2012, **488**, 70–72.
2 A. G. Chmielewski, *Encyclopedia of Life Support Systems*, 2008.
3 A. M. Appel, J. E. Bercaw, A. B. Bocarsly, H. Dobbek, D. L. DuBois, M. Dupuis, J. G. Ferry, E. Fujita, R. Hille, P. J. A. Kenis, C. A. Kerfeld, R. H. Morris, C. H. F. Peden, A. R. Portis, S. W. Ragsdale, T. B. Rauchfuss, J. N. H. Reek, L. C. Seefeldt, R. K. Thauer and G. L. Waldrop, *Chem. Rev.*, 2013, **113**, 6621–6658.
4 *Bulletin of the American Meteorological Society*, ed. J. Blunden and D. S. Arndt, 2020, vol. 101, pp. S1–S429.
5 M. E. Boot-Handford, J. C. Abanades, E. J. Anthony, M. J. Blunt, S. Brandani, N. Mac Dowell, J. R. Fernández, M.-C. Ferrari, R. Gross, J. P. Hallett, R. S. Haszeldine, P. Heptonstall, A. Lyngfelt, Z. Makuch, E. Mangano, R. T. J. Porter, M. Pourkashanian, G. T. Rochelle, N. Shah, J. G. Yao and P. S. Fennell, *Energy Environ. Sci.*, 2014, **7**, 130–189.
6 G. Centi and S. Perathoner, *Catal. Today*, 2009, **148**, 191–205.
7 K. S. Lackner, *Annu. Rev. Energy Environ.*, 2002, **27**, 193–232.
8 D. T. Whipple and P. J. A. Kenis, *J. Phys. Chem. Lett.*, 2010, **1**, 3451–3458.
9 H.-R. ''Molly'' Jhong, S. Ma and P. J. A. Kenis, *Curr. Opin. Chem. Eng.*, 2013, **2**, 191–199.
10 R. Francke, B. Schille and M. Roemelt, *Chem. Rev.*, 2018, **118**, 4631–4701.
11 E. E. Benson, C. P. Kubiak, A. J. Sathrum and J. M. Smieja, *Chem. Soc. Rev.*, 2009, **38**, 89–99.
12 S. Zhang, Q. Fan, R. Xia and T. J. Meyer, *Acc. Chem. Res.*, 2020, **53**, 255–264.
13 R. W. Dorner, D. R. Hardy, F. W. Williams and H. D. Willauer, *Energy Environ. Sci.*, 2010, **3**, 884–890.
14 Y. Hori, *Handb. Fuel Cells*, 2010.
15 K. E. Dalle, J. Warnan, J. J. Leung, B. Reuillard, I. S. Karmel and E. Reisner, *Chem. Rev.*, 2019, **119**, 2752–2875.
16 B. Kumar, M. Llorente, J. Froehlich, T. Dang, A. Sathrum and C. P. Kubiak, *Annu. Rev. Phys. Chem.*, 2012, **63**, 541–569.
17 M. P. Johnson, *Essays Biochem.*, 2016, **60**, 255–273.
18 C. Welte and U. Deppenmeier, in *Methods in Methane Metabolism, Part A*, ed. A. C. Rosenzweig and S. W. B. T.-M. E. Ragsdale, Academic Press, 2011, vol. 494, pp. 257–280.
19 J. L. Peel, R. Haeuber, V. Garcia, A. G. Russell and L. Neas, *Biogeochemistry*, 2013, **114**, 121–134.
20 M. Graetzel, *Acc. Chem. Res.*, 1981, **14**, 376–384.
21 A. J. Bard and M. A. Fox, *Acc. Chem. Res.*, 1995, **28**, 141–145.
22 E. Lamy, L. Nadjo and J. M. Saveant, *J. Electroanal. Chem. Interfacial Electrochem.*, 1977, **78**, 403–407.
23 H. A. Schwarz and R. W. Dodson, *J. Phys. Chem.*, 1989, **93**, 409–414.
24 C. Costentin, M. Robert and J.-M. Savéant, *Chem. Soc. Rev.*, 2013, **42**, 2423–2436.
25 J. A. Bassham, A. A. Benson and M. Calvin, *J. Biol. Chem.*, 1950, **185**, 781–787.
26 S. W. Ragsdale and E. Pierce, *Biochim. Biophys. Acta, Proteins Proteomics*, 2008, **1784**, 1873–1898.
27 B. B. Buchanan and D. I. Arnon, *Photosynth. Res.*, 1990, **24**, 47–53.
28 M. C. Evans, B. B. Buchanan and D. I. Arnon, *Proc. Natl. Acad. Sci. U. S. A.*, 1966, **55**, 928–934.
29 G. Fuchs, *Annu. Rev. Microbiol.*, 2011, **65**, 631–658.
30 V. Svetlitchnyi, C. Peschel, G. Acker and O. Meyer, *J. Bacteriol.*, 2001, **183**, 5134–5144.
31 B. Zhang, C. F. Hemann and R. Hille, *J. Biol. Chem.*, 2010, **285**, 12571–12578.
32 H. Dobbek, L. Gremer, R. Kiefersauer, R. Huber and O. Meyer, *Proc. Natl. Acad. Sci. U. S. A.*, 2002, **99**, 15971–15976.
33 S. W. Ragsdale and M. Kumar, *Chem. Rev.*, 1996, **96**, 2515–2540.
34 Z. Hu, N. J. Spangler, M. E. Anderson, J. Xia, P. W. Ludden, P. A. Lindahl and E. Münck, *J. Am. Chem. Soc.*, 1996, **118**, 830–845.
35 Y. Kung and C. L. Drennan, *Curr. Opin. Chem. Biol.*, 2011, **15**, 276–283.
36 T. I. Doukov, T. M. Iverson, J. Seravalli, S. W. Ragsdale and C. L. Drennan, *Science*, 2002, **298**, 567–572.
37 H. Dobbek, V. Svetlitchnyi, J. Liss and O. Meyer, *J. Am. Chem. Soc.*, 2004, **126**, 5382–5387.
38 Y. Kung, T. I. Doukov, J. Seravalli, S. W. Ragsdale and C. L. Drennan, *Biochemistry*, 2009, **48**, 7432–7440.
39 J.-H. Jeoung and H. Dobbek, *Science*, 2007, **318**, 1461–1464.
40 V. J. DeRose, J. Telser, M. E. Anderson, P. A. Lindahl and B. M. Hoffman, *J. Am. Chem. Soc.*, 1998, **120**, 8767–8776.
41 E. J. Kim, J. Feng, M. R. Bramlett and P. A. Lindahl, *Biochemistry*, 2004, **43**, 5728–5734.
42 C. L. Drennan, J. Heo, M. D. Sintchak, E. Schreiter and P. W. Ludden, *Proc. Natl. Acad. Sci. U. S. A.*, 2001, **98**, 11973–11978.
43 B. Mondal, J. Song, F. Neese and S. Ye, *Curr. Opin. Chem. Biol.*, 2015, **25**, 103–109.
44 I. G. Shabalin, K. M. Polyakov, V. I. Tishkov and V. O. Popov, *Acta Nat.*, 2009, **1**, 89–93.
45 E. V. Filippova, K. M. Polyakov, T. V. Tikhonova, T. N. Stekhanova, K. M. Boiko and V. O. Popov, *Crystallogr. Rep.*, 2005, **50**, 796–800.
46 R. K. Thauer, *FEBS Lett.*, 1972, **27**, 111–115.
47 T. Reda, C. M. Plugge, N. J. Abram and J. Hirst, *Proc. Natl. Acad. Sci. U. S. A.*, 2008, **105**, 10654–10658.
48 J. C. Boyington, V. N. Gladyshev, S. V. Khangulov, T. C. Stadtman and P. D. Sun, *Science*, 1997, **275**, 1305–1308.
49 H. C. A. Raaijmakers and M. J. Romão, *JBIC, J. Biol. Inorg. Chem.*, 2006, **11**, 849–854.
50 V. N. Gladyshev, J. C. Boyington, S. V. Khangulov, D. A. Grahame, T. C. Stadtman and P. D. Sun, *J. Biol. Chem.*, 1996, **271**, 8095–8100.

51 H. Dobbek, *Coord. Chem. Rev.*, 2011, **255**, 1104–1116.
52 H. Raaijmakers, S. Macieira, J. M. Dias, S. Teixeira, S. Bursakov, R. Huber, J. J. G. Moura, I. Moura and M. J. Romão, *Structure*, 2002, **10**, 1261–1272.
53 S. V. Khangulov, V. N. Gladyshev, G. C. Dismukes and T. C. Stadtman, *Biochemistry*, 1998, **37**, 3518–3528.
54 G. N. George, C. M. Colangelo, J. Dong, R. A. Scott, S. V. Khangulov, V. N. Gladyshev and T. C. Stadtman, *J. Am. Chem. Soc.*, 1998, **120**, 1267–1273.
55 C. S. Mota, M. G. Rivas, C. D. Brondino, I. Moura, J. J. G. Moura, P. J. González and N. M. F. S. A. Cerqueira, *JBIC, J. Biol. Inorg. Chem.*, 2011, **16**, 1255–1268.
56 M. Aresta, C. F. Nobile, V. G. Albano, E. Forni and M. Manassero, *J. Chem. Soc., Chem. Commun.*, 1975, 636–637.
57 S. Meshitsuka, M. Ichikawa and K. Tamaru, *J. Chem. Soc., Chem. Commun.*, 1974, 158–159.
58 B. Fisher and R. Eisenberg, *J. Am. Chem. Soc.*, 1980, **102**, 7361–7363.
59 J. Hawecker, J.-M. Lehn and R. Ziessel, *J. Chem. Soc., Chem. Commun.*, 1984, **3**, 328–330.
60 J. Hawecker, J. Lehn and R. Ziessel, *Helv. Chim. Acta*, 1986, **69**, 1990.
61 H. Ishida, K. Tanaka and T. Tanaka, *Organometallics*, 1987, **6**, 181–186.
62 C. Mark Bolinger, B. Nicole Story, P. Sullivan and T. J. Meyer, *Inorg. Chem.*, 1988, **27**, 4582–4587.
63 M. R. Bruce, E. Megehee, B. P. Sullivan, H. Thorn, T. R. O'Toole, A. Downard and T. J. Meyer, *Organometallics*, 1988, **7**, 238–240.
64 J. M. Smieja and C. P. Kubiak, *Inorg. Chem.*, 2010, **49**, 9283–9289.
65 J. M. Smieja, E. E. Benson, B. Kumar, K. A. Grice, C. S. Seu, A. J. M. Miller, J. M. Mayer and C. P. Kubiak, *Proc. Natl. Acad. Sci. U. S. A.*, 2012, **109**, 15646–15650.
66 M. Bourrez, F. Molton, S. Chardon-Noblat and A. Deronzier, *Angew. Chem., Int. Ed.*, 2011, **50**, 9903–9906.
67 J. M. Smieja, M. D. Sampson, K. A. Grice, E. E. Benson, J. D. Froehlich and C. P. Kubiak, *Inorg. Chem.*, 2013, **52**, 2484–2491.
68 M. D. Sampson, A. D. Nguyen, K. A. Grice, C. E. Moore, A. L. Rheingold and C. P. Kubiak, *J. Am. Chem. Soc.*, 2014, **136**, 5460–5471.
69 M. D. Sampson and C. P. Kubiak, *J. Am. Chem. Soc.*, 2016, **138**, 1386–1393.
70 A. Zhanaidarova, H. Steger, M. H. Reineke and C. P. Kubiak, *Dalton Trans.*, 2017, **46**, 12413–12416.
71 M. L. Clark, K. A. Grice, C. E. Moore, A. L. Rheingold and C. P. Kubiak, *Chem. Sci.*, 2014, **5**, 1894–1900.
72 J. Agarwal, T. W. Shaw, C. J. Stanton, G. F. Majetich, A. B. Bocarsly and H. F. Schaefer, *Angew. Chem., Int. Ed.*, 2014, **53**, 5152–5155.
73 F. Franco, C. Cometto, F. F. Vallana, F. Sordello, E. Priola, C. Minero, C. Nervi and R. Gobetto, *Chem. Commun.*, 2014, **50**, 14670–14673.
74 N. P. Liyanage, H. A. Dulaney, A. J. Huckaba, J. W. Jurss and J. H. Delcamp, *Inorg. Chem.*, 2016, **55**, 6085–6094.
75 K. T. Ngo, M. McKinnon, B. Mahanti, R. Narayanan, D. C. Grills, M. Z. Ertem and J. Rochford, *J. Am. Chem. Soc.*, 2017, **139**, 2604–2618.
76 S. Sung, D. Kumar, M. Gil-Sepulcre and M. Nippe, *J. Am. Chem. Soc.*, 2017, **139**, 13993–13996.
77 S. Sung, X. Li, L. M. Wolf, J. R. Meeder, N. S. Bhuvanesh, K. A. Grice, J. A. Panetier and M. Nippe, *J. Am. Chem. Soc.*, 2019, **141**, 6569–6582.
78 E. Haviv, D. Azaiza-Dabbah, R. Carmieli, L. Avram, J. M. L. Martin and R. Neumann, *J. Am. Chem. Soc.*, 2018, **140**, 12451–12456.
79 A. W. Nichols, S. Chatterjee, M. Sabat and C. W. MacHan, *Inorg. Chem.*, 2018, **57**, 2111–2121.
80 A. N. Hellman, R. Haiges and S. C. Marinescu, *Dalton Trans.*, 2019, **48**, 14251–14255.
81 D. Z. Zee, M. Nippe, A. E. King, C. J. Chang and J. R. Long, *Inorg. Chem.*, 2020, **59**, 5206–5217.
82 S. Slater and J. H. Wagenknecht, *J. Am. Chem. Soc.*, 1984, **106**, 5367–5368.
83 A. Szymaszek and F. P. Pruchnik, *J. Organomet. Chem.*, 1989, **376**, 133–140.
84 D. L. Dubois, *Comments Inorg. Chem.*, 1997, **19**, 307–325.
85 A. M. Brun and A. Harriman, *J. Am. Chem. Soc.*, 1991, **113**, 8153–8159.
86 B. D. Steffey, A. Miedaner, M. L. Maciejewski-Farmer, P. R. Bernatis, A. M. Herring, V. S. Allured, V. Carperos and D. L. DuBois, *Organometallics*, 1994, **13**, 4844–4855.
87 P. Kang, C. Cheng, Z. Chen, C. K. Schauer, T. J. Meyer and M. Brookhart, *J. Am. Chem. Soc.*, 2012, **134**, 5500–5503.
88 A. Miedaner, C. J. Curtis, R. M. Barkley and D. L. DuBois, *Inorg. Chem.*, 1994, **33**, 5482–5490.
89 B. D. Steffey, C. J. Curtis and D. L. DuBois, *Organometallics*, 1995, **14**, 4937–4943.
90 A. Miedaner, B. C. Noll and D. L. DuBois, *Organometallics*, 1997, **16**, 5779–5791.
91 D. L. Delaet, R. Del Rosario, P. E. Fanwick and C. P. Kubiak, *J. Am. Chem. Soc.*, 1987, **109**, 754–758.
92 E. Simón-Manso and C. P. Kubiak, *Organometallics*, 2005, **24**, 96–102.
93 R. J. Haines, R. E. Wittrig and C. P. Kubiak, *Inorg. Chem.*, 1994, **33**, 4723–4728.
94 D. A. Morgenstern, G. M. Ferrence, J. Washington, J. I. Henderson, L. Rosenhein, J. D. Heise, P. E. Fanwick and C. P. Kubiak, *J. Am. Chem. Soc.*, 1996, **118**, 2198–2207.
95 S. Roy, B. Sharma, J. Pécaut, P. Simon, M. Fontecave, P. D. Tran, E. Derat and V. Artero, *J. Am. Chem. Soc.*, 2017, **139**, 3685–3696.
96 C. S. Seu, A. M. Appel, M. D. Doud, D. L. Dubois and C. P. Kubiak, *Energy Environ. Sci.*, 2012, **5**, 6480–6490.
97 B. R. Galan, M. L. Reback, A. Jain, A. M. Appel and W. J. Shaw, *Eur. J. Inorg. Chem.*, 2013, 5366–5371.
98 B. R. Galan, J. Schöffel, J. C. Linehan, C. Seu, A. M. Appel, J. A. S. Roberts, M. L. Helm, U. J. Kilgore, J. Y. Yang, D. L. Dubois and C. P. Kubiak, *J. Am. Chem. Soc.*, 2011, **133**, 12767–12779.
99 L. Chen, Z. Guo, X. G. Wei, C. Gallenkamp, J. Bonin, E. Anxolabéhère-Mallart, K. C. Lau, T. C. Lau and M. Robert, *J. Am. Chem. Soc.*, 2015, **137**, 10918–10921.

100 A. Taheri, E. J. Thompson, J. C. Fettinger and L. A. Berben, *ACS Catal.*, 2015, **5**, 7140–7151.
101 A. Taheri and L. A. Berben, *Inorg. Chem.*, 2016, **55**, 378–385.
102 D. Lexa, J. M. Savéant and D. L. Wang, *Organometallics*, 1986, **5**, 1428–1434.
103 D. Lexa, J. M. Saveant, K. B. Su and D. L. Wang, *J. Am. Chem. Soc.*, 1988, **110**, 7617–7625.
104 C. Gueutin, D. Lexa, J. M. Savéant and D. L. Wang, *Organometallics*, 1989, **8**, 1607–1613.
105 D. Lexa, J. M. Savéant, K. B. Su and D. L. Wang, *J. Am. Chem. Soc.*, 1987, **109**, 6464–6470.
106 D. Lexa, J. M. Savéant, K. B. Su, D. L. Wang, H. J. Schäfer and B. Vering, *J. Am. Chem. Soc.*, 1990, **112**, 6162–6177.
107 M. Hammouche, D. Lexa, J. M. Savéant and M. Momenteau, *J. Electroanal. Chem.*, 1988, **249**, 347–351.
108 M. Hammouche, D. Lexa, J. M. Savêant and M. Momenteau, *J. Am. Chem. Soc.*, 1991, **113**, 8455–8466.
109 I. Bhugun, D. Lexa and J. M. Savéant, *J. Phys. Chem.*, 1996, **100**, 19981–19985.
110 I. Bhugun, D. Lexa and J. M. Savéant, *J. Am. Chem. Soc.*, 1994, **116**, 5015–5016.
111 E. A. Mohamed, Z. N. Zahran and Y. Naruta, *Chem. Commun.*, 2015, **51**, 16900–16903.
112 C. Costentin, S. Drouet, G. Passard, M. Robert and J. M. Savéant, *J. Am. Chem. Soc.*, 2013, **135**, 9023–9031.
113 C. Costentin, M. Robert, J. M. Savéant and C. Tard, *Acc. Chem. Res.*, 2014, **47**, 271–280.
114 C. Costentin, S. Drouet, M. Robert and J.-M. Savéant, *Science*, 2012, **338**, 90–94.
115 C. Costentin, G. Passard, M. Robert and J. M. Savéant, *Proc. Natl. Acad. Sci. U. S. A.*, 2014, **111**, 14990–14994.
116 S. Sinha and J. J. Warren, *Inorg. Chem.*, 2018, **57**, 12650–12656.
117 M. H. Abraham, P. L. Grellier, D. V. Prior, J. J. Morris and P. J. Taylor, *J. Chem. Soc., Perkin Trans. 2*, 1990, 521–529.
118 M. H. Abraham, P. L. Grellier, D. V. Prior, P. P. Duce, J. J. Morris and P. J. Taylor, *J. Chem. Soc., Perkin Trans. 2*, 1989, 699–711.
119 C. Costentin, M. Robert, J. M. Savéant and A. Tatin, *Proc. Natl. Acad. Sci. U. S. A.*, 2015, **112**, 6882–6886.
120 C. Costentin, G. Passard, M. Robert and J. M. Savéant, *J. Am. Chem. Soc.*, 2014, **136**, 11821–11829.
121 P. Kumar Das, K. Mittra and A. Dey, *Chem. Commun.*, 2014, **50**, 5218–5220.
122 K. Mittra, S. Chatterjee, S. Samanta, K. Sengupta, H. Bhattacharjee and A. Dey, *Chem. Commun.*, 2012, **48**, 10535–10537.
123 K. Mittra, S. Chatterjee, S. Samanta and A. Dey, *Inorg. Chem.*, 2013, **52**, 14317–14325.
124 B. Mondal, A. Rana, P. Sen and A. Dey, *J. Am. Chem. Soc.*, 2015, **137**, 11214–11217.
125 I. Azcarate, C. Costentin, M. Robert and J. M. Savéant, *J. Am. Chem. Soc.*, 2016, **138**, 16639–16644.
126 A. Khadhraoui, P. Gotico, B. Boitrel, W. Leibl, Z. Halime and A. Aukauloo, *Chem. Commun.*, 2018, **54**, 11630–11633.
127 C. G. Margarit, C. Schnedermann, N. G. Asimow and D. G. Nocera, *Organometallics*, 2019, **38**, 1219–1223.
128 K. Guo, X. Li, H. Lei, W. Zhang and R. Cao, *ChemCatChem*, 2020, **12**, 1591–1595.
129 E. M. Nichols, J. S. Derrick, S. K. Nistanaki, P. T. Smith and C. J. Chang, *Chem. Sci.*, 2018, **9**, 2952–2960.
130 P. Sen, B. Mondal, D. Saha, A. Rana and A. Dey, *Dalton Trans.*, 2019, **48**, 5965–5977.
131 P. Gotico, B. Boitrel, R. Guillot, M. Sircoglou, A. Quaranta, Z. Halime, W. Leibl and A. Aukauloo, *Angew. Chem., Int. Ed.*, 2019, **58**, 4504–4509.
132 C. G. Margarit, N. G. Asimow, C. Costentin and D. G. Nocera, *ACS Energy Lett.*, 2020, **5**, 72–78.
133 R. K. Parsapur, S. Chatterjee and K.-W. Huang, *ACS Energy Lett.*, 2020, 2881–2885.
134 M. L. Pegis, J. A. S. Roberts, D. J. Wasylenko, E. A. Mader, A. M. Appel and J. M. Mayer, *Inorg. Chem.*, 2015, **54**, 11883–11888.
135 W. Zhang, W. Lai and R. Cao, *Chem. Rev.*, 2017, **117**, 3717–3797.
136 S. Dey, B. Mondal, S. Chatterjee, A. Rana, S. Amanullah and A. Dey, *Nat. Rev. Chem.*, 2017, **1**, 98.
137 S. Amanullah, A. Singha and A. Dey, *Coord. Chem. Rev.*, 2019, **386**, 183–208.
138 T. Sakai, D. Mersch and E. Reisner, *Angew. Chem., Int. Ed.*, 2013, **52**, 12313–12316.
139 F. Lakadamyali, M. Kato, N. M. Muresan and E. Reisner, *Angew. Chem., Int. Ed.*, 2012, **51**, 9381–9384.
140 J. G. Kleingardner, B. Kandemir and K. L. Bren, *J. Am. Chem. Soc.*, 2014, **136**, 4–7.
141 B. Kandemir, L. Kubie, Y. Guo, B. Sheldon and K. L. Bren, *Inorg. Chem.*, 2016, **55**, 1355–1357.
142 D. W. Wakerley and E. Reisner, *Energy Environ. Sci.*, 2015, **8**, 2283–2295.
143 N. Kaeffer, A. Morozan and V. Artero, *J. Phys. Chem. B*, 2015, **119**, 13707–13713.
144 B. Mondal and A. Dey, *Chem. Commun.*, 2017, **53**, 7707–7715.
145 M. E. Ahmed, S. Dey, M. Y. Darensbourg and A. Dey, *J. Am. Chem. Soc.*, 2018, **140**, 12457–12468.
146 S. Samanta, K. Sengupta, K. Mittra, S. Bandyopadhyay and A. Dey, *Chem. Commun.*, 2012, **48**, 7631–7633.
147 B. Mondal, P. Sen, A. Rana, D. Saha, P. Das and A. Dey, *ACS Catal.*, 2019, **9**, 3895–3899.
148 S. Meshitsuka, M. Ichikawa and K. Tamaru, *J. Chem. Soc., Chem. Commun.*, 1974, 158–159.
149 M. Beley, J. P. Collin, R. Ruppert and J. P. Sauvage, *J. Chem. Soc., Chem. Commun.*, 1984, **2**, 1315–1316.
150 M. Beley, J. P. Collin, R. Ruppert and J. P. Sauvage, *J. Am. Chem. Soc.*, 1986, **108**, 7461–7467.
151 J. P. Collin, A. Jouaiti and J. P. Sauvage, *Inorg. Chem.*, 1988, **27**, 1986–1990.
152 G. B. Balazs and F. C. Anson, *J. Electroanal. Chem.*, 1992, **322**, 325–345.
153 G. B. Balazs and F. C. Anson, *J. Electroanal. Chem.*, 1993, **361**, 149–157.
154 K. Bujno, R. Bilewicz, L. Siegfried and T. A. Kaden, *J. Electroanal. Chem.*, 1998, **445**, 47–53.

155 E. Fujita, J. Haff, R. Sanzenbacher and H. Elias, *Inorg. Chem.*, 1994, **33**, 4627–4628.
156 J. Schneider, H. Jia, K. Kobiro, D. E. Cabelli, J. T. Muckerman and E. Fujita, *Energy Environ. Sci.*, 2012, **5**, 9502–9510.
157 P. J. Connolly and E. J. Billo, *Inorg. Chem.*, 1987, **26**, 3224–3226.
158 J. D. Froehlich and C. P. Kubiak, *Inorg. Chem.*, 2012, **51**, 3932–3934.
159 J. Song, E. L. Klein, F. Neese and S. Ye, *Inorg. Chem.*, 2014, **53**, 7500–7507.
160 J. D. Froehlich and C. P. Kubiak, *J. Am. Chem. Soc.*, 2015, **137**, 3565–3573.
161 C. R. Schneider and H. S. Shafaat, *Chem. Commun.*, 2016, **52**, 9889–9892.
162 E. M. Nichols and C. J. Chang, *Organometallics*, 2019, **38**, 1213–1218.
163 A. Chapovetsky, T. H. Do, R. Haiges, M. K. Takase and S. C. Marinescu, *J. Am. Chem. Soc.*, 2016, **138**, 5765–5768.
164 E. X. Zhang, D. X. Wang, Z. T. Huang and M. X. Wang, *J. Org. Chem.*, 2009, **74**, 8595–8603.
165 D. C. Lacy, C. C. L. McCrory and J. C. Peters, *Inorg. Chem.*, 2014, **53**, 4980–4988.
166 X. Su, K. M. McCardle, J. A. Panetier and J. W. Jurss, *Chem. Commun.*, 2018, **54**, 3351–3354.
167 T. Fogeron, T. K. Todorova, J. P. Porcher, M. Gomez-Mingot, L. M. Chamoreau, C. Mellot-Draznieks, Y. Li and M. Fontecave, *ACS Catal.*, 2018, **8**, 2030–2038.
168 S. Dey, M. E. Ahmed and A. Dey, *Inorg. Chem.*, 2018, **57**, 5939–5947.
169 M. E. Ahmed, A. Rana, R. Saha, S. Dey and A. Dey, *Inorg. Chem.*, 2020, **59**, 5292–5302.
170 S. Dey, T. K. Todorova, M. Fontecave and V. Mougel, *Angew. Chem., Int. Ed.*, 2020, **59**, 15726–15733.
171 B. M. Ceballos and J. Y. Yang, *Proc. Natl. Acad. Sci. U. S. A.*, 2018, **115**, 12686–12691.
172 Y. Matsubara, *ACS Energy Lett.*, 2017, **2**, 1886–1891.
173 K. Roy and P. L. A. Popelier, *J. Phys. Org. Chem.*, 2009, **22**, 186–196.
174 J. Song, E. L. Klein, F. Neese and S. Ye, *Inorg. Chem.*, 2014, **53**, 7500–7507.
175 O. Einsle, A. Messerschmidt, R. Huber, P. M. H. Kroneck, F. Neese and A. Strukturforschung, *J. Am. Chem. Soc.*, 2002, **124**, 11737–11745.
176 L. B. Maia and J. J. G. Moura, *Chem. Rev.*, 2014, **114**, 5273–5357.
177 D. P. Summers and S. Chang, *Nature*, 1993, **365**, 630–633.
178 B. Burlat, J. D. Gwyer, S. Poock, T. Clarke, J. A. Cole, A. M. Hemmings, M. R. Cheesman and J. N. Butt, *Biochem. Soc. Trans.*, 2005, **33**, 137–140.
179 M. Kern, *Biochem. Soc. Trans.*, 2008, **36**, 1011–1016.
180 B. C. Berks, S. J. Ferguson, J. W. B. Moir and D. J. Richardson, *Biochim. Biophys. Acta, Bioenerg.*, 1995, **1232**, 97–173.
181 V. A. Bamford, H. C. Angove, H. E. Seward, A. J. Thomson, J. A. Cole, J. N. Butt, A. M. Hemmings and D. J. Richardson, *Biochemistry*, 2002, **41**, 2921–2931.
182 S. A. T. Å. Resolution, I. Binding, H. Motifs, O. Einsle, P. Stach, A. Messerschmidt, A. Kro, R. Huber and P. M. H. Kroneck, *J. Biol. Chem.*, 2000, **275**, 39608–39616.
183 O. Einsle, P. Stach, A. Messerschmidt and È. Simon, *Acta Crystallogr., Sect. D: Biol. Crystallogr.*, 2002, **58**, 341–342.
184 O. Einsle, A. Messerschmidt, P. Stach, G. P. Bourenkov, H. D. Bartunik, R. Huber and P. M. H. Kroneck, *Nature*, 1999, **400**, 476–480.
185 C. A. Cunha, S. Macieira, M. Dias, G. Almeida, L. L. Gonc, C. Costa, J. Lampreia, R. Huber, J. G. Moura, I. Moura and M. Joa, *J. Biol. Chem.*, 2003, **278**, 17455–17465.
186 M. G. Almeida, S. Macieira, L. L. Gonc, R. Huber, C. A. Cunha, C. Costa, J. Lampreia and M. Joa, *Eur. J. Biochem.*, 2003, **270**, 3904–3915.
187 F. Oliveira and M. L. Rodrigues, *EMBO J.*, 2006, **25**, 5951–5960.
188 M. Youngblut, E. T. Judd, S. J. Elliott, M. Schmidt and A. A. Pacheco, *J. Biol. Inorg. Chem.*, 2012, **17**, 647–662.
189 E. T. Judd, M. Youngblut, A. Andrew Pacheco and S. J. Elliott, *Biochemistry*, 2012, **51**, 10175–10185.
190 K. M. Polyakov, K. M. Boyko, T. V. Tikhonova, A. Slutsky, A. N. Antipov, R. A. Zvyagilskaya, A. N. Popov, G. P. Bourenkov, V. S. Lamzin and V. O. Popov, *J. Mol. Biol.*, 2009, **389**, 846–862.
191 P. Rydberg, E. Sigfridsson and U. Ryde, *J. Biol. Inorg. Chem.*, 2004, **9**, 203–223.
192 N. Stein, D. Love, E. T. Judd, S. J. Elliott, B. Bennett and A. A. Pacheco, *Biochemistry*, 2015, **54**, 3749–3758.
193 C. W. J. Lockwood, M. R. Cheesman, M. Kern, J. Simon, T. A. Clarke, D. J. Richardson and J. N. Butt, *J. Am. Chem. Soc.*, 2015, **137**, 3059–3068.
194 P. Stach, O. Einsle, W. Schumacher, E. Kurun and P. M. H. Kroneck, *J. Inorg. Biochem.*, 2000, **79**, 381–385.
195 P. Lukat, M. Rudolf, P. Stach, A. Messerschmidt, P. M. H. Kroneck and O. Einsle, *Biochemistry*, 2008, **47**, 2080–2086.
196 M. Sjo, *Phys. Chem. Chem. Phys.*, 2004, **6**, 4851–4858.
197 D. Bykov and F. Neese, *J. Biol. Inorg. Chem.*, 2011, **16**, 417–430.
198 E. T. Judd, N. Stein, A. A. Pacheco and S. J. Elliott, *Biochemistry*, 2014, **53**, 5638–5646.
199 Bruker, Apex Ii, 2013, Bruker AXS Inc., Madison, Wisconsin, USA.
200 M. G. Almeida, C. M. Silveira, B. Guigliarelli, P. Bertrand, J. J. G. Moura, I. Moura and C. Léger, *FEBS Lett.*, 2007, **581**, 284–288.
201 T. A. Clarke, G. L. Kemp, J. H. Van Wonderen, R. A. S. Doyle, J. A. Cole, N. Tovell, M. R. Cheesman, J. N. Butt, D. J. Richardson and A. M. Hemmings, *Biochemistry*, 2008, **47**, 3789–3799.
202 D. Bykov and F. Neese, *Inorg. Chem.*, 2015, **54**, 9303–9316.
203 D. Bykov, M. Plog and F. Neese, *J. Biol. Inorg. Chem.*, 2014, **19**, 97–112.
204 G. Martins, L. Rodrigues, F. M. Cunha, D. Matos, P. Hildebrandt, D. H. Murgida, A. C. Pereira and S. Todorovic, *J. Phys. Chem. B*, 2010, **114**, 5563–5566.
205 M. Ali, N. Stein, Y. Mao, S. Shahid, M. Schmidt, B. Bennett and A. A. Pacheco, *J. Am. Chem. Soc.*, 2019, **141**, 13358–13371.
206 D. Bykov and F. Neese, *J. Biol. Inorg. Chem.*, 2012, 741–760.

207 J. H. Enemark and R. D. Feltham, *Coord. Chem. Rev.*, 1974, **13**, 339–406.
208 L. E. Goodrich, F. Paulat, V. K. K. Praneeth and N. Lehnert, *Inorg. Chem.*, 2010, **49**, 6293–6316.
209 G. R. A. Wyllie and W. R. Scheidt, *Chem. Rev.*, 2002, **102**, 1067–1089.
210 L. W. Olson, D. Schaeper, D. Lançon and K. M. Kadish, *J. Am. Chem. Soc.*, 1982, **104**, 2042–2044.
211 D. Lançon and K. M. Kadish, *J. Am. Chem. Soc.*, 1983, **105**, 5610–5617.
212 I. K. Choi, Y. Liu, D. W. Feng, K. J. Paeng and M. D. Ryan, *Inorg. Chem.*, 1991, **30**, 1832–1839.
213 K. Fischer, G. G. Barbier, H. J. Hecht, R. R. Mendel, W. H. Campbell and G. Schwarz, *Plant Cell*, 2005, **17**, 1167–1179.
214 E. Frı, L. M. Rubio, A. Herrero and E. Flores, *Photosynth. Res.*, 2005, **83**, 117–133.
215 D. B. Knaff and M. Hirasawa, *Biochim. Biophys. Acta*, 1991, **1056**, 93–125.
216 M. Hirasawa, K. Fukushima, G. Tamuna and D. B. Knaff, *Biochim. Biophys. Acta*, 1984, **791**, 145–154.
217 C. Pino, F. Olmo-Mira, P. Cabello, M. Martínez-Luque, F. Castillo, M. D. Roldán and C. Moreno-Vivián, *Biochem. Soc. Trans.*, 2006, **34**, 127–129.
218 S. S. Merchant, D. B. Knaff and J. P. Allen, *Photosynth. Res.*, 2010, **103**, 67–77.
219 U. Swamy, M. Wang, J. N. Tripathy, S. K. Kim, M. Hirasawa, D. B. Knaff and J. P. Allen, *Biochemistry*, 2005, **44**, 16054–16063.
220 A. J. Gates, V. M. Luque-Almagro, A. D. Goddard, S. J. Ferguson, M. D. Roldán and D. J. Richardson, *Biochem. J.*, 2011, **435**, 743–753.
221 N. R. Harborne, L. Griffiths, S. J. W. Busby and J. A. Cole, *Mol. Microbiol.*, 1992, **6**, 2805–2813.
222 S. Nakano, M. Takahashi, A. Sakamoto, H. Morikawa and K. Katayanagi, *Protein Sci.*, 2012, **21**, 383–395.
223 S. Nakano, M. Takahashi, A. Sakamoto, H. Morikawa and K. Katayanagi, *Proteins: Struct., Funct., Bioinf.*, 2012, **80**, 2035–2045.
224 M. J. Murphy, L. M. Siegel, S. R. Tove and H. Kamin, *Proc. Natl. Acad. Sci. U. S. A.*, 1974, **71**, 612–616.
225 P. Sétif, M. Hirasawa, N. Cassan, B. Lagoutte, J. N. Tripathy and D. B. Knaff, *Biochemistry*, 2009, **48**, 2828–2838.
226 M. Hirasawa, G. Tollin, Z. Salamon and D. B. Knaff, *Biochim. Biophys. Acta*, 1994, **1185**, 336–345.
227 K. Parey, E. Warkentin, P. M. H. Kroneck and U. Ermler, *Biochemistry*, 2010, **49**, 8912–8921.
228 S. Kuznetsova, D. B. Knaff, M. Hirasawa, P. Sétif and T. A. Mattioli, *Biochemistry*, 2004, **43**, 10765–10774.
229 A. M. V. Brânzanic, U. Ryde and R. Silaghi-Dumitrescu, *Chem. Commun.*, 2019, **55**, 14047–14049.
230 S. Rinaldo, G. Giardina, N. Castiglione, V. Stelitano and F. Cutruzzolà, *Biochem. Soc. Trans.*, 2011, **39**, 195–200.
231 W. G. Zumft, *Microbiol. Mol. Biol. Rev.*, 1997, **61**, 533–616.
232 F. Cutruzzolà, *Biochim. Biophys. Acta, Bioenerg.*, 1999, **1411**, 231–249.
233 D. Nurizzo, F. Cutruzzolà, M. Arese, D. Bourgeois, M. Brunori, C. Cambillau and M. Tegoni, *Biochemistry*, 1998, **37**, 13987–13996.
234 F. Cutruzzolà, K. Brown, E. K. Wilson, A. Bellelli, M. Arese, M. Tegoni, C. Cambillau and M. Brunori, *Proc. Natl. Acad. Sci. U. S. A.*, 2001, **98**, 2232–2237.
235 W. Sun, M. Arese, M. Brunori, F. Cutruzzolà, D. Nurizzo, K. Brown, C. Cambillau and M. Tegoni, *Biochem. Biophys. Res. Commun.*, 2002, **291**, 1–7.
236 S. C. Baker, N. F. W. Saunders, A. C. Willis, S. J. Ferguson, J. Hajdu and V. Fülöp, *J. Mol. Biol.*, 1997, **269**, 440–455.
237 M. R. Cheesman, S. J. Ferguson, J. W. B. Moir, D. J. Richardson, W. G. Zumft and A. J. Thomson, *Biochemistry*, 1997, **36**, 16267–16276.
238 A. Jafferji, J. W. A. Allen, S. J. Ferguson and V. Fulop, *J. Biol. Chem.*, 2000, **275**, 25089–25094.
239 P. A. Williams, V. Fülöp, E. F. Carman, N. F. W. Saunders, S. J. Ferguson and J. Hajdu, *Nature*, 1997, **389**, 406–412.
240 I. V. Pearson, M. D. Page, R. J. M. Van Spanning and S. J. Ferguson, *J. Bacteriol.*, 2003, **185**, 6308–6315.
241 T. Hard, H. J. Barnes, C. Larsson, J.-A. Gustafsson and J. Lund, *Nature*, 1995, **2**, 983–989.
242 E. Vijgenboom, J. E. Busch and G. W. Canters, *Microbiology*, 1997, **143**, 2853–2863.
243 F. Rinaldo and S. Cutruzzola, *Biology of the nitrogen cycle*, Elsevier, Amsterdam, 2007.
244 W. Wu and C. K. Chang, *J. Am. Chem. Soc.*, 1987, **109**, 3149–3150.
245 D. Nurizzo, F. Cutruzzolà, M. Arese, D. Bourgeois, M. Brunori, C. Cambillau and M. Tegoni, *J. Biol. Chem.*, 1999, **274**, 14997–15004.
246 D. Nurizzo, M. C. Silvestrini, M. Mathieu, F. Cutruzzolà, D. Bourgeois, V. Fülöp, J. Hajdu, M. Brunori, M. Tegoni and C. Cambillau, *Structure*, 1997, **5**, 1157–1171.
247 V. Fülöp, J. W. B. Moir, S. J. Ferguson and J. Hajdu, *Cell*, 1995, **81**, 369–377.
248 R. S. Zajicek, M. L. Cartron and S. J. Ferguson, *Biochemistry*, 2006, **45**, 11208–11216.
249 F. Cutruzzolà, M. Arese, S. Grasso, A. Bellelli and M. Brunori, *FEBS Lett.*, 1997, **412**, 365–369.
250 M. Radoul, F. Centola, S. Rinaldo, F. Cutruzzolá, I. Pecht and D. Goldfarb, *Inorg. Chem.*, 2009, 48, 3913–3915.
251 T. Sjögren and J. Hajdu, *J. Biol. Chem.*, 2001, **276**, 29450–29455.
252 B. Samyn, B. C. Berks, M. D. Page, S. J. Ferguson and J. J. Van Beeumen, *Eur. J. Biochem.*, 1994, **219**, 585–594.
253 A. Koppenhöfer, K. L. Turner, J. W. A. Allen, S. K. Chapman and S. J. Ferguson, *Biochemistry*, 2000, **39**, 4243–4249.
254 K. A. Sam, M. J. F. Strampraad, S. De Vries and S. J. Ferguson, *J. Biol. Chem.*, 2008, **283**, 27403–27409.
255 J. Yi, M. K. Safo and G. B. Richter-Addo, *Biochemistry*, 2008, **47**, 8247–8249.
256 J. Yi, A. M. Orville, J. M. Skinner, M. J. Skinner and G. B. Richter-Addo, *Biochemistry*, 2010, **49**, 5969–5971.
257 D. M. Copeland, A. S. Soares, A. H. West and G. B. Richter-Addo, *J. Inorg. Biochem.*, 2006, **100**, 1413–1425.

258 K. Brown, V. Roig-Zamboni, F. Cutruzzola', M. Arese, W. Sun, M. Brunori, C. Cambillau and M. Tegoni, *J. Mol. Biol.*, 2001, **312**, 541–554.
259 S. Rinaldo, A. Arcovito, M. Brunori and F. Cutruzzolà, *J. Biol. Chem.*, 2007, **282**, 14761–14767.
260 G. Ranghino, E. Scorza, T. Sjogren, P. A. Williams, M. Ricci and J. Hajdu, *Biochemistry*, 2000, **39**, 10958–10966.
261 E. G. Moore and Q. H. Gibson, *J. Biol. Chem.*, 1976, **251**, 2788–2794.
262 P. Sarti, A. Giuffré, E. Forte, D. Mastronicola, M. C. Barone and M. Brunori, *Biochem. Biophys. Res. Commun.*, 2000, **274**, 183–187.
263 S. J. George, J. W. A. Allen, S. J. Ferguson and R. N. F. Thorneley, *J. Biol. Chem.*, 2000, **275**, 33231–33237.
264 Y. Wang and B. A. Averill, *J. Am. Chem. Soc.*, 1996, **118**, 3972–3973.
265 S. Rinaldo, M. Brunori and F. Cutruzzolà, *Biochem. Biophys. Res. Commun.*, 2007, **363**, 662–666.
266 O. Farver, M. Brunori, F. Cutruzzolà, S. Rinaldo, S. Wherland and I. Pecht, *Biophys. J.*, 2009, **96**, 2849–2856.
267 O. Farver, P. M. H. Kroneck, I. Pecht and W. G. Zumft, *Proc. Natl. Acad. Sci. U. S. A.*, 2003, **100**, 7622–7625.
268 S. Rinaldo, K. A. Sam, N. Castiglione, V. Stelitano, A. Arcovito, M. Brunori, J. W. A. Allen, S. J. Ferguson and F. Cutruzzolà, *Biochem. J.*, 2011, **435**, 217–225.
269 C. D. Richter, J. W. A. Allen, C. W. Higham, A. Koppenhöfer, R. S. Zajicek, N. J. Watmough and S. J. Ferguson, *J. Biol. Chem.*, 2002, **277**, 3093–3100.
270 K. A. Sam, J. D. Tolland, S. A. Fairhurst, C. W. Higham, D. J. Lowe, R. N. F. Thorneley, J. W. A. Allen and S. J. Ferguson, *Biochem. Biophys. Res. Commun.*, 2008, **371**, 719–723.
271 G. W. Watt and J. D. Chrisp, *Anal. Chem.*, 1952, **24**, 2006–2008.
272 K. A. Sam, S. A. Fairhurst, R. N. F. Thorneley, J. W. A. Allen and S. J. Ferguson, *J. Biol. Chem.*, 2008, **283**, 12555–12563.
273 M. Radoul, D. Bykov, S. Rinaldo, F. Cutruzzolà, F. Neese and D. Goldfarb, *J. Am. Chem. Soc.*, 2011, **133**, 3043–3055.
274 J. W. A. Allen, P. D. Barker, O. Daltrop, J. M. Stevens, E. J. Tomlinson, N. Sinha and S. J. Ferguson, *Dalton Trans.*, 2005, 3410–3418.
275 K. Kobayashi, A. Koppenhöfer, S. J. Ferguson and S. Tagawa, *Biochemistry*, 1997, **36**, 13611–13616.
276 L. L. Perissinotti, M. A. Marti, F. Doctorovich, F. J. Luque and D. A. Estrin, *Biochemistry*, 2008, **47**, 9793–9802.
277 B. Wang, Y. Shi, J. Tejero, S. M. Powell, L. M. Thomas, M. T. Gladwin, S. Shiva, Y. Zhang and G. B. Richter-Addo, *Biochemistry*, 2018, **57**, 4788–4802.
278 M. Tiso, J. Tejero, S. Basu, I. Azarov, X. Wang, V. Simplaceanu, S. Frizzell, T. Jayaraman, L. Geary, C. Shapiro, C. Ho, S. Shiva, D. B. Kim-Shapiro and M. T. Gladwin, *J. Biol. Chem.*, 2011, **286**, 18277–18289.
279 R. Silaghi-Dumitrescu, *Inorg. Chem.*, 2004, **43**, 3715–3718.
280 H. Li, A. Samouilov, X. Liu and J. L. Zweier, *Biochemistry*, 2003, **42**, 1150–1159.
281 H. Li, C. Hemann, T. M. Abdelghany, M. A. El-Mahdy and J. L. Zweier, *J. Biol. Chem.*, 2012, **287**, 36623–36633.
282 P. Corti, M. Ieraci and J. Tejero, *Nitric Oxide*, 2016, **53**, 22–34.
283 C. Gautier, E. Van Faassen, I. Mikula, P. Martasek and A. Slama-Schwok, *Biochem. Biophys. Res. Commun.*, 2006, **341**, 816–821.
284 J. Tejero, C. E. Sparacino-Watkins, V. Ragireddy, S. Frizzell and M. T. Gladwin, *Biochemistry*, 2015, **54**, 722–733.
285 D. B. Kim-Shapiro and M. T. Gladwin, *Nitric Oxide*, 2014, **38**, 58–68.
286 A. F. Vanin, L. M. Bevers, A. Slama-Schwok and E. E. Van Faassen, *Cell. Mol. Life Sci.*, 2007, **64**, 96–103.
287 B. J. Reeder and J. Ukeri, *Nitric Oxide*, 2018, **72**, 16–23.
288 G. Da Silva, E. M. Kennedy and B. Z. Dlugogorski, *J. Phys. Chem. A*, 2006, **110**, 11371–11376.
289 A. J. Bard, R. Parsons and J. Jordan, *Standard Potentials in Aqueous Solution*, Dekker, New York, 1985.
290 J. Heinecke and P. C. Ford, *Coord. Chem. Rev.*, 2010, **254**, 235–247.
291 B. R. Crane, L. M. Siegel and E. D. Getzoff, *Biochemistry*, 1997, **36**, 12120–12137.
292 H. Nasri, Y. Wang, B. H. Huynh and W. R. Scheldt, *J. Am. Chem. Soc.*, 1991, **113**, 717–719.
293 J. B. Fernandes, D. W. Feng, A. Chang, A. Keyser and M. D. Ryan, *Inorg. Chem.*, 1986, **25**, 2606–2610.
294 M. G. Finnegan, A. G. Lappin and W. R. Scheidt, *Inorg. Chem.*, 1990, **29**, 181–185.
295 H. Nasri, W. R. Scheidt, Y. Wang, B. H. Huynh and F. A. Walker, *Inorg. Chem.*, 1991, **30**, 1483–1489.
296 Z. Wei and M. D. Ryan, *Inorg. Chim. Acta*, 2001, **314**, 49–57.
297 H. Nasri, M. K. Ellison, S. Chen, B. H. Huynh and W. R. Scheldt, *J. Am. Chem. Soc.*, 1997, **119**, 6274–6283.
298 J. Lee, A. Y. Kovalevsky, I. V. Novozhilova, K. A. Bagley, P. Coppens and G. B. Richter-Addo, *J. Am. Chem. Soc.*, 2004, **126**, 7180–7181.
299 I. V. Novozhilova, P. Coppens, J. Lee, G. B. Richter-Addo and K. A. Bagley, *J. Am. Chem. Soc.*, 2006, **128**, 2093–2104.
300 K. S. Suslick and R. A. Watson, *Inorg. Chem.*, 1991, **30**, 912–919.
301 K. M. Kadish, V. A. Adamian, E. Van Caemelbecke, Z. Tan, P. Tagliatesta, P. Bianco, T. Boschi, G.-B. Yi, M. A. Khan and G. B. Richter-Addo, *Inorg. Chem.*, 1996, **35**, 1343–1348.
302 K. M. Miranda, X. Bu, I. Lorković and P. C. Ford, *Inorg. Chem.*, 1997, **36**, 4838–4848.
303 F. A. Leal, I. M. Lorkovic, P. C. Ford, J. Lee, L. Chen, L. Torres, M. A. Khan and G. B. Richter-Addo, *Can. J. Chem.*, 2003, **81**, 872–881.
304 D. Awasabisah and G. B. Richter-Addo, *NO_x* linkage isomerization in metal complexes, Elsevier Inc., 1st edn, 2015, vol. 67.
305 J. L. Heinecke, J. Yi, J. C. M. Pereira, G. B. Richter-Addo and P. C. Ford, *J. Inorg. Biochem.*, 2012, **107**, 47–53.
306 T. S. Kurtikyan and P. C. Ford, *Coord. Chem. Rev.*, 2008, **252**, 1486–1496.
307 C. K. Chang, *J. Biol. Chem.*, 1985, 9520–9522.
308 D. Feng, Y. S. Ting and M. D. Ryan, *Inorg. Chem.*, 1985, **24**, 612–617.

309 Y. Liu and M. D. Ryan, *Inorg. Chim. Acta*, 1994, **225**, 57–66.
310 A. M. Stolzenberg, S. H. Strauss and R. H. Holm, *J. Am. Chem. Soc.*, 1981, **103**, 4763–4778.
311 A. M. Stolzenberg, L. O. Spreer and R. H. Holm, *J. Am. Chem. Soc.*, 1980, **102**, 364–370.
312 A. M. Stolzenberg, L. O. Spreer and R. H. Holm, *J. Chem. Soc., Chem. Commun.*, 1979, 1077–1078.
313 C. K. Chang and J. Fajer, *J. Am. Chem. Soc.*, 1980, **102**, 848–851.
314 C. K. Chang, K. M. Barkigia, L. K. Hanson and J. Fajer, *J. Am. Chem. Soc.*, 1986, **108**, 1352–1354.
315 P. F. Richardson, C. K. Chang, L. K. Hanson, L. D. Spaulding and J. Fajer, *J. Phys. Chem.*, 1979, **83**, 3420–3424.
316 C. K. Chang, L. K. Hanson, P. F. Richardson, R. Young and J. Fajer, *Proc. Natl. Acad. Sci. U. S. A.*, 1981, **78**, 2652–2656.
317 E. Fujita and J. Fajer, *J. Am. Chem. Soc.*, 1983, **105**, 6743–6745.
318 S. Ozawa, E. Sakamoto, Y. Watanabe and I. Morishima, *J. Chem. Soc., Chem. Commun.*, 1994, **3**, 935–936.
319 S. Ozawa, E. Sakamoto, T. Ichikawa, Y. Watanabe and I. Morishima, *Inorg. Chem.*, 1995, **34**, 6362–6370.
320 Y. Liu, C. DeSilva and M. D. Ryan, *Inorg. Chim. Acta*, 1997, **258**, 247–255.
321 M. H. Barley, K. Takeuchi, W. R. Murphy and T. J. Meyer, *J. Chem. Soc., Chem. Commun.*, 1985, 507–508.
322 M. H. Barley, K. J. Takeuchi and T. J. Meyer, *J. Am. Chem. Soc.*, 1986, **108**, 5876–5885.
323 M. R. Kumar, D. Pervitsky, L. Chen, T. Poulos, S. Kundu, M. S. Hargrove, E. J. Rivera, A. Diaz, J. L. Colón and P. J. Farmer, *Biochemistry*, 2009, **48**, 5018–5025.
324 R. Lin and P. J. Farmer, *J. Am. Chem. Soc.*, 2000, **122**, 2393–2394.
325 L. E. Goodrich, S. Roy, E. E. Alp, J. Zhao, M. Y. Hu and N. Lehnert, *Inorg. Chem.*, 2013, **52**, 7766–7780.
326 M. H. Rahman and M. D. Ryan, *Inorg. Chem.*, 2017, **56**, 3302–3309.
327 Y. Liu and M. D. Ryan, *J. Electroanal. Chem.*, 1994, **368**, 209–219.
328 J. Pellegrino, S. E. Bari, D. E. Bikiel and F. Doctorovich, *J. Am. Chem. Soc.*, 2010, **132**, 989–995.
329 S. Amanullah and A. Dey, *Chem. Sci.*, 2020, **11**, 5909–5921.
330 A. J. Timmons and M. D. Symes, *Chem. Soc. Rev.*, 2015, **44**, 6708–6722.
331 I. K. Choi and M. D. Ryan, *Inorg. Chim. Acta*, 1988, **153**, 25–30.
332 Y. O. Kim and H. M. Goff, *Inorg. Chem.*, 1990, **29**, 3907–3908.
333 S. Amanullah, P. Saha, R. Saha and A. Dey, *Inorg. Chem.*, 2019, **58**, 152–164.
334 T. K. Das, E. K. Wilson, F. Cutruzzolà, M. Brunori and D. L. Rousseau, *Biochemistry*, 2001, **40**, 10774–10781.
335 X.-J. Zhao, V. Sampath and W. S. Caughey, *Biochem. Biophys. Res. Commun.*, 1994, 537–543.
336 J. C. Maxwell and W. S. Caughey, *Biochemistry*, 1976, **15**, 388–396.
337 D. S. Bohle and C.-H. Hung, *J. Am. Chem. Soc.*, 1995, **117**, 9584–9585.
338 Z. Wei and M. D. Ryan, *Inorg. Chem.*, 2010, **49**, 6948–6954.
339 A. E. Servid, A. L. McKay, C. A. Davis, E. M. Garton, A. Manole, P. S. Dobbin, M. A. Hough and C. R. Andrew, *Biochemistry*, 2015, **54**, 3320–3327.
340 J. J. Warren, T. A. Tronic and J. M. Mayer, *Chem. Rev.*, 2010, **110**, 6961–7001.
341 D. D. M. Wayner and V. D. Parker, *Acc. Chem. Res.*, 1993, **26**, 287–294.
342 E. Wiberg, N. Wiberg and A. F. Holleman, *Inorganic chemistry*, Academic Press, De Gruyter, San Diego; Berlin; New York, 2001.
343 N. S. Lewis, *Science*, 2007, **315**, 798–801.
344 J. A. Turner, *Science*, 2004, **305**, 972–974.
345 K. A. Vincent, A. Parkin and F. A. Armstrong, *Chem. Rev.*, 2007, **107**, 4366–4413.
346 D. Mersch, C.-Y. Lee, J. Z. Zhang, K. Brinkert, J. C. Fontecilla-Camps, A. W. Rutherford and E. Reisner, *J. Am. Chem. Soc.*, 2015, **137**, 8541–8549.
347 W. Lubitz, E. J. Reijerse and J. Messinger, *Energy Environ. Sci.*, 2008, **1**, 15–31.
348 C. Mealli and T. B. Rauchfuss, *Angew. Chem., Int. Ed.*, 2007, **46**, 8942–8944.
349 V. Artero, M. Chavarot-Kerlidou and M. Fontecave, *Angew. Chem., Int. Ed.*, 2011, **50**, 7238–7266.
350 M. Wang, L. Chen and L. Sun, *Energy Environ. Sci.*, 2012, **5**, 6763–6778.
351 D. V. Esposito, S. T. Hunt, Y. C. Kimmel and J. G. Chen, *J. Am. Chem. Soc.*, 2012, **134**, 3025–3033.
352 R. B. Gordon, M. Bertram and T. E. Graedel, *Proc. Natl. Acad. Sci. U. S. A.*, 2006, **103**, 1209–1214.
353 D. G. Nocera, *Acc. Chem. Res.*, 2017, **50**, 616–619.
354 P. M. Vignais, B. Billoud and J. Meyer, *FEMS Microbiol. Rev.*, 2001, **25**, 455–501.
355 P. M. Vignais and B. Billoud, *Chem. Rev.*, 2007, **107**, 4206–4272.
356 P. Tamagnini, R. Axelsson, P. Lindberg, F. Oxelfelt, R. Wünschiers and P. Lindblad, *Microbiol. Mol. Biol. Rev.*, 2002, **66**, 1–20.
357 R. K. Thauer, A.-K. Kaster, M. Goenrich, M. Schick, T. Hiromoto and S. Shima, *Annu. Rev. Biochem.*, 2010, **79**, 507–536.
358 R. Cammack, M. Frey and R. Robson, *Hydrogen as a Fuel Learning from Nature*, Taylor & Francis, 11 New Fetter Lane, London EC4P 4EE, 2001.
359 C. Madden, M. D. Vaughn, I. Díez-Pérez, K. A. Brown, P. W. King, D. Gust, A. L. Moore and T. A. Moore, *J. Am. Chem. Soc.*, 2012, **134**, 1577–1582.
360 H. R. Pershad, J. L. C. Duff, H. A. Heering, E. C. Duin, S. P. J. Albracht and F. A. Armstrong, *Biochemistry*, 1999, **38**, 8992–8999.
361 A. K. Jones, E. Sillery, S. P. J. Albracht and F. A. Armstrong, *Chem. Commun.*, 2002, 866–867.
362 D. J. Evans and C. J. Pickett, *Chem. Soc. Rev.*, 2003, **32**, 268–275.

363 S. Dey, P. K. Das and A. Dey, *Coord. Chem. Rev.*, 2013, **257**, 42–63.
364 K. Schütz, T. Happe, O. Troshina, P. Lindblad, E. Leitão, P. Oliveira and P. Tamagnini, *Planta*, 2004, **218**, 350–359.
365 A. Melis, L. Zhang, M. Forestier, M. L. Ghirardi and M. Seibert, *Plant Physiol.*, 2000, **122**, 127–136.
366 M. L. Ghirardi, *Indian J. Biochem. Biophys.*, 2006, **43**, 201–210.
367 W. Lubitz, H. Ogata, O. Rüdiger and E. Reijerse, *Chem. Rev.*, 2014, **114**, 4081–4148.
368 J. C. Fontecilla-Camps, A. Volbeda, C. Cavazza and Y. Nicolet, *Chem. Rev.*, 2007, **107**, 4273–4303.
369 J. C. Fontecilla-Camps, P. Amara, C. Cavazza, Y. Nicolet and A. Volbeda, *Nature*, 2009, **460**, 814–822.
370 S. Shima and R. K. Thauer, *Chem. Rec.*, 2007, **7**, 37–46.
371 S. Rospert, J. Breitung, K. Ma, B. Schwörer, C. Zirngibl, R. K. Thauer, D. Linder, R. Huber and K. O. Stetter, *Arch. Microbiol.*, 1991, **156**, 49–55.
372 Y. Nicolet, C. Piras, P. Legrand, C. E. Hatchikian and J. C. Fontecilla-Camps, *Structure*, 1999, **7**, 13–23.
373 J. W. Peters, W. N. Lanzilotta, B. J. Lemon and L. C. Seefeldt, *Science*, 1998, **282**, 1853–1858.
374 W. Roseboom, A. L. De Lacey, V. M. Fernandez, E. C. Hatchikian and S. P. J. Albracht, *JBIC, J. Biol. Inorg. Chem.*, 2006, **11**, 102–118.
375 Z. Chen, B. J. Lemon, S. Huang, D. J. Swartz, J. W. Peters and K. A. Bagley, *Biochemistry*, 2002, **41**, 2036–2043.
376 P. E. M. Siegbahn, J. W. Tye and M. B. Hall, *Chem. Rev.*, 2007, **107**, 4414–4435.
377 A. L. de Lacey, E. C. Hatchikian, A. Volbeda, M. Frey, J. C. Fontecilla-Camps and V. M. Fernandez, *J. Am. Chem. Soc.*, 1997, **119**, 7181–7189.
378 C. V. Popescu and E. Münck, *J. Am. Chem. Soc.*, 1999, **121**, 7877–7884.
379 Y. Nicolet, A. L. de Lacey, X. Vernède, V. M. Fernandez, E. C. Hatchikian and J. C. Fontecilla-Camps, *J. Am. Chem. Soc.*, 2001, **123**, 1596–1601.
380 O. F. Erdem, L. Schwartz, M. Stein, A. Silakov, S. Kaur-Ghumaan, P. Huang, S. Ott, E. J. Reijerse and W. Lubitz, *Angew. Chem., Int. Ed.*, 2011, **50**, 1439–1443.
381 W. Lubitz, E. Reijerse and M. van Gastel, *Chem. Rev.*, 2007, **107**, 4331–4365.
382 A. Silakov, B. Wenk, E. Reijerse and W. Lubitz, *Phys. Chem. Chem. Phys.*, 2009, **11**, 6592–6599.
383 P. Rodríguez-Maciá, K. Pawlak, O. Rüdiger, E. J. Reijerse, W. Lubitz and J. A. Birrell, *J. Am. Chem. Soc.*, 2017, **139**, 15122–15134.
384 A. Adamska, A. Silakov, C. Lambertz, O. Rüdiger, T. Happe, E. Reijerse and W. Lubitz, *Angew. Chem., Int. Ed.*, 2012, **51**, 11458–11462.
385 J. H. Artz, D. W. Mulder, M. W. Ratzloff, C. E. Lubner, O. A. Zadvornyy, A. X. LeVan, S. G. Williams, M. W. W. Adams, A. K. Jones, P. W. King and J. W. Peters, *J. Am. Chem. Soc.*, 2017, **139**, 9544–9550.
386 A. S. Pandey, T. V. Harris, L. J. Giles, J. W. Peters and R. K. Szilagyi, *J. Am. Chem. Soc.*, 2008, **130**, 4533–4540.
387 M. Senger, S. Mebs, J. Duan, O. Shulenina, K. Laun, L. Kertess, F. Wittkamp, U.-P. Apfel, T. Happe, M. Winkler, M. Haumann and S. T. Stripp, *Phys. Chem. Chem. Phys.*, 2018, **20**, 3128–3140.
388 M. W. Ratzloff, J. H. Artz, D. W. Mulder, R. T. Collins, T. E. Furtak and P. W. King, *J. Am. Chem. Soc.*, 2018, **140**, 7623–7628.
389 C. Sommer, A. Adamska-Venkatesh, K. Pawlak, J. A. Birrell, O. Rüdiger, E. J. Reijerse and W. Lubitz, *J. Am. Chem. Soc.*, 2017, **139**, 1440–1443.
390 M. L. K. Sanchez, C. Sommer, E. Reijerse, J. A. Birrell, W. Lubitz and R. B. Dyer, *J. Am. Chem. Soc.*, 2019, **141**, 16064–16070.
391 A. Volbeda, E. Garcin, C. Piras, A. L. de Lacey, V. M. Fernandez, E. C. Hatchikian, M. Frey and J. C. Fontecilla-Camps, *J. Am. Chem. Soc.*, 1996, **118**, 12989–12996.
392 A. Volbeda, M.-H. Charon, C. Piras, E. C. Hatchikian, M. Frey and J. C. Fontecilla-Camps, *Nature*, 1995, **373**, 580–587.
393 H. Ogata, W. Lubitz and Y. Higuchi, *Dalton Trans.*, 2009, 7577–7587.
394 T. R. Simmons, G. Berggren, M. Bacchi, M. Fontecave and V. Artero, *Coord. Chem. Rev.*, 2014, **270–271**, 127–150.
395 R. P. Happe, W. Roseboom, A. J. Pierik, S. P. J. Albracht and K. A. Bagley, *Nature*, 1997, **385**, 126.
396 H. S. Shafaat, O. Rüdiger, H. Ogata and W. Lubitz, *Biochim. Biophys. Acta, Bioenerg.*, 2013, **1827**, 986–1002.
397 S. Foerster, M. Stein, M. Brecht, H. Ogata, Y. Higuchi and W. Lubitz, *J. Am. Chem. Soc.*, 2003, **125**, 83–93.
398 M. Brecht, M. van Gastel, T. Buhrke, B. Friedrich and W. Lubitz, *J. Am. Chem. Soc.*, 2003, **125**, 13075–13083.
399 S. J. George, S. Kurkin, R. N. F. Thorneley and S. P. J. Albracht, *Biochemistry*, 2004, **43**, 6808–6819.
400 H. Ogata, K. Nishikawa and W. Lubitz, *Nature*, 2015, **520**, 571–574.
401 M. Kampa, M.-E. Pandelia, W. Lubitz, M. van Gastel and F. Neese, *J. Am. Chem. Soc.*, 2013, **135**, 3915–3925.
402 H. Ogata, S. Hirota, A. Nakahara, H. Komori, N. Shibata, T. Kato, K. Kano and Y. Higuchi, *Structure*, 2005, **13**, 1635–1642.
403 R. K. Thauer, A. R. Klein and G. C. Hartmann, *Chem. Rev.*, 1996, **96**, 3031–3042.
404 C. Zirngibl, R. Hedderich and R. K. Thauer, *FEBS Lett.*, 1990, **261**, 112–116.
405 C. Zirngibl, W. Van Dongen, B. Schwörer, R. Von Bünau, M. Richter, A. Klein and R. K. Thauer, *Eur. J. Biochem.*, 1992, **208**, 511–520.
406 T. Hiromoto, E. Warkentin, J. Moll, U. Ermler and S. Shima, *Angew. Chem., Int. Ed.*, 2009, **48**, 6457–6460.
407 A. Dey, *J. Am. Chem. Soc.*, 2010, **132**, 13892–13901.
408 G. J. Kubas, *Chem. Rev.*, 2007, **107**, 4152–4205.
409 G. J. Kubas, R. R. Ryan, B. I. Swanson, P. J. Vergamini and H. J. Wasserman, *J. Am. Chem. Soc.*, 1984, **106**, 451–452.
410 G. J. Kubas, *J. Organomet. Chem.*, 2001, **635**, 37–68.
411 R. H. Crabtree, *Angew. Chem., Int. Ed. Engl.*, 1993, **32**, 789–805.

412 G. J. Kubas, *Proc. Natl. Acad. Sci. U. S. A.*, 2007, **104**, 6901–6907.
413 R. H. Morris, *Coord. Chem. Rev.*, 2008, **252**, 2381–2394.
414 J. Chatt and L. A. Duncanson, *J. Chem. Soc.*, 1953, 2939–2947.
415 M. J. S. Dewar, *Bull. Soc. Chim. Fr.*, 1951, **18**, C71.
416 A. D. Wilson, R. H. Newell, M. J. McNevin, J. T. Muckerman, M. Rakowski DuBois and D. L. DuBois, *J. Am. Chem. Soc.*, 2006, **128**, 358–366.
417 C. J. Curtis, A. Miedaner, R. Ciancanelli, W. W. Ellis, B. C. Noll, M. Rakowski DuBois and D. L. DuBois, *Inorg. Chem.*, 2003, **42**, 216–227.
418 A. D. Wilson, K. Fraze, B. Twamley, S. M. Miller, D. L. DuBois and M. Rakowski DuBois, *J. Am. Chem. Soc.*, 2008, **130**, 1061–1068.
419 W. Zhu, A. C. Marr, Q. Wang, F. Neese, D. J. E. Spencer, A. J. Blake, P. A. Cooke, C. Wilson and M. Schröder, *Proc. Natl. Acad. Sci. U. S. A.*, 2005, **102**, 18280–18285.
420 A. D. Wilson, R. K. Shoemaker, A. Miedaner, J. T. Muckerman, D. L. DuBois and M. R. DuBois, *Proc. Natl. Acad. Sci. U. S. A.*, 2007, **104**, 6951–6956.
421 T. W. Woolerton, S. Sheard, Y. S. Chaudhary and F. A. Armstrong, *Energy Environ. Sci.*, 2012, **5**, 7470–7490.
422 C. Léger and P. Bertrand, *Chem. Rev.*, 2008, **108**, 2379–2438.
423 H. Reihlen, A. Gruhl and G. v. Hessling, *Justus Liebigs Ann. Chem.*, 1929, **472**, 268–287.
424 D. Seyferth, G. B. Womack, M. K. Gallagher, M. Cowie, B. W. Hames, J. P. Fackler and A. M. Mazany, *Organometallics*, 1987, **6**, 283–294.
425 J. T. Kleinhaus, F. Wittkamp, S. Yadav, D. Siegmund and U.-P. Apfel, *Chem. Soc. Rev.*, 2021, Advance Article, DOI: 10.1039/D0CS01089H.
426 J.-F. Capon, F. Gloaguen, F. Y. Pétillon, P. Schollhammer and J. Talarmin, *Coord. Chem. Rev.*, 2009, **253**, 1476–1494.
427 G. A. N. Felton, C. A. Mebi, B. J. Petro, A. K. Vannucci, D. H. Evans, R. S. Glass and D. L. Lichtenberger, *J. Organomet. Chem.*, 2009, **694**, 2681–2699.
428 D. Schilter, J. M. Camara, M. T. Huynh, S. Hammes-Schiffer and T. B. Rauchfuss, *Chem. Rev.*, 2016, **116**, 8693–8749.
429 F. Gloaguen, J. D. Lawrence and T. B. Rauchfuss, *J. Am. Chem. Soc.*, 2001, **123**, 9476–9477.
430 G. Eilers, L. Schwartz, M. Stein, G. Zampella, L. de Gioia, S. Ott and R. Lomoth, *Chem. – Eur. J.*, 2007, **13**, 7075–7084.
431 B. E. Barton and T. B. Rauchfuss, *Inorg. Chem.*, 2008, **47**, 2261–2263.
432 F. Wang, M. Wang, X. Liu, K. Jin, W. Dong and L. Sun, *Dalton Trans.*, 2007, 3812–3819.
433 U.-P. Apfel, C. R. Kowol, F. Kloss, H. Görls, B. K. Keppler and W. Weigand, *J. Organomet. Chem.*, 2011, **696**, 1084–1088.
434 H.-G. Cui, M. Wang, W.-B. Dong, L.-L. Duan, P. Li and L.-C. Sun, *Polyhedron*, 2007, **26**, 904–910.
435 R. J. Wright, C. Lim and T. D. Tilley, *Chem. – Eur. J.*, 2009, **15**, 8518–8525.
436 G. Qian, W. Zhong, Z. Wei, H. Wang, Z. Xiao, L. Long and X. Liu, *New J. Chem.*, 2015, **39**, 9752–9760.
437 D. Chong, I. P. Georgakaki, R. Mejia-Rodriguez, J. Sanabria-Chinchilla, M. P. Soriaga and M. Y. Darensbourg, *Dalton Trans.*, 2003, 4158–4163.
438 Z. Yu, M. Wang, P. Li, W. Dong, F. Wang and L. Sun, *Dalton Trans.*, 2008, 2400–2406.
439 Y. Si, M. Hu and C. Chen, *C. R. Chim.*, 2008, **11**, 932–937.
440 Y. Na, M. Wang, J. Pan, P. Zhang, B. Åkermark and L. Sun, *Inorg. Chem.*, 2008, **47**, 2805–2810.
441 C. M. Thomas, O. Rüdiger, T. Liu, C. E. Carson, M. B. Hall and M. Y. Darensbourg, *Organometallics*, 2007, **26**, 3976–3984.
442 M. L. Singleton, R. M. Jenkins, C. L. Klemashevich and M. Y. Darensbourg, *C. R. Chim.*, 2008, **11**, 861–874.
443 Z. Wang, W. Jiang, J. Liu, W. Jiang, Y. Wang, B. Åkermark and L. Sun, *J. Organomet. Chem.*, 2008, **693**, 2828–2834.
444 P. Li, M. Wang, L. Chen, J. Liu, Z. Zhao and L. Sun, *Dalton Trans.*, 2009, 1919–1926.
445 E. S. Donovan, J. J. McCormick, G. S. Nichol and G. A. N. Felton, *Organometallics*, 2012, **31**, 8067–8070.
446 J. Chen, A. K. Vannucci, C. A. Mebi, N. Okumura, S. C. Borowski, M. Swenson, L. T. Lockett, D. H. Evans, R. S. Glass and D. L. Lichtenberger, *Organometallics*, 2010, **29**, 5330–5340.
447 H.-M. Lin, C. Mu, A. Li, X.-F. Liu, Y.-L. Li, Z.-Q. Jiang and H.-K. Wu, *Transition Met. Chem.*, 2019, **44**, 491–498.
448 G. Durgaprasad, R. Bolligarla and S. K. Das, *J. Organomet. Chem.*, 2012, **706–707**, 37–45.
449 R. M. Bullock and M. L. Helm, *Acc. Chem. Res.*, 2015, **48**, 2017–2026.
450 J.-F. Capon, S. Ezzaher, F. Gloaguen, F. Y. Pétillon, P. Schollhammer and J. Talarmin, *Chem. – Eur. J.*, 2008, **14**, 1954–1964.
451 S. Ott, M. Kritikos, B. Åkermark, L. Sun and R. Lomoth, *Angew. Chem., Int. Ed.*, 2004, **43**, 1006–1009.
452 Y. Si, C. Ma, M. Hu, H. Chen, C. Chen and Q. Liu, *New J. Chem.*, 2007, **31**, 1448–1454.
453 T. Liu, M. Wang, Z. Shi, H. Cui, W. Dong, J. Chen, B. Åkermark and L. Sun, *Chem. – Eur. J.*, 2004, **10**, 4474–4479.
454 L.-C. Song, J.-H. Ge, X.-G. Zhang, Y. Liu and Q.-M. Hu, *Eur. J. Inorg. Chem.*, 2006, 3204–3210.
455 L.-C. Song, J.-H. Ge, X.-F. Liu, L.-Q. Zhao and Q.-M. Hu, *J. Organomet. Chem.*, 2006, **691**, 5701–5709.
456 W.-G. Wang, H.-Y. Wang, G. Si, C.-H. Tung and L.-Z. Wu, *Dalton Trans.*, 2009, 2712–2720.
457 S. Jiang, J. Liu, Y. Shi, Z. Wang, B. Åkermark and L. Sun, *Dalton Trans.*, 2007, 896–902.
458 L.-C. Song, B.-S. Yin, Y.-L. Li, L.-Q. Zhao, J.-H. Ge, Z.-Y. Yang and Q.-M. Hu, *Organometallics*, 2007, **26**, 4921–4929.
459 L.-C. Song, L.-X. Wang, B.-S. Yin, Y.-L. Li, X.-G. Zhang, Y.-W. Zhang, X. Luo and Q.-M. Hu, *Eur. J. Inorg. Chem.*, 2008, 291–297.
460 W. Gao, J. Liu, C. Ma, L. Weng, K. Jin, C. Chen, B. Åkermark and L. Sun, *Inorg. Chim. Acta*, 2006, **359**, 1071–1080.

461 W. Gao, J. Sun, T. Åkermark, M. Li, L. Eriksson, L. Sun and B. Åkermark, *Chem. – Eur. J.*, 2010, **16**, 2537–2546.
462 C. Costentin, *Chem. Rev.*, 2008, **108**, 2145–2179.
463 G. A. N. Felton, R. S. Glass, D. L. Lichtenberger and D. H. Evans, *Inorg. Chem.*, 2006, **45**, 9181–9184.
464 J.-F. Capon, F. Gloaguen, P. Schollhammer and J. Talarmin, *J. Electroanal. Chem.*, 2004, **566**, 241–247.
465 J.-F. Capon, F. Gloaguen, P. Schollhammer and J. Talarmin, *J. Electroanal. Chem.*, 2006, **595**, 47–52.
466 S. Jiang, J. Liu and L. Sun, *Inorg. Chem. Commun.*, 2006, **9**, 290–292.
467 M. Y. Darensbourg, E. J. Lyon and J. J. Smee, *Coord. Chem. Rev.*, 2000, **206–207**, 533–561.
468 C. Tard and C. J. Pickett, *Chem. Rev.*, 2009, **109**, 2245–2274.
469 M. E. Ahmed and A. Dey, *Curr. Opin. Electrochem.*, 2019, **15**, 155–164.
470 J.-X. Jian, C. Ye, X.-Z. Wang, M. Wen, Z.-J. Li, X.-B. Li, B. Chen, C.-H. Tung and L.-Z. Wu, *Energy Environ. Sci.*, 2016, **9**, 2083–2089.
471 M. Cheng, M. Wang, S. Zhang, F. Liu, Y. Yang, B. Wan and L. Sun, *Faraday Discuss.*, 2017, **198**, 197–209.
472 R. Mejia-Rodriguez, D. Chong, J. H. Reibenspies, M. P. Soriaga and M. Y. Darensbourg, *J. Am. Chem. Soc.*, 2004, **126**, 12004–12014.
473 F. Quentel, G. Passard and F. Gloaguen, *Energy Environ. Sci.*, 2012, **5**, 7757–7761.
474 S. Dey, A. Rana, S. G. Dey and A. Dey, *ACS Catal.*, 2013, **3**, 429–436.
475 M. E. Ahmed, S. Dey, B. Mondal and A. Dey, *Chem. Commun.*, 2017, **53**, 8188–8191.
476 V. Vijaikanth, J.-F. Capon, F. Gloaguen, F. Y. Pétillon, P. Schollhammer and J. Talarmin, *J. Organomet. Chem.*, 2007, **692**, 4177–4181.
477 A. Le Goff, V. Artero, R. Metayé, F. Moggia, B. Jousselme, M. Razavet, P. D. Tran, S. Palacin and M. Fontecave, *Int. J. Hydrogen Energy*, 2010, **35**, 10790–10796.
478 E. S. Andreiadis, P.-A. Jacques, P. D. Tran, A. Leyris, M. Chavarot-Kerlidou, B. Jousselme, M. Matheron, J. Pécaut, S. Palacin, M. Fontecave and V. Artero, *Nat. Chem.*, 2013, **5**, 48–53.
479 C. Caix, S. Chardon-Noblat, A. Deronzier and R. Ziessel, *J. Electroanal. Chem.*, 1996, **403**, 189–202.
480 I. Sádaba, M. López Granados, A. Riisager and E. Taarning, *Green Chem.*, 2015, **17**, 4133–4145.
481 R. H. Morris, *Chem. Rev.*, 2016, **116**, 8588–8654.
482 K. Abdur-Rashid, T. P. Fong, B. Greaves, D. G. Gusev, J. G. Hinman, S. E. Landau, A. J. Lough and R. H. Morris, *J. Am. Chem. Soc.*, 2000, **122**, 9155–9171.
483 X. Zhao, I. P. Georgakaki, M. L. Miller, J. C. Yarbrough and M. Y. Darensbourg, *J. Am. Chem. Soc.*, 2001, **123**, 9710–9711.
484 X. Zhao, I. P. Georgakaki, M. L. Miller, R. Mejia-Rodriguez, C.-Y. Chiang and M. Y. Darensbourg, *Inorg. Chem.*, 2002, **41**, 3917–3928.
485 I. P. Georgakaki, M. L. Miller and M. Y. Darensbourg, *Inorg. Chem.*, 2003, **42**, 2489–2494.
486 T. Xu, D. Chen and X. Hu, *Coord. Chem. Rev.*, 2015, **303**, 32–41.
487 M. T. Olsen, B. E. Barton and T. B. Rauchfuss, *Inorg. Chem.*, 2009, **48**, 7507–7509.
488 M. T. Olsen, T. B. Rauchfuss and S. R. Wilson, *J. Am. Chem. Soc.*, 2010, **132**, 17733–17740.
489 J. M. Camara and T. B. Rauchfuss, *J. Am. Chem. Soc.*, 2011, **133**, 8098–8101.
490 J. M. Camara and T. B. Rauchfuss, *Nat. Chem.*, 2012, **4**, 26–30.
491 N. Wang, M. Wang, T. Zhang, P. Li, J. Liu and L. Sun, *Chem. Commun.*, 2008, 5800–5802.
492 N. Wang, M. Wang, J. Liu, K. Jin, L. Chen and L. Sun, *Inorg. Chem.*, 2009, **48**, 11551–11558.
493 S. Ghosh, G. Hogarth, N. Hollingsworth, K. B. Holt, S. E. Kabir and B. E. Sanchez, *Chem. Commun.*, 2014, **50**, 945–947.
494 N. Wang, M. Wang, Y. Wang, D. Zheng, H. Han, M. S. G. Ahlquist and L. Sun, *J. Am. Chem. Soc.*, 2013, **135**, 13688–13691.
495 K. A. Vincent, A. Parkin, O. Lenz, S. P. J. Albracht, J. C. Fontecilla-Camps, R. Cammack, B. Friedrich and F. A. Armstrong, *J. Am. Chem. Soc.*, 2005, **127**, 18179–18189.
496 K. D. Swanson, M. W. Ratzloff, D. W. Mulder, J. H. Artz, S. Ghose, A. Hoffman, S. White, O. A. Zadvornyy, J. B. Broderick, B. Bothner, P. W. King and J. W. Peters, *J. Am. Chem. Soc.*, 2015, **137**, 1809–1816.
497 S. Dey, A. Rana, D. Crouthers, B. Mondal, P. K. Das, M. Y. Darensbourg and A. Dey, *J. Am. Chem. Soc.*, 2014, **136**, 8847–8850.
498 S. T. Stripp, G. Goldet, C. Brandmayr, O. Sanganas, K. A. Vincent, M. Haumann, F. A. Armstrong and T. Happe, *Proc. Natl. Acad. Sci. U. S. A.*, 2009, **106**, 17331–17336.
499 M. K. Bruska, M. T. Stiebritz and M. Reiher, *J. Am. Chem. Soc.*, 2011, **133**, 20588–20603.
500 M. T. Stiebritz and M. Reiher, *Inorg. Chem.*, 2009, **48**, 7127–7140.
501 C. Lambertz, N. Leidel, K. G. V. Havelius, J. Noth, P. Chernev, M. Winkler, T. Happe and M. Haumann, *J. Biol. Chem.*, 2011, **286**, 40614–40623.
502 C. Orain, L. Saujet, C. Gauquelin, P. Soucaille, I. Meynial-Salles, C. Baffert, V. Fourmond, H. Bottin and C. Léger, *J. Am. Chem. Soc.*, 2015, **137**, 12580–12587.
503 A. Kubas, D. De Sancho, R. B. Best and J. Blumberger, *Angew. Chem., Int. Ed.*, 2014, **53**, 4081–4084.
504 S. Fukuzumi, Y.-M. Lee and W. Nam, *Coord. Chem. Rev.*, 2018, **355**, 54–73.
505 S. Kaur-Ghumaan and M. Stein, *Dalton Trans.*, 2014, **43**, 9392–9405.
506 F. Möller, S. Piontek, R. G. Miller and U.-P. Apfel, *Chem. – Eur. J.*, 2018, **24**, 1471–1493.
507 Y. Ohki and K. Tatsumi, *Eur. J. Inorg. Chem.*, 2011, 973–985.
508 D. Brazzolotto, M. Gennari, N. Queyriaux, T. R. Simmons, J. Pécaut, S. Demeshko, F. Meyer, M. Orio, V. Artero and C. Duboc, *Nat. Chem.*, 2016, **8**, 1054–1060.

509 Y. Oudart, V. Artero, J. Pécaut, C. Lebrun and M. Fontecave, *Eur. J. Inorg. Chem.*, 2007, 2613–2626.
510 S. Canaguier, M. Fontecave and V. Artero, *Eur. J. Inorg. Chem.*, 2011, 1094–1099.
511 S. Ogo, R. Kabe, K. Uehara, B. Kure, T. Nishimura, S. C. Menon, R. Harada, S. Fukuzumi, Y. Higuchi, T. Ohhara, T. Tamada and R. Kuroki, *Science*, 2007, **316**, 585–587.
512 L.-C. Song, J.-P. Li, Z.-J. Xie and H.-B. Song, *Inorg. Chem.*, 2013, **52**, 11618–11626.
513 V. Fourmond, S. Canaguier, B. Golly, M. J. Field, M. Fontecave and V. Artero, *Energy Environ. Sci.*, 2011, **4**, 2417–2427.
514 B. E. Barton and T. B. Rauchfuss, *J. Am. Chem. Soc.*, 2010, **132**, 14877–14885.
515 B. E. Barton, C. M. Whaley, T. B. Rauchfuss and D. L. Gray, *J. Am. Chem. Soc.*, 2009, **131**, 6942–6943.
516 L. Vaccaro, V. Artero, S. Canaguier, M. Fontecave and M. J. Field, *Dalton Trans.*, 2010, **39**, 3043–3049.
517 L.-C. Song, Y. Lu, L. Zhu and Q.-L. Li, *Organometallics*, 2017, **36**, 750–760.
518 O. A. Ulloa, M. T. Huynh, C. P. Richers, J. A. Bertke, M. J. Nilges, S. Hammes-Schiffer and T. B. Rauchfuss, *J. Am. Chem. Soc.*, 2016, **138**, 9234–9245.
519 L.-C. Song, X.-Y. Yang, M. Cao, X.-Y. Gao, B.-B. Liu, L. Zhu and F. Jiang, *Chem. Commun.*, 2017, **53**, 3818–3821.
520 T. R. Simmons and V. Artero, *Angew. Chem., Int. Ed.*, 2013, **52**, 6143–6145.
521 S. Ogo, K. Ichikawa, T. Kishima, T. Matsumoto, H. Nakai, K. Kusaka and T. Ohhara, *Science*, 2013, **339**, 682–684.
522 G. M. Chambers, M. T. Huynh, Y. Li, S. Hammes-Schiffer, T. B. Rauchfuss, E. Reijerse and W. Lubitz, *Inorg. Chem.*, 2016, **55**, 419–431.
523 S. Canaguier, M. Field, Y. Oudart, J. Pécaut, M. Fontecave and V. Artero, *Chem. Commun.*, 2010, **46**, 5876–5878.
524 F. Dole, A. Fournel, V. Magro, E. C. Hatchikian, P. Bertrand and B. Guigliarelli, *Biochemistry*, 1997, **36**, 7847–7854.
525 S. Niu, L. M. Thomson and M. B. Hall, *J. Am. Chem. Soc.*, 1999, **121**, 4000–4007.
526 L. De Gioia, P. Fantucci, B. Guigliarelli and P. Bertrand, *Inorg. Chem.*, 1999, **38**, 2658–2662.
527 K. Weber, T. Krämer, H. S. Shafaat, T. Weyhermüller, E. Bill, M. van Gastel, F. Neese and W. Lubitz, *J. Am. Chem. Soc.*, 2012, **134**, 20745–20755.
528 G. Gezer, S. Verbeek, M. A. Siegler and E. Bouwman, *Dalton Trans.*, 2017, **46**, 13590–13596.
529 G. Gezer, D. Durán Jiménez, M. A. Siegler and E. Bouwman, *Dalton Trans.*, 2017, **46**, 7506–7514.
530 H. Tang and M. B. Hall, *J. Am. Chem. Soc.*, 2017, **139**, 18065–18070.
531 D. Balestri, Y. Roux, M. Mattarozzi, C. Mucchino, L. Heux, D. Brazzolotto, V. Artero, C. Duboc, P. Pelagatti, L. Marchiò and M. Gennari, *Inorg. Chem.*, 2017, **56**, 14801–14808.
532 D. Brazzolotto, L. Wang, H. Tang, M. Gennari, N. Queyriaux, C. Philouze, S. Demeshko, F. Meyer, M. Orio, V. Artero, M. B. Hall and C. Duboc, *ACS Catal.*, 2018, **8**, 10658–10667.
533 L.-C. Song, X.-F. Han, W. Chen, J.-P. Li and X.-Y. Wang, *Dalton Trans.*, 2017, **46**, 10003–10013.
534 S. Ding, P. Ghosh, M. Y. Darensbourg and M. B. Hall, *Proc. Natl. Acad. Sci. U. S. A.*, 2017, **114**, E9775–E9782.
535 S. Ding, P. Ghosh, A. M. Lunsford, N. Wang, N. Bhuvanesh, M. B. Hall and M. Y. Darensbourg, *J. Am. Chem. Soc.*, 2016, **138**, 12920–12927.
536 P. Ghosh, M. Quiroz, N. Wang, N. Bhuvanesh and M. Y. Darensbourg, *Dalton Trans.*, 2017, **46**, 5617–5624.
537 P. Ghosh, S. Ding, R. B. Chupik, M. Quiroz, C.-H. Hsieh, N. Bhuvanesh, M. B. Hall and M. Y. Darensbourg, *Chem. Sci.*, 2017, **8**, 8291–8300.
538 M. E. Ahmed, S. Chattopadhyay, L. Wang, D. Brazzolotto, D. Pramanik, D. Aldakov, J. Fize, A. Morozan, M. Gennari, C. Duboc, A. Dey and V. Artero, *Angew. Chem., Int. Ed.*, 2018, **57**, 16001–16004.
539 N. T. Nguyen, Y. Mori, T. Matsumoto, T. Yatabe, R. Kabe, H. Nakai, K.-S. Yoon and S. Ogo, *Chem. Commun.*, 2014, **50**, 13385–13387.
540 T. Matsumoto, B. Kure and S. Ogo, *Chem. Lett.*, 2008, **37**, 970–971.
541 G. M. Chambers, J. Mitra, T. B. Rauchfuss and M. Stein, *Inorg. Chem.*, 2014, **53**, 4243–4249.
542 B. Kure, T. Matsumoto, K. Ichikawa, S. Fukuzumi, Y. Higuchi, T. Yagi and S. Ogo, *Dalton Trans.*, 2008, 4747–4755.
543 M. Isegawa, A. K. Sharma, S. Ogo and K. Morokuma, *ACS Catal.*, 2018, **8**, 10419–10429.
544 J. Kalms, A. Schmidt, S. Frielingsdorf, T. Utesch, G. Gotthard, D. von Stetten, P. van der Linden, A. Royant, M. A. Mroginski, P. Carpentier, O. Lenz and P. Scheerer, *Proc. Natl. Acad. Sci. U. S. A.*, 2018, **115**, E2229–E2237.
545 N. J. Lindenmaier, S. Wahlefeld, E. Bill, T. Szilvási, C. Eberle, S. Yao, P. Hildebrandt, M. Horch, I. Zebger and M. Driess, *Angew. Chem., Int. Ed.*, 2017, **56**, 2208–2211.
546 X. Yang, L. C. Elrod, J. H. Reibenspies, M. B. Hall and M. Y. Darensbourg, *Chem. Sci.*, 2019, **10**, 1368–1373.
547 B. Ginovska-Pangovska, A. Dutta, M. L. Reback, J. C. Linehan and W. J. Shaw, *Acc. Chem. Res.*, 2014, **47**, 2621–2630.
548 R. M. Bullock, A. M. Appel and M. L. Helm, *Chem. Commun.*, 2014, **50**, 3125–3143.
549 M. Rakowski DuBois and D. L. DuBois, *Chem. Soc. Rev.*, 2009, **38**, 62–72.
550 W. J. Shaw, M. L. Helm and D. L. DuBois, *Biochim. Biophys. Acta, Bioenerg.*, 2013, **1827**, 1123–1139.
551 J. Y. Yang, S. Chen, W. G. Dougherty, W. S. Kassel, R. M. Bullock, D. L. DuBois, S. Raugei, R. Rousseau, M. Dupuis and M. R. DuBois, *Chem. Commun.*, 2010, **46**, 8618–8620.
552 J. Y. Yang, R. M. Bullock, M. R. DuBois and D. L. DuBois, *MRS Bull.*, 2011, **36**, 39–47.
553 D. L. DuBois and R. M. Bullock, *Eur. J. Inorg. Chem.*, 2011, 1017–1027.
554 U. J. Kilgore, J. A. S. Roberts, D. H. Pool, A. M. Appel, M. P. Stewart, M. R. DuBois, W. G. Dougherty, W. S. Kassel,

R. M. Bullock and D. L. DuBois, *J. Am. Chem. Soc.*, 2011, **133**, 5861–5872.
555 S. Raugei, M. L. Helm, S. Hammes-Schiffer, A. M. Appel, M. O'Hagan, E. S. Wiedner and R. M. Bullock, *Inorg. Chem.*, 2016, **55**, 445–460.
556 S. Horvath, L. E. Fernandez, A. V. Soudackov and S. Hammes-Schiffer, *Proc. Natl. Acad. Sci. U. S. A.*, 2012, **109**, 15663–15668.
557 A. Dutta, S. Lense, J. Hou, M. H. Engelhard, J. A. S. Roberts and W. J. Shaw, *J. Am. Chem. Soc.*, 2013, **135**, 18490–18496.
558 T. Liu, X. Wang, C. Hoffmann, D. L. DuBois and R. M. Bullock, *Angew. Chem., Int. Ed.*, 2014, **53**, 5300–5304.
559 T. Liu, D. L. DuBois and R. M. Bullock, *Nat. Chem.*, 2013, **5**, 228–233.
560 T. Liu, S. Chen, M. J. O'Hagan, M. Rakowski DuBois, R. M. Bullock and D. L. DuBois, *J. Am. Chem. Soc.*, 2012, **134**, 6257–6272.
561 N. Wang, H. Zheng, W. Zhang and R. Cao, *Chin. J. Catal.*, 2018, **39**, 228–244.
562 H. Lei, X. Li, J. Meng, H. Zheng, W. Zhang and R. Cao, *ACS Catal.*, 2019, **9**, 4320–4344.
563 T. Nakae, M. Hirotsu and I. Kinoshita, *Organometallics*, 2015, **34**, 3988–3997.
564 C. H. Lee, D. K. Dogutan and D. G. Nocera, *J. Am. Chem. Soc.*, 2011, **133**, 8775–8777.
565 A. Kochem, M. O'Hagan, E. S. Wiedner and M. van Gastel, *Chem. – Eur. J.*, 2015, **21**, 10338–10347.
566 D. K. Bediako, B. H. Solis, D. K. Dogutan, M. M. Roubelakis, A. G. Maher, C. H. Lee, M. B. Chambers, S. Hammes-Schiffer and D. G. Nocera, *Proc. Natl. Acad. Sci. U. S. A.*, 2014, **111**, 15001–15006.
567 D. J. Graham and D. G. Nocera, *Organometallics*, 2014, **33**, 4994–5001.
568 A. Dutta, J. A. S. Roberts and W. J. Shaw, *Angew. Chem., Int. Ed.*, 2014, **53**, 6487–6491.
569 A. Dutta, D. L. DuBois, J. A. S. Roberts and W. J. Shaw, *Proc. Natl. Acad. Sci. U. S. A.*, 2014, **111**, 16286–16291.
570 P. Das, M.-H. Ho, M. O'Hagan, W. J. Shaw, R. Morris Bullock, S. Raugei and M. L. Helm, *Dalton Trans.*, 2014, **43**, 2744–2754.
571 A. Rana, B. Mondal, P. Sen, S. Dey and A. Dey, *Inorg. Chem.*, 2017, **56**, 1783–1793.
572 M. Aresta, A. Dibenedetto and A. Angelini, *Chem. Rev.*, 2014, **114**, 1709–1742.
573 S. Chatterjee, K. Sengupta, S. Dey and A. Dey, *Inorg. Chem.*, 2013, **52**, 14168–14177.